University of Alberta

Synthesis and Investigation of Viral Cysteine Protease Inhibitors and Biosynthetic Studies on Subtilosin A

by

Venugopal Rao Miyyapuram

A thesis submitted to the Faculty of Graduate Studies and Research
in partial fulfillment of the requirements for the degree of

Doctor of Philosophy

Department of Chemistry

Fall 2009

Edmonton, Alberta

Examining Committee

Dr. John C. Vederas (Supervisor) ; Department of Chemistry

Dr. Frederick G. West ; Department of Chemistry

Dr. Jillian M. Buriak ; Department of Chemistry

Dr. Robert E. Campbell ; Department of Chemistry

Dr. David Bressler ; Department of Agriculture, Food and Nutrional Science

Dr. Erika Plettner (External) ; Department of Chemistry, Simon Fraser University, British Columbia

ABSTRACT

This thesis discusses the synthesis and evaluation of cysteine protease inhibitors, the asymmetric reduction of pseudoxazolones, and the study of the mechanism of subtilosin A biosynthesis.

Five classes of compounds, including pyridinylamines and ethers, have been designed with the aim of developing non-covalent inhibitors of SARS–CoV $3CL^{pro}$, a chymotrypsin-like cysteine protease vital to the life cycle of the SARS coronavirus. These compounds were synthesized and screened against SARS–CoV $3CL^{pro}$. 3-Bromo-5-[5-(4-nitro-phenyl)-furan-2-ylmethoxy]-pyridine (**37**), 5-Bromo-*N*-((5-(4-nitrophenyl)furan-2-yl)methyl)pyridin-3-amine (**54**), *N*-((5-(4-Aminophenyl)furan-2-yl)methyl)-5-bromopyridin-3-amine (**61**) and *N*-{5-[5-(4-Nitro-phenyl)-furan-2-ylmethylene]-4-oxo-2-thioxo-thiazolidin-3-yl}-acetamide **(67)** show very good inhibition with IC_{50} values ranging from 12 μM to 31 μM. Mechanism studies suggest that these compounds are reversible inhibitors.

Inhibitors against Israel acute paralysis virus (IAPV), which is associated with Colony Collapse Disorder (CCD) in honeybees, have been designed with a glutamine residue at the P1 position based on sequence comparisons between IAPV $3C^{pro}$ and known 3C proteases. Two fluorogenic peptide substrates, Abz-QTTTQAG-Y(NO_2)-E (**95**) and Abz-EVSMQVD-Y(NO_2)-D (**98**), were synthesized. However, both compounds show no activity. As a different strategy,

a peptidyl fluoromethyl ketone, Ac-Val-Thr(OBn)-Leu-6-fluoro-N,N-dimethyl-S-oxohexanamide (**77**), incorporating the SARS recognition sequence, has also been synthesized, and testing of its activity is in progress.

Asymmetric reduction of pseudoxazolones containing an imine moiety can serve as a method for preparing enantiopure amino acids. Several conditions were tried but without success. Although the results are not encouraging, attempts to prepare pseudoxazolone derivatives with increased reactivity led to synthesis of highly substituted olefins.

Subtilosin A, a ribosomally synthesized antimicrobial cyclic peptide from *Bacillus subtilis*, is posttranslationally modified to contain unusual thioether cross-links between cysteine sulfurs and alpha-carbons of phenylalanines and threonine. The *sbo-alb* gene locus is required for the production of subtilosin A as well as for immunity, but the exact roles of these genes are unclear. In order to elucidate the roles of *albA*, *albE* and *albF* genes that may be responsible for the posttranslational modifications, three potential substrates were designed and synthesized. In addition to these biosynthetic studies, subtilosin A1, a T6I mutant of subtilosin A, was purified and characterized. It was found to show hemolytic activity and altered bactericidal activity compared to that of the parent.

ACKNOWLEDGEMENTS

Doing research as well as living in a country with a different culture constituted a challenge from which I had a lot to learn. I made a big step forward and it is my pleasure to take this opportunity to acknowledge all the people contributing to it.

I start by expressing my deepest appreciation and gratitude to Dr. John C. Vederas for his guidance, excellent support and for sharing his vast scientific knowledge. Dr. Vederas provided a perfect environment for me to grow as a chemist and as an individual. It has been truly memorable and educative being a member of his research group.

I owe my special thanks to Dr. Wei Liu and Sabesan (Jay) Yoganathan, Clarissa Sit and Avena Ross for proof-reading this thesis and providing invaluable suggestions for its improvement.

I thank Dr. Michael N. G. James, Dr. Jiang Yin (Biochemistry Department, University of Alberta), Dr. Linsay Eltis, Dr. Carly Huitema (Department of Microbiology and Immunology, University of British Columbia) and Dr. Michiko M. Nakano (Department of Science & Engineering, School of Medicine, Oregon Health & Science University) for their collaborative efforts.

I thank Dr. Randy Whittal, Dr. Angie Morales-Izquierdo, Jing Zheng, Mark Miskolzie, Nupur Dabral and Wayne Moffat in spectral and analytical services in the Department of Chemistry for their expertise and technical support.

The University of Alberta Chemistry Department is gratefully acknowledged for providing the infrastructure and financial support.

The day-by-day life, especially the breaks would have not had the salt and pepper without the lab mates, both present and past. I would like to thank one and all for making my stay a pleasant one.

Mere words cannot enunciate my gratitude and affection to Mahendra Sandbhor, Dahnanjay Kendre, Ravi, Jianmin Zhang, Patrick Liu, Leah Martin-Visscher, Jay, Chenguang Fan and Zedu Haung who have not only stood by me in the most difficult times, but also by their own special ways, made my stint a thoroughly enjoyable and memorable one.

I find it difficult to verbalize my deepest sense of indebtedness to my family members for all their sacrifice and blessings.

TABLE OF CONTENTS

CHAPTER 1: SYNTHESES AND EVALUATION OF SEVERE ACUTE RESPIRATORY SYNDROME (SARS) 3CL^{PRO} INHIBITORS

1.1 INTRODUCTION.....1

1.1.1 Severe acute respiratory syndrome (SARS).....1

1.1.2 Coronaviruses.....1

1.1.3 Picornaviruses 2

1.1.4 SARS coronavirus (SARS-CoV).....2

1.1.5 Coronavirus life cycle 3

1.1.6 Symptoms and Treatment of SARS.....4

1.1.7 Structure and function of SARS 3C-like protease (3CL^{pro}).....5

1.1.8 Crystal structure of SARS-CoV 3CL^{pro}.....8

1.1.9 Design of inhibitors against SARS 3CL^{pro}.....9

1.1.10 Covalent Inhibitors.....10

1.1.10.1 Chloromethyl ketone (CMK).....11

1.1.10.2 Ruprintrivir (**2**) and analogues as Michael acceptors.....12

1.1.10.3 Benzotriazole esters.....15

1.1.10.4 Thiophenecarboxylates and
biological evaluation using FRET.....16

1.1.10.5 Heteroaromatic esters.....19

1.1.10.6 Fluoromethylene ketones (FMK).....22

1.1.11 Non-covalent inhibitors.....23

1.1.11.1 Bifunctional phenyl boronic acids.....23

1.1.11.2 Phthalhydrazide substituted
keto-glutamine analogues.....25

1.1.11.3 Isatin derivatives.....29

1.1.11.4 Aryl methylene ketones.....31

1.1.12 Objectives: Synthesis and evaluation of SARS 3CL^{pro}
inhibitors.....34

1.2 RESULTS AND DISCUSSION.....36

1.2.1 Pyridinyl ethers.....36

1.2.2 Pyridinylamines.....43

1.2.3 Hybrid peptide.....49

1.2.4 Rhodanine derivative.....50

1.2.5 Oxazole derivatives.....51

1.2.6 Inhibition mechanism studies.....54

1.2.7 Conclusions and future work.....58

CHAPTER 2: INHIBITORS OF INSECT VIRAL CYSTEINE PROTEASES

2.1 INTRODUCTION.....61

2.1.1 Picornaviruses 61

2.1.2 Colony Collapse Disorder (CCD).....64

2.1.3 Design of inhibitors against insect viral 3C proteases.....65

2.1.4 Objectives: synthesis and evaluation of

insect viral cysteine protease inhibitors.....67

2.2 RESULTS AND DISCUSSION.....69

2.2.1 Peptidyl fluoromethyl ketone.....69

2.2.2 Cricket paralysis virus (CrPV) peptide substrate.....74

2.2.3 Israel acute paralysis virus (IAPV) peptide substrate.....77

2.2.4 Conclusions and future work.....89

CHAPTER 3: ASYMMETRIC REDUCTION OF PSEUDOXAZOLONES

3.1 INTRODUCTION.....90

3.1.1 Asymmetric synthesis of alpha-amino acid.....90

3.1.2 Objectives: Asymmetric reduction of pseudoxazolones.....94

3.2 RESULTS AND DISCUSSION.....95

3.2.1 Reactions attempted.....96

3.2.2 Preparation of 2-dichloromethylene pseudoxazolone.....100

3.2.3 Attempts to synthesize 2-dicyano and

2-dimethyl ester analogues of pseudoxazolones.....101

3.2.4 Conclusions and future direction.....109

CHAPTER 4: BIOSYNTHETIC STUDIES ON SUBTILOSIN A

4.1 INTRODUCTION.....110

4.1.1 Mechanism of action.....114

4.1.2 Structural elucidation studies of subtilosin A.....114

4.1.3 Physical properties.....118

4.1.4 Plausible mechanisms of formation of thioether

linkages and N-C cyclization.....119

4.1.4.1 Thioether linkages.....119

4.1.4.2 N-C cyclization.....122

4.1.5 Objectives: Biosynthetic studies.....129

4.2 RESULTS AND DISCUSSION.....130

4.2.1 Synthesis of mature peptide.....133

4.2.2 Synthesis of the subtilosin A precursor linear peptide.....138

4.2.3 Synthesis of cyclic peptide.....140

4.2.4 Conclusions and future direction.....143

CHAPTER 5: EXPERIMENTAL PROCEDURES

5.1 GENERAL PROCEDURES.....145

5.1.1 Reagents, solvents, and solutions.....145

5.1.2 Purification techniques.....146

5.1.3 Instrumentation for compound characterization.....147

5.1.4 Manual Fmoc solid phase peptide synthesis (SPPS).....148

5.1.5 Automated Fmoc SPPS.....149

5.2 EXPERIMENTAL PROCEDURES AND DATA

FOR COMPOUNDS.....150

[5-(4-Chloro-phenyl)furan-2-yl]methanol (**32**).....150

3-Chloro-5-((5-(4-chlorophenyl)furan-2-yl)methoxy)pyridine (**33**).....151

3-Bromo-5-((5-(4-chlorophenyl)furan-2yl)methoxy)pyridine (**34**).....152

5-[5-(4-Chloro-phenyl)-furan-2-ylmethoxy]-2-methyl-pyridine (**35**).....153

2-(4-Chlorophenyl)-5-((3-(trifluoromethyl)phenoxy)methyl)furan (**36**).154

3-Bromo-5-[5-(4-nitro-phenyl)-furan-2-ylmethoxy]-pyridine (**37**).....155

2-[5-(4-Chloro-phenyl)-furan-2-ylmethylsulfanyl]-pyridine (**38**).....156

3-(Thiophen-2-ylmethoxy)-pyridine (**39**).....157

2-Methyl-5-(thiophen-2-ylmethoxy)pyridine (**40**).....158

3-Bromo-5-((5-(3-nitrophenyl)furan-2-yl)methoxy)pyridine (**41**).....159

[5-(3-Nitrophenyl)furan-2-yl)]methanol (**44**).....160

3-Bromo-5-(4-methoxy-benzylsulfanyl)-pyridine (**45**).....161

5-Bromo-*N*-((5-(4-nitrophenyl)furan-2-yl)methyl)

pyridin-3-amine (**54**).....162

(5-Bromo-pyridin-3-yl)-[5-(4-chloro-phenyl)-furan-2-

ylmethyl]-amine (**55**).....163

(5-Bromo-pyridin-3-yl)-furan-2-ylmethyl-amine (**56**).....164

Benzofuran-2-ylmethyl-(5-bromo-pyridin-3-yl)-amine (**57**).....165

Benzo[*b*]thiophen-2-ylmethyl-(5-bromo-pyridin-3-yl)-amine (**58**).....166

N-((1*H*-indol-3-yl)methyl)-5-bromopyridin-3-amine (**59**).....167

(5-Bromo-pyridin-3-yl)-(1-methyl-1*H*-indol-3-ylmethyl)-amine (**60**)....168

N-((5-(4-Aminophenyl)furan-2-yl)methyl)-5-bromopyridin-3-amine (**61**).....169

N-(4-(5-((5-bromopyridin-3-ylamino)methyl)furan-2-yl) phenyl)methanesulfonamide (**62**).....170

Ethyl-(5-bromo-pyridin-3-yl)-[5-(4-nitro-phenyl)-furan-2-ylmethyl]-amine (**63**).....171

N-(5-bromopyridin-3-yl)-*N*-((5-(4-chlorophenyl)furan-2-yl)methyl)-cyclopropanecarboxamide (**64**).....172

(*S*)-5-(4-Chlorophenyl)-*N*-(6-(dimethylamino)-1-(1,4-dioxo-3,4-dihydrophthalazin-2(1*H*)-yl)-2,6-dioxohexan-3-yl)furan-2-carboxamide **(65)**.....173

N-{5-[5-(4-Nitro-phenyl)-furan-2-ylmethylene]-4-oxo-2-thioxo-thiazolidin-3-yl}-acetamide (**67**).....174

5-((5-Bromopyridin-3-yloxy)methyl)-2-(4-chlorophenyl)oxazole (**69**)..175

5-Bromo-*N*-((2-(4-chlorophenyl)oxazol-5-yl)methyl)pyridin-3-amine (**70**).....176

Ethyl 3-diazo-2-oxopropanoate (**72**).....177

2-(4-Chloro-phenyl)-oxazole-5-carboxylic acid ethyl ester (**73**).....178

[2-(4-Chloro-phenyl)-oxazol-5-yl]-methanol (**74**).....179

2-(4-Chloro-phenyl)-oxazole-5-carbaldehyde (**75**).....180

(*S*)-2-((2*S*,3*S*)-2-((*S*)-2-Acetamido-3-methylbutanamido)-3-(benzyloxy)butanamido)-4-methylpentanoic acid (**76**).....180

(*S*)-4-((*S*)-2-((2*S*,3*R*)-2-((*S*)-2-Acetamido-3-methylbutanamido)-3-(benzyloxy)butanamido)-4-methylpentanamido)-6-fluoro-*N*,*N*-dimethyl 5-oxohexanamide **(77)**.....182

(*S*)-*tert*-Butyl 6-(dimethylamino)-1-fluoro-2,6-dioxohexan-3-ylcarbamate (**78**).....184

2-*tert*-Butoxycarbonylamino-4-dimethylcarbamoyl-butyric acid benzyl ester (**80**).....185

2-*tert*-Butoxycarbonylamino-4-dimethylcarbamoyl-butyric acid (**81**)....186

Dibenzyl 2-fluoromalonate (**83**).....187

3-(Benzyloxy)-2-fluoro-3-oxopropanoic acid (**84**).....188

Benzyl fluoromalonate, magnesium salt (**85**).....189

(*S*)-*tert*-Butyl-6-(dimethylamino)-1-fluoro-2-hydroxy-6-oxohexan-3-ylcarbamate (**92**).....190

CrPV peptide substrate (**95**).....191

Precursor for CrPV (**96**).....192

IAPV Fluorescent Peptide (**98**).....193

(*S*)-5-*tert*-Butoxy-2-(2-(*tert*-butoxycarbonylamino)benzamido)-5-oxopentanoic acid (**105**).....194

Precurosor for IAPV Fluorescent Peptide (**106**).....195

2-Benzhydrylidene-4-methyl-2*H*-oxazol-5-one (**109**).....196

2-Diphenylacetylamino-propionic acid methyl ester (**110**).....197

Methyl-2-2-diphenyl acetate (**111**).....198

4-hydroxy-5-methyl-3,3-diphenylpyrrolidin-2-one **(112)**.....199

2-Dichloromethylene-4-methyl-2*H*-oxazol-5-one (**113**).....199

Phenyltrichloroacetate **(117)**.....200

2-(2,2,2-Trichloroacetamido)propanoic acid (**118**).....201

1,1-Dimethyl-1-phenylbromomethanetricarboxylate (**121**).....202

Dimethyl-2,3-dicarbomethoxy)butendioate **(123)**.....202

2-Methoxycarbonyl-malonic acid methyl ester phenyl ester (**125**).....203

1,1-Diethyl-2,2-dimethylethene-1,1,2,2-tetracarboxylate **(128)**.....204

2-*tert*-Butoxycarbonylamino-benzoic acid (**132**).....205

Subtilosin A mature linear peptide.....206

Subtilosin A precursor linear peptide.....207

Subtilosin A mature cyclic peptide.....208

H_2N-Abz-Ser-OH.....209

5.3 ENZYMATIC ACTIVITY ASSAY.....210

6. REFERENCES.....212

7. APPENDIX A: ISOLATION AND CHARACTERIZATION OF SUBTILOSIN A1 WITH HEMOLYTIC ACTIVITY.....236

7.1 Subtilosin A1.....236

7.2 Objective.....237

7.3 Isolation and purification of subtilosin A1.....238

7.4 Mass spectrometry studies.....238

7.5 Antibacterial and hemolytic activity of subtilosin A and subtilosin A1 240

7.6 Conclusions and future direction 241

7.7 Experimental procedures 242

7.7.1 Growth and purification of subtilosin A1 242

7.7.2 HPLC purification 243

7.7.3 Mass spectrometry analysis 244

7.8 References 245

8. APPENDIX B: SYNTHESIS AND TESTING OF SMALL MOLECULE INHIBITOR OF *hi*GlmU AGAINST *mtb*GlmU 246

8.1 Introduction 246

8.2 Objective 250

8.3 Results and discussion 251

8.4 Summary and future direction 252

8.5 Experimental procedures and data for compounds 253

8.6 References 255

LIST OF TABLES

Table 1. Synthesis of pyridinyl ethers **35**-**40**.....37

Table 2. Evaluation of pyridinyl ethers as SARS-CoV M^{pro} inhibitors.....38

Table 3. Synthesis of pyridinylamines by reductive amination and their inhibition results.....45

Table 4. FRET assay results showing the observed inhibition.....54

Table 5. Reduction reactions attempted with diphenyl pseuodoxazolone **109**.....97

LIST OF FIGURES

Figure 1. Schematic representation of the SARS coronavirus.....3

Figure 2. Life cycle of coronaviruses.....4

Figure 3. The SARS-CoV $3CL^{pro}$ polyproteins and the positions of cleavage sites predicted to be processed by $PL2^{pro}$ (blue) and $3CL^{pro}$ (red).....6

Figure 4. The standard nomenclature used for substrate residues and their corresponding binding sites.....7

Figure 5. The SARS-CoV $3CL^{pro}$ monomer structure.....8

Figure 6. Structure of CMK (**1**) and mechanism of covalent attachment.....11

Figure 7. Dimer structure of SARS Co-V M^{pro} complexed with CMK (**1**).....12

Figure 8. Structure of Ruprintrivir (**2**).....13

Figure 9. Mechanism of inactivation of the enzyme via formation of a thioether bond.....14

Figure 10. Structures of **3** and **4** 14

Figure 11. Proposed acylation mechanism with benzotriazole ester **5**.....16

Figure 12. A quenched-FRET assay for evaluating SARS-CoV 3CL^{pro} activity..17

Figure 13. Structure of pyridinyl ester **6** shows that it can undergo nucleophilic attack by cysteine thiol of the enzyme.....18

Figure 14. Structures of pyridinyl ester analogs.....20

Figure 15. Docking studies (by Dr. Chunying Niu) of inhibitors **8** and **9** in the SARS-CoV 3CL^{pro} active site.....21

Figure 16. Mechanism of enzyme inactivation by fluoromethyl ketones.....22

Figure 17. Structures of dipeptidyl glutaminyl fluoromethyl ketones **16** and **17**.....23

Figure 18. Active site of SARS-CoV 3CL^{pro} showing serine residues 139, 144 and 147 and catalytic Cys145 and His41.....24

Figure 19. Structure of bifunctional phenyl boronic acid **18**.....25

Figure 20. Structure of **19**.....26

Figure 21. Ketoglutamine analogs as the potent inhibitors of SARS 3CL^{pro}.....26

Figure 22. Interactions between inhibitor **20** and SARS 3CL^{pro} showing episulfide and thioacyl forms.....27

Figure 23. Structure of an isatin derivative **26**.....29

Figure 24. Docking studies of compound **26** showing hydrogen bonding interactions.....30

Figure 25. Structure of 5-halopyridin-3-yl aromatic ester **27** that was designed based on **6**.....31

Figure 26. Structure of aryl methylene ketones **28**-**30**.....32

Figure 27. Modelling conformations (by Dr. Chunying Niu) of **28** (white carbon sticks), **29** (cyan), and **30** (yellow) at the active site of SARS-CoV M^{pro}.....33

Figure 28. SARS $3CL^{pro}$ inhibitor **28** and potential sites of modification.....34

Figure 29. Representative examples of targets **A** to **E**.....35

Figure 30. Mass spectral evaluation of the inhibition mechanism.....55

Figure 31. Parts of the NMR spectra showing the peaks for **A**. Ethyl mercaptan; **B:** Inhibitor **54**.....57

Figure 32. Generalized schematic representation of picornaviral polyprotein processing.....62

Figure 33. Mechanism of protease hydrolysis by HAV $3C^{pro}$ at the 2B/2C junction.....63

Figure 34. Structure of Abz-SVTLQ/SGY(NO_2)R.....67

Figure 35. Structures of fluorescent peptide substrates for CrPV and IAPV.....68

Figure 36. Structure of SARS 3CL^{pro} recognition tripeptide **76**.....69

Figure 37. General structure of pseudoxazolone (unsaturated).....92

Figure 38. Amino acid sequences of presubtilosin and subtilosin

A. Backbone cyclization between the N- and C- termini and

B. Cross-link between cysteine sulfur and α-carbon in Phe.....111

Figure 39. Structure of cyclothiazomycin.....113

Figure 40. The proposed primary structure of subtilosin A by Babasaki *et al*...115

Figure 41. The *sbo-alb* locus in *Bacillus subtilis*.....116

Figure 42. The subtilosin A structure proposed by Stein and coworkers.....117

Figure 43. Structure of microcin J25.....122

Figure 44. Cyanobactin assembly lines in cyanobacteria.....123

Figure 45. Cleavage of precursor peptide by PatA.....124

Figure 46. PagG mediated cleavage showing the formation of eptidemnamide and recognition peptide.....125

Figure 47. Proposed transamidation mechanism.....126

Figure 48. Structure of microviridin B.....128

Figure 49. Amino acid sequences of the mature, cyclic and precursor peptides.....130

Figure 50. Structure of Fmoc-Ala-Thr(ΨMe,Me Pro)-OH.....131

Figure 51. Structure of Fmoc-Asp(O^{t}Bu)-(Dmb)Gly-OH.....133

Figure 52. MS/MS fragmentation nomenclature and analysis of decapeptide indicating modifications on tryptophan residue.....135

Figure 53. MS / MS analysis of subtilosin A mature linear peptide.....138

Figure 54. MS / MS analysis of subtilosin A precursor linear peptide.....140

APPENDIX A

Figure 1. Amino acid sequence of subtilosin A1.....236

Figure 2. MALDI-TOF mass spectrum of subtilosin A1.....239

Figure 3. Hemolytic activity produced by *B. subtilis* and the variant subtilosin A1.....241

APPENDIX B

Figure 1. Schematic representation of *hi*GlmU showing hydrogen-bonding interactions.....250

LIST OF SCHEMES

Scheme 1. Proposed mechanisms accounting for reversible and irreversible inhibition….....…….…….....28

Scheme 2. Synthesis of pyridinyl ethers **33** and **34**.....36

Scheme 3. Synthesis of H_2N-Abz-Ser-OH.....39

Scheme 4. Synthesis of **41**.....40

Scheme 5. Synthesis of pyridinyl thioether **45**.....41

Scheme 6. Retrosynthetic analysis of target **48**.....41

Scheme 7. Efforts to deprotect PMB group.....42

Scheme 8. Efforts to synthesize **50**.....43

Scheme 9. Preparation of pyridinylamine **54**.....44

Scheme 10. Reduction of nitro derivative **54**.....46

Scheme 11. Proposed mechanism of decomposition of **61**.....47

Scheme 12. Synthesis of mesylated derivative **62**.....47

Scheme 13. Synthesis of alkylated and amide derivatives **63** and **64**.....48

Scheme 14. Synthesis of hybrid peptide **65**.....49

Scheme 15. Reagents and conditions for the synthesis of rhodanine analog **67**...50

Scheme 16. Synthesis of oxazole ether **69**.....52

Scheme 17. Preparation of oxazole amine derivative **70**.....53

Scheme 18. Retrosynthetic analysis of target fluoromethyl peptide **77**.....70

Scheme 19. Synthesis of *N*,*N*-dimethylglutamine derivative **81**.....71

Scheme 20. Synthesis of *N*,*N*-dimethylglutamine-fluoroketone **78**.....72

Scheme 21. Synthesis of recognition tripeptide **76**.....73

Scheme 22. Synthesis of target peptidyl fluoromethyl ketone **77**.....74

Scheme 23. Synthesis of nonamer precursor **96** for Cricket paralysis virus (CrPV) peptide substrate.....75

Scheme 24. Synthesis of CrPV peptide substrate **95** from **96**.....77

Scheme 25. Synthesis of precursor **99** for IAPV peptide substrate.....78

Scheme 26. Attempted synthesis of IAPV peptide substrate showing the formation of the undesired aminobenzoyl adducts.....80

Scheme 27. Proposed mechanism for the formation of Abz adducts.....82

Scheme 28. Plausible mechanism of cleavage of peptide via diketopiperazine adduct formation.....83

Scheme 29. Retro-synthetic analysis of **98**.....84

Scheme 30. Synthesis of Abz peptide **105** on a 2-chlorotrityl chloride resin.....85

Scheme 31. Synthesis of precursor peptide **106**.....87

Scheme 32. Final synthesis of **98**.....88

Scheme 33. Synthetic approaches toward chiral α-amino acids.....91

Scheme 34. Approach for the synthesis of enantiopure aminoacids.....94

Scheme 35. Approach for making new amino acids.....94

Scheme 36. Synthesis of pseudoxazolone.....95

Scheme 37. $NaBH_3CN$ reduction of alanine diphenyl pseudoxazolone.....96

Scheme 38. Proposed mechanism for the formation of **112**.....99

Scheme 39. Structures of **113, 114** and **115**.....100

Scheme 40. Synthesis of 2-dichloromethylene pseudoxazolone (**113)**.....101

Scheme 41. Attempts to synthesize 2-dicyano analogue **114**. Also shown are possible sites of attack.....102

Scheme 42. Retrosynthetic analysis of **115**.....103

Scheme 43. Attempts to synthesize **121**.....103

Scheme 44. Proposed mechanism for the formation of **123**.....104

Scheme 45. Alternative strategy showing the synthesis of **121**.....104

Scheme 46. Attempted synthesis of **122**.....105

Scheme 47. Plausible debromination mechanism.....105

Scheme 48. Attempts of Nucleophilic additions on **109** and **113**.....106

Scheme 49. Preparation of tertrasubstituted olefin **123**.....107

Scheme 50. Synthesis of unsymmetrically substituted olefin **128**.....108

Scheme 51. Nucleophilic attack of cysteine thiol on a highly reactive *N*-acyl iminium moiety.....119

Scheme 52. Proposed imine formation mechanisms.....120

Scheme 53. Schematic representation of the reaction involving radical SAM...121

Scheme 54. Proposed diradical mechanism.....121

Scheme 55. Biosynthetic mechanisms mediated by ATP-grasp enzymes.....127

Scheme 56. A possible mechanism of N-C cyclization.....129

Scheme 57. Mechanism of aspartimide and related by-product formation.....132

Scheme 58. Synthesis of the heptapeptide.....133

Scheme 59. A plausible mechanism for the tryptophan reduction.....136

Scheme 60. Synthesis of the subtilosin A mature linear peptide.....137

Scheme 61. Extension of the mature peptide to the precursor peptide.....139

Scheme 62. Synthesis of a precursor for the cyclic peptide.....142

Scheme 63. Synthesis of the cyclic peptide by an on-resin head-to-tail cyclization strategy.....143

APPENDIX B

Scheme 1. Biosynthetic pathway for UDP-GlcNAc.....247

Scheme 2. Mechanism showing the formation of UDP-GlcNAc.....249

Scheme 3. Synthesis of piperidine derivative.....251

EQUATION

Equation 1. Equation depicting mechanism based inhibition.....15

LIST OF ABBREVIATIONS

[α]	specific rotation
Abz	aminobenzoyl
Ac	acetyl
AcOH	acetic acid
Aq	aqueous
atm	atmosphere
Ar	aryl
Bis-Tris	2-(bis(2-hydroxyethyl)imino)-2-(hydroxymethyl)-1,3-propanediol
Bn	benzyl
Boc	*tert*-butoxycarbonyl
br	broad
tert-Bu	*tertiary*-butyl
c	concentration
calcd	calculated
Cbz	benzyloxycarbonyl
CDI	1,1'-carbonyldiimidazole
$3CL^{pro}$	3C-like protease
CMK	chloromethyl ketone
CoV	coronavirus

CPE	cytopathogenic effect
Cys	cysteine
δ	chemical shift in parts per million downfield from tetramethylsilane
d	doublet
Da	Dalton
DBU	1,8-Diazabicyclo[5.4.0]undec-7-ene
DCC	1,3-dicyclohexylcarbodiimide
DCM	dichloromethane
DEAD	diethyl azodicarboxylate
DIC	diisopropyl carbodimide
DIPEA	diisopropylethyl amine
DMB	dimethoxybenzyl
DMF	dimethylformamide
DMP	Dess-Martin periodinane
DMSO	dimethylsulfoxide
DTT	dithiothreitol
EC_{50}	concentration causing 50% of a maximum effect
EDCI	1-(3-dimethylaminopropyl)-3-ethylcarbodiimide
EDTA	ethylenediaminetetraacetic acid
EI	electron impact ionization
Enz	enzyme
ES	electrospray ionization
Et	ethyl

Et_2O	diethyl ether
EtOAc	ethyl acetate
EtOCOCl	ethyl chloroformate
EtOH	ethanol
Eq	equivalents
FMK	fluoromethyl ketone
Fmoc	fluoren-9-ylmethyloxycarbonyl
FRET	fluorescence resonance energy transfer
Gln	glutamine
Glu	glutamic acid
Gly	glycine
GST	glutathione-*S*-transferase
h	hour
HAV	hepatitis A virus
HBTU	*O*-benzotriazol-1-tetramethyluroniumhexafluorophosphate
His	histidine
HIV	human immunodeficiency virus
HOBt	*N*-hydroxybenzotriazole
HPLC	high performance liquid chromatography
HRMS	high-resolution mass spectrometry
HRV	human rhinovirus
HTS	high throughput screening

IC_{50}	concentration causing 50% inhibition
Ile	isoleucine
IR	infrared
IUPAC	International Union of Pure and Applied Chemistry
J	coupling constant
KDa	kilo Dalton
k_i	inhibition rate constant
K_i	dissociation constant of enzyme-inhibitor complex
k_{inact}	rate of enzyme inactivation
LDA	lithium diisopropylamine
Leu	leucine
LiHMDS	lithium bis(trimethylsilyl) amide
m	multiplet
MALDI-TOF MS	matrix-assisted laser desorption/ionization time-of-flight mass spectrometry
Me	methyl
MeCN	acetonitrile
MeOH	methanol
MHz	megahertz
min	minute
M^{pro}	main protease
MS	mass spectrometry
m/z	mass to charge ratio

mM	millimolar
N^{τ}	the distal nitrogen atom of imidazole ring of histidine relative to the side chain – IUPAC Compendium of Chemical Terminolgy
NMM	*N*-methylmorpholine
NMP	*N*-methyl-2-pyrrolidone
NMR	nuclear magnetic resonance
PMB	*para*-methoxybenzyl
Ph	phenyl
Phe	phenylalanine
PPh_3	triphenylphosphine
ppm	parts per million
psi	pounds per square inch
Py or Pyr	pyridine
PyBOP	benzotriazole-1-yl-oxy-trispyrrolidinophosphonium hexafluorophosphate
Q	glutamine
q	quartet
quant	quantitative
rt	room temperature
s	singlet
SAR	structure activity relationship
SARS	severe acute respiratory syndrome
Ser	serine
sub	subtilosin

t	triplet
TGEV	porcine transmissible gastroenteritis virus
TFA	trifluoroacetic acid
TFAA	trifluoroacetic anhydride
TFE	trifluoroethanol
THF	tetrahydrofuran
TLC	thin layer chromatography
Thr	threonine
TIPS	triisopropylsilane
TMS	tetramethylsilane
TMSCl	trimethylsilyl chloride
μM	micromolar
Val	valine

CHAPTER 1: SYNTHESES AND EVALUATION OF SEVERE ACUTE RESPIRATORY SYNDROME (SARS) 3CL^{PRO} INHIBITORS

1.1 INTRODUCTION

1.1.1 Severe acute respiratory syndrome (SARS)

In November 2002, a new human respiratory disease, known as severe acute respiratory syndrome (SARS) emerged in Guangdong province of Southern China and rapidly spread to several other countries (>25) during late 2002 and early 2003.[1,2] According to the World Health Organization (WHO), 8098 people became sick worldwide with SARS and 774 of the infected patients died. The rapid transmission and the high overall mortality rate (~10%) in 2002-2003 make SARS a potential global threat. A new coronavirus that was never before seen in humans was found to be the causative agent of SARS.[1,2,3] Studies suggest that the virus emerged from non-human sources (Palm Civets and Raccoon Dogs).[4,5]

1.1.2 Coronaviruses

Coronaviruses are positive-sense (RNA that acts as mRNA for direct synthesis of viral protein) single-stranded enveloped RNA viruses.[6,7,8] They are named after their crown-like appearance when observed under electron microscopy. Coronaviruses are normally associated with respiratory, gastrointestinal and neurological disorders. They typically cause upper-respiratory-tract infections in

humans and are responsible for a large proportion of common colds.[9] Interest in coronaviruses has grown following the outbreaks of SARS, as coronaviruses with similar genome sequences were isolated in China where the first SARS cases appeared. Since coronaviruses and picornaviruses share some similarities in their substrate specificities, a brief account of picornaviruses is presented.

1.1.3 Picornaviruses

Picornaviruses are small positive strand RNA viruses that cause a wide variety of infections in humans and animals. All picornaviruses have a protease that processes an initially synthesized viral polyprotein to mature proteins that are ultimately required for the generation of new viral particles. This protease contains a cysteine nucleophile that is involved in the breakdown of peptide bonds of proteins. The protease is called a 3C protease, because its active site topology resembles that of chymotrypsin-like serine proteases.

1.1.4 SARS coronavirus (SARS-CoV)

A diagrammatic representation of the structure of a SARS coronavirus (SARS-CoV) is shown in Figure 1. Coronaviruses are enveloped viruses. The envelope consists of a lipid bilayer membrane containing transmembrane glycoproteins, spike proteins and envelope proteins. This envelope surrounds the nucleocapsid, a complex of the viral RNA genome with viral capsid proteins.

Figure 1. Schematic representation of the SARS coronavirus (adapted with permission from Stadler *et al*.[9])

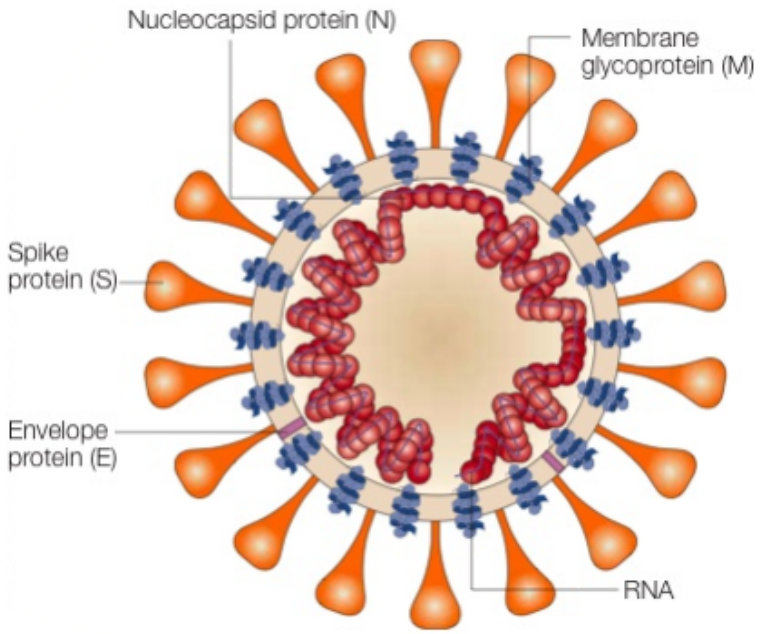

1.1.5 Coronavirus life cycle

The coronavirus begins its life cycle (Figure 2) by binding its spike protein, a structural protein, to a host cell surface receptor. After binding, the virus enters the host cell by membrane fusion. The viral RNA genome is then released into the cytoplasm where it undergoes a replication cycle involving transcription, translation and extensive proteolytic processing leading to viral maturation. Finally the virus is released from the host cell to start the cycle again.

Figure 2. Life cycle of coronaviruses (adapted with permission from Stadler *et al*.[9])

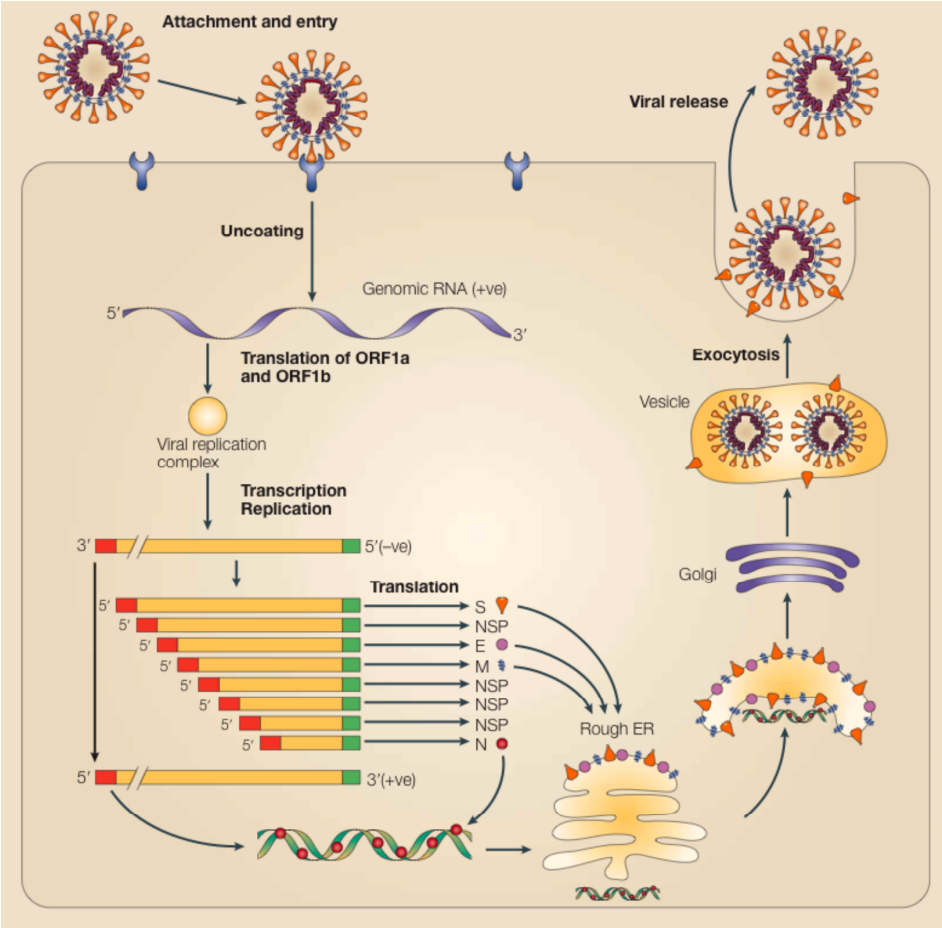

1.1.6 Symptoms and treatment of SARS

The signs and symptoms of SARS resemble those of influenza and include high fever, malaise, rigor, headache, cough and shortness of breath and may gradually progress to generalized interstitial infiltrates (collection of fluid in the interstices

of a tissue) in the lung.[10] In severe cases, patients may require oxygen support and mechanical help to breathe.

There is currently no efficacious treatment for SARS available. However a combination of the antiviral drug Ribavarin and corticosteroids are frequently administered for treating SARS.[11] According to Health Canada,[12] patients infected with SARS will receive the same treatment given to any patient with serious pneumonia including oxygen support, as needed. Glycyrrhizin, an active ingredient of liquorice roots having some anti-HIV activity, has shown some promise against SARS.[9] Likewise β-interferon,[13] which interferes with SARS replication, has been investigated as a possible drug. However, there is currently no clinical evidence to support the efficacy of any of these treatments.

1.1.7 Structure and function of SARS 3C-like protease ($3CL^{pro}$)

The SARS coronavirus replicase gene encodes for two overlapping polyproteins (Figure 3)[14] called pp1a (486 kDa) and pp1b (790 kDa). These polyproteins are cleaved into smaller functional (endowed with enzymatic activity) polypeptides of the replicase. These functional subunits will form into a replication complex to ultimately carry out viral replication and transcription.[14,15] The key enzyme that performs the polyprotein cleavage is a 33.8-kDa cysteine protease called 3C-like protease ($3CL^{pro}$) to indicate its substrate specificity similar to picornaviral 3C proteases.

Figure 3. The SARS-CoV 3CL^{pro} polyproteins and the positions of cleavage sites predicted to be processed by PL2^{pro} (blue) and 3CL^{pro} (red) (from Theil *et al*.[14])

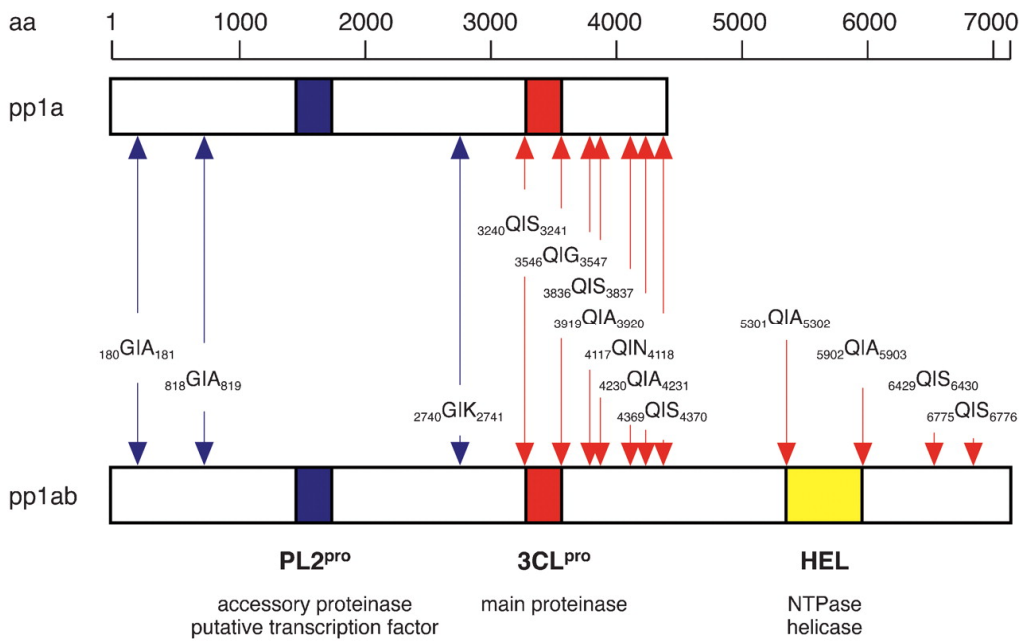

The other protease is a papain-like cysetine accessory protease (PL2^{pro}) that cleaves the pp1a and pp1b polyproteins (Figure 3) at three N-proximal sites (blue arrows).[14] The 3CL^{pro}, part of the 790 kDa polyprotein (pp1b), in addition to catalyzing its own release from the polyprotein, directs the processing of all downstream domains through at-least 11 conserved sites (red arrows). The 3CL^{pro} is sometimes called the main protease (M^{pro}) to indicate its dominant role in the viral polyprotein cleavage. The standard nomenclature devised by Schechter and Berger is adopted for describing inhibitor residues (*e.g*. P3, P2, P1, P1', P2', P3')

that are bound to the corresponding enzyme subsites (*e.g*. S3, S2, S1, S1', S2', S3') is shown in Figure 4. Clevage occurs between P1 and P1' residues.

Figure 4. The standard nomenclature used for substrate residues and their corresponding binding sites.[16]

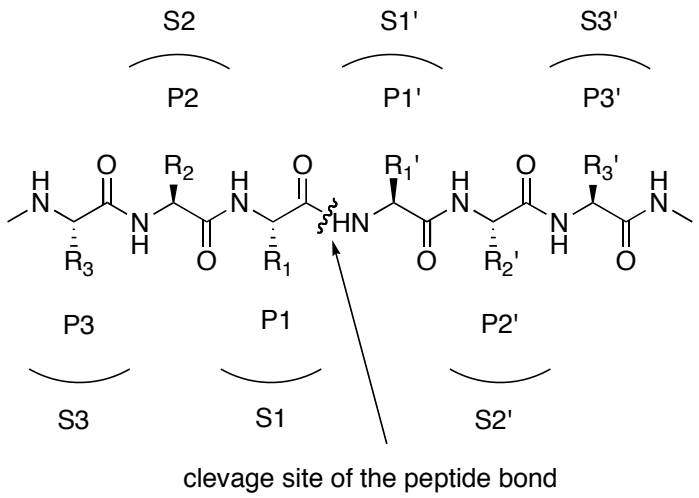

The polyproteins encoded by SARS-CoV replicase are conserved among other known coronaviruses including human CoV (HcoV). Comparison of substrate specificities of five coronavirus main proteases indicated heavy sequence conservation at the P2, P1, P1' and P2' positions.[17] The P2 and P1 positions have an absolute preference for Leu and Gln respectively while the P2' position prefers either an Asn or Gly. The P1' position is preferentially occupied by small aliphatic residues such as an Ala or Ser. In SARS-CoV $3CL^{pro}$, the P1 position has a similar preference for a Gln residue while P1' prefers Ala/Ser.[14]

1.1.8 Crystal structure of SARS-CoV 3CL^{pro}

The crystal structures of HCoV (strain 229) M^{pro} and SARS-CoV 3CL^{pro} have already been solved and published.[18-20] SARS-CoV 3CL^{pro} forms an enzymatically active dimer [21] and each monomer is composed of three domains (Figure 5).

Figure 5. The SARS-CoV 3CL^{pro} monomer structure (from Tan *et al*.[20])

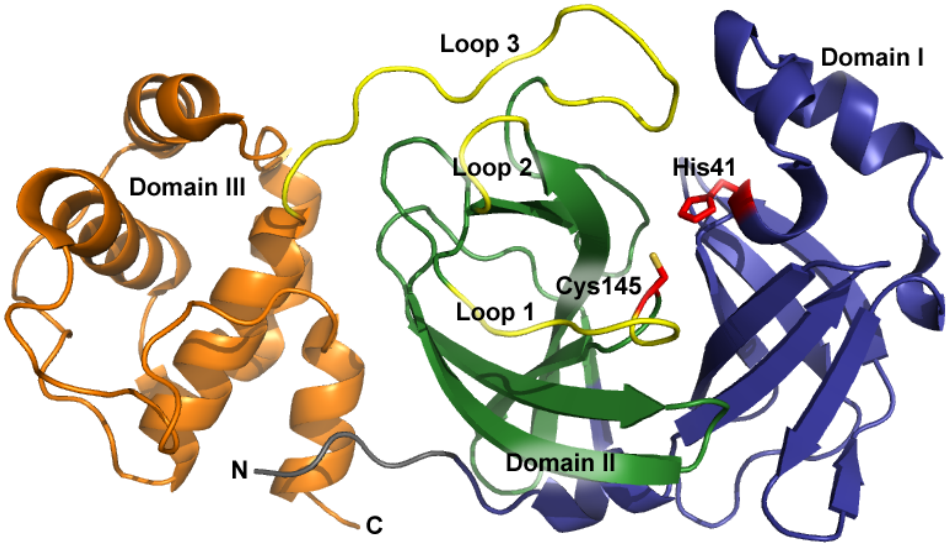

Domains I (blue) and II (green) have an anti-parallel β-barrel structure, similar to the serine protease of the chymotrypsin family, but different from the picornaviral 3C proteases. Domain III (orange) contains antiparallel α-helices arranged into a globular cluster and is connected to domain II via a 16 amino acid long loop region.[19] The active site constituting the catalytic diad and the substrate binding sites are located in a cleft formed by domains I and II. In contrast to common serine proteases, the SARS 3CL^{pro} has a Cys-His catalytic diad (Cys-145 and His-

41) in which the cysteine thiol functions as a nucleophile while the histidine functions as a general acid-base catalyst. It has been shown that domain III stabilizes the dimer thus maintaining the activity of the SARS $3CL^{pro}$.[22]

1.1.9 Design of inhibitors against SARS 3C-like protease ($3CL^{pro}$)

A SARS-CoV global pandemic was prevented from spreading by the implementation of strict quarantine measures. Transmission of SARS from infected animals[23,24] (the natural reservoir) to humans may pose the greatest risk in the future. Additionally, the accidental infection risk of researchers[25] handling the pathogenic virus could precipitate another outbreak.[9] Currently there are no approved drugs available to cure SARS, therefore new antiviral drugs for the treatment and eradication of SARS are needed. Some of the common approaches of drug development against viruses include the prevention of viral entry into the host and interference with the intracellular life cycles.[26,27] These intracellular activities are mediated by the viral proteases that process initially expressed high-molecular-weight polyprotein precursors into mature functional proteins. These then assemble into replication complexes to generate the viral genome. Therefore viral proteases represent one of the attractive targets for antiviral drug design. The design of inhibitors of the SARS-CoV $3CL^{pro}$ that controls the activities of the coronavirus replication complex has been the focus of several research groups and drug companies.

A major decision in drug development is whether to design a reversible or an irreversible inhibitor.[28] Reversible inhibitors form noncovalent interactions with

the enzyme. The inhibitor is free to associate and dissociate and an equilibrium is established between the bound and unbound form of the inhibitor. Irreversible inhibitors form a stable covalent bond with the enzyme. Once bound to the enzyme, the inhibitor can not be released.[29] Although, irreversible inhibitors may be of some use in acute disease treatment and as tools in investigating protease catalytic mechanisms, they always bear the risk of non-specific interactions with host cells, which can enhance their toxicity. In general reversible non-covalent inhibitors provide better selectivity and cause fewer side effects than covalently binding ones and are thus more suitable for therapeutic development.

Several covalent and non-covalent small molecule inhibitors of SARS $3CL^{pro}$ have been reported in the literature. Some of them are chloromethyl ketone (CMK) and ruprintrivir analogues,[19,30] bifunctional phenyl boronic acids, thiophenecarboxylates,[31] heteroaromatic esters,[32] benzotriazole esters,[33] phthalhydrazide substituted keto-glutamine analogues,[34] heteroaromatic esters[32] and isatin derivatives.[35]

1.1.10 Covalent inhibitors

These cysteine protease inhibitors usually contain an electrophilic functional group (warhead) that binds covalently to the active site cysteine of the target enzyme.

1.1.10.1 Chloromethyl ketone (CMK)

The chloromethyl ketone **1** (Figure 6) was the first reported inhibitor of SARS 3CL^{pro}. A covalent bond is formed between the enzyme and the α-methylene carbon.[19]

Figure 6. Structure of CMK (**1**) and mechanism of covalent attachment

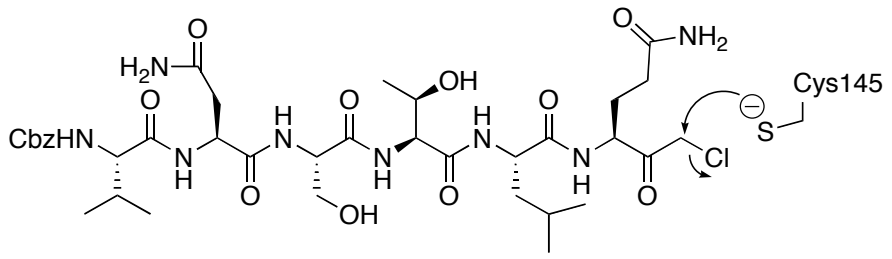

1

Comparison of the crystal structure of the human coronavirus M^{pro} to the CMK inhibitor complexed with a porcine transmissible gastroenteritis (corona) virus (TGEV) M^{pro} indicated similar substrate specificities among coronavirus main proteases.[18] This suggests that inhibitors of coronaviruses could be potentially tested against SARS-CoV 3CL^{pro}. This was supported by the SARS-CoV 3CL^{pro} mediated cleavage of CMK (**1**) and a crystal structure of the SARS-CoV 3CL^{pro} in complex with the CMK inhibitor (Figure 7).[19]

Figure 7. Dimer structure of SARS-CoV M^{pro} complexed with CMK (**1**). Arrows show inhibitors (CMK) at the active site (from Yang *et al*.[19])

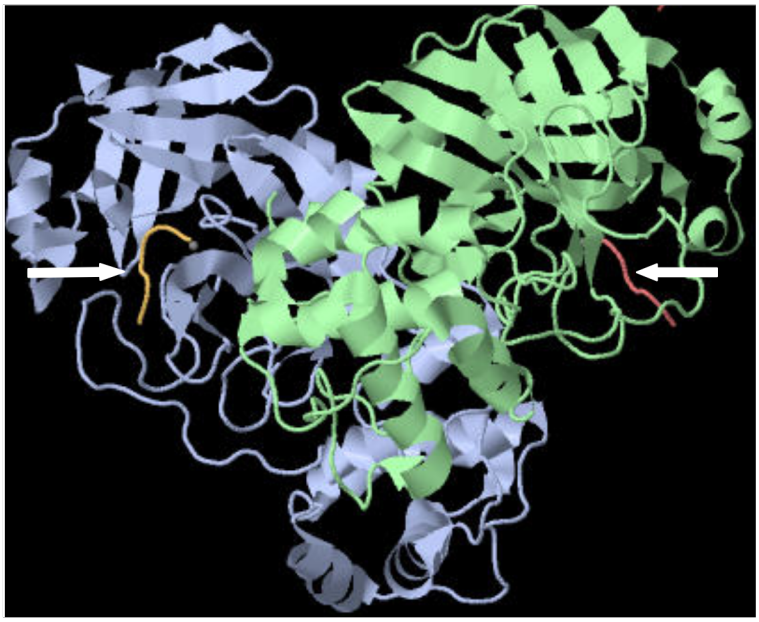

Although CMK (**1**) can react with a variety of nucleophiles making it unsuitable for drug development, it can be utilized as an excellent model substrate for the anti-SARS drug design.

1.1.10.2 Ruprintrivir (2) and analogues as Michael acceptors

Several of the inhibitors designed for cysteine proteases are substrate derived. However, the peptide bonds in these substrates are susceptible to proteolytic cleavages leading to poor pharmacologic profiles. One way to tackle this problem

is to use electrophilic warheads with diminished peptide character. Some of these warheads include aldehydes, ketones, epoxides and α,β unsaturated esters.[36] Introducing an α,β unsaturated ester as the Michael acceptor mimicking the peptide cleavage site at the P1 position of the SARS-CoV 3CL^{pro} active site gave rise to several cysteine protease inhibitors.[30] Ruprintrivir (**2**) is a human rhinovirus (HRV) inhibitor that is currently in clinical trials for the treatment of common cold (Figure 8).[30]

Figure 8. Structure of Ruprintrivir (**2**)

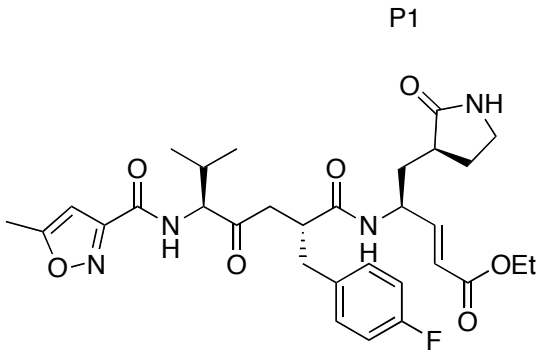

2

Ruprintrivir structure contains an α,β unsaturated ester that can undergo a Michael addition with the cysteine thiol of the target protease to form a covalent bond thereby inactivating the protease (Figure 9).

Figure 9. Mechanism of inactivation of the enzyme via formation of a thioether bond

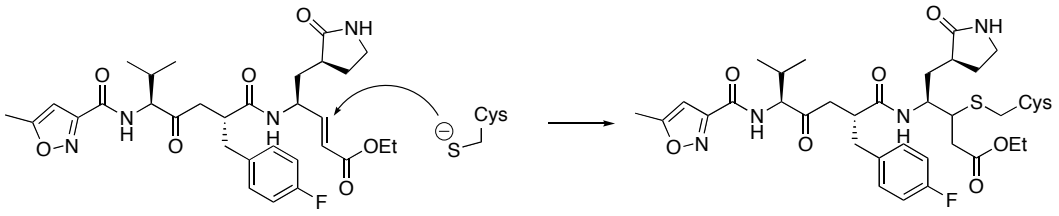

2

Comparison of the stereo images of the TGEV M^{pro} complexed with CMK and rhinovirus $3C^{pro}$ (a picornavirus) in complex with **2** suggested some similar binding interactions. Interestingly, both corona[37] and picornaviruses[38,39] share high similarities in their substrate specifcities at the P4, P1 and P1' sites.[18] Based on these observations, **2** was modified to provide two analogs **3** and **4**, which were found to be active aginst SARS $3CL^{pro}$(Figure 10).[30] A crystal structure in which **4** was covalently linked to SARS $3CL^{pro}$ was reported and showed hydrogen bonding interactions to His-164 and Glu-166 at the active site of SARS $3CL^{pro}$ providing clues to the molecular recognition for such inhibitors.

Figure 10. Structures of **3** and **4**

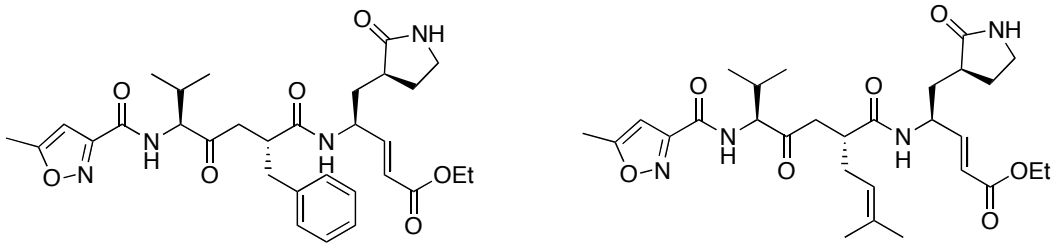

3 **4**

1.1.10.3 Benzotriazole esters

Some of the inhibitors developed against SARS 3CL^{pro} are mechanism-based inhibitors. In mechanism-based inhibition, the inhibitor forms a reversible complex with the enzyme and then reacts irreversibly with the enzyme leading to the formation of a covalent bond (Equation 1).

Equation 1. Equation depicting mechanism based inhibition

$$E + I \underset{k_2}{\overset{k_1}{\rightleftharpoons}} EI \xrightarrow{k_i} E\text{-}I \qquad K_i = k_2/k_1$$

K_i, represented as k_2/k_1 is the dissociation constant for the initial reversible inhibitor enzyme complex EI. It measures the affinity or strength of binding between the enzyme and inhibitor; k_i is the first-order rate constant for the second irreversible reaction. Wu and coworkers[33] designed several stable benzotriazole esters as potent mechanism-based irreversible SARS 3CL^{pro} inhibitors with a k_{inact} of 0.0011 s^{-1} and a K_i of 7.5 nM. A covalent bond (acylation) formation was suggested between the active site at Cys145 and the inhibitor **5** (Figure 11).

Figure 11. Proposed acylation mechanism with benzotriazole ester **5**

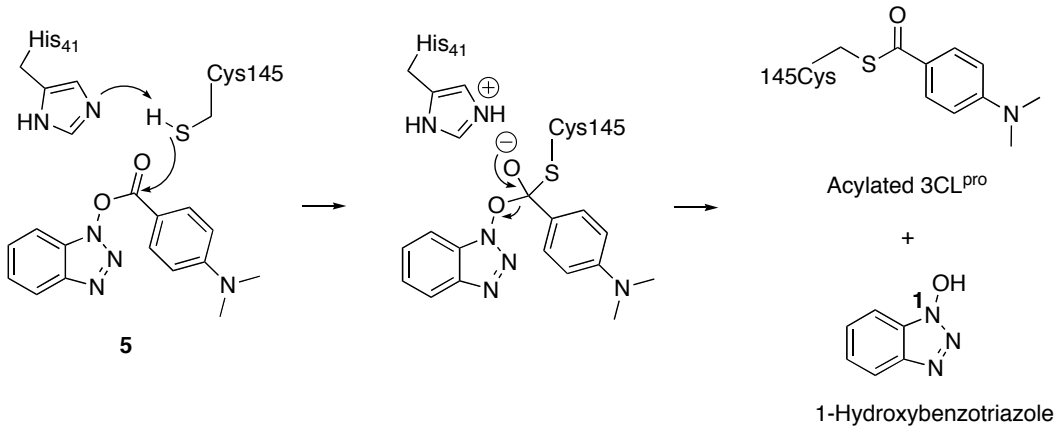

1.1.10.4 Thiophenecarboxylate and biological evaluation using fluorescence resonance energy transfer (FRET)

One of the in vitro techniques that has gained widespread popularity in the screening of large libraries of small molecules against SARS 3CL^{pro} is the quenched fluorescence resonance energy transfer (FRET) assay. As an integral part of developing innovative inhibitors against newly emerging diseases, Brown and coworkers[31] developed a quenched fluorescence resonance energy transfer (FRET) assay for 3CL^{pro}. The assay is primarily based on the principle that enzymatic cleavage of a fluorescent peptide substrate results in increased fluorescent emission.[31] The fluorescent substrate contains a N-terminal amino benzoyl donor and a C-terminal nitrotyrosine acceptor for FRET. When the enzyme SARS 3CL^{pro} binds to an inhibitor, the fluorescent substrate remains

intact and all the excited energy is transferred from the donor to the acceptor. Little if any fluorescence of the donor is detected. However, when the enzyme cleaves the substrate, energy is not transferred efficiently as the donor and acceptor moieties are far apart and increased fluorescence of the donor is detected (Figure 12).

Figure 12. A quenched-FRET assay for evaluating SARS-CoV 3CL^{pro} activity

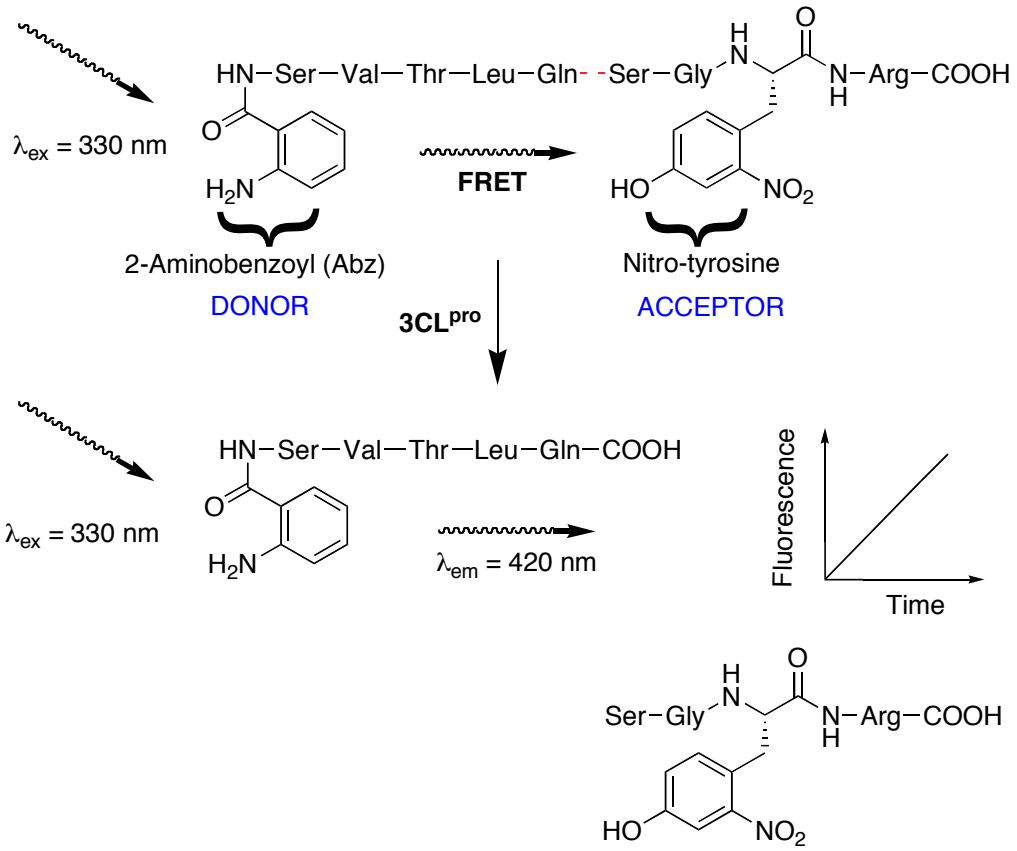

Using the FRET assay, Brown and coworkers[31] screened about 50,000 small molecules; of these, five potent lead compounds were identified with IC_{50} values in the low micro molar range (0.5-7 μM). This means that when the inhibitor was added, that enzyme was less able to cleave the fluorescent peptide and so less fluorescence was detected. The thiophene containing aromatic ester **6** (Figure 13) was the most potent inhibitor with an IC_{50} of 0.5 μM. The aromatic ester **6** contains an electrophilic site with which the nucleophilic thiolate of cysteine could form a covalent adduct. Such reaction is the basis for several peptide based inhibitors of cysteine proteases such as α-β unsaturated ketones, esters, amides and nitriles.

Figure 13. Structure of pyridinyl ester **6** shows that it can undergo nucleophilic attack by cysteine thiol of the enzyme

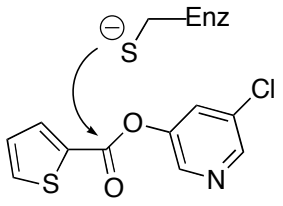

6

Although these compounds may react nonspecifically with bioactive thiol functionalities rendering them unsuitable as drug candidates, they could be useful for giving insight into the catalytic mechanism of SARS-CoV $3CL^{pro}$.

1.1.10.5 Heteroaromatic esters

The high potency and relatively simple structure of **6** was quite encouraging. To further investigate the structure activity relationships of compounds related to **6**, Dr. Jianmin Zhang, a former graduate student from our laboratory synthesized amides and a focused library of esters by coupling several commercially available carboxylic acids to 5-chloro/bromo-3-pyridinol and tested them against SARS $3CL^{pro}$ using the fluorometric assay described above.[32] Many of them showed good inhibition and some esters (*e.g.* **7**, **8)** (Figure 14) were extremely potent inhibitors of SARS $3CL^{pro}$ with IC_{50} values in the low nanomolar range. Structure activity relationship studies revealed some interesting results. In comparison, amides **10** and **11** were inactive even at 100 μM concentration. Strong inhibition was observed with compounds in which the pyridine ring carried an ester functionality at the meta position (*e.g.* **7**, **8)**. Poor (*e.g.* **12**) or almost no inhibition (*e.g.* **13)** was observed when the pyridine ring carried an ester functionality either at the ortho or para positions. Reversal of the ester linkage as in **14** resulted in poor inhibition. In addition to the ester, the pyridinyl ring shows preference for meta substituents such as halogens and compounds carrying a bromine (*e.g.* **8)** gave the most potent inhibition. Weaker inhibition was observed with analog **15** where an extra carbon was inserted between the pyridine ring and the oxygen atom.

Figure 14. Structures of pyridinyl ester analogs[32]

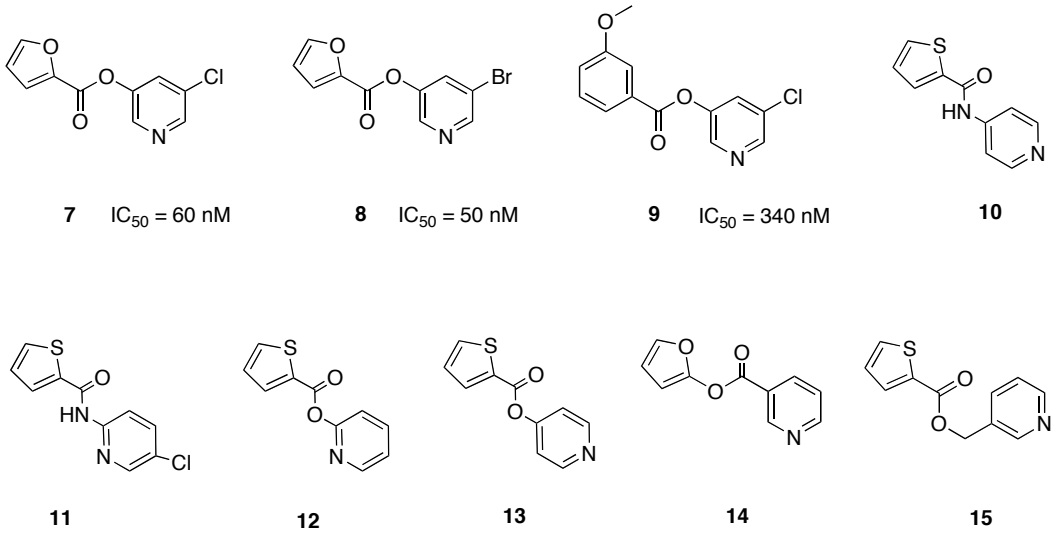

Molecular modeling studies by James and co-workers[40] proposed an S1-S2 binding mode for this class of compounds, suggesting they primarily occupy the volume extending from the S2 to S1 binding sites (Figure 15).

Figure 15. Docking studies (by Dr. Chunying Niu) of inhibitors **8** and **9** in the SARS-CoV 3CL^{pro} active site (from Zhan *et al*.[32]) in which inhibitors **8** (yellow) and **9** (white) are shown as sticks (chlorine is green; bromine is orange; oxygen atoms are red; nitrogen atoms are blue)

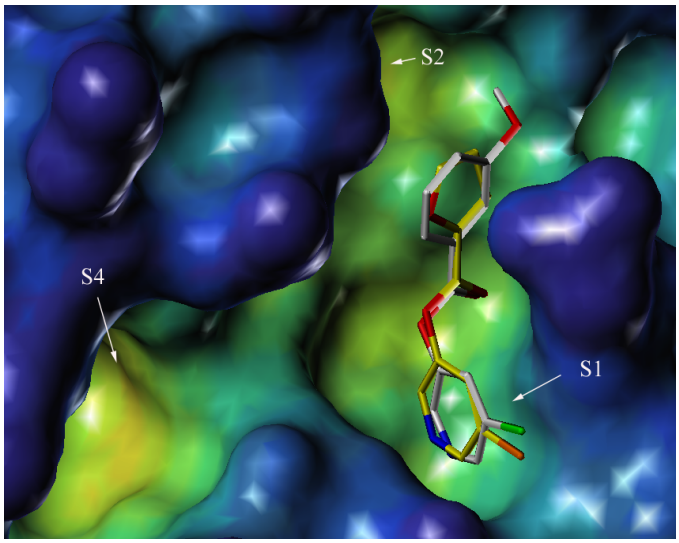

The halopyridinyl moiety fits into the S1 pocket in an orientation parallel to the S1 walls and van der Waals forces play key roles in the initial *in vitro* binding interactions. The nitrogen atom in the pyridine ring forms a hydrogen bond with the NH of the imidazole ring (N^{τ}, the symbol recommended by IUPAC to denote the distal nitrogen atom of imidazole ring relative to the side chain) of His163, which is the P1 specificity-determining residue. The carbonyl oxygen points to the 3CL^{pro} oxyanion hole to receive a hydrogen bond from the main chain NH of Gly143. Inhibition mechanism studies suggest covalent adduct formation with the nucleophilic sulfur of cys145.[32]

1.1.10.6 Fluoromethylene ketones (FMK)

The advantages of fluoroketones as protease inhibitors were first reported in 1986.[41] The introduction of a fluorine atom into the backbone of protease substrates can result in effective and selective peptidyl fluoroketones.[42] Although fluoride is often inert to nucleophilic displacement, a rate enhancement for this process can be anticipated within the enzyme-inhibitor complex thereby minimizing the side reactions elsewhere.[43] Flouomethylene ketones (FMK) inactivate the enzymes via formation of thioether linkages (Figure 16).

Figure 16. Mechanism of enzyme inactivation by fluoromethyl ketones

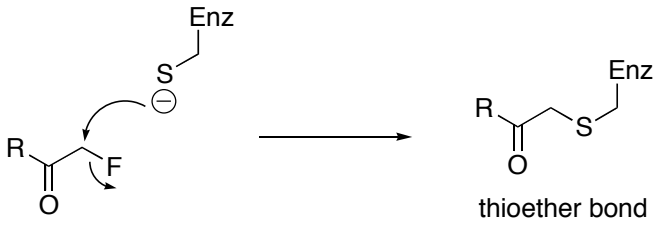

Due to the differences in the reactivities of serine and cysteine proteases, peptidyl fluoromethyl ketones were found to be selective and effective inhibitors of cysteine proteases but only marginally active inhibitors of their mammalian serine counterparts.[44] Caspases are a class of cysteine proteases that play an important role in apoptosis (programmed cell death).[45] Based on caspase inhibitors, a series of dipeptidyl glutaminyl fluoromethyl ketones were reported as potential inhibitors of SARS-CoV M^{pro}.[46] Compound **16** was found to be a potent inhibitor with low toxicity in cells with an EC_{50} of 2.5 μM and a selectivity index (SI = CC_{50}/EC_{50}) of greater than 40. Structure activity relationship studies (SAR)

indicated a Gln residue is necessary as the P1 amino acid although an *N,N*-dimethylglutamine is tolerated at P1. Leucine is accepted at P2, but can be replaced with isoleucine or valine. Another derivative **17** was found less toxic in mice during a safety profile study of fluoromethyl ketones. (Figure 17).[46]

Figure 17. Structures of dipeptidyl glutaminyl fluoromethyl ketones **16** and **17**

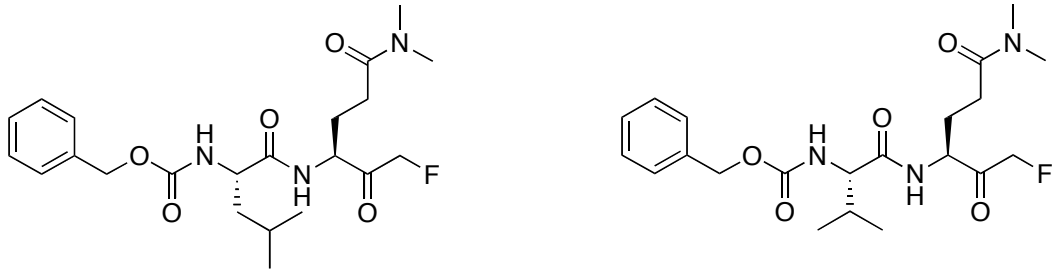

16 **17**

1.1.11 Non-covalent inhibitors

As the name suggests these inhibitors will undergo non-covalent interactions with the enzyme. These inhibitors bind reversibly either with the enzyme or enzyme-substrate complex thereby slowing or preventing the turnover of the enzyme.[47]

1.1.11.1 Bifunctional phenyl boronic acids

Barrila *et al* identified a cluster of serine residues[48] near the active site of SARS-CoV 3CL^{pro} (Figure 18). Since boronic acids are known to react with serine

hydroxyl groups, a series of bifunctional aryl boronic acids were evaluated as potential inhibitors of the SARS coronavirus $3CL^{pro}$.

Figure 18. Active site of SARS-CoV $3CL^{pro}$ showing serine residues 139, 144 and 147 and catalytic Cys145 and His41 (from Barrila *et al*.[48])

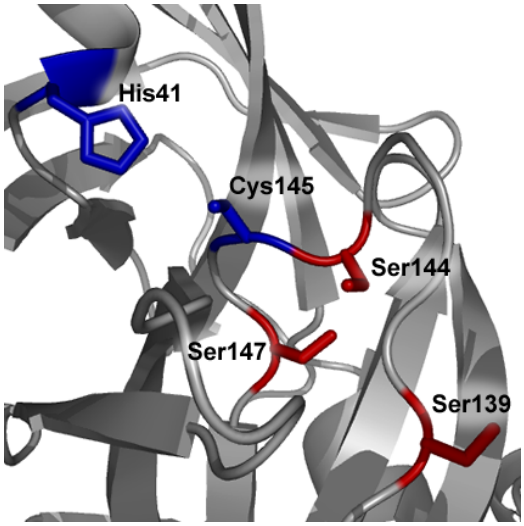

This serine cluster was found to be highly conserved in 20 other coronaviruses, suggesting an attractive target for the development of a broad spectrum of inhibitors for coronaviruses. A compound named FL-166 (**18**), a bifunctional phenyl boronic acid (Figure 19) was a very effective reversible inhibitor of SARS $3CL^{pro}$ protease with a K_i (inhibition constant) of 40 nM.[48]

Figure 19. Structure of bifunctional phenyl boronic acid **18**

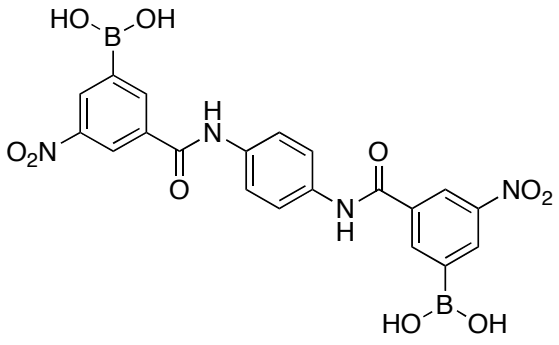

18

1.1.11.2 Phthalhydrazide substituted keto-glutamine analogues

The 3C proteases of picornaviruses (human rhinovirus (HRV), hepatitis A virus (HAV) and coronavirus (SARS) share some substrate specificities, and this is particularly true at the P4, P1 and P1' positions.[37] Crystal structure studies of picronavirus 3C proteases, such as HAV and HRV, established that a Gln residue at the P1 position is a key recognition element as its side chain amide oxygen is involved in the formation of hydrogen bonding with a His191 at the S1 subsite of the enzyme.[49,50] This suggests that inhibitors developed against picornavirus $3C^{pro}$ could potentially serve as templates for further refinements for anti SARS drug development. Our group has previously demonstrated that ketoglutamine tetrapeptides with a phthalahydrazide moiety at the α-position (*e.g.* **19**) are potent inhibitors of the HAV 3C protease with IC_{50} values in the low micromolar range (Figure 20).[51]

Figure 20. Structure of **19**

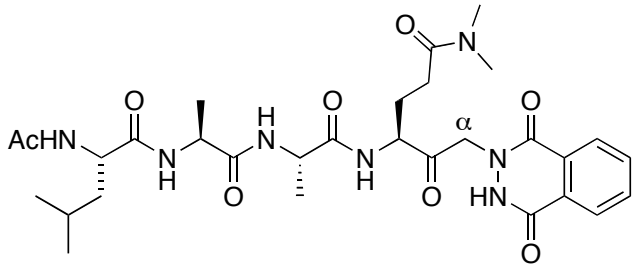

19, IC_{50} = 13 μM

Based on these observations and the observation that some coronaviruses prefer a bulky hydrophobic residue such as a Leu at the P2 position, phthalhydrazide derivatives incorporating a tripeptide (Ac-Val-Thr-Leu) were prepared and tested against SARS $3CL^{pro}$.[34] Compounds **20**-**23** containing the tripeptide displayed much improved inhibition with IC_{50} values ranging from 0.6 to 3.4 μM (Figure 21). Modeling studies indicated the residues were involved in key interactions at the active site.[34]

Figure 21. Ketoglutamine analogs as the potent inhibitors of SARS $3CL^{pro}$

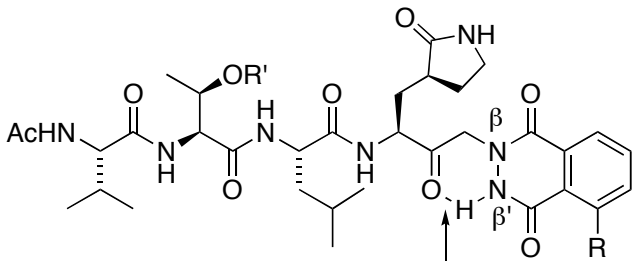

20 : R = H, R' = Bn

21 : R = H, R' = H

22 : R = NO_2, R' = Bn

23 : R = NO_2, R' = H

The inhibition mechanism studies of these compounds revealed interesting results. Initial kinetic experiments using the FRET based assay suggested that compound **20** was a competitive and reversible inhibitor with a K_i of 250 nM. No evidence of covalent bond formation was observed when one equivalent of enzyme was pre-incubated with 10 equivalents of inhibitor **20** for short period of time (15 min to 1 h). However the crystal structure of SARS 3CL^{pro} in complex with inhibitor **20** that was grown over a period of 2 to 3 days revealed the formation of a covalent thioether bond. Surprisingly, two forms of covalently modified enzyme were observed. The inhibitor **20** when soaked into the pre-grown SARS-CoV M^{pro} crystals forms an unusual episulfide cation ring intermediate **24** (Figure 22) with the sulfur atom of Cys145. However a thioacyl form **25** (Figure 22) was observed through co-crystallizing inhibitor **20** with SARS 3CL^{pro}.

Figure 22. Interactions between inhibitor **20** and SARS 3CL^{pro} showing episulfide and thioacyl forms

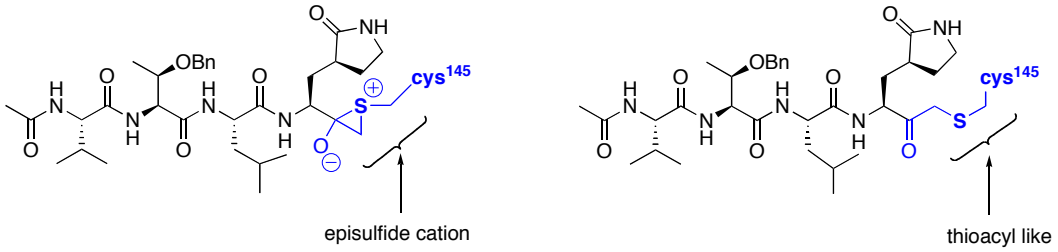

24 **25**

The inhibition mechanism was further investigated by subjecting the co-crystal of the SARS 3CL^{pro}-inhibitor complex to electrospray ionization-mass spectrometry

(ESI-MS). A peak with a mass of 34480 Da corresponding to the mass of SARS 3CL^{pro}-inhibitor complex (without phthalhydrazide) suggested a covalent bond between inhibitor **20** and the enzyme. In order to account for these discrepancies, the authors proposed an inhibition mechanism (Scheme 1).[52] In the first step, a tetrahedral intermediate **20a** is formed (arrow a) resulting from the attack of a nucleophilic sulfur atom of SARS 3CL^{pro} onto the ketone carbon of inhibitor **20**. The tetrahedral intermediate **20a** is thermodynamically unstable and could collapse either way giving back (arrow b) the inhibitor **20** and the catalytic cysteine in a short period of time, or going forward (arrow c) over a long period time via the unusual three-membered episulfide cationic intermediate **24** to form the stable covalent thioether adduct **25** (revealed from crystallography). The preformed crystal of the SARS 3CL^{pro} with no inhibitor is able to trap **24**.

Scheme 1. Proposed mechanisms accounting for reversible and irreversible inhibition

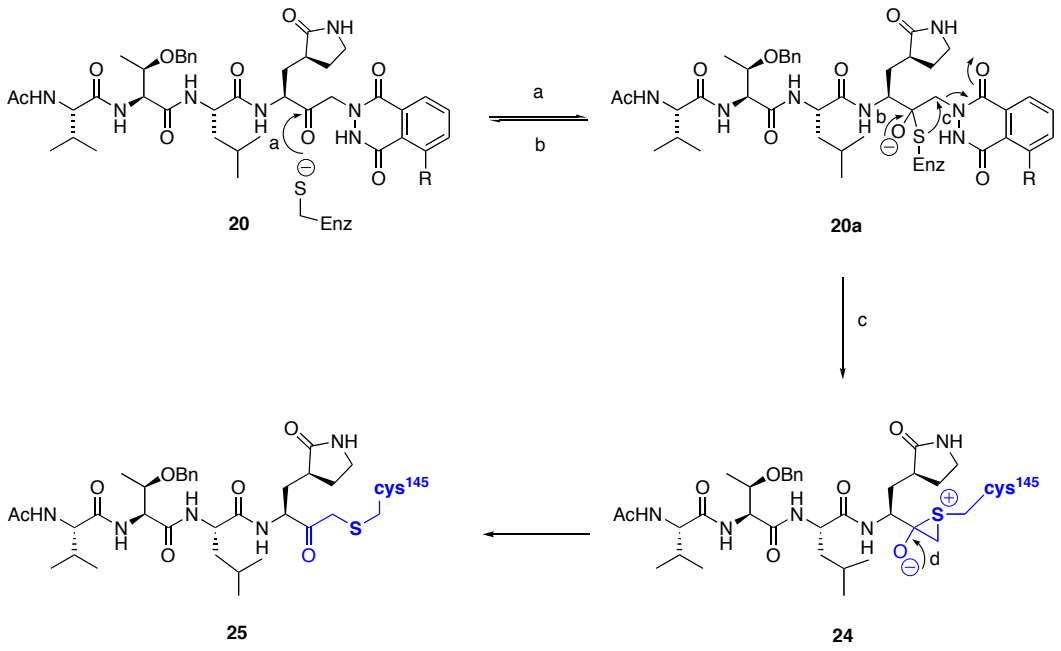

1.1.11.3 Isatin derivatives

The active site domain of SARS $3CL^{pro}$ is similar to other picornavirus 3C proteases such as HRV. Certain *N*-substituted isatin (2,3-dioxindole) derivatives effective against HRV $3C^{pro}$ were developed as potent and selective inhibitors of SARS $3CL^{pro}$.[53] As SARS-CoV $3CL^{pro}$ has a preference for Gln at the P1 site, introdution of an amide group on the isatin molecule may mimic the P1 Gln side chain that can form hydrogen bonds with Phe140 and His163 residues at the active site. Based on these observations Lai and coworkers synthesized a series of *N*-substituted 5-carboxamide-isatin derivatives and tested them against SARS $3CL^{pro}$.[35] Mass spectrometry and enzyme pre-incubation studies indicated non-covalent interactions. Compound **26** showed significant inhibition with an IC_{50} of 0.37 μM (Figure 23).

Figure 23. Structure of an isatin derivative **26**

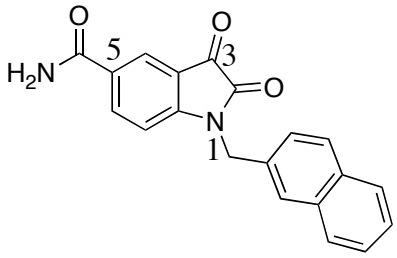

26

SAR studies demonstrated that the C-5 position preferred a carboxamide group while large hydrophobic residues such as naphthyl were preferred at the N-1

position. Modelling studies[35] suggested hydrogen bonding interactions between the carbonyl oxygens of **26** and SARS 3CL^{pro} active site residues (Figure 24). The C-3 carbonyl oxygen forms a hydrogen bond to Cys145 (Figure 24). The other carbonyl oxygen at the C-2 position forms a hydrogen bond with the His41. The side chain amide of **26** forms hydrogen bonds to His163 and Phe140 at the active site.

Figure 24. Docking studies of compound **26** showing hydrogen bonding interactions[35]

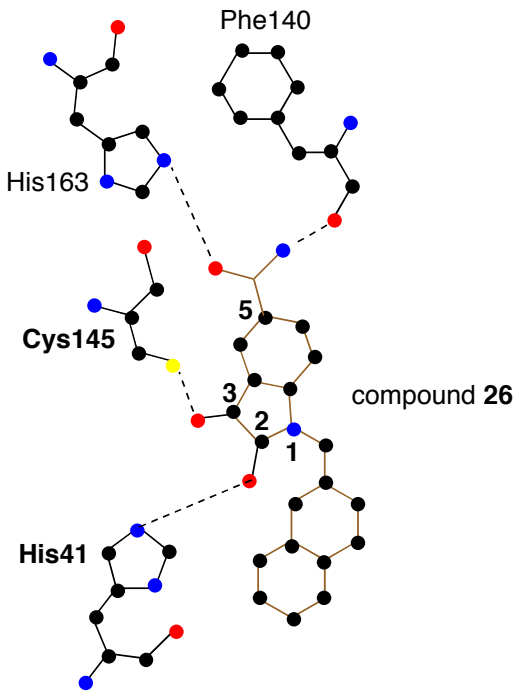

1.1.11.4 Aryl methylene ketones

It was previously demonstrated by Dr. Jianmin Zhang in our group that a series of 5-halopyridin-3-yl aromatic esters (*e.g.* **27**) based on a small molecule hetero aromatic ester **6**, are very potent covalent inhibitors of SARS 3CL^{pro} (Figure 25).[32]

Figure 25. Structure of 5-halopyridin-3-yl aromatic ester **27** that was designed based on **6**

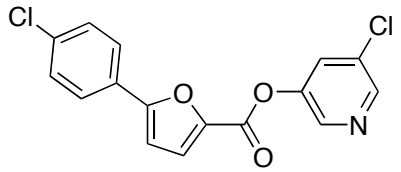

27, 98% inhibition at 1 mM, IC_{50} = 63 nM

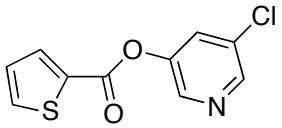

6

These esters could acylate the enzyme thiol and thereby inactivate the enzyme. Structure-activity relationship (SAR) and modeling studies suggest that both the three aromatic rings and 5-halopyridin-3-yl components are essential for good inhibition. Despite potent inhibition, these esters are not suitable as drug candidates due to their inherent susceptibility to hydrolysis and other non-specific reactions potentially enhancing their side effects. The search for non-covalent and reversible inhibitors continued in our group. It had been well known that compounds containing a carbonyl functionality (an aldehyde or a ketone) were

reactive towards nucleophiles, such as cysteine proteases, and could form hemithioacetals. Also, introducing a fluorine substituent alpha to a carbonyl carbon makes it more electrophilic, thereby enhancing its reactivity towards nucleophiles. Based on this assumption, some fluorinated and non-fluorinated ketone derivatives **28**, **29** and **30** (Figure 26) were synthesized and tested against SARS M^{pro} using the fluorometric assay.[54]

Figure 26. Structure of aryl methylene ketones **28**-**30**

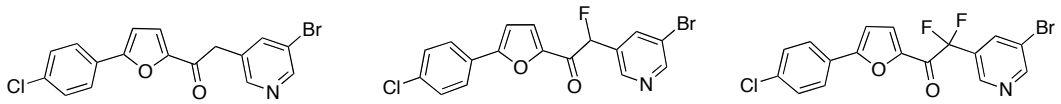

28 **29** **30**

Among them, compound **28** was the most potent inhibitor with an IC_{50} of 13 μM. Interestingly, mass spectrometry and enzymatic studies indicated non-covalent and reversible inhibition. To further explore the possible binding modes of ketone based inhibitors with this enzyme, modeling studies were performed by Dr. Chunying Niu[54] at the University of Alberta Biochemistry Department. An S4-S1 binding model was proposed for compounds with three aromatic rings (Figure 27).

Figure 27. Modelling conformations (by Dr. Chunying Niu) of **28** (white carbon sticks), **29** (cyan), and **30** (yellow) at the active site of SARS-CoV M^{pro} (from Zhang *et al*.[54]) (oxygen-red; nitrogen-blue; chlorine-green; bromine-maroon; and fluorine-purple).

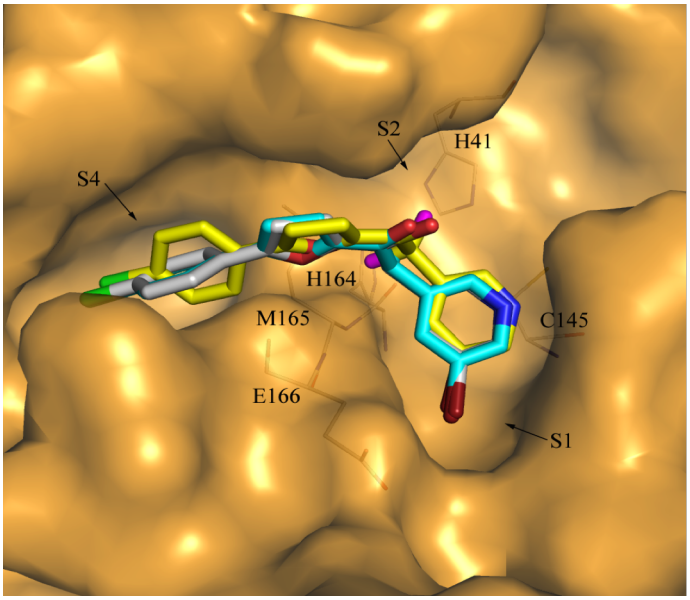

According to this model, the three-aromatic-ring compounds are oriented from the S4 to the S1 pocket in an extended conformation and the furan ring oxygen atom can form a hydrogen bond with the backbone NH of Glu166. By blocking the entry of substrates into the active site, the three aromatic-ring-compounds exhibit non-covalent and reversible inhibition against SARS $3CL^{pro}$. The pyridinyl portion fits into the S1 pocket limiting the orientation of substituents at the α-position of the keto group.

1.1.12 Objectives: Synthesis and evaluation of SARS 3CL^{pro} inhibitors

Our objective is to develop stable and potent non-covalent inhibitors against SARS 3CL^{pro}. The ketone analog **28**, because of its potency and non-covalent nature of inhibition represents an attractive lead compound for further modifications. The potential sites of modifications are shown in Figure 28. Further crystallographic studies could provide important clues in understanding the inhibition mechanism.

Figure 28. SARS 3CL^{pro} inhibitor **28** and potential sites of modification

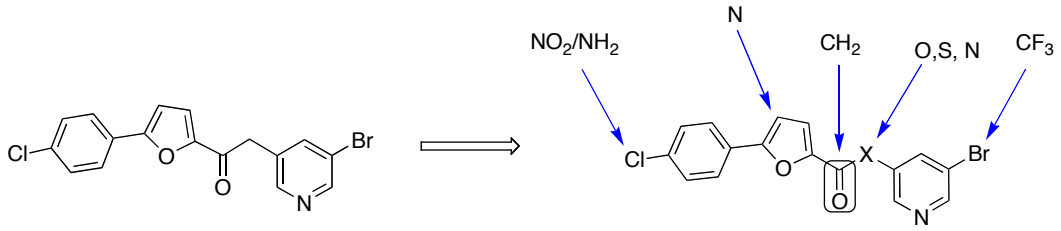

SARS 3CL^{pro} inhibitor,
IC_{50} = 13 μM
non-covalent and reversible inhibitor
(Dr. Jianmin Zhang)

To this end, a series of pyridinyl ethers (Target **A**), pyridinylamines and their derivatives (Target **B**), a hybrid compound (Target **C**), a rhodanine derivative (Target **D**) incorporating the previously established key structural features and

relatively stable oxazole derivatives (Target **E**) have been designed, synthesized and screened as possible reversible inhibitors of SARS 3CL^{pro} (Figure 29).

Figure 29. Representative examples of targets **A** to **E**

Target **A**

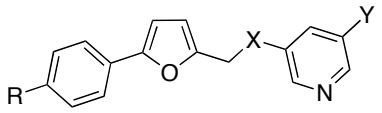

33: R = Cl, X = O, Y = Cl

34: R = Cl, X = O, Y = Br

36: R = Cl, X = O, Y = CF_3

38: R = Cl, X = S, Y = H

Target **B**

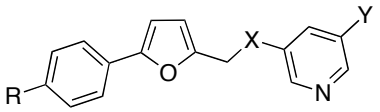

54: R = NO_2, X = NH, Y = Br

55: R = Cl, X = NH, Y = Br

61: R = NH2, X = NH, Y = Br

63: R = NO_2, X = N-Et, Y = Br

Target **C**

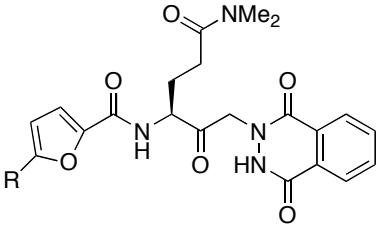

65: R = 4-Chlorophenyl

Target **D**

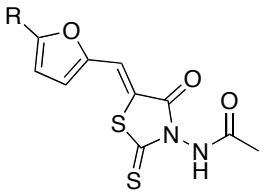

67: R = 4-Chlorophenyl

Target **E**

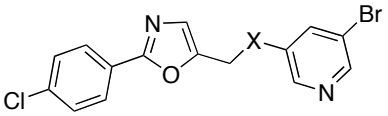

69: X = O

70: X = N

Enzyme kinetics and spectrometry studies will aid in evaluating their inhibition mechanism. Crystal structures of these inhibitors with SARS CL^{pro} will help develop a better understanding of the inhibition mechanism.

1.2 RESULTS AND DISCUSSION

1.2.1 Pyridinyl ethers

A Mitsunobu reaction is used for the key step in the synthesis of pyridinyl ethers and thioethers. Reduction of a commercially available furfural derivative **31** with lithium aluminium hydride (LAH) provides the corresponding alcohol **32** in quantitative yield. Mitsunobu reaction of **32** with either 3-chloro or 3-bromo-5-pyridinol as nucleophiles affords the desired ethers **33** and **34** in 60% yield (Scheme 2).

Scheme 2. Synthesis of pyridinyl ethers **33** and **34**

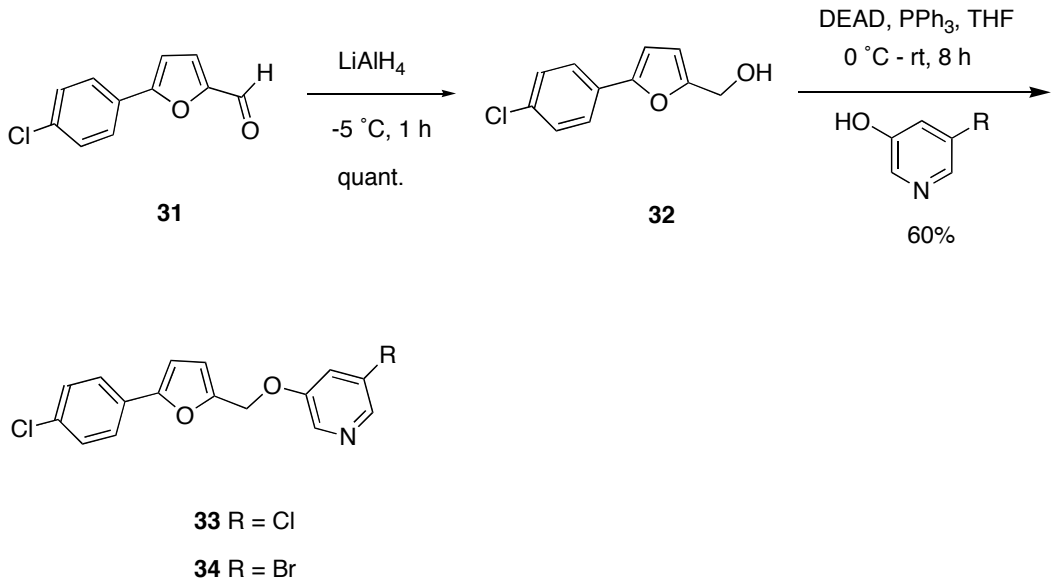

Compounds **33** and **34** were initially tested using a quenched fluorescence resonance energy transfer (FRET) assay (details in experimental section). Both ethers **33** and **34** show 50% inhibition at 100 μM concentration indicating chloro and bromo substituents have similar effects on inhibition. Although the ethers showed moderate inhibition (50%), the results were encouraging and prompted us to make a series of pyridinyl ethers using various alcohols as substrates and substituted pyridines as nucleophiles (Table 1).

Table 1. Synthesis of pyridinyl ethers **35**-**40**

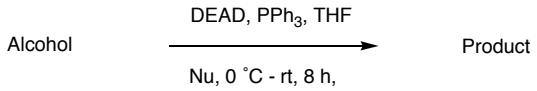

Alcohol	Nu	Product	Comp. No.
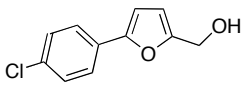	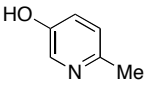	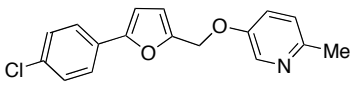	**35**
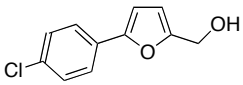	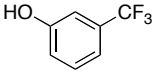	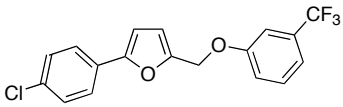	**36**
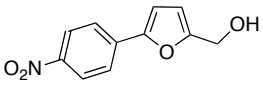	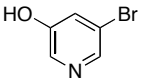	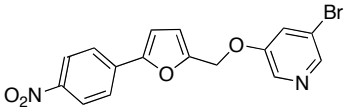	**37**
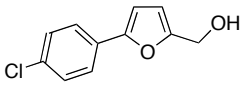	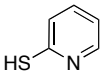	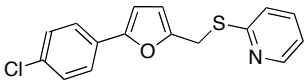	**38**
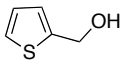	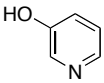	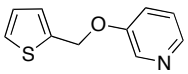	**39**
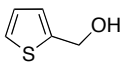	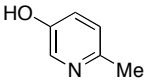	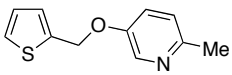	**40**

The compounds were tested against the SARS 3CL^{pro} using the FRET assay as described above and the results are shown in table **2**.

Table 2. Evaluation of pyridinyl ethers as SARS-CoV M^{pro} inhibitors

Comp. No.	Product	% Inhibition at 100 μM	IC_{50} (μM)
35	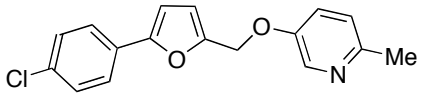	33	-
36	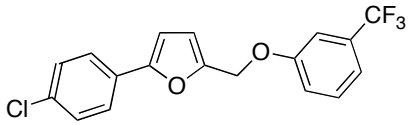	54	120
37	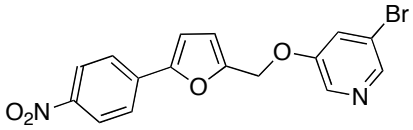	90	31
38	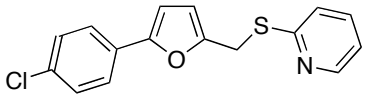	50	-
39	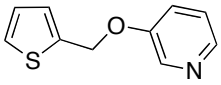	53	-
40	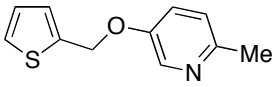	23	-

In cases where the inhibition was equal to or greater than 90% at 100 μM, control experiments were done to determine whether quenching (or enhancing) of the fluorescence of the product from the enzymatic cleavage reaction was due to the inhibitor molecules. In this experimnt, a fragment of the fluorescent substrate for the SARS 3CL^{pro} containing the donor (H_2N-Abz-Ser-OH) was synthesized

(Scheme 3) and its fluorescence was compared in both the presence and absence of the inhibitors. No significant change in the fluorescence was observed.

Scheme 3. Synthesis of H_2N-Abz-Ser-OH

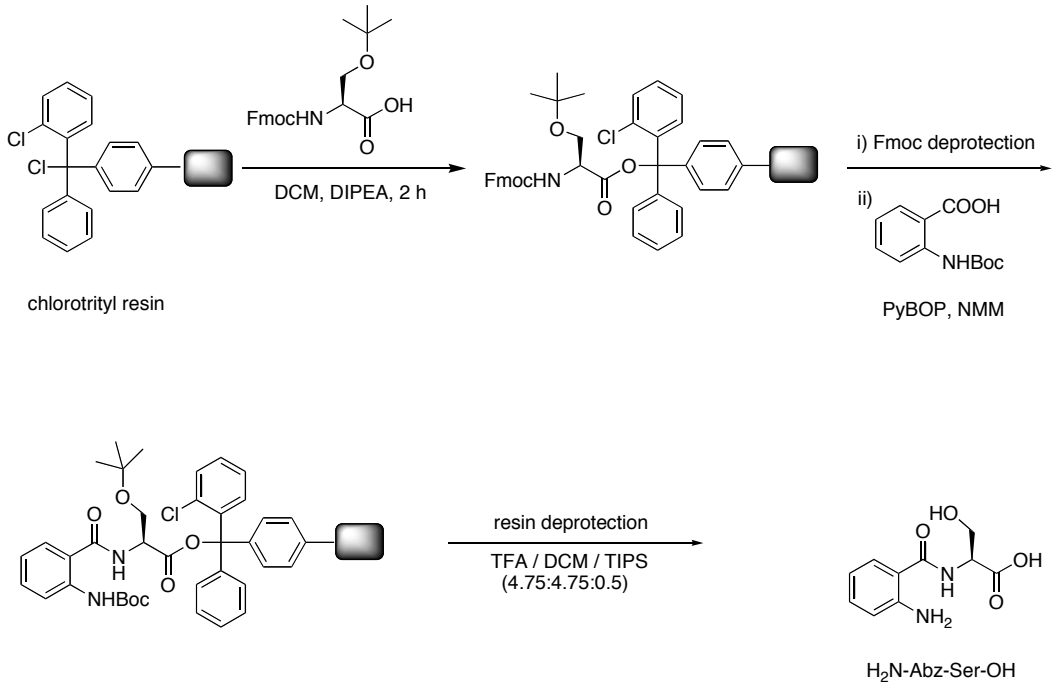

Most of the pyridinyl ethers (**33**, **34**, **36**, **37**, **38** and **39**) display moderate (54%) to very good (90%) inhibition. Some interesting structure activity relationships can be drawn from the testing results. For pyridinyl ethers, substituents meta to the pyridinyl nitrogen result in better inhibition (**33**, **34**, **36**, **37**). Compounds with two aromatic rings (**39** and **40**) display poorer inhibition. Introducing a relatively strong electron withdrawing group (CF_3, *e.g.* **36**) on the pyridine has little effect on degree of inhibition compared to thioether **38**, which shows moderate inhibition (50%), compared to the ether analogues. Introducing a nitro group (*e.g.* **37**) on the other ring dramatically increases the inhibition. In order to examine the

influence of substituent position around the phenyl ring, a pyridinyl ether **41** carrying a nitro group meta to the furan substituent was prepared and tested (Scheme 4). The commercially available *meta*-nitrophenyl furanoic acid **42** was activated as its anhydride derivative **43** by treating with ethyl chloroformate. Reduction of **43** provides the corresponding alcohol **44**. Mitsunobu reaction of **44** with 3-bromo-5-pyridinol as a nucleophile affords the desired ether **41** in 40% yield.

Scheme 4. Synthesis of **41**

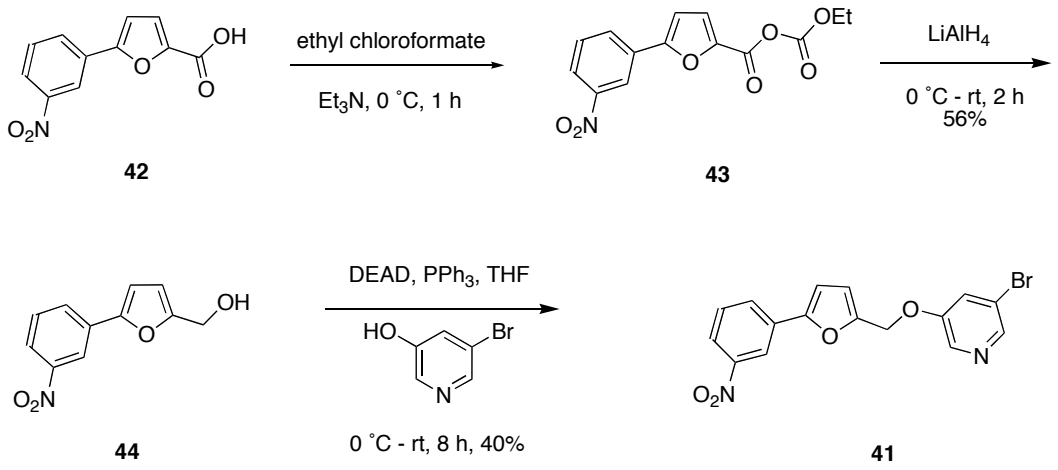

Compound **41** shows moderate inhibition (53%) of SARS $3CL^{pro}$ compared to **37** demonstrating that a nitro group para to the furan substituent results in much stronger inhibition. As the thioether **38** shows some promise (50% inhibition at 100 μM conc.), the synthesis of more thioethers was undertaken.

The thioether **45** was prepared according to the literature procedure.[55] Alkylation of dibromopyridine **46** with 4-methoxybenzylthiol (**47**) using sodium hydride affords the pyridinyl thioether **45** (Scheme 5)

Scheme 5. Synthesis of pyridinyl thioether **45**

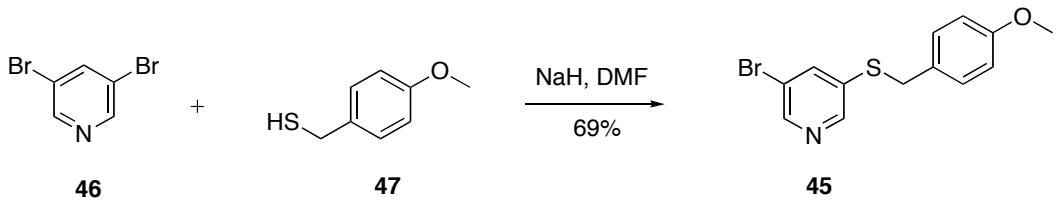

For the synthesis of another thioether **48**, a retrosynthetic analysis suggested that it could be prepared from **49** and **32**, and **49** could be prepared from **45** by deprotection of the *para*-methoxybenzyl (PMB) group (Scheme 6).

Scheme 6. Retrosynthetic analysis of target **48**

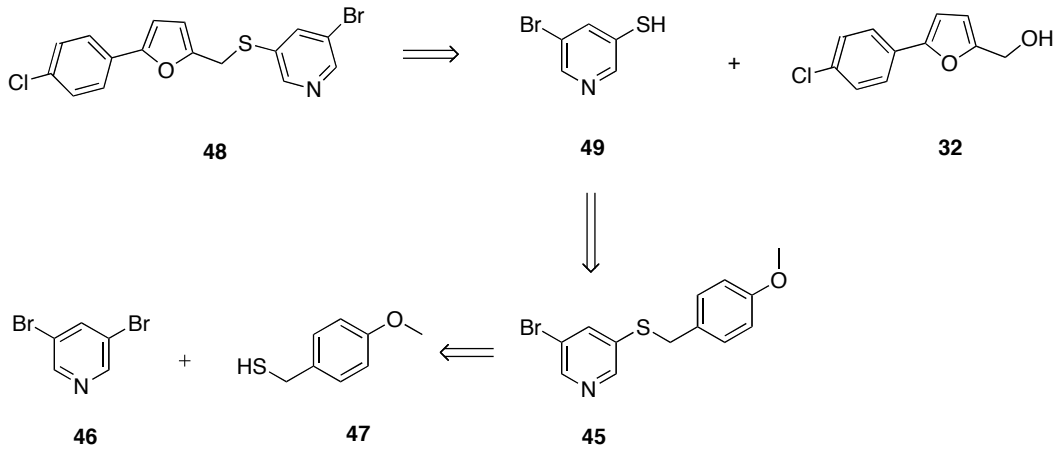

Efforts to deblock the PMB group of **45** were unsuccessful. Refluxing **45** in a 1:1 mixture of trifluoroacetic acid (TFA) and *meta*-cresol for 2 h did not provide **49** and yielded unreacted starting materials. Another method was attempted using 2 eq each of $Hg(OAc)_2$ and a strong reducing agent such as dithiothreitol (DTT) in TFA to effect cleavage but this reaction was unsuccessful with the recovery of starting material (Scheme 7).

Scheme 7. Efforts to deprotect PMB group

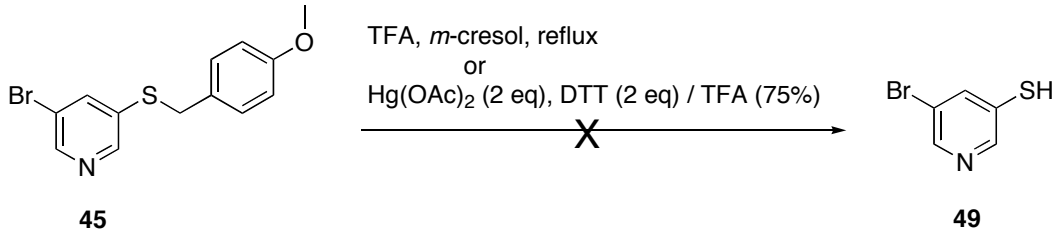

As efforts to deprotect the PMB group failed, it was decided to synthesize **50** with a triphenylmethyl group that could be easily removed by treatment with acid. However, alkylation of dibromopyridine **46** with tritylthiol (**51)** using conditions similar to the synthesis of **45** also failed and yielded unreacted starting materials (Scheme 8).

Scheme 8. Efforts to synthesize **50**

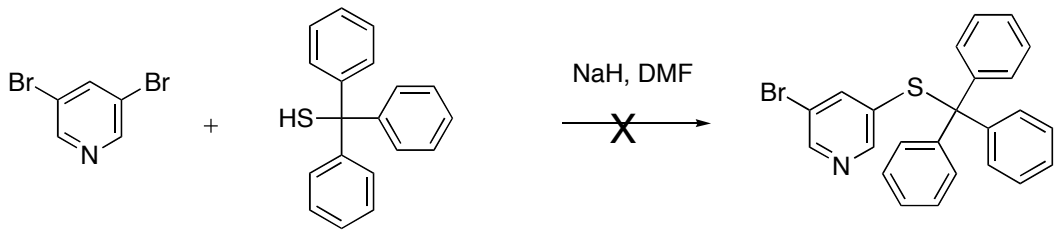

46 **51** **50**

Failure to obtain the product **50** could be attributed to the steric bulk of **51**. Since the efforts to synthesize **50** were unsuccessful and since testing results with ethers and thioethers were not so promising except for the inhibitor carrying a NO_2 substituent (**37**), attention was focused on making pyridinylamines.

1.2.2 Pyridinylamines

Because heteroaromatic esters (*e.g.* **7** and **8**) containing halopyridinyl functionalities have been demonstrated as potent inhibitors of SARS $3CL^{pro}$, pyridinylamines incorporating such key structural elements were synthesized. For the synthesis of pyridinylamines, reductive amination was used as the key reaction. A commercially available furfural derivative **52** condensed with 3-amino-5-bromopyridine (**53**), and the product was then reduced with sodium triacetoxyborohydride to provide the corresponding pyridinylamine **54** in 76% yield (Scheme 9).

Scheme 9. Preparation of pyridinylamine **54**

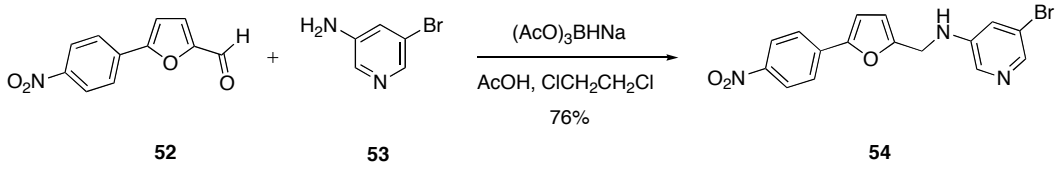

Compound **54** was tested against SARS 3CL^{pro} using the fluorometric assay. The result was promising as the amine derivative **54** showed very good inhibition of about 92% at 100 μM concentration with an IC_{50} of 24 μM. Based on these encouraging results, a small library of amines focused around the bromopyrdinyl moiety using several aldehyde substrates was made (Table 3). Several aldehydes were condensed with a bromopyridinylamine **53** followed by reduction with sodium triacetoxyborohydride to provide the corresponding pyridinylamines.

Table 3. Synthesis of pyridinylamines by reductive amination and their inhibition results

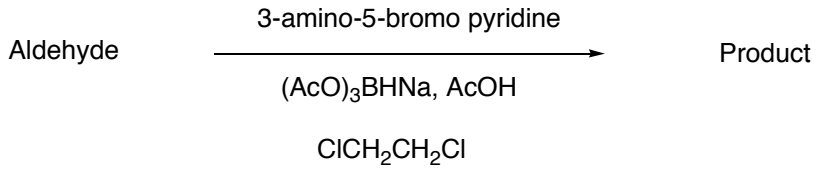

Aldehyde	Product	Compound No.	% Inhibition (100 μM)
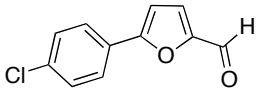	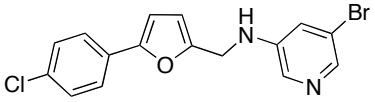	**55**	40
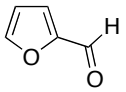	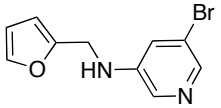	**56**	37
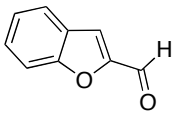	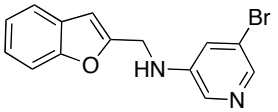	**57**	27
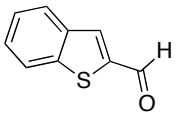	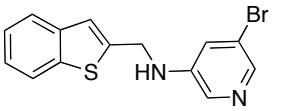	**58**	61
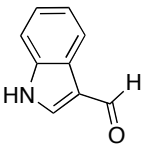	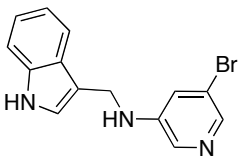	**59**	45
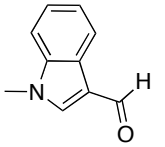	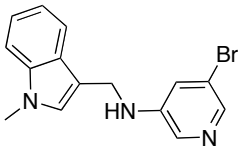	**60**	35

The pyridinylamines **55**-**60** were tested against SARS-CoV M^{pro} and the results are shown in Table 3. Compound **55** shows moderate inhibition. In the fused

heterocyclic systems, thiophene derivative **58** shows the best activity. These results suggest that electron withdrawing nitro group at the para position of the phenyl ring provides the best inhibition. Compound **54** (Scheme 9) is a better inhibitor than **55** carrying a *para*-chloro substituent (Table 3). In order to further study the infuence of groups at the para position of phenyl ring, the nitro group of **54** was reduced with hydrazine hydrate in the presence of iron and charcoal in ethanol to afford the corresponding amine derivative **61** in 61% yield (Scheme 10).

Scheme 10. Reduction of nitro derivative **54**

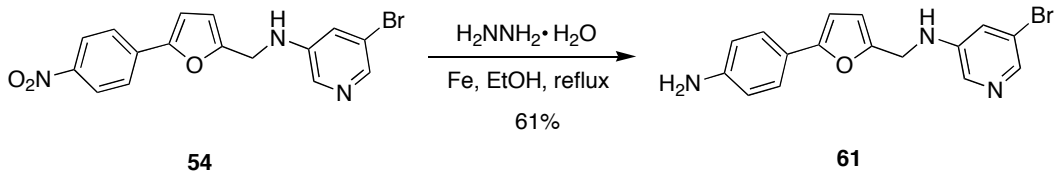

Compound **61** was tested against SARS 3CL^{pro} using a fluorometric assay. The amine derivative **61** displays potent inhibition (92% inhibition at 100 μM concentration) with an IC_{50} of 12 μM. This is the most potent inhibitor in the pyridinylamine series. However, **61** is unstable even in slightly acidic conditions and decomposes on silica gel and in chloroform. NMR and mass spectra indicated that 5-bromopyridin-3-amine (**53**) was a product of decomposition. A possible mechanism for its degradation is proposed in Scheme 11.

Scheme 11. Proposed mechanism of decomposition of **61**

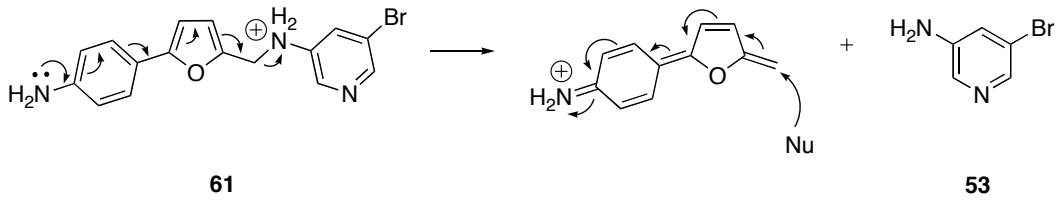

The corresponding ether analog **37** is also potent and has an IC_{50} of 31μM. Hence, the pyridinylamines **54** and **61** seemed a good choice for further modifications to improve the stability and to extend the inhibitor into the S2 and S4 pockets of the enzyme. The primary amine **61** was selected for further modifications. Treatment of **61** with methanesulfonyl chloride in the presence of triethylamine provides the corresponding mesylated derivative **62** (Scheme 12).

Scheme 12. Synthesis of mesylated derivative **62**

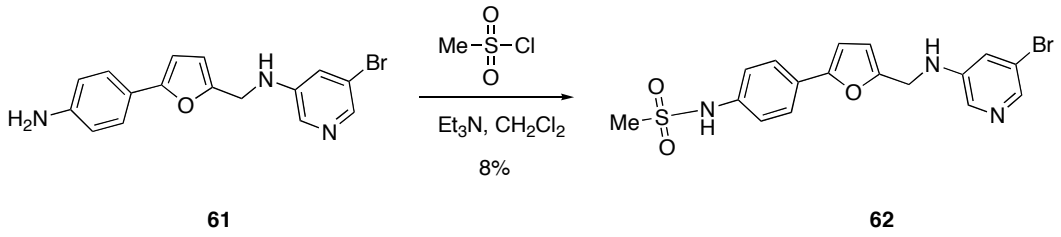

Compound **62** shows 88% inhibition of SARS $3CL^{pro}$ at 100 μM concentration, which is somewhat less than **61** (92% inhibition at 100 μM).

Docking studies of three-aromatic-ring compounds suggest substituents can be introduced on to the secondary amino group which can extend into the S2 pocket, as described previously. Accordingly, the secondary amine **54** was modified by introducing an alkyl or acyl group (Scheme 13). Reductive amination of **54** with acetaldehyde, affords the desired *N*-alkylated derivative **63** in 22% yield. Treatment of **54** with cyclopropanecarbonyl chloride affords the desired tertiary amide **64.**

Scheme 13. Synthesis of alkylated and amide derivatives **63** and **64**

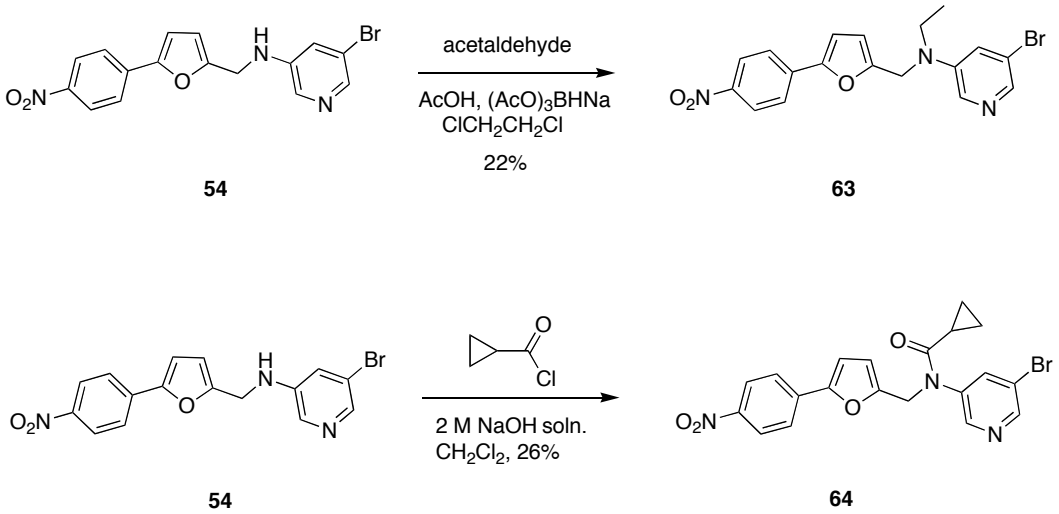

Both the *N*-substituted amine derivatives **63** and **64** display good inhibition. Compound **63** shows 90% inhibition of SARS $3CL^{pro}$ at 100 μM concentration with an IC_{50} of 35 μM, which is slightly poorer than **54** (IC_{50} 24 μM). The compound **64** displayed 73% inhibition at 100 μM. These results demonstrate that

tertiary and secondary amine analogs may be better inhibitors than the previously synthesized ethers. However, stability issues prevent the use of a favourable para amino group on the aromatic ring.

1.2.3 Hybrid peptide

It was previously demonstrated that a series of 5-halopyridin-3-yl aromatic esters and *N*,*N*-dimethylglutamine analogs are very potent inhibitors of SARS 3CL^{pro}.[32,51] Studies indicate that *para*-chlorophenyl furanyl, *N*,*N*-dimethylglutamine and phthalhydrazide moieties are key structural features for potent inhibition. Based on this observation, a mix-and-match strategy was used to synthesize a hybrid molecule **65** incorporating such key structural features. Removal of the Boc protecting group of precursor **66** with TFA, followed by coupling with 5-(4-chlorophenyl)furan-2-carboxylic acid affords the desired hybrid peptide **65** in 40% yield (Scheme 14).

Scheme 14. Synthesis of hybrid peptide **65**

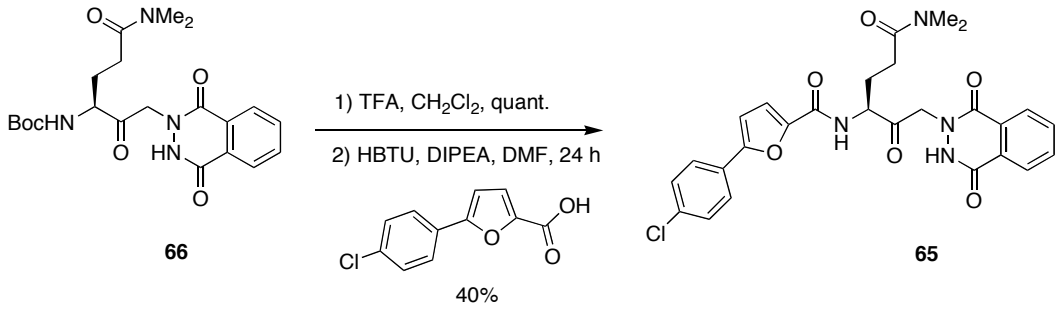

The hybrid peptide **65** shows good inhibition (86% inhibition at 100 μM) of SARS 3CL^{pro} supporting this mix-and-match strategy.

1.2.4 Rhodanine derivative

Rhodanine based molecules have been known to possess antibacterial, antiviral and antidiabetic properties[56]. However, they have never been tested against SARS-CoV 3CL^{pro}. Our screening results against SARS 3CL^{pro} have shown that pyridinyl amines containing a 2-(4-nitrophenyl)furanyl moiety display good inhibition. Based on this observation, we believe the 2-(4-nitrophenyl)furanyl unit may be an important structural feature for such effective inhibition. It also seemed reasonable to prepare a mix-and-match analogue combining the rhodanine and furanyl moieties. It was hoped that the rhodanine moiety might occupy the same site as the pyridinyl group and the amide carbonyl could bind at or near the active site. The rhodanine analog **67** was prepared in high yield (90%) via a Knoevenagel like condensation between aldehyde **52** and the *N*-acylthioxothiazolidinone derivative **68** (Scheme 15).

Scheme 15. Reagents and conditions for the synthesis of rhodanine analog **67**

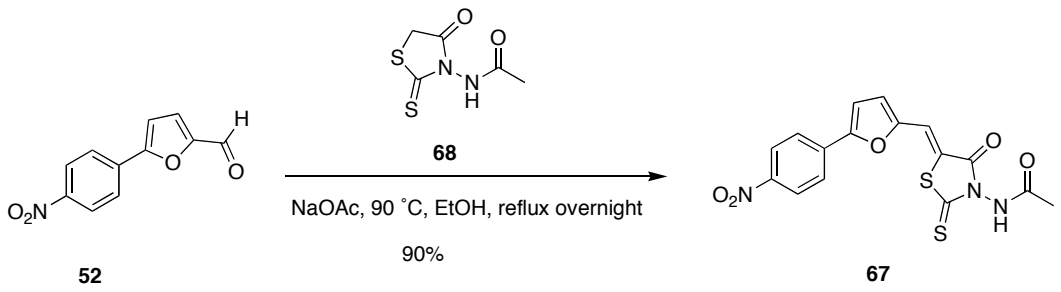

Compound **67** was tested against SARS $3CL^{pro}$ using a continuous fluorometric assay as described before. Gratifyingly, rhodanine derivative **67** shows good inhibition of SARS $3CL^{pro}$ (65% inhibition at 100 μM) with an IC_{50} value of 26 μM. This result shows **67** may be an interesting lead compound for making more potent inhibitors against SARS $3CL^{pro}$. To the best of our knowledge, rhodanine derivatives have never been tested against SARS and compound **67** is the first in this class that was tested against SARS-CoV M^{pro}. However, it should be noted that this compound may also be a Michael acceptor and may react with thiols.

1.2.5 Oxazole derivatives

Although furan rings are found in several drug molecules (*e.g.* furosemide, prazosin, cimetidine, rantidine) and natural products (*e.g.* ascorbic acid, furfuryl thiol, perillene, furan epothilones, *Galerucella* pheromone), they have some propensity to be rapidly metabolized in mammalian cells thereby limiting their usefulness.[54] In order to develop stable and non-covalent inhibitors, two additional oxazole derivatives, an ether **69** and an amine **70**, were synthesized and examined. The oxazole ether **69** was prepared from commercially available ethyl 2-chloro-2-oxoacetate **71**. Nucleophilic reaction of **71** with trimethylsilyl diazomethane ($TMSCHN_2$) affords the diazo derivative **72** in 70% yield.[57] Reaction of **72** with the copper salt $Cu(acac)_2$ generates the in-situ carbene, which reacts readily with 4-chlorobenzonitrile via a formal [3+2] cyclo-addition to form an ester derivative

73 containing the desired oxazole functionality. Reduction of **73** with diisobutylaluminium hydride (DIBALH) provides the corresponding alcohol **74** in 51% yield. A Mitsunobu reaction of **74** with 3-bromo-5-pyridinol as the nucleophile affords the desired oxazole ether **69** in 58% yield (Scheme 16).

Scheme 16. Synthesis of oxazole ether **69**

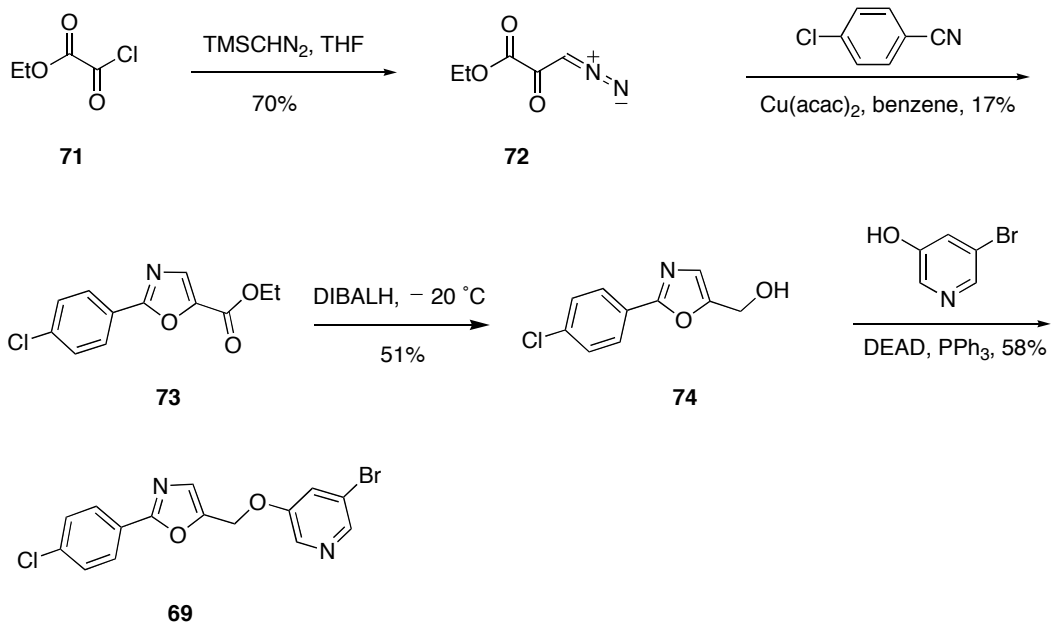

The desired oxazole amine derivative **70** was prepared from the previously synthesized intermediate **74**. Oxidation of **74** with Dess-Martin periodinane (DMP) affords the aldehyde **75** in 72% yield. Reductive amination of **75** with 3-amino-5-bromopyridine **53** affords the desired oxazole amine derivative **70** (Scheme 17).

Scheme 17. Preparation of oxazole amine derivative **70**

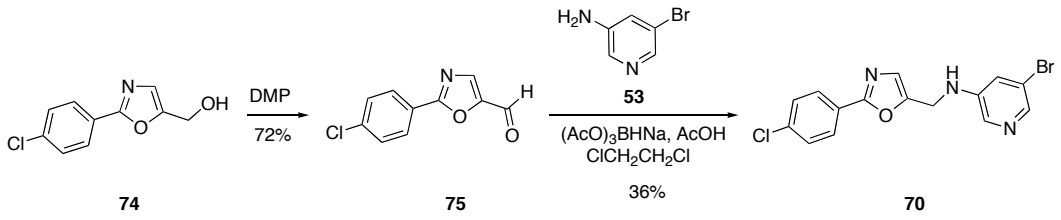

Both the oxazole derivatives **69** and **70** were tested against SARS 3CL^{pro} using a continuous fluorometric assay as described previously. Compound **69** shows weak inhibition (10%) and compound **70** shows about 21% inhibition at 100 μM concentration.

The majority of the enzyme inhibitors bind to their targets through a combination of non-covalent forces such as van der Waals, electrostatic forces, hydrogen bonding and hydrophobic interactions.[58] For inhibitors with three aromatic rings, hydrogen bonding is predicted between the oxygen atom of the furan ring and the SARS 3CL^{pro} active site. The low electron density of this oxygen in the oxazole rings of **69** and **70** might be responsible for the weaker binding that results in poor inhibition.

1.2.6 Inhibition mechanism studies

Enzyme kinetics, mass spectrometry studies and NMR experiments are used as tools to elucidate the inhibition mechanism of these compounds. The pyridinylamine derivative **54** will be discussed as a representative example of these methods. The FRET assay was performed by preincubating a mixture of a buffer, the inhibitor **54** (10 μM) and the enzyme (SARS $3CL^{pro}$) for varying lengths of time followed by adding the fluorescent substrate and recording fluorescence. Reversible inhibitors will inhibit the enzyme to the same amount, irrespective of the preincubation time period.[47] The percentage inhibitions both at 0 ˚C and at rt were the same (Table 4) for the recorded time intervals suggesting a non-covalent, rapid and reversible inhibition.

Table 4. FRET assay results showing the observed inhibition

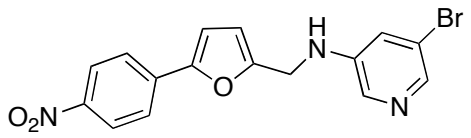

54

Temperature (˚C)	Time (min)	% inhibition (100 μM)
rt	0	25
rt	15	25
rt	30	24
rt	60	23

Temperature (˚C)	Time (min)	% inhibition (100 μM)
0	0	25
0	10	26
0	30	26
0	60	21

The inhibition mechanism was further investigated using electrospray ionization mass spectrometry (ESI-MS). In this study, one equivalent of the enzyme (SARS $3CL^{pro}$) was mixed with 5 equivalents of inhibitor **54** and incubated for 10 min. Analysis by ESI-MS indicated a peak at 33843 Da ($[M+H]^+$) (Figure 30A) corresponding to the mass of the enzyme suggesting no covalent modifications of the enzyme. The peak at 374 Da (Figure 30B) showed the presence of the intact inhibitor. These results are consistent with a non-covalent and reversible inhibition mechanism.

Figure 30. Mass spectral evaluation of the inhibition mechanism; **A:** Peak showing the mass of the enzyme; **B:** Mass of the intact inhibitor **54**

A: Mass of the enzyme (33843 Da) ($[M+H]^+$)

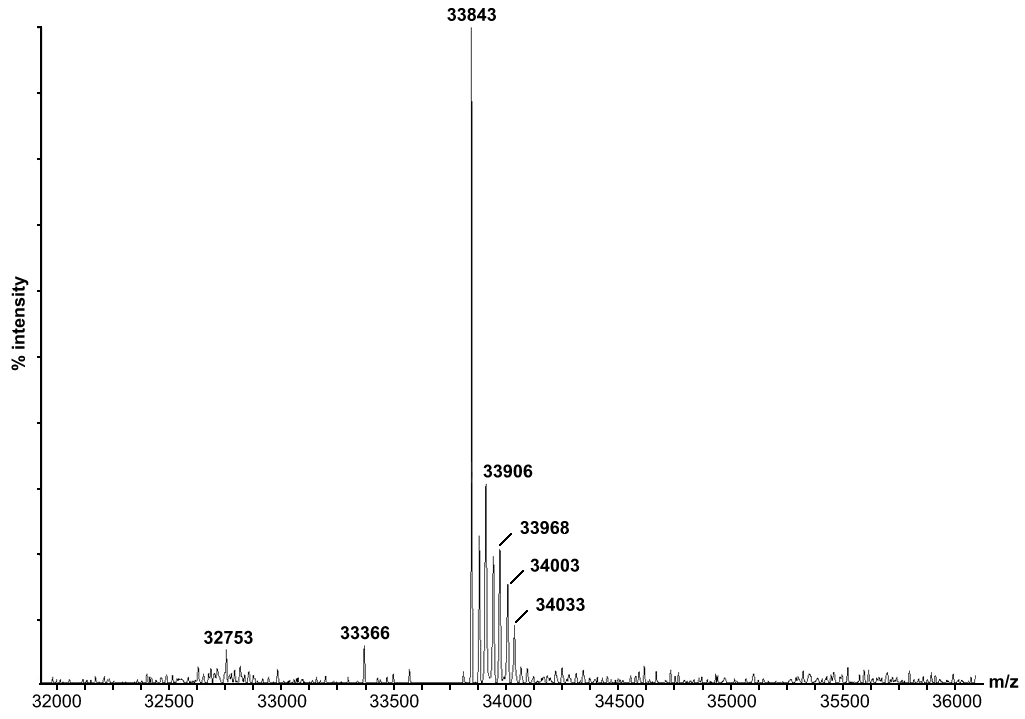

B: Mass of the intact inhibitor **54** (374 Da) ($[M+H]^+$)

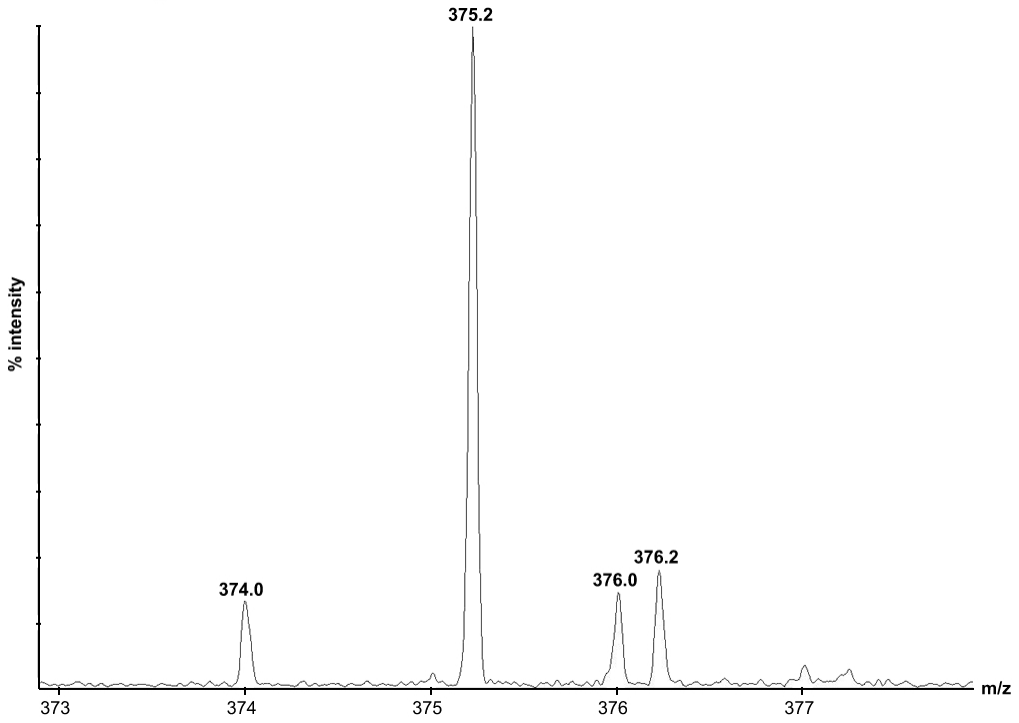

The inhibition mechanism was also examined using NMR studies. Ethyl mercaptan was used as a model of the enzyme's thiol nucleophile. Initially a 1:6 solution of D_2O and DMSO-d_6 containing Bis-tris buffer (20 mM) and ethyl mercaptan (1.0 eq) was prepared and its spectrum recorded at 0.5 seconds. Ethyl mercaptan showed two peaks, one quartet at 2.44 ppm and a triplet at 1.19 ppm corresponding to methylene and methyl protons respectively (Figure 31A). To this solution was added the inhibitor **54** (1.0 eq) and its spectra recorded at specified time intervals. A change in peak positions and integration values of the

protons are expected if a covalent bond between ethyl mercaptan and the inhibitor **54** is involved. No change in chemical shifts or integration values of the protons of either the ethyl mercaptan or the inhibitor **54** (Figure 31B) was observed demonstrating additional evidence of reversible and non-covalent inhibition.

Figure 31. Parts of the NMR spectra showing the peaks for **A**. Ethyl mercaptan; **B:** Inhibitor **54**

A: Ethyl mercaptan

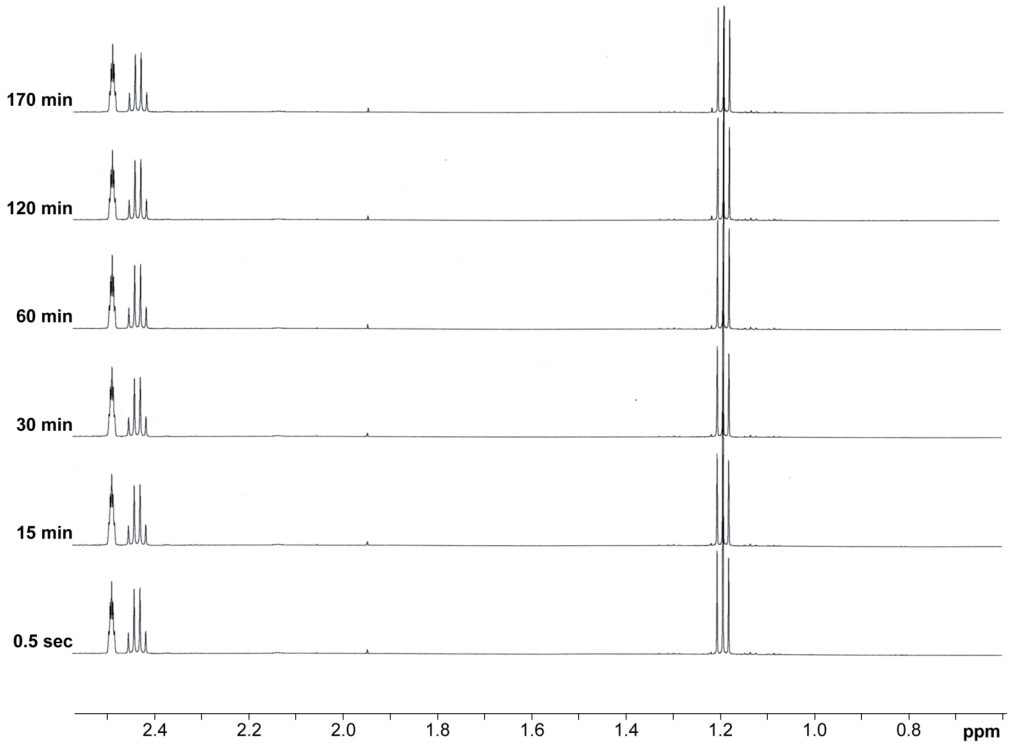

B: Inhibitor **54**

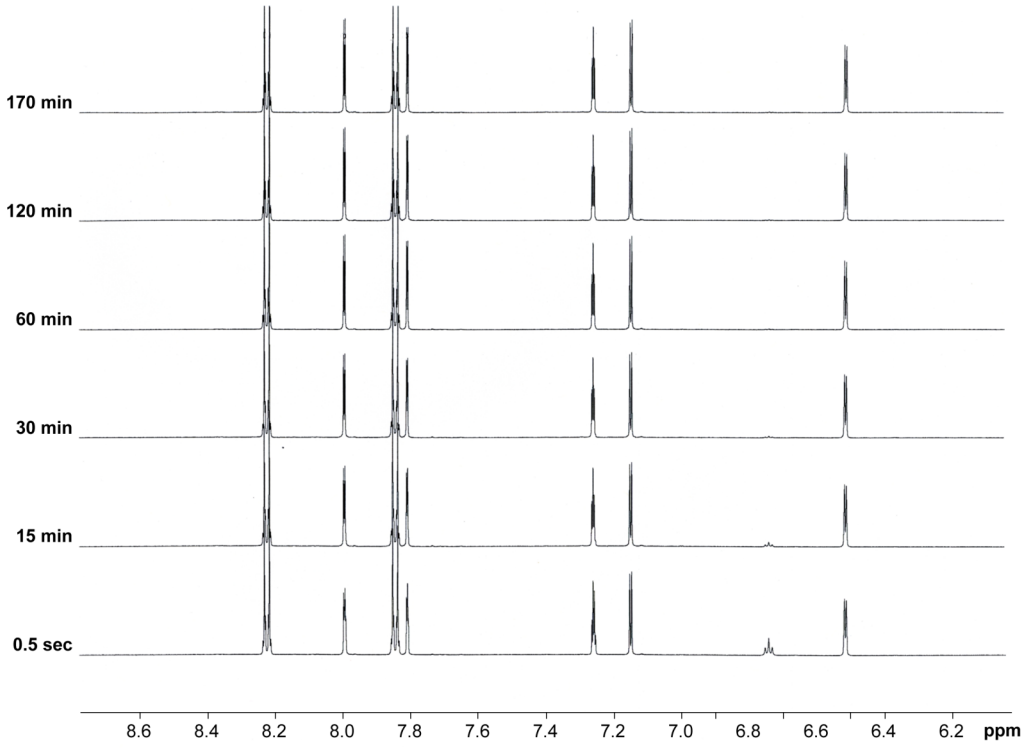

All lines of evidence taken together suggest a covalent bond is not formed between the SARS 3CL^{pro} and the pyridinylamine-derived inhibitor **54**.

1.2.7 Conclusions and future work

A series of pyridinyl ethers and amines, oxazoles and other compounds using a mix-and-match strategy have been synthesized and tested. The results are promising with several compounds showing moderate to very good inhibition

(92% at 100 μM concentration). Some interesting structure activity relationships can be drawn. Compared to ethers, pyridinylamines display better inhibition. Compound **61** having a primary amine functionality para to the furan moiety shows very good inhibition (92%) against SARS $3CL^{pro}$ with the lowest IC_{50} of 12 μM. Substituents at meta postion to the pyridinyl nitrogen enhance inhibition. Compounds with either two aromatic rings or fused heterocyclic rings display poor inhibition. Compounds carrying a strong electron-withdrawing (NO_2) group at the para position of the phenyl ring show strong inhibition. Introduction of substituents (such as compounds containing 3 aromatic rings) that can extend into the S2 and S4 pockets of the proposed S4-S1 binding model gave inhibitors with better activity. Docking studies predict that for inhibitors with three aromatic rings, hydrogen bonding is involved between the oxygen atom of the furan ring and the SARS $3CL^{pro}$ active site. Substitution of a furan ring with an oxazole moiety results in decreased inhibition. The low electron density of oxazole rings of **69** and **70** might be responsible for the weaker binding that results in poor inhibition. Testing results for the hybrid peptide **65** indicate that *para*-chlorophenyl furanyl, *N*,*N*-dimethylglutamine and phthalhydrazide moieties are key structural elements for strong inhibition. Further modifications such as replacing *N*,*N*-dimethylglutamine with a γ-lactam or substituting a *p*-chlorophenyl furanyl group with a *p*-nitrophenyl furanyl moiety could give better inhibitors. Since the subtrate specificities of picornavirus $3C^{pro}$ and coronavirus 3CL proteases are similar, inhibitors developed against SARS $3CL^{pro}$ could potentially be applied to other pathogenic picorna and corona viruses. Further crystallization

studies of these inhibitors with SARS $3CL^{pro}$ will assist in understanding the inhibition mechanism.

CHAPTER 2: INHIBITORS OF INSECT VIRAL CYSTEINE PROTEASES

2.1 INTRODUCTION

Proteases are a group of enzymes that catalyze the hydrolysis (breakdown) of proteins and are involved in virtually all biological functions. In addition to serving as key regulators of several physiological processes in humans, proteases are essential for the replication of pathogenic viruses, bacteria and parasites that cause infectious diseases.[59] As such, proteases constitute attractive drug targets against a variety of pathogens. Cysteine proteases, one major class of proteases, have been found in plants and animals as well as in bacteria and viruses.[36] They are implicated in a wide variety of diseases including cardiovascular, inflammatory, neurological, respiratory, viral, musculoskeletal, immunological, CNS disorders and cancer.[60] The cysteine proteases of picornaviruses (HAV, HRV) and coronaviruses (TGEV, HCoV, SARS-CoV) play a crucial role in viral life cycle processes such as replication and transcription. As such, cysteine proteases hold significant promise as drug targets.

2.1.1 Picornaviruses

The picornavirus (pico meaning small, and RNA referring to ribonucleic acid) family comprises small icosahedral positive-sense single stranded RNA viruses. All picornaviruses have a 3C protease, a cysteine protease much like the SARS $3CL^{pro}$ previously discussed. The 3C proteases in these viruses process an initially

synthesized viral polyprotein into smaller structural and functional proteins, and are crucial for viral maturation and replication. In its life cycle, the picornavirus infects the host by attachment to a specific cell surface receptor followed by releasing the positive-sense single stranded RNA into the cytosol where it functions as a mRNA to produce a single polyprotein of about 250 kDa (Figure 32).[49] This polyprotein is cleaved by the viral 3C protease to produce the structural (capsid, P1) and nonstructural (P2-P3) protein precursors which then assemble to new viral particles.[49]

Figure 32. Generalized schematic representation of picornaviral polyprotein processing

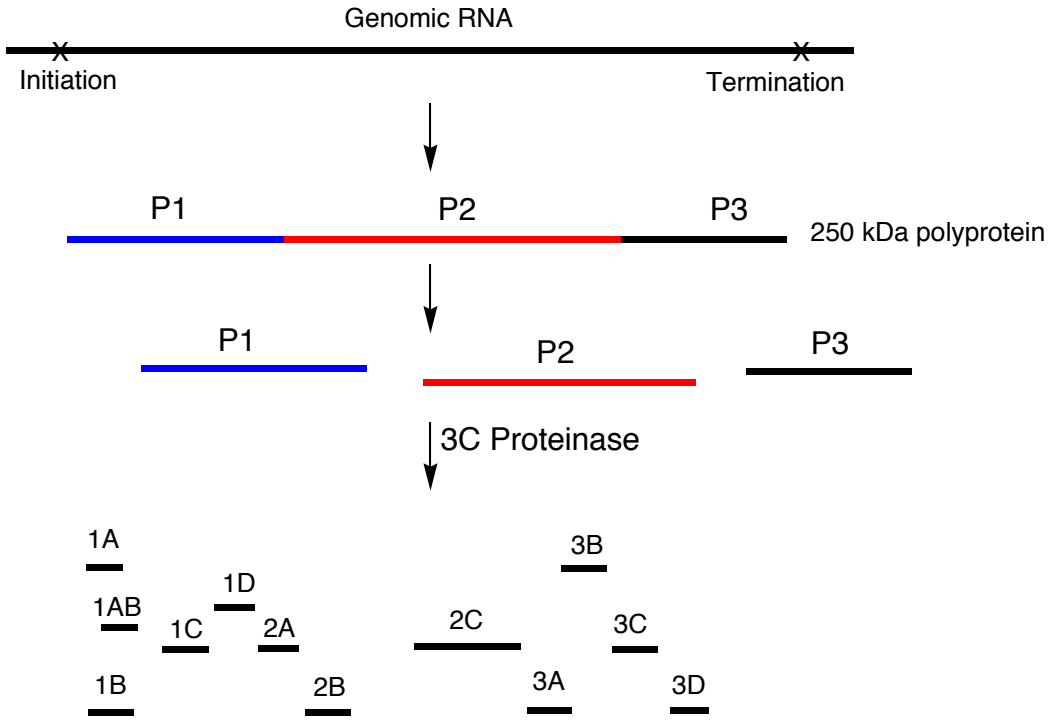

In the hepatitis A virus (HAV), the cysteine side-chain thiolate of the $3C^{pro}$ acts as a nucleophile during peptide bond cleavage of the polyprotein precursor, and this is assisted by a histidine in the protease, which serves as a general acid-base catalyst (Figure 33).[61]

Figure 33. Mechanism of protease hydrolysis by HAV $3C^{pro}$ at the 2B/2C junction

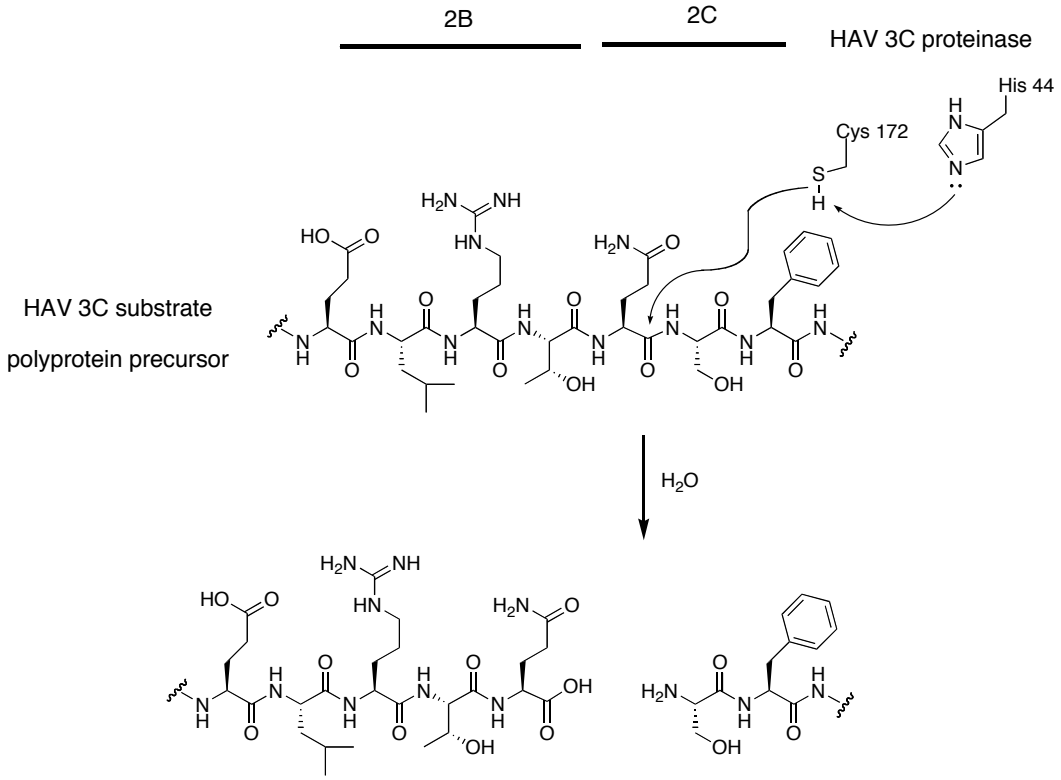

A thioester is formed by the nucleophilic attack of a thiolate anion on the carbonyl carbon of the substrate. Subsequent hydrolysis of the thioester bond releases the carboxylic acid moiety, thereby regenerating the free enzyme.

Picornaviruses cause a wide variety of illnesses in humans and animals.[62] Some of these include human rhinovirus (HRV) that causes the common cold, the hepatitis A virus (HAV), human poliovirus, enterovirus that causes aseptic meningitis (inflammation of the meninges, the membranes that cover the brain and spinal cord) and foot and mouth disease (FMD) virus, that causes the highly contagious diseases in cloven-hooved mammals in animals. Picornaviruses are also linked to the recent mysterious disappearance of honeybees called Colony Collapse Disorder (CCD).[63] An insect picorna-like virus called Israel acute paralysis virus (IAPV) is implicated in CCD.[64]

2.1.2 Colony Collapse Disorder (CCD)

In the beginning of October 2006, an alarming number of honeybee colonies began to die in the United States with beekeepers reporting losses of 30-90% of their hives. Similar colony declines have occurred in the past, with documented reports in both 1986 and in 2004. This phenomenon is called "Colony Collapse Disorder" (CCD) and has affected as many as 23% of beekeeping operations in the United States alone. The affected beekeepers have lost about 45% of their operations making an enormous horticultural and economic impact worldwide. CCD is characterized by an inexplicable loss of adult bee colonies, with little or no build-up of dead bees found inside or around the colonies.[65,66] Although, there is no consensus on the origin of the disorder, it has been attributed to biotic factors (such as *Varroa* mites and insect diseases), stress related to environmental change, malnutrition, and even cell phone radiation. Exposure to pesticides, which

can affect the bee immune system may be another contributing factor for developing the viral infection.[64] Using a metagenomic technique in which the genetic material of affected and healthy bees from environmental samples are collected and analysed, Lipkin and coworkers[64] have identified a virus called Israel acute paralysis virus (IAPV) as a putative marker for colony collapse disorder. They found the virus in most of the affected colonies but in almost no healthy bees. Sela and coworkers[67,68] demonstrated that injection of IAPV into bees caused paralysis and death in 98% of bees within a matter of days. When IAPV was fed to bees, they survived a few days longer. IAPV was initially identified in Israel in 2002 and significantly associated with affected hives. Based on homology and genetic sequence, IAPV belongs to the *Dicistroviridae* family.[69] Members of the *Dicistroviridae* have similarities to other viruses having a positive-sense ssRNA genomes within the "picornavirus-like superfamily" indicating IAPV most likely has a $3C^{pro}$. Most members of the family *Dicistroviridae* are pathogenic and infect honeybees, flies, aphids, ants, leafhoppers, silkworms and shrimp. The best understood of these insect picorna-like viruses is cricket paralysis virus (CrPV) and it is expected to behave very similarly to IAPV.

2.1.3 Design of inhibitors against insect viral 3C proteases

The precursor proteins in dicistroviruses are processed by a $3C^{pro}$-like protease that is structurally similar to the 3C protease of picornaviruses. It is this structural conservation that makes the 3C proteases ideal targets for the design of insect

picorna-like viral $3C^{pro}$ inhibitors. Interruption of these 3C proteases could prevent the formation of new virions and thus combat CCD. However, the 3C proteases of insect picorna-like viruses are not well studied. No crystallographic data or kinetic studies have been reported in the literature. The $3C^{pro}$ is found within the same polyprotein that it cleaves. Therefore if the N and C termini of the $3C^{pro}$ can be determined, the cleavage sites within the substrate can be found. This is because when the $3C^{pro}$ cleaves the polyprotein it simultaneously liberates itself.

Our collaborators, Dr. Lindsay Eltis and coworkers at the University of British Columbia (UBC) and at the University of Alberta (Dr. Michael James and coworkers) tentatively predicted the cleavage sites by aligning the sequences of the IAPV and the related CrPV to those of known 3C proteases and scanning putative N- and C- terminini of 3C-like proteinases for potential cleavage sites in the replicases of these viruses. Their alignment suggests that there exists a highly conserved histidine (corresponding to His191 in HAV $3C^{pro}$), which is the major determinant of substrate specificity for characterized 3C proteases. Interestingly, Dr. Carly Huitema (Ph.D. thesis, 2009) from UBC demonstrated a partially purified glutathione-S-transferase tagged (GST-tagged) IAPV $3C^{pro}$ efficiently cleaved the SARS-P2 substrate (Abz-SVTLQ/SGY(NO_2)R) (Figure 34).[70] This indicates that peptide sequences having a Gln residue at the P1 position could potentially be a good starting framework for the design of inhibitors against IAPV $3C^{pro}$.

Figure 34. Structure of Abz-SVTLQ/SGY(NO_2)R

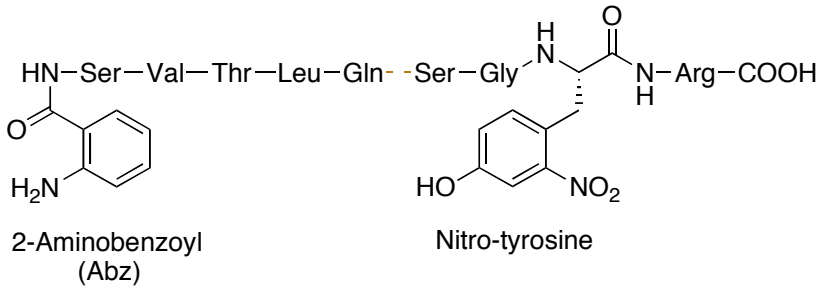

Tate *et al*[71] performed alignment studies in which the amino acid sequences of capsid proteins of CrPV are compared with those of other picorna-like viruses. These authors demonstrated significant sequence similarities and conservation between insect viruses and picornaviruses. Substantial structural similarities were also found between cricket paralysis virus and picorna-like insect viruses.[71]

2.1.4 Objectives: Synthesis and evaluation of insect viral cysteine protease inhibitors

The objective is to design, synthesize and test fluoroscent peptide inhibitors against the $3C^{pro}$ of IAPV that has been associated with CCD. As CrPV is the best characterized insect picorna-like virus and both IAPV and CrPV are dicistroviruses, an inhibitor designed for CrPV might also inhibit IAPV. Our collaborators at UBC were initially unsure if the IAPV protease could be purified. As such, it was decided to synthesize the CrPV peptide substrate. An important

consideration in the peptide substrate design is the selection of an optimum donor-acceptor pair for FRET. Earlier studies of SARS $3CL^{pro}$ suggested that an anthranilate-nitrotyrosine (Abz-YNO_2), derived from anthranilic acid and tyrosine respectively, would be a better donor-acceptor pair for the FRET assay. Accordingly, the peptide substrates were designed incorporating 2-aminobenzoyl (Abz) as a donor and nitro-tyrosine (YNO_2) as an acceptor on opposite sides of the predicted cleavage sites. The alignment studies discussed above led us to design and synthesize the following two-fluoroscent peptides (Figure 35). The arrows indicate the sites of predicted cleavage. For example in IAPV, the peptide (amide) bond between glutamine and valine could be cleaved by IAPV $3C^{pro}$.

Figure 35. Structures of fluorescent peptide substrates for CrPV and IAPV

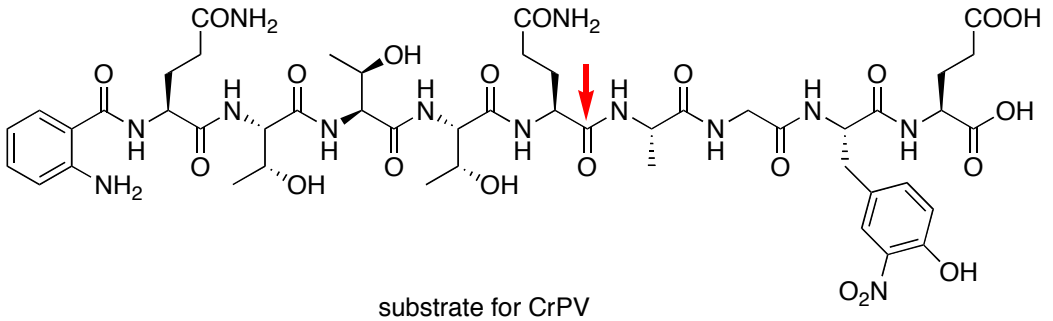

substrate for CrPV

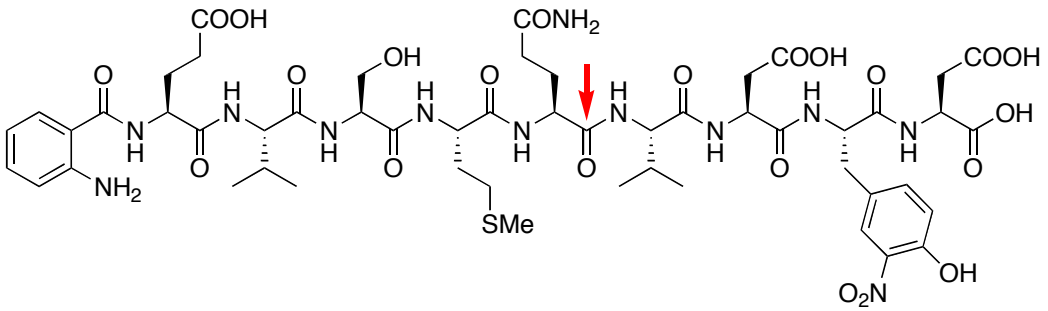

substrate for IAPV

A peptidyl fluoromethyl ketone is also synthesized incorporating the SARS recognition tripeptide (Figure 36) discussed previously. This was based on the observation, that IAPV 3C^{pro} cleaves the SARS-P2 substrate and thus SARS inhibitors may also be effective against IAPV.

Figure 36. Structure of SARS 3CL^{pro} recognition tripeptide **76**

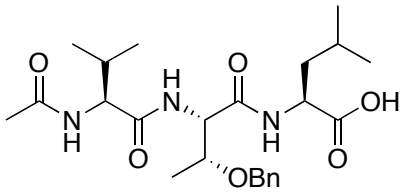

76
SARS recognition tripeptide

2.2 RESULTS AND DISCUSSION

2.2.1 Peptidyl fluoromethyl ketone

The peptidyl fluoromethyl ketone **77** was designed based on the results of our collaborators that a partially purified IAPV 3C^{pro} efficiently cleaved the SARS-P2 substrate. A retrosynthetic analysis of the peptidyl fluoromethyl ketone derivative **77** is shown in Scheme 18.

Scheme 18. Retrosynthetic analysis of target fluoromethyl peptide **77**

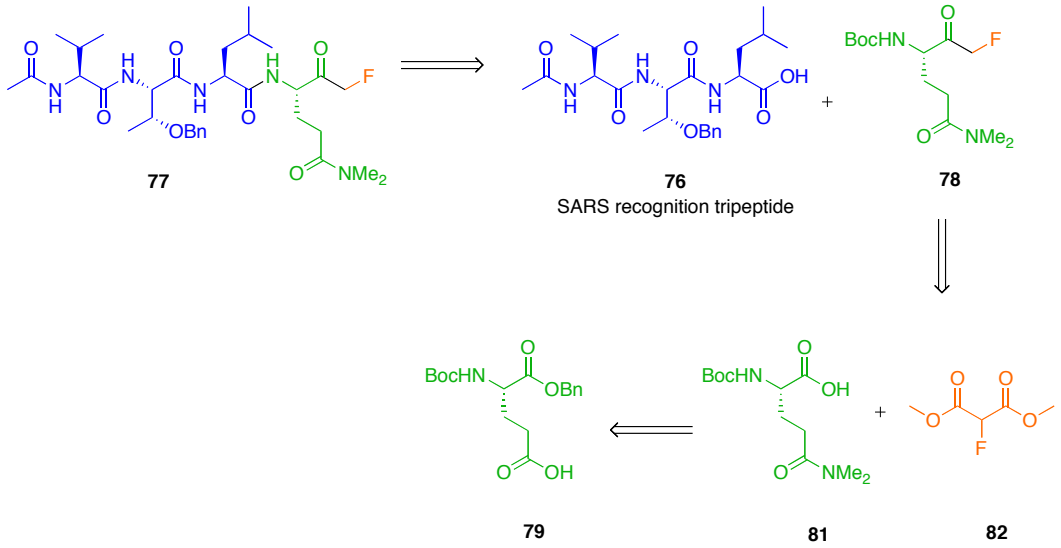

As outlined in scheme 18, we envisioned that the peptidyl fluoromethylene ketone **77** could be obtained from the SARS recognition tripeptide **76** and *N*,*N*-dimethylglutamine-fluoroketone **78**. The fluoroketone **78** could be prepared from commercially available glutamic acid derivative **79** and dimethyl fluoromalonate **82**.

The *N*,*N*-dimethylglutamine **81** derivative can be prepared by a literature procedure previously established in our group[72] in which treatment of the commercially available benzyl protected L-glutamic acid derivative **79** with ethyl chloroformate followed by addition of $NHMe_2$•HCl and Et_3N generates the

corresponding amide **80**. Removal of the benzyl group by palladium-mediated hydrogenolysis affords the desired free acid **81** (Scheme 19).

Scheme 19. Synthesis of *N*,*N*-dimethylglutamine derivative **81**

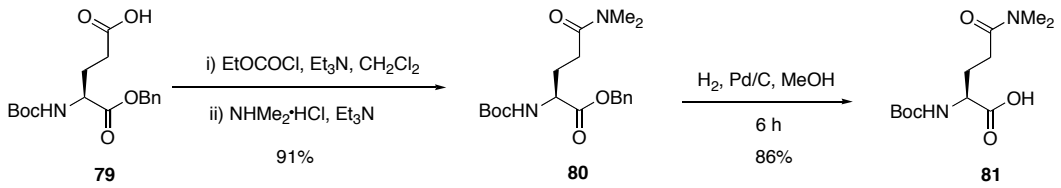

The *N*,*N*-dimethylglutamine-fluoroketone **78** was synthesized according to the patented procedure of Palmer.[73] Transesterification of dimethyl fluoromalonate **82** with benzyl alcohol provides the dibenzyl fluoromalonate **83**. Hydrolysis with one equivalent of base generates the mono ester **84**, which is subsequently treated with magnesium ethoxide to afford the magnesium salt **85**. Activation of glutamic acid **81** with carbonyl diimidazole (CDI) followed by enolate condensation with the magnesium salt **85** affords intermediate **86** as a mixture of diastereomers. The intermediate **86**, without isolation, was subjected to palladium catalyzed hydrogenolysis to afford the desired *N*,*N*-dimethylglutamine- fluoroketone **78** (Scheme 20).

Scheme 20. Synthesis of *N*,*N*-dimethylglutamine-fluoroketone **78**

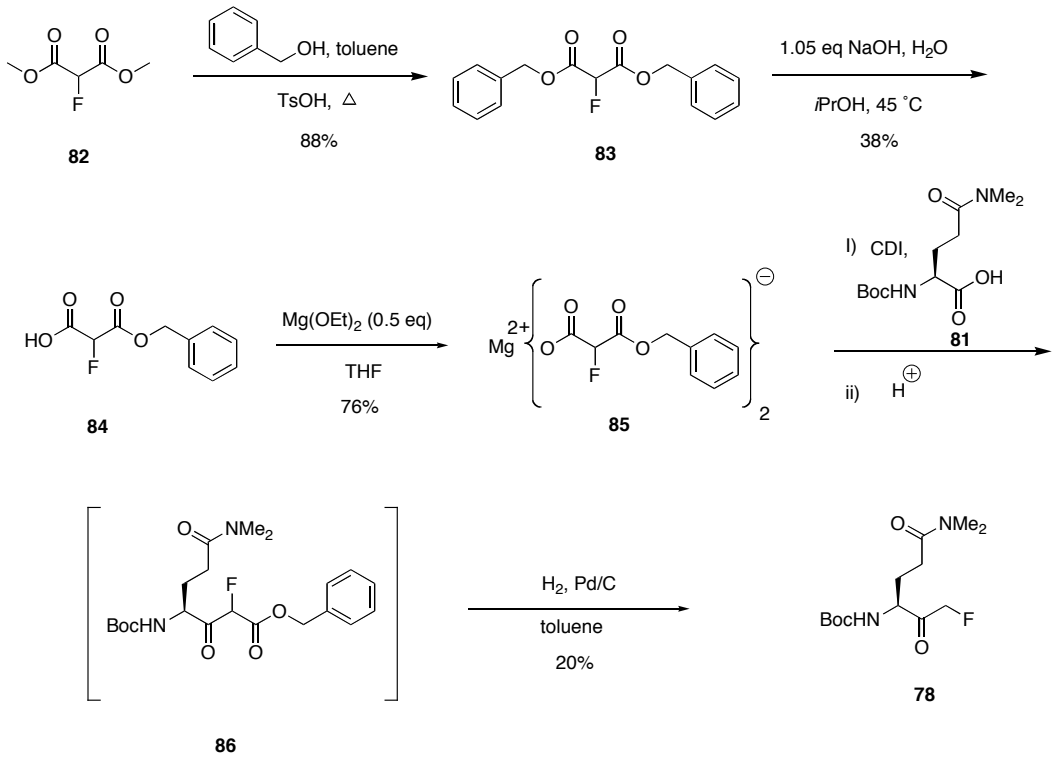

The SARS recognition tripeptide **76** is prepared according to a procedure developed in our group.[34] Conversion of leucine (**87**) to the corresponding methyl ester **88** followed by treatment with pre-activated Boc-Thr(OBn)-OH/EtOCOCl solution affords the dipeptide **89**. The Boc protecting group is removed with TFA and the resulting dipeptide is coupled with Boc-Val-OH to afford the tripeptide **90**. Removal of the Boc group, followed by acylation of the free amine with acetic anhydride generates the *N*-acyl derivative **91**. Base hydrolysis of **91** provides the

desired tripeptide **76** (Scheme 21).

Scheme 21. Synthesis of recognition tripeptide **76**

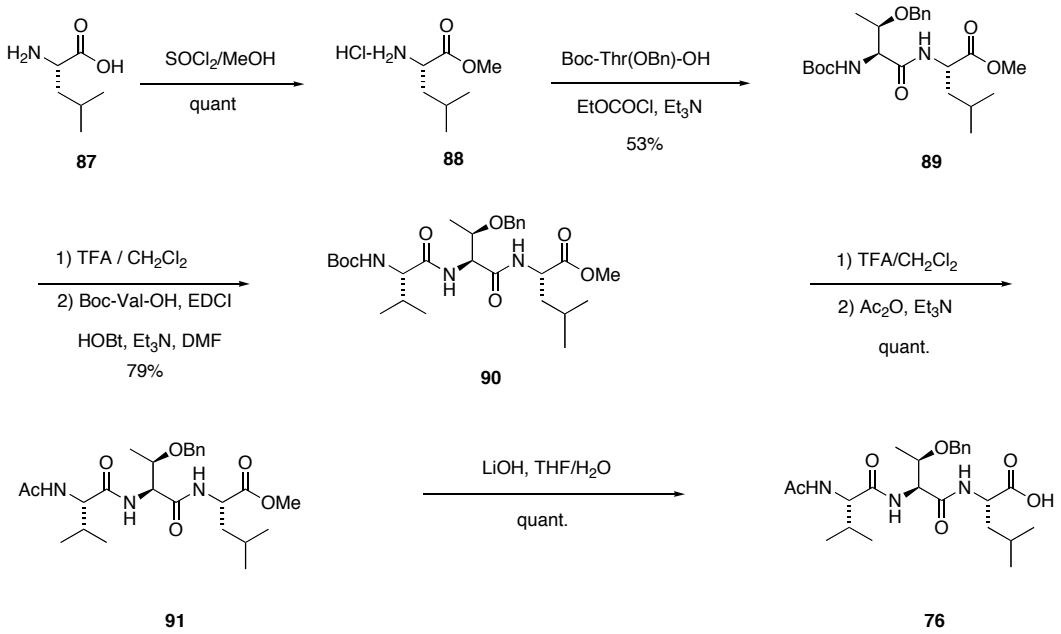

With the tripeptide **76** and *N*,*N*-dimethylglutamine-fluoroketone **78** in hand, the desired peptidylfluoromethyl ketone **77** was synthesized as described in Scheme 22. In order to prevent the formation of an imine derivative between the electrophilic α-fluoro ketone moiety of one molecule and the Boc deprotected primary amine of another molecule, the ketone functionality in **78** was masked as an alcohol. Reduction of **78** with sodium borohydride ($NaBH_4$) followed by acidic work up provides the corresponding alcohol **92**. Removal of the Boc group with TFA affords the salt **93** that is coupled without isolation to the previously synthesized tripeptide **76** to afford the fluoro alcohol derivative **94**. Oxidation of **94** with Dess-Martin periodinane (DMP) provides the desired product **77**.

Scheme 22. Synthesis of target peptidyl fluoromethyl ketone **77**

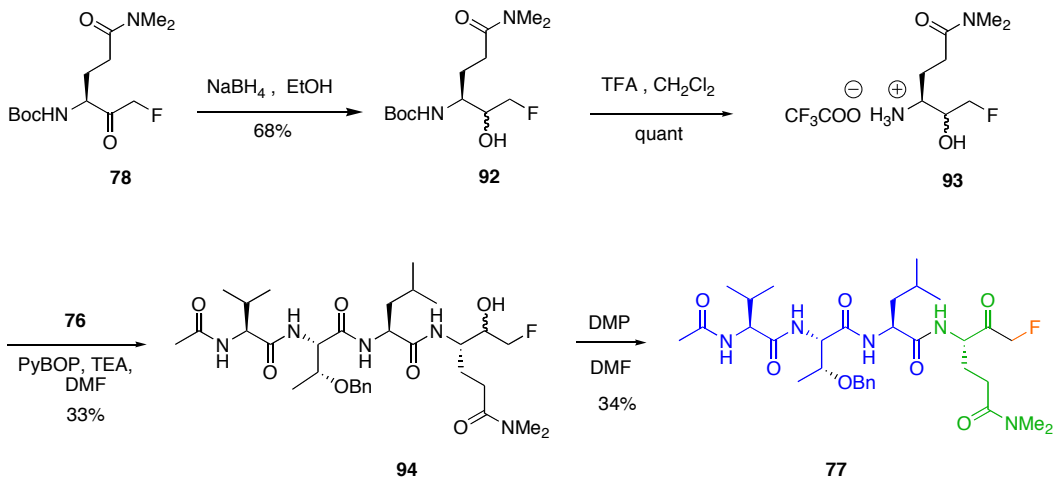

2.2.2 Cricket paralysis virus (CrPV) peptide substrate

Synthesis of CrPV peptide substrate **95** was done using an automated ABI 433A peptide synthesizer. A Wang resin preloaded with Fmoc-Glu(O*t*Bu)-OH is used as the C-terminal amino acid. The next eight amino acid residues are introduced using the peptide synthesizer with Fmoc solid phase protocols in the order: Fmoc-Tyr(NO_2)-OH, Fmoc-Gly-OH, Fmoc-Ala-OH, Fmoc-Gln(Trt)-OH, Fmoc-Thr(*t*Bu)-OH, Fmoc-Thr(*t*Bu)-OH, Fmoc-Thr(*t*Bu)-OH, Fmoc-Gln(Trt)-OH. The N-terminal Fmoc group is then removed manually with 20% piperidine followed by treatment of the resin bound peptide with (95:2.5:2.5) TFA / TIPS / H_2O to cleave the product from the solid support. Analysis by MALDI-TOF MS showed a peak for the desired precursor **96** (Scheme 23).

Scheme 23. Synthesis of nonamer precursor **96** for Cricket paralysis virus (CrPV) peptide substrate

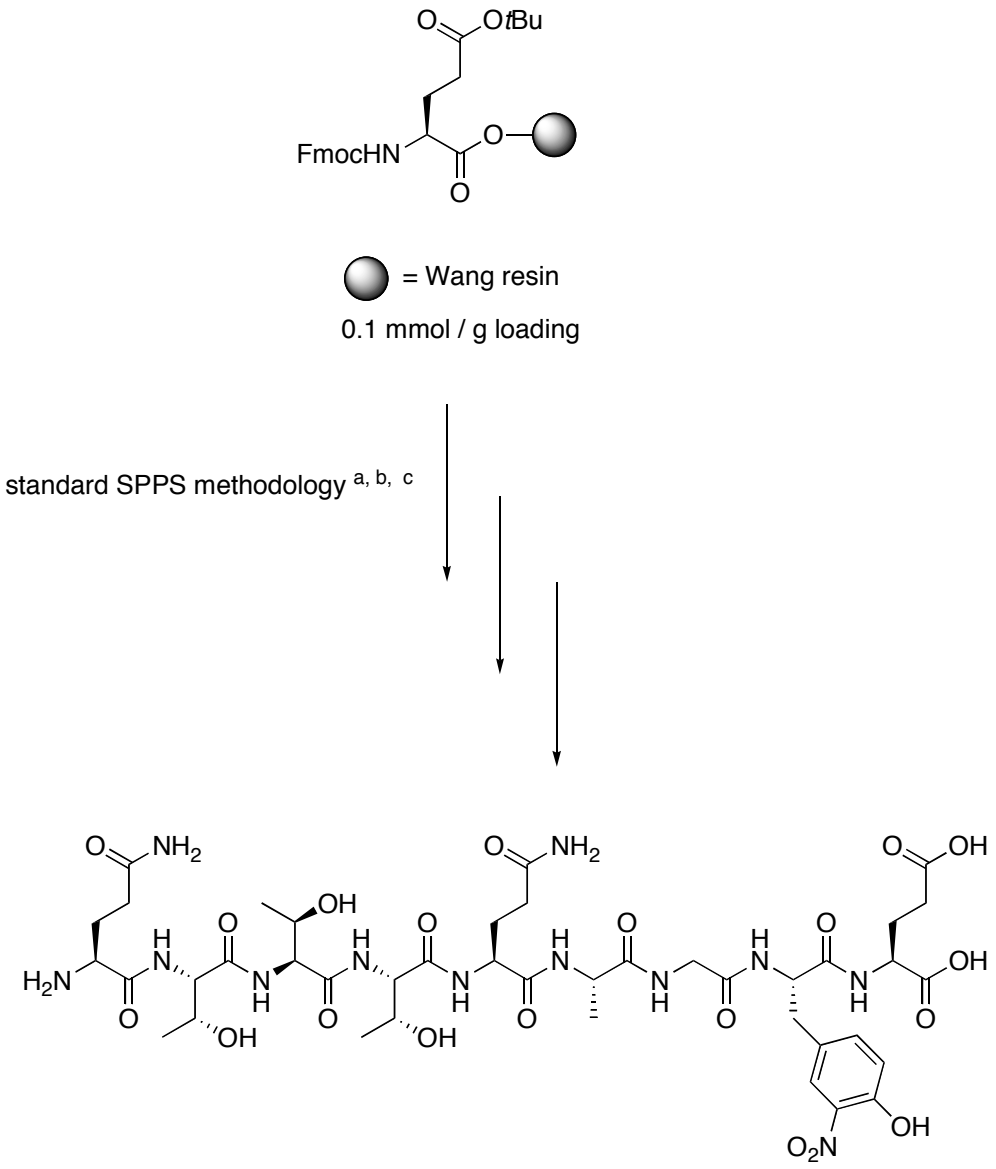

96

[a] Conditions used in the peptide synthesizer: (i) 22% piperidine in NMP, (ii) HBTU, HOBt, DIPEA, NMP, (iii) Fmoc-Tyr(NO_2)-OH [b] Repeat (i) and (ii) for amino acids; Fmoc-Gly-OH, Fmoc-Ala-OH, Fmoc-Gln(Trt)-OH, Fmoc-Thr(*t*Bu)-OH, Fmoc-Thr(*t*Bu)-OH, Fmoc-Thr(*t*Bu)-OH and Fmoc-Gln(Trt)-OH [c] (i) 20% piperidine in DMF, (ii) (95:2.5:2.5:) TFA / TIPS / H_2O

Coupling of the last residue 2-(Fmoc-amino)benzoic acid (Fmoc-Abz-OH) using benzotriazole-1-yl-oxy-trispyrrolidinophosphonium hexafluorophosphate (PyBOP) as the coupling reagent followed by cleavage from the resin with TFA / TIPS / H_2O affords the peptide. Analysis by MALDI-TOF MS revealed a major peak at 1184.4 ($[M+Na]^+$) for the desired product **95** in the positive mode as well as a peak at 1160.5 ($[M-H]^-$) in the negative mode along with another major peak, 238 Da higher than the desired product. Careful analysis suggested the mass of the undesired peak corresponds to the desired peptide plus two additional aminobenzoyl (Abz) units (Scheme 24). The desired product was then purified by reverse phase HPLC.

Scheme 24. Synthesis of CrPV peptide substrate **95** from **96**

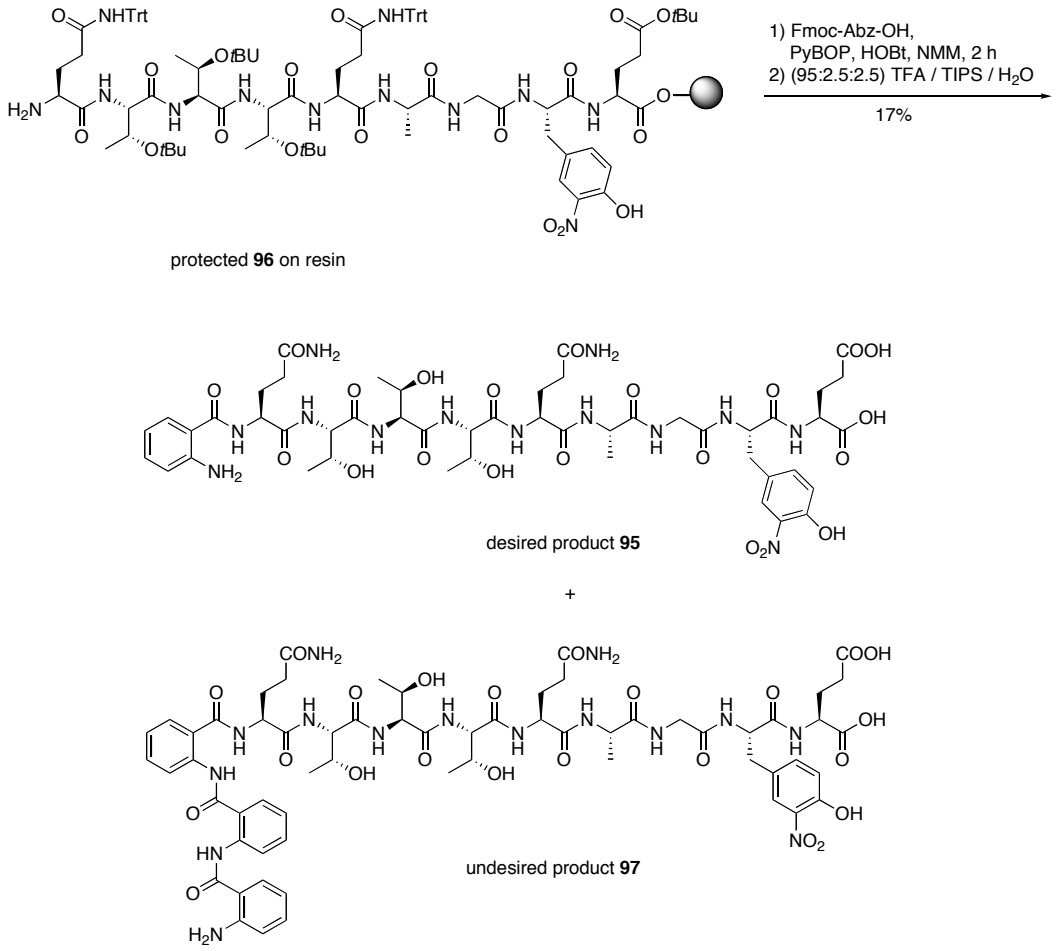

2.2.3 Israel acute paralysis virus (IAPV) peptide substrate

For the synthesis of an IAPV peptide substrate **98**, a strategy similar to the synthesis of **95** can be used. A commercial Wang resin preloaded with the C-terminal amino acid Fmoc-Asp(O*t*Bu)-OH is used. As described previously, using

an automated ABI 433A peptide synthesizer, the next eight residues are introduced in the order: Fmoc-Tyr(NO_2)-OH, Fmoc-Asp(O*t*Bu)-OH, Fmoc-Val-OH, Fmoc-Gln(Trt)-OH, Fmoc-Met-OH, Fmoc-Ser(*t*Bu)-OH, Fmoc-Val-OH and Fmoc-Glu(O*t*Bu)-OH. Removal of the N-terminal Fmoc group is effected with 20% piperidine. Cleavage of a small portion of the resin bound peptide with TFA followed by MALDI-TOF MS analysis reveals the precursor peptide **99** (Scheme 25). The remaining synthesis is done manually.

Scheme 25. Synthesis of precursor **99** for IAPV peptide substrate

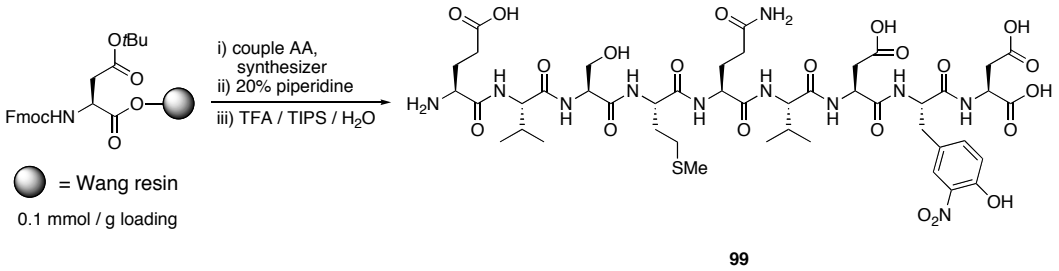

The peptide **99** is coupled to *N*-Boc-anthranilic acid (**132**, Boc-Abz-OH, 4 eq to resin) using PyBOP as the coupling reagent. Cleavage of a small sample with using (95:2.5:2.5) TFA / TIPS / H_2O and subsequent analysis by MALDI-TOF MS indicates none of the desired product. Interestingly, a major peak 238 Da higher in mass than the desired product is observed suggesting the formation of a peptide adduct **101** containing two aminobenzoyl units (Scheme 26). This analysis is further supported by NMR data. A higher ratio of aromatic protons

than would be expected for the product is observed in the NMR of crude material supporting the formation of peptide adducts with anthranilic acid. Initial unexpected results could be due to some mechanical errors in the peptide synthesizer. Also the coupling reagents and conditions used in the automated synthesizer are different from the ones used in manual synthesis. The solid phase synthesis is therefore used to manually introduce all of the residues using only 3 eq of *N*-Boc-anthranilic acid (**132**) in the final step to minimize the formation of Abz adducts. No product is seen in the analysis by MALDI-TOF MS but interestingly a peak with a mass 119 units higher than the desired product is observed along with some unreacted precursor **99**. Analysis of the undesired peak suggests the formation of the product adduct **100** with one additional aminobenzoyl unit attached (Scheme 26).

Scheme 26. Attempted synthesis of IAPV peptide substrate showing the formation of the undesired aminobenzoyl adducts.

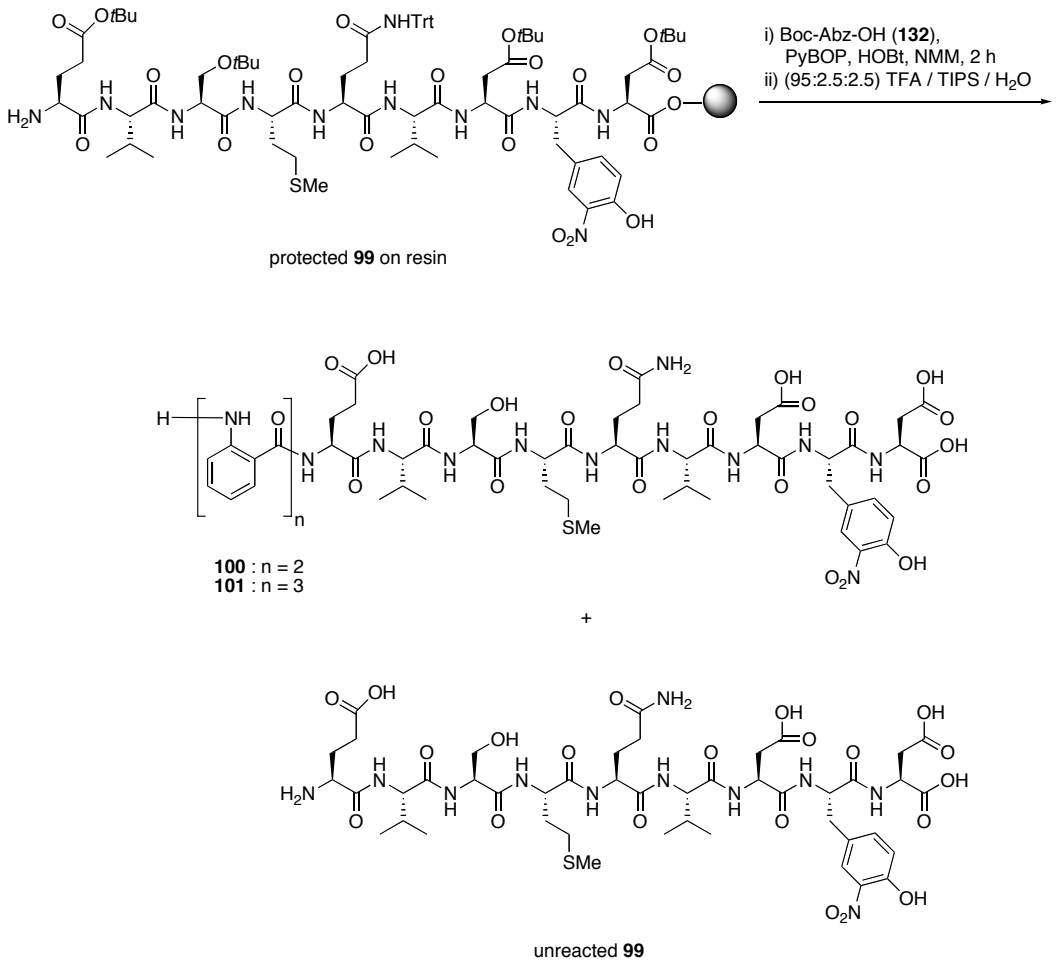

Similar results are observed when coupling reactions are run using reagents such as 1-hydroxybenzotriazole (HOBt) or using different coupling reagents such as diisopropyl carbodimide (DIC) and *O*-benzotriazole-N, N, N', N'-tetramethyl-uronium-hexafluorophosphate (HBTU). The Kaiser[74] test is used as a qualitative test for the presence or absence of free primary amino groups, and can be used to

ascertain the completeness of coupling reactions in solid phase peptide synthesis. The test gives a characteristic dark blue color in the presence of primary amines. Inconclusive test results are observed after coupling the last residue, either *N*-Boc-anthranilic acid or 2-(Fmoc-amino)benzoic acid, to the pre-made nonamer precursor peptide **99**. The beads are always blue colored indicating an incomplete coupling step. However, cleavage of a small sample of resin and analysis by MADI-TOF MS indicated the formation of product adducts **100** and **101** as before having one or two additional Abz units respectively along with unreacted precursor **99**. When the MALDI-TOF MS was run in negative mode, some desired product was observed along with the mono Abz adduct **100** and unreacted precursor **99**. Similar results were obtained when the samples were run using ES-MS in negative mode but no peaks were observed in the positive mode. Although the mechanism for the formation of the aminobenzoyl (Abz) adducts (**100** and **101**) is not clear at this point, one plausible mechanism (Scheme 27) could be proposed. In this mechanism under basic conditions, intramolecular attack of the carboxylate anion onto the carbamate carbonyl of anthranilic acid **102** could give the dione derivative **103**. Nucleophilic attack by the peptide N-terminus followed by elimination of carbon dioxide could generate a free amine **104**, which can couple to another anthranilic acid (Scheme 27).

Scheme 27. Proposed mechanism for the formation of Abz adducts

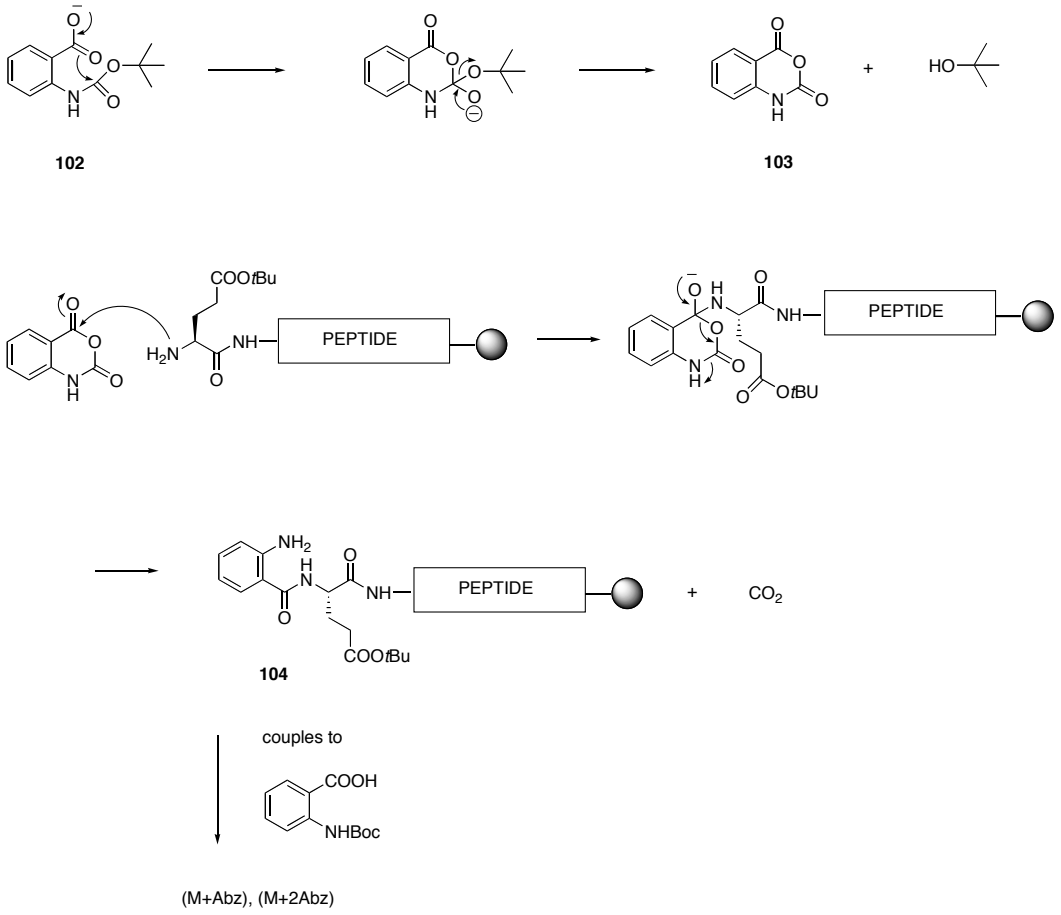

The fact that the product and product adduct peaks are seen in the negative ion mode is not surprising as the final peptide contains several acidic residues (a total of 4 acidic sites including the free C-terminal carboxylic acid). Efforts to purify the desired peptide substrate by HPLC were unsuccessful due to the overlap of product and several other undesired peaks. Some synthetic difficulties were also encountered during manual synthesis. During the monitoring of Fmoc deprotection by UV-Visible spectroscopy, several unusual peaks were observed

after the nitro tyrosine was introduced. The filtrate was yellow colored during deprotection steps suggesting loss of a peptide or part of the peptide during the solid phase assembly. One possible cause of peptide loss could be the formation of a diketopiperazine adducts leading to the loss of a di-peptide containing the nitro-tyrosine residue from the resin. The diketopiperazine formation is a well-known side reaction seen at the dipeptide stage in solid phase peptide synthesis with non-bulky resins (*e.g.* Wang resin) and is particularly observed in Fmoc based SPPS because of its mechanism. In order to confirm the diketopiperazine adduct formation at the dipeptide stage, a small sample of filtrate solution after Fmoc deprotection was submitted for ES-MS analysis. A peak at 402.1 ($[M+Na]^+$) in the positive mode and one at 378.1 ($[M-H]^-$) in the negative mode support the formation of this expected diketopiperazine adduct. A mechanism is proposed (Scheme 28).

Scheme 28. Plausible mechanism of cleavage of peptide via diketopiperazine adduct formation

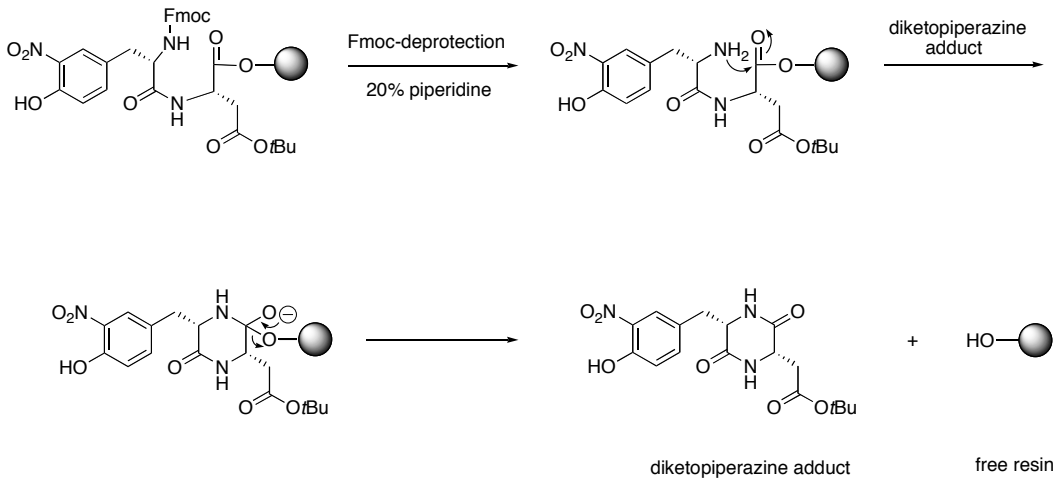

As discussed before, attempts to synthesize the IAPV peptide substrate **98** always led to the formation of peptide adducts **100** and **101** after coupling the last residue either *N*-Boc-anthranilic acid **(132)** or 2-(Fmoc-amino)benzoic acid. One way to avoid this problem could be to introduce the troublesome residue in the form of a dipeptide that could couple to a premade octamer **106** on resin. A retrosynthetic analysis of **98** is outlined in Scheme 29. Accordingly, the synthesis of an protected aminobenzoyl dipeptide **105** (Abz peptide) was undertaken (Scheme 30).

Scheme 29. Retrosynthetic analysis of **98**

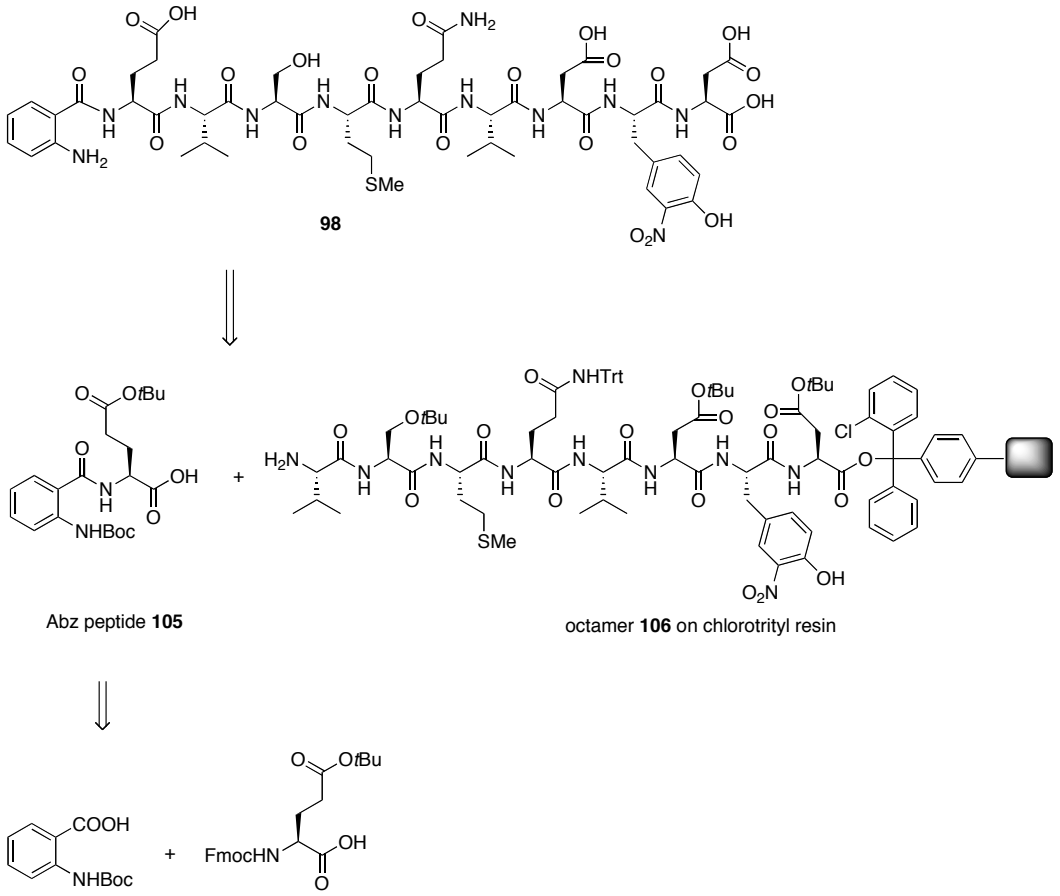

The first step towards the synthesis of **105** is the attachment of Fmoc-Glu(O*t*Bu)-OH onto the commercially available bulky 2-chlorotrityl chloride resin with a loading of 1.1 mmol/g. In the next step, the Fmoc group is removed with 20% piperidine in DMF and the resulting free amine is coupled to *N*-Boc-anthranilic acid using benzotriazole-1-yl-oxy-trispyrrolidinophosphonium hexafluorophosphate (PyBOP) as the coupling reagent to afford the protected peptide. Finally the dipeptide is cleaved from the resin using the mild cleavage cocktail (6:2:2) DCM / TFE / AcOH to afford the desired protected Abz dipeptide **105** as a white solid (Scheme 30).

Scheme 30. Synthesis of Abz peptide **105** on a 2-chlorotrityl chloride resin

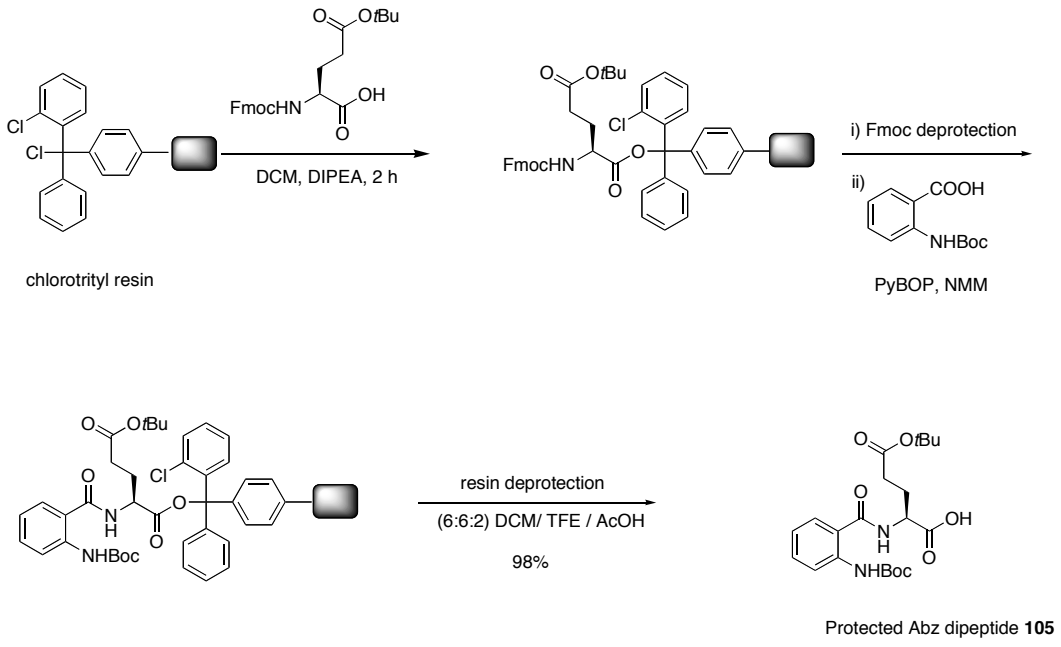

The precursor octamer peptide **106** was synthesized using an ABI 433A peptide synthesizer. A commercially available preloaded resin H-Asp(O^{t}Bu)-2-ClTrt with a substitution capacity of 0.77 mmol/g was used (Scheme 31). Following preswelling of the resin in NMP for 20 min, the amino acids are introduced in the order: Fmoc-Tyr(NO_2)-OH, Fmoc-Asp(O*t*Bu)-OH, Fmoc-Val-OH, Fmoc-Gln(Trt)-OH, Fmoc-Met-OH, Fmoc-Ser(*t*Bu)-OH and Fmoc-Val-OH. Global deprotection using (95:2.5:2.5) TFA / TIPS / H_2O followed by MALDI-TOF analysis indicated a peak at 1023.6 ($[M+Na]^+$) consistent with the calculated mass (1023.4 Da) of the desired precursor peptide **106** (Scheme 31).

Scheme 31. Synthesis of precursor peptide **106**

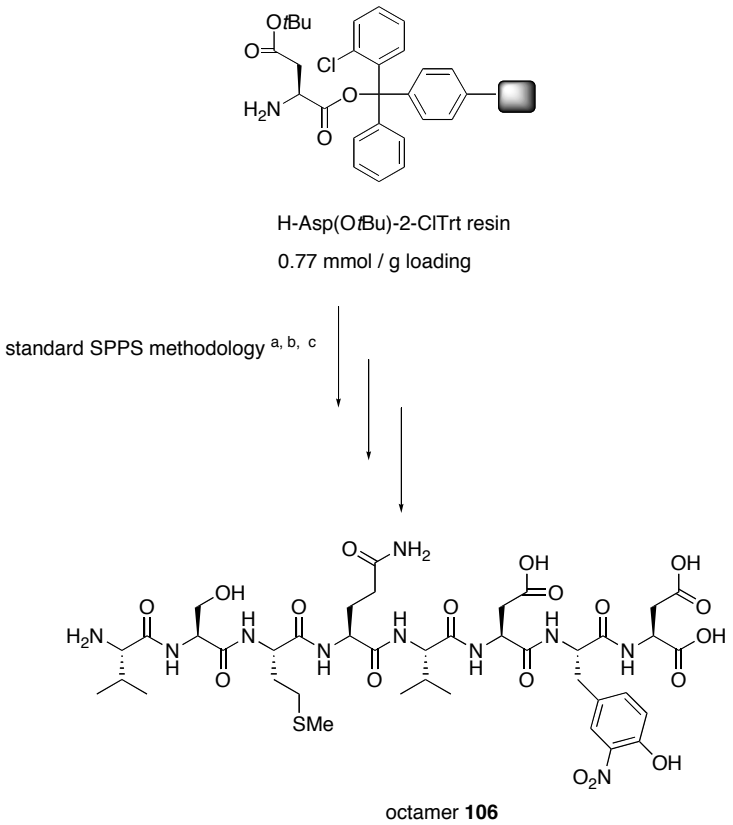

[a] Conditions used in the peptide synthesizer: (i) HBTU, HOBt, DIPEA, NMP, (ii) Fmoc-Tyr(NO_2)-OH, iii) 22% piperidine in NMP,; [b] Repeat (i) and (ii) and iii) for amino acids; Fmoc-Gly-OH, Fmoc-Ala-OH, Fmoc-Gln(Trt)-OH, Fmoc-Thr(*t*Bu)-OH, Fmoc-Thr(*t*Bu)-OH, Fmoc-Thr(*t*Bu)-OH and Fmoc-Gln(Trt)-OH [c] (95:2.5:2.5:) TFA / TIPS / H_2O.

The protected Abz peptide **105** was then coupled to the precursor octamer **106** on resin using PyBOP as the coupling reagent. Global deprotection using (95:2.5:2.5) TFA / TIPS / H_2O followed by MALDI-TOF MS analysis indicates a peak at 1271.7 Da ($[M+Na]^+$) consistent with the calculated mass (1271.5 Da) of the

desired peptide **98** (Scheme 32).

Scheme 32. Final synthesis of **98**

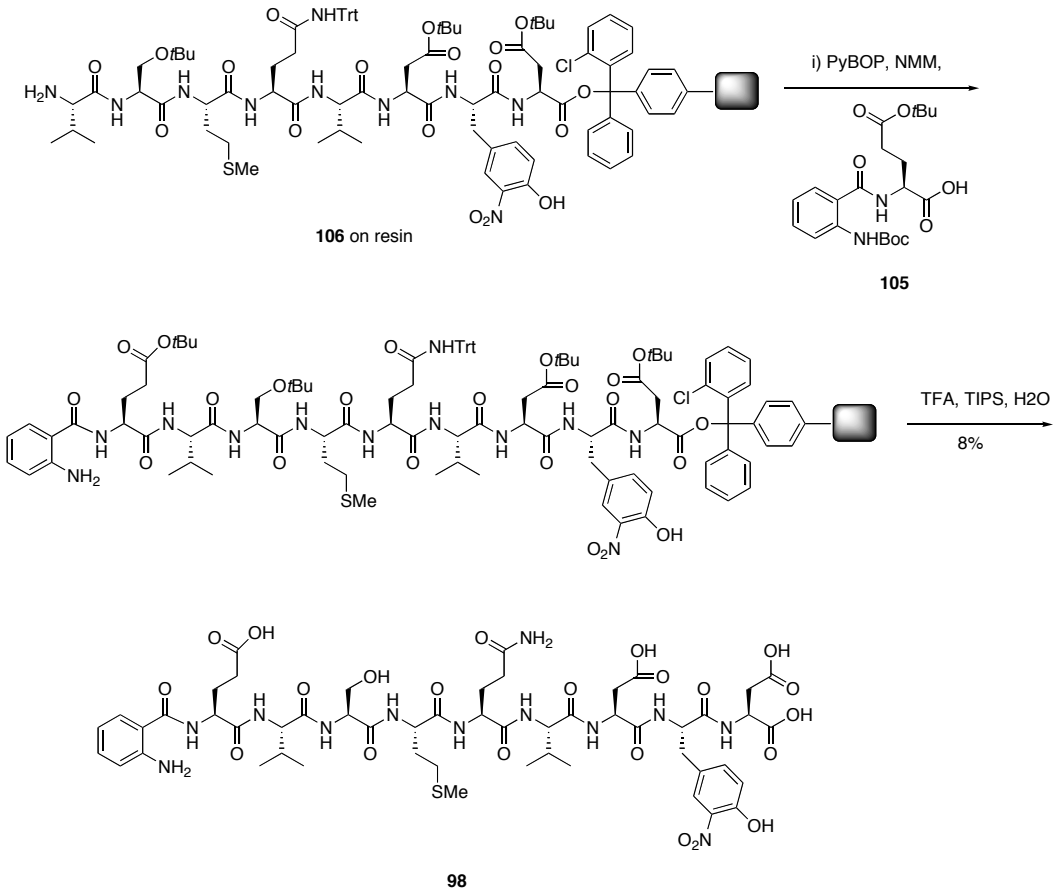

No Abz adducts (**100** and **101)** were observed and the desired product **98** was purified by reverse phase HPLC. Our collaborators at UBC tested the peptide substrates against CrPV and IAPV $3C^{pro}$. Unfortunately no activity was observed. The reason for this is not clear for CrPV $3C^{pro}$. However for IAPV, mass spectrometry analysis of a portion of replicase including $3C^{pro}$ identified a peptide

TPIVIE that could correspond to the 3A/3B cleavage site in the IAPV replicase.[70] This peptide containing a Glu suggests that Gln may not be a correct choice for cleavage by IAPV $3C^{pro}$.

2.2.4 Conclusions and future work

Two fluorescent peptide substrates for IAPV and CrPV were designed and synthesized. Plausible mechanisms for the formation of diketopiperazine and Abz adducts along with some spectroscopic evidence are presented. A strategy was developed in which the use of a pre-made aminobenzoyl dipeptide **105** (Abz peptide) eliminated the formation of Abz adducts and could possibly be applied to the synthesis of internally quenched fluorescent peptides containing *ortho*-aminobenzoic acid as the donor. Although no activity was observed with the peptide substrates **95** and **98**, proper identification of cleavage sites may help in the design of better inhibitors. A peptidyl fluoromethyl ketone based on the SARS-CoV $3CL^{pro}$ recognition tripeptide was successfully synthesized. The testing of its biological activity is in progress. The fluoromethyl ketone was also tested against SARS $3CL^{pro}$ and displays very good inhibition (95%). In the future, these peptides can also be tested against other insect picorna-like 3C proteases including the highly virulent CrPV that causes the paralysis and death of insects. Enzymatic and crystallographic studies of these inhibitors could provide further insights in understanding the inhibition mechanism.

CHAPTER 3. ASYMMETRIC REDUCTION OF PSEUDOXAZOLONES

3.1 INTRODUCTION

Amino acids are critical to life and play important roles both as building blocks of proteins and as intermediates in protein metabolism. There are 21 natural protein amino acids including selenocysteine and most of them are found in their optically pure form. The vast majority of amino acids found in proteins are L-amino acids.

3.1.1 Asymmetric synthesis of alpha-amino acids

Asymmetric synthesis of amino acids has been the subject of intense study for synthetic chemists because of their extensive use in pharmaceuticals, agrochemicals and their applications as chiral ligands. Earlier methods of preparing optically pure amino acids relied on enzymatic resolution of racemic amino acids.[75,76] However, with the advancement of synthetic organic chemistry, many approaches[77,78] have been developed for the synthesis of chiral α-amino acids (Scheme 33). Some of these include (A) Schollkopf's bis-lactim ethers,[79,80] (B) Seebach's cyclic aminals,[81] (C) Williams oxazinone,[82] (D) Evans oxazolidinone,[83] (E) asymmetric Strecker reaction[84] and (F) asymmetric hydrogenation of dehydroamino acids (Noyori).[85]

Scheme 33. Synthetic approaches toward chiral α-amino acids

32A. Schollkopf's bis-lactim ethers

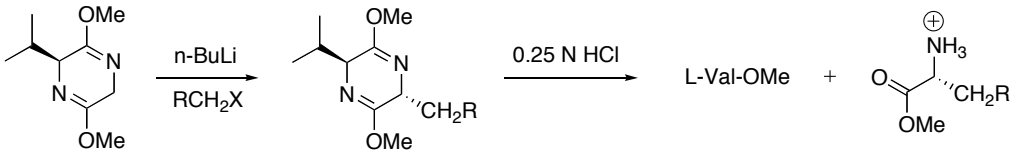

32B. Seebach's cyclic aminals

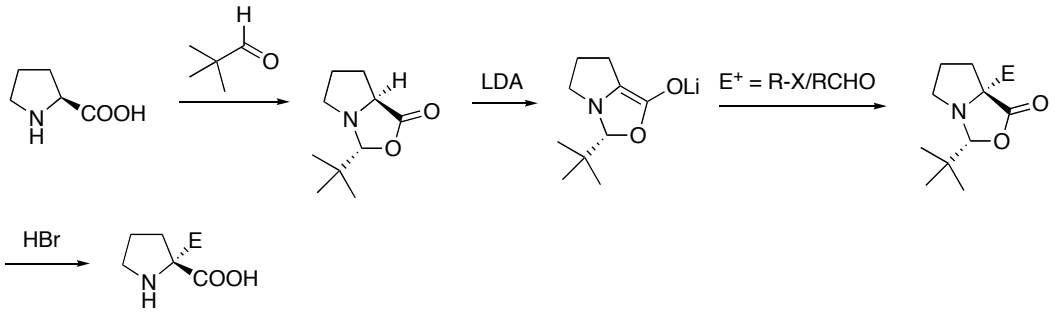

32C. Williams oxazinone

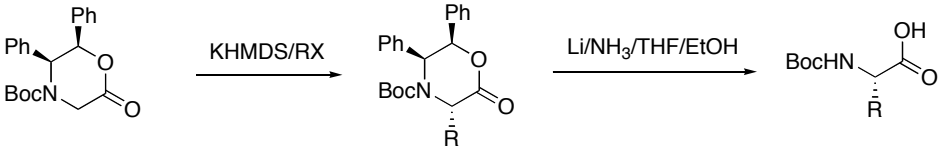

32D. Evans oxazolidinone

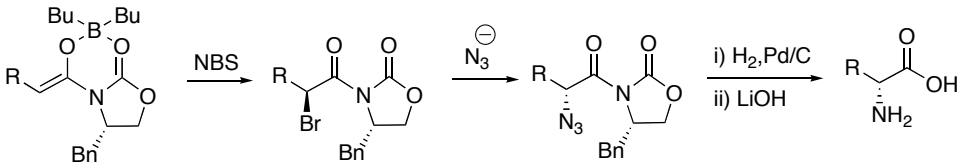

32E. Asymmetric Strecker reaction

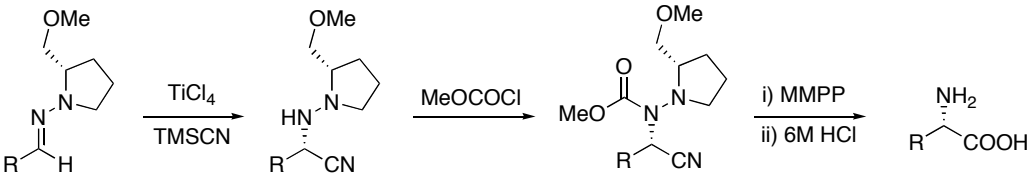

MMPP = Magnesium monoperoxy phthalate

32F. Asymmetric hydrogenation of dehydroamino acids

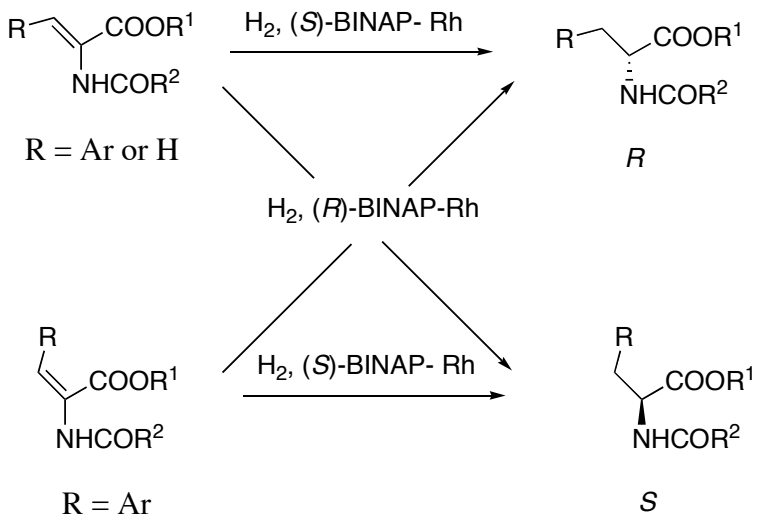

Although the synthetic routes given above are available for the preparation of optically pure amino acids, asymmetric reduction is considered one of the best methods in the literature. There are a number of advanced precursors, which can be subjected to asymmetric reduction for this purpose, including imines and dehydroamino acids. One interesting class of compounds that contains imine functionalities is the pseudoxazolones (or 3-oxazoline-5-one) (Figure 37), which could be amenable to asymmetric reduction. These heterocyclic compounds are also explored in the literature as building blocks to synthesize a variety of organic molecules.

Figure 37. General structure of pseudoxazolone (unsaturated)

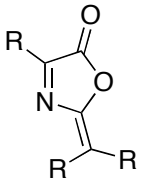

They have also been explored by our group as inhibitors of cysteine proteases.[62,72,86] Several methods for asymmetric reduction of imines have been developed. Some of them use a variety of transformations such as the (a) asymmetric transfer hydrogenation of imines with chiral Rh complexes with diamine ligands,[87,88] (b) hydrogenation in the presence of chiral Ir diphosphine complexes,[89] (c) asymmetric hydrosilylation[90] and (d) oxazaborolidine-mediated asymmetric reduction of an imine using borane-THF as the reducing agent.[91] Since pseudoxazolones are prepared in high yields from simple racemic amino acid precursors, asymmetric reduction could be employed to generate either of the desired enantiomers.

There are a number of unnatural or nonprotein amino acids, such as homocysteine, thyroxine, gamma-aminobutyric acid (GABA), L-DOPA (3,4-dihydroxy phenyl L-alanine) and L-citruline, are found in several natural products and various synthetic drugs. Furthermore, nonprotein amino acids could be used for preparing synthetic enzymes, hormones and peptide based drugs. In the area of protein engineering, non-protein amino acids can be incorporated into proteins for studying protein structure and function. This has led to increased interest in developing synthetic methodologies to prepare such amino acids. Asymmetric reduction of pseudoxazolones may also provide a way to prepare nonprotein amino acids, which could be precursors for the synthesis of such compounds mentioned above.

3.1.2 Objectives: Asymmetric reduction of pseudoxazolones

Our group has hypothesized that an asymmetric reduction strategy of pseudoxazolones followed by ring opening could generate optically pure amino acids (Scheme 34). This approach could be applied to various substrates to yield amino acids with different substituents at the alpha-position.

Scheme 34. Approach for the synthesis of enantiopure aminoacids

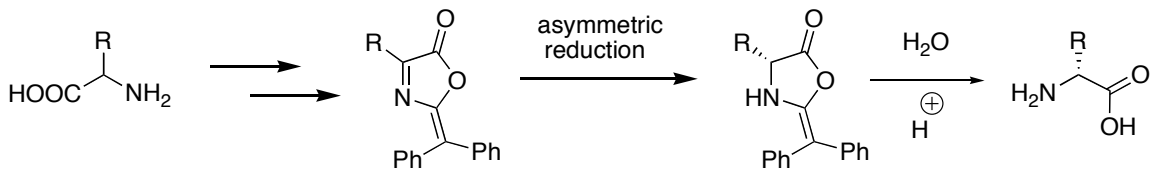

It is also postulated that the reactivity of imine may provide an oppurtunity for nucleophilic addition to install various groups at the alpha position. Therefore, another proposed approach is to synthesize pseudoxazolone derivatives with increased reactivity at the imine carbon. This could facilitate the addition of nucleophiles thereby providing access to new, unnatural amino acids (Scheme 35).

Scheme 35. Approach for making new amino acids

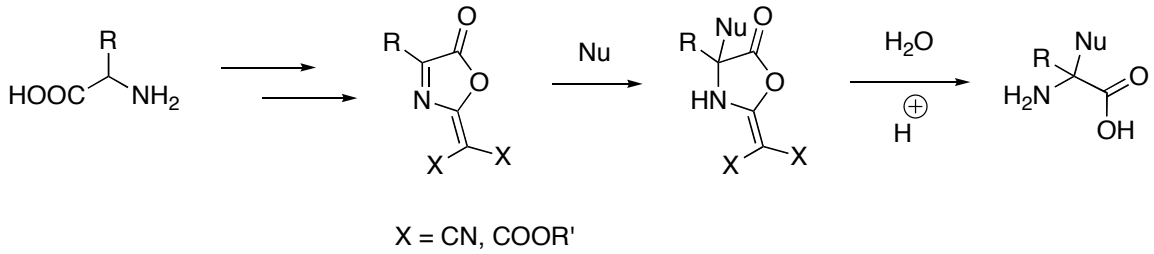

3.2 RESULTS AND DISCUSSION

For the asymmetric reduction, diphenyl pseudoxazolone was chosen as the model substrate since it can be easily prepared in high yields from simple amino acids. The diphenyl pseudoxazolone is prepared using a modified literature procedure established in our group (Scheme 36).[92] Commercially available alanine, **107** reacts with 2-chloro-2,2-diphenylacetyl chloride in the presence of propylene oxide as an acid scavenger to give the chloro-adduct **108**, which is then cyclized with trifluoroacetic anhydride followed by elimination of HCl to afford the desired pseudoxazolone **109**.

Scheme 36. Synthesis of pseudoxazolone

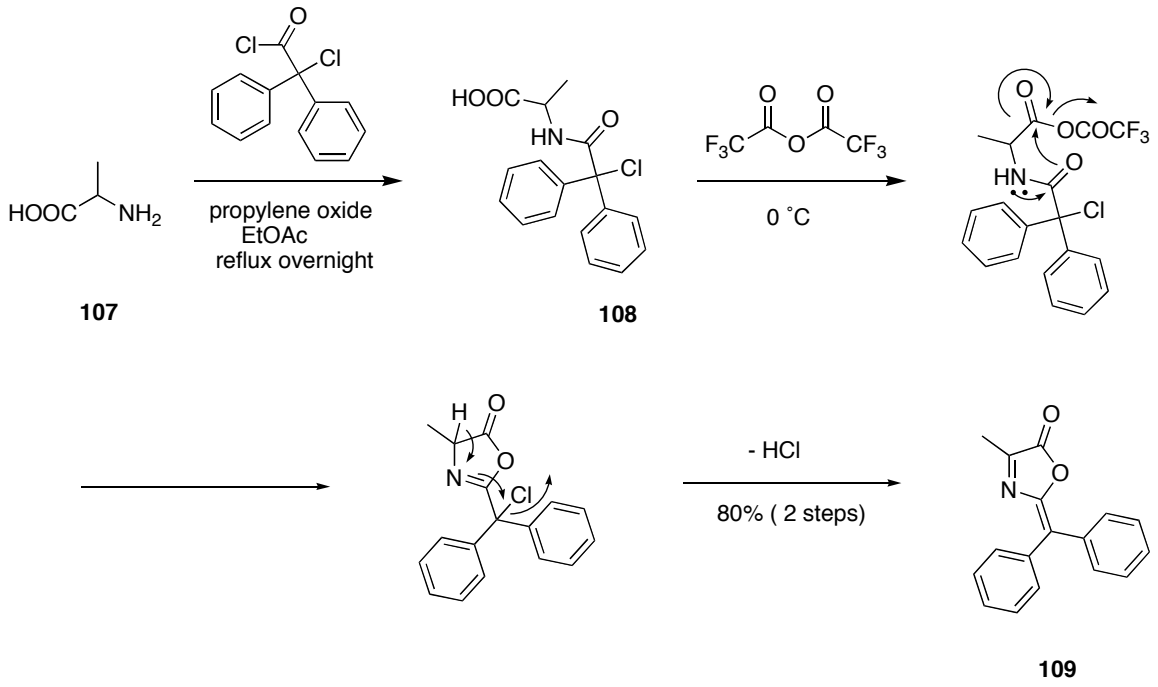

3.2.1 Reactions attempted

It is known that treating alanine diphenyl pseudoxazolone (**109**) with $NaBH_4$ in MeOH results in reduction of the imine functionality with simultaneous ring opening providing the methylated ester derivative **110**. Similar results are observed with sodium cyanoborohydride (Scheme 37).

Scheme 37. $NaBH_3CN$ reduction of alanine diphenyl pseudoxazolone

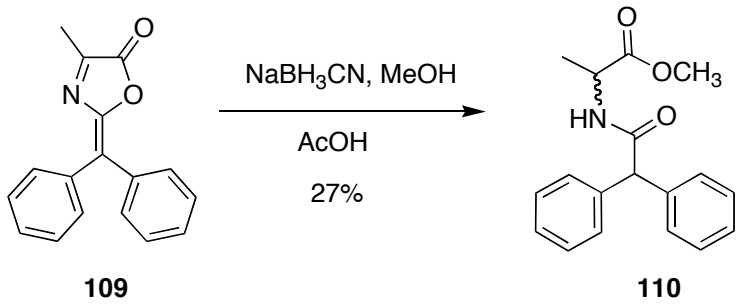

The initial results suggest that reduction of the pseudoxazolone is a feasible strategy; however, this strategy provides a racemic mixture of products. In order to do the same reaction to afford a selected enantiomer, the pseudoxazolone **109** was subjected to asymmetric reduction using several reaction conditions. Efforts to reduce the imine functionality of diphenyl pseudoazolone **109** by Dr. Nathaniel Martin, a former graduate student in our group, with several imine reducing agents, have failed.[92] Accordingly, some carbonyl reduction conditions along with a chiral Ru catalyzed asymmetric transfer hydrogenation that was developed for imines, were used. The results are tabulated (Table 5).

Table 5. Reduction reactions attempted with diphenyl pseudoxazolone **109**

Catalyst / Ligand / Reagent	Conditions	Solvent	Results
Asymmetric transfer hydrogenation			
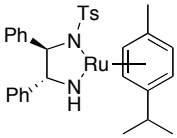	a) rt,isopropanol 24 h b) 60 ˚C isopropanol 24 h / 48 h	isopropanol	no reaction recovered substrate
Asymmetric hydrogenation			
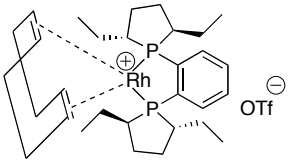	a) H_2, 55 psi, rt, 48 h	a) MeOH	recovered substrate
	b) H_2, 400 psi, 42 ˚C 24 h	b) EtOAc	recovered substrate
	c) H_2,100 psi, 50 ˚C 24 h	c) MeOH	recovered substrate and 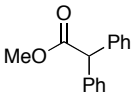 **111**
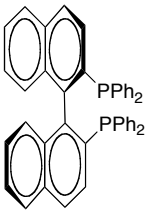 *R* - BINAP Pd(II)trifluoro acetate	a) H_2, 1500 psi rt 24 h b) H_2, 400 psi 40 ˚C 30 h	CF_3CH_2OH	no reaction recovered substrate
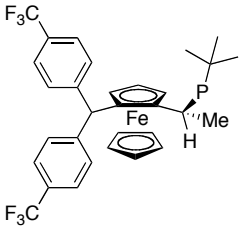 chiral ligand	a) chloro(1,5-cyclo octadiene)Rh(I) dimer, H_2, 100 psi, rt, 24 h	MeOH	no reaction recovered substrate

Table 5 (continued)

Catalyst / Ligand / Reagent	Conditions	Solvent	Results
Boron reducing agents Lithium triethyl borohydride (super hydride)	a) 0 ˚C, 20 min b) - 70 ˚C, 20 min	THF	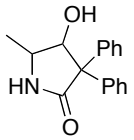 **112**
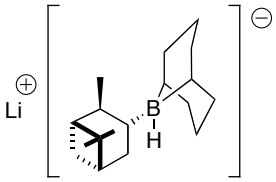 *R*-Alpine-Hydride	- 30 ˚C, 5 min	THF	complex mixtures
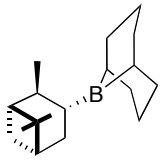 *R*-Alpine-borane	rt, 20 h	THF	starting compound and complex mixtures
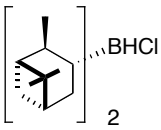 DIP-Cl	rt, 42 h	THF	starting compound and complex mixtures

In most cases, the reactions provide either starting materials or a complicated mixture of products (Table 5). Reduction seen in some cases (*e.g*. $NaBH_3CN$) is also accompanied by ring opening. In some cases ring cleavage is observed to give compound **111**. Strong reducing agents such as superhydride provided the

undesired amide derivative **112**. The formation of **112** instead of the expected lactol derivative was somewhat surprising. Analysis suggested the lactol derivative that could form in the beginning of the reaction is unstable and could rearrange to the more stable amide derivative **112**. A reasonable mechanism could be proposed (Scheme 38).

Scheme 38. Proposed mechanism for the formation of **112**

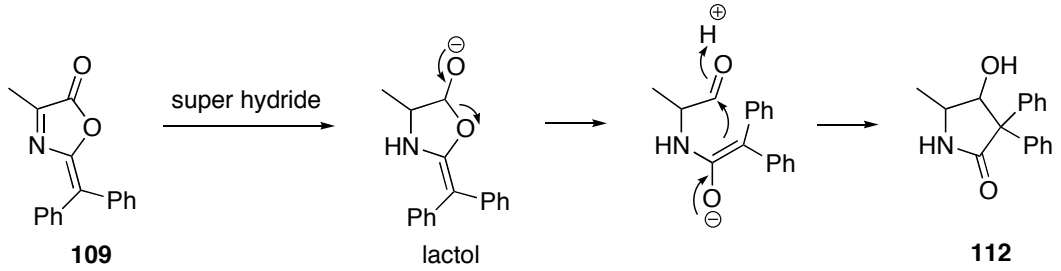

The above reduction results indicate that pseuodoxazolones are much less reactive than the carbonyl and imine counterparts. The reason for this lack of reactivity towards several reducing agents could be attributed to the imine functionality being part of an extensive conjugated system.

As the efforts of reducing diphenyl pseudoxazolone were unsuccessful, an attempt to synthesize analogs with increased reactivity at the imine carbon was undertaken.

3.2.2 Preparation of 2-dichloromethylene pseudoxazolone

The 2-dichloromethylene pseudoxazolone **113**, which can be the precursor for the 2-dicyano **114** and di-ester **115** derivatives (Scheme 39), can be prepared according to a literature procedure.[93]

Scheme 39. Structures of **113, 114** and **115**

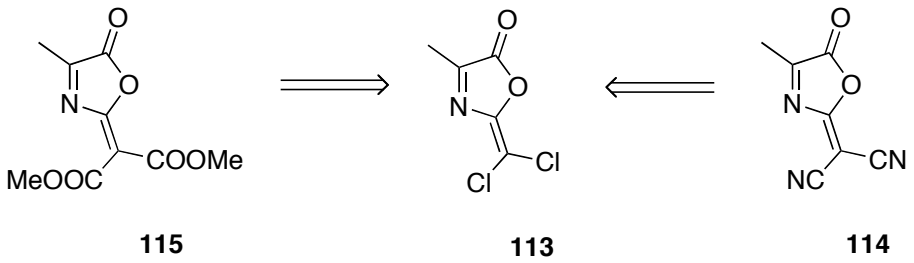

Treatment of trichloroacetyl chloride **116** with phenol under refuxing conditions affords phenyl trichloroacetate **117,** which reacts with alanine **107** to afford the corresponding amide derivative **118**. Compound **118** can be activated with phosphorous oxychloride followed by cyclization to provide the trichloro adduct, which spontaneously loses HCl to give the desired product **113** (Scheme 40).

Scheme 40. Synthesis of 2-dichloromethylene pseudoxazolone (**113)**

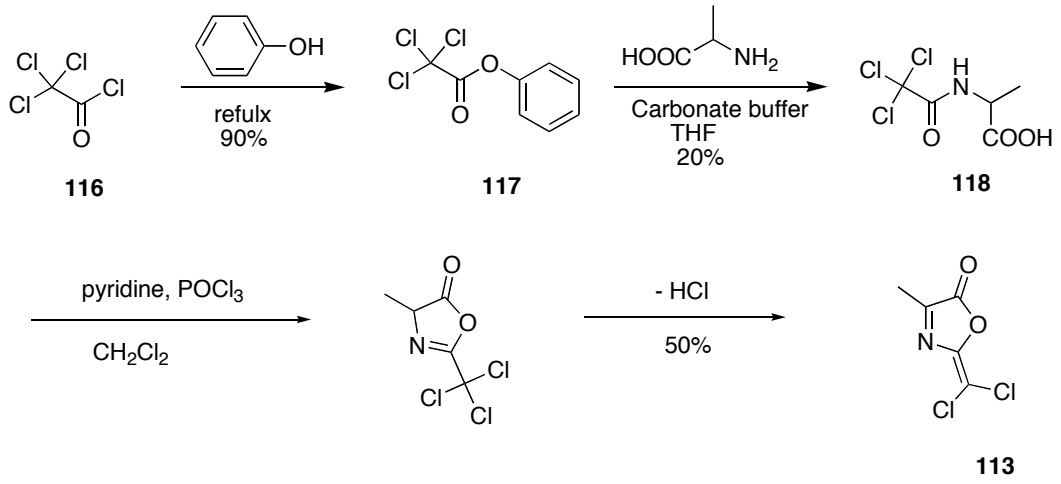

3.2.3 Attempts to synthesize 2-dicyano and 2-dimethyl ester analogs of pseudoxazolones

In order to synthesize dicyano **(114)** and diester (**115**) analogs, 2,2-dichloromethylene pseudoxazolone (**113)** is used as the precursor. Initial attempts to prepare dicyano analog using either sodium or potassium cyanide gave a complex mixture of decomposed products presumably through nucleophilic reactions of cyanide at several possible electrophilic sites (Scheme 41).

Scheme 41. Attempts to synthesize 2-dicyano analogue **114**. Also shown are possible sites of attack

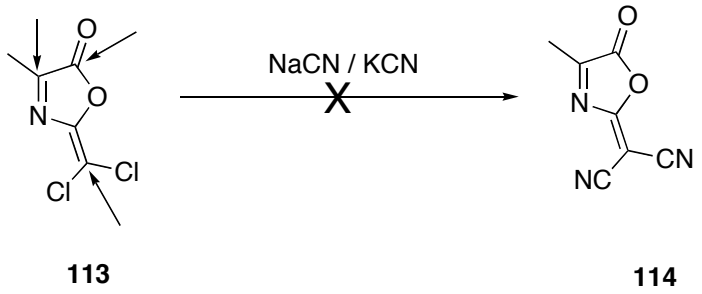

NMR stability studies on 2,2-dichloromethylene pseudoxazolone (**113**) were done to evaluate the stability of the substrate. Compound **113** decomposes in about 4 hours in aqueous media. These findings suggest that compound **113** is unstable and nucleophilic substitution at a selected site may not be possible. As the attempts to prepare the cyano derivative failed, we then shifted our focus to prepare the diester analog **115**. In order to prepare the ester analogue **115**, commercially available dimethyl bromomalonate could be used as a starting material. A retrosynthetic analysis is outlined in Scheme 42.

Scheme 42. Retrosynthetic analysis of **115**

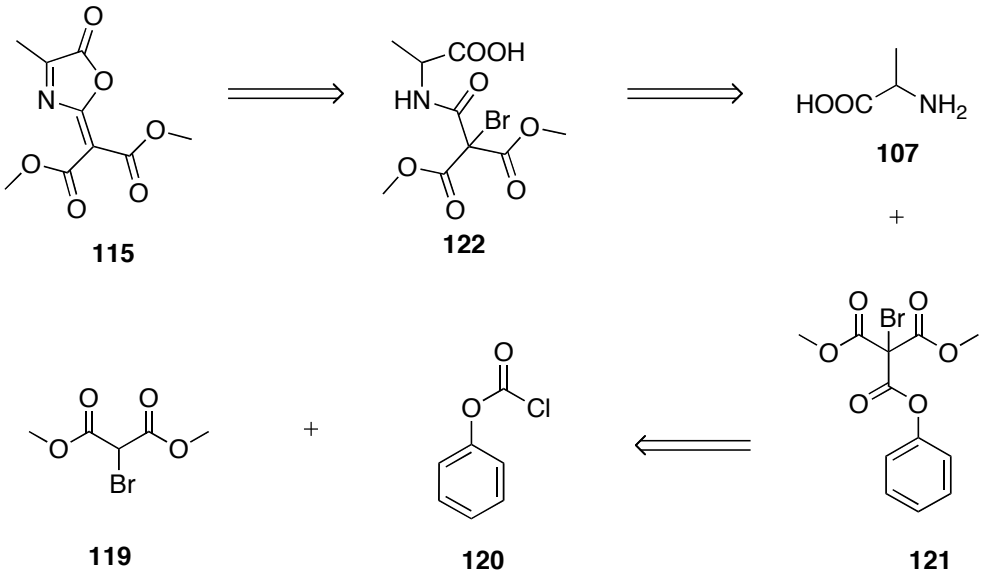

Treatment of **119** with phenyl chloroformate fails to provide the desired bromo tricarboxylate derivative **121** (Scheme 43). Interestingly formation of tetrasubstituted olefin **123** is observed.

Scheme 43. Attempts to synthesize **121**

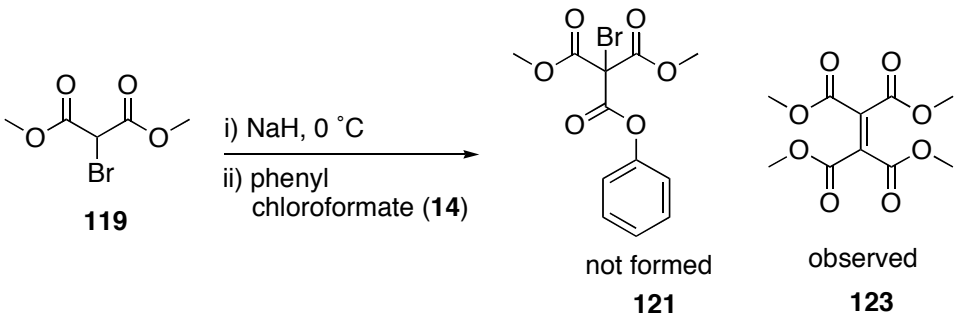

A mechanism can be proposed for the formation of tetrasubstituted olefin **17** (Scheme 44).

Scheme 44. Proposed mechanism for the formation of **123**

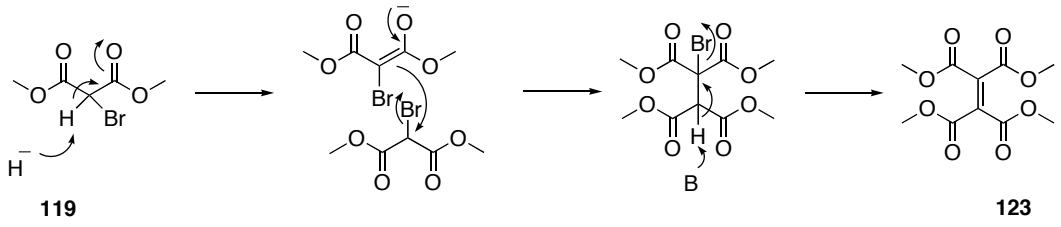

In an alternative strategy, an enolate of malonate **124** is treated with phenyl chloroformate to provide the triester derivative **125**. Bromination of **125** gives the desired bromo derivative **121** in 90% yield (Scheme 45).

Scheme 45. Alternative strategy showing the synthesis of **121**

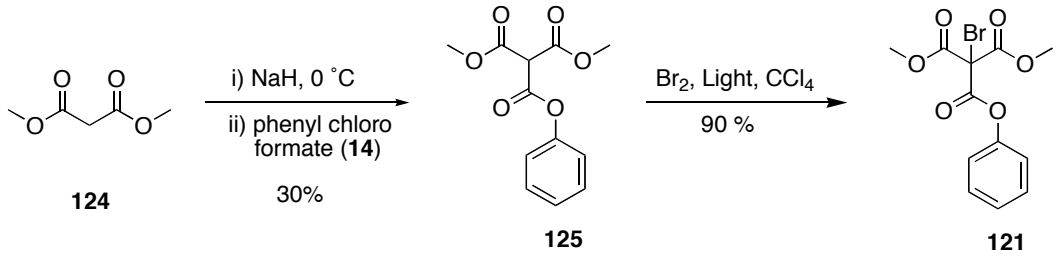

Attempts to prepare the amide derivative **122** under buffered (pH 8.0) or refluxing conditions failed and led to the generation of the debromo derivative **125** and alanine (**107**) (Scheme 46).

Scheme 46. Attempted synthesis of **122**

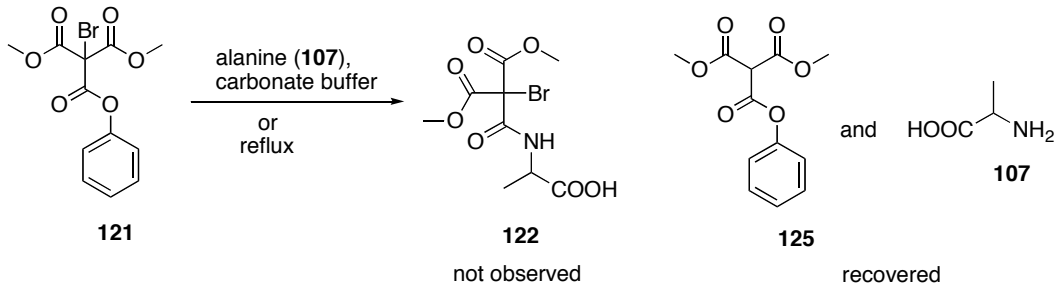

In the above reaction, it is possible that loss of a bromine atom generates a highly stabilized radical system that combines with a hydrogen atom to give the debrominated derivative **125** (Scheme 47). Alternatively, the bromine in **121** could be attacked by a nucleophile (OH^- ?) to give a highly stabilized anion. This could then be protonated.

Scheme 47. Possible debromination mechanism

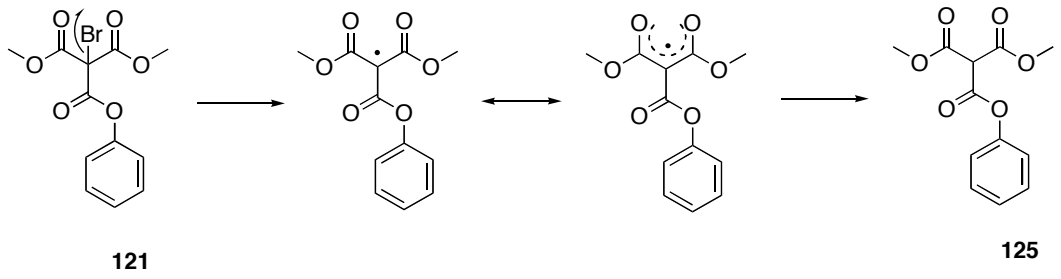

As the efforts to make analogs with increased reactivity were not successful, an attempt was made to add two nucleophiles to the available diphenyl **109** and

dichlro pseudoxazolone analog **113**. Both allyl iodide and trimethylsilyl cyanide were tested but without success. This could be attributed to the presence of a highly conjugated system in **109** (Scheme 48).

Scheme 48. Attempts of Nucleophilic additions on **109** and **113**

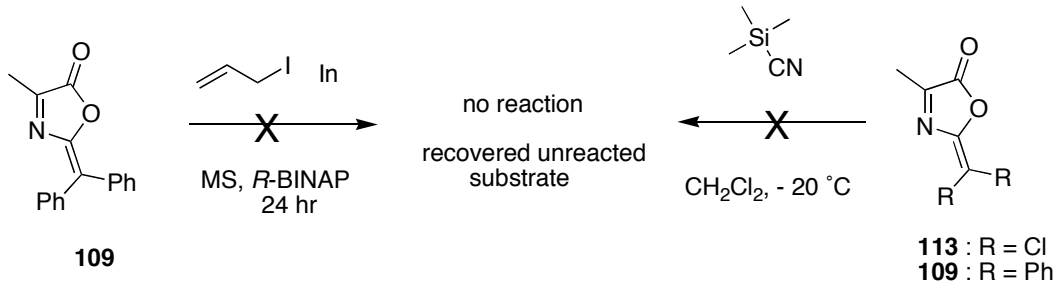

From earlier reactions, one of the observed side products during the attempted synthesis of **121** is an olefin **123**. As the olefin **123** is symmetrical and heavily substituted, we decided to briefly explore this chemistry to synthesize some functionalized olefins. Treatment of commercially available dimethyl bromomalonate **119** with sodium hydride provides the symmetrically functionalized olefin **123** in 60% yield (Scheme 49).

Scheme 49. Preparation of tetrasubstituted olefin **123**

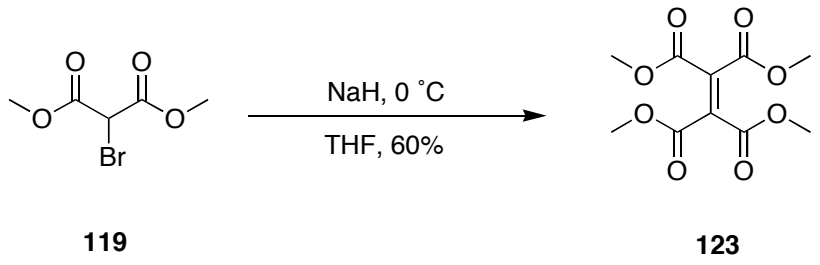

These results suggest that similar methods could be used to synthesize unsymmetrically substituted olefins. Slow addition of diethyl bromomalonate **126** to the sodium enolate of dimethyl fluoromalonate **127** affords 1,1-diethyl-2,2-dimethyl ethane-1,1,2,2-tetracarboxylate (**128)**, an unsymmetrically substituted olefin. To the best of our knowledge, there is only one literature precedent[94] in which **128** was observed during studies on the effects of pi-electron accepting substituents in thiiranes. Efforts to optimize the reaction conditions gave a maximum yield of 20%. The low yield can be attributed to the dehalogenation of the starting compounds and other side products indicated by mass spectrometry (Scheme 50).

Scheme 50. Synthesis of unsymmetrically substituted olefin **128**

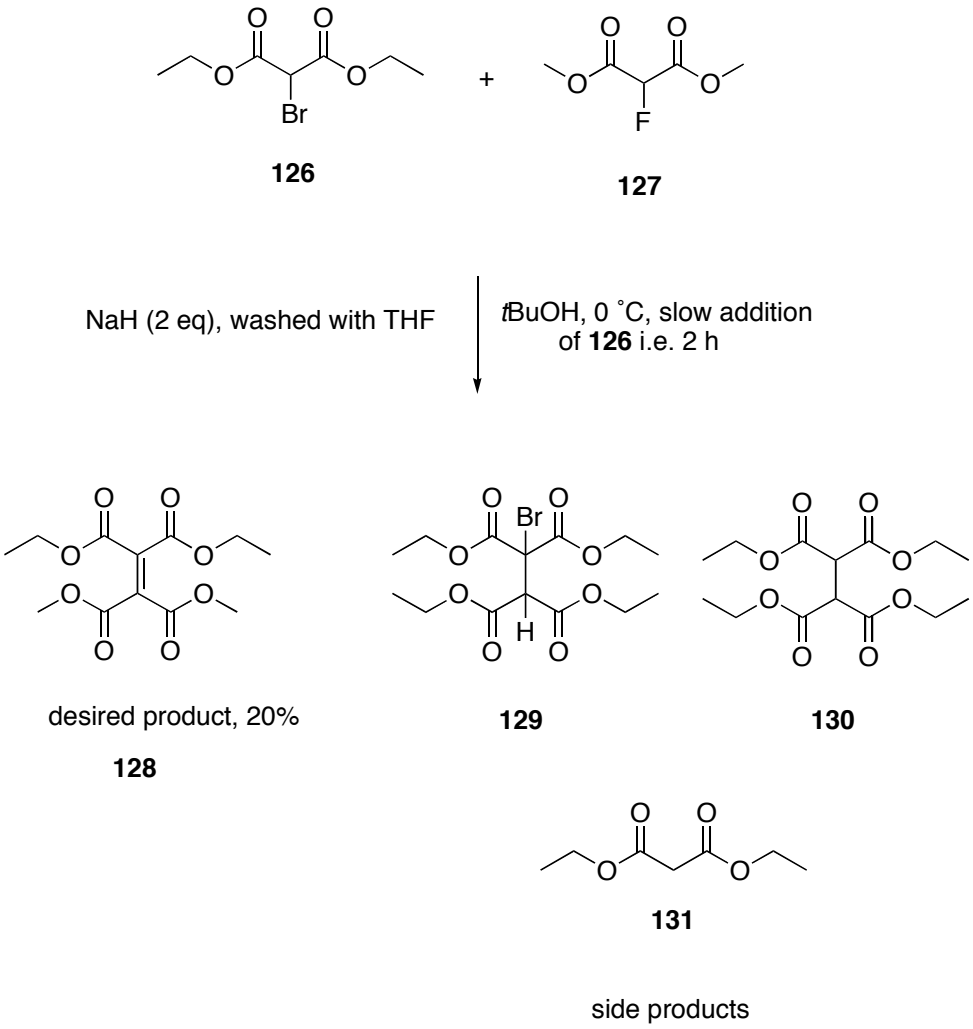

3.2.4 Conclusions and future direction

Several conditions were used in an attempt to reduce pseudoxazolones but without success and this could be due to the stability of the imine as part of a highly conjugated system. The formation of a tetrasubstituted olefin as one of the by products has led to the development of a methodology to prepare highly substituted olefins such as **17** and **22**. These methods could possibly be developed to synthesize symmetrical and unsymmetrical olefins.

CHAPTER 4: BIOSYNTHETIC STUDIES ON SUBTILOSIN A

4.1 INTRODUCTION

Subtilosin A is an antimicrobial peptide produced by the Gram-positive soil bacterium *Bacillus subtilis*.[95] It is anionic in character, resistant to proteolysis and stable to moderate heat and mildly acidic conditions. Subtilosin A is classified as a bacteriocin. Bacteriocins are defined as antimicrobial peptides produced by bacteria that inhibit the growth of similar or closely related bacterial strains.[96,97] Bacteriocins are generally cationic and mostly 35 to 78 amino acids in length.[98] Colicin from *Escherichia coli* was first detected in 1925 as an antimicrobial substance.[99] These small, gene-encoded and ribosomally produced bacteriocins are biosynthesized as precursors that often undergo posttranslational modifications during maturation to yield biologically active peptides.[100]

There are several classification schemes and revisions available for bacteriocins.[101-103] The classification scheme proposed by Cotter *et al*.[104] divides bacteriocins into two distinct categories: Class I includes lantibiotics that are highly posttranslationally modified and contain characteristic cyclic thioether amino acids such as lanthionine or β-methyl lanthionine; Class II includes non-lantibiotic bacteriocins. Circular bacteriocins[105,106] that undergo posttranslational modifications for cyclizing their N- and C-termini are included in class II. Unlike other non-lantibiotic bacteriocins, subtilosin A is anionic and extensively

posttranslationally modified. Subtilosin A is synthesized as a precursor peptide consisting of 43 amino acids including a very short (compared to some bacteriocins)[100,107] eight amino acid leader peptide. The mature product could be formed by the loss of the leader peptide, cyclization of the N- and C-termini and formation of unusual cross-links between the cysteine sulfurs and alpha-carbons of phenylalanines and a threonine (Figure 38A & 38B).[108]

Figure 38A. Amino acid sequences of presubtilosin and subtilosin **A**. Backbone cyclization between the N- and C- termini is shown by a solid line. Positions of sulfur to α-carbon linkages are indicated by solid lines

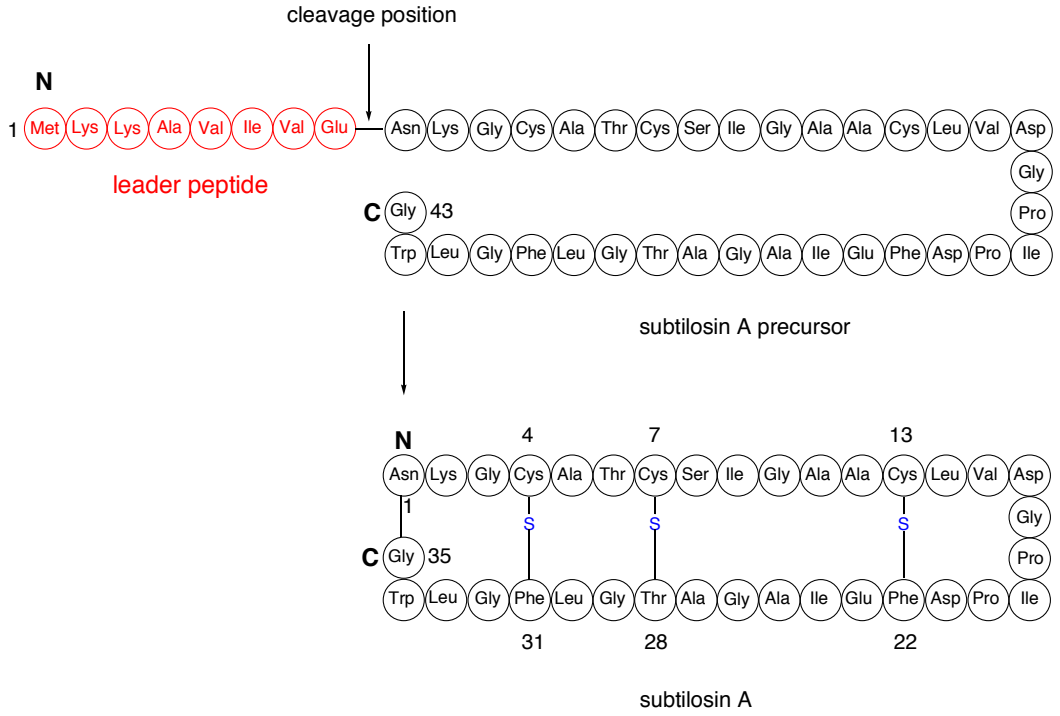

Figure 38B. Cross-link between cysteine sulfur and α-carbon in phenylalanine. The stereochemistries are predicted by NMR analysis. [109,108]

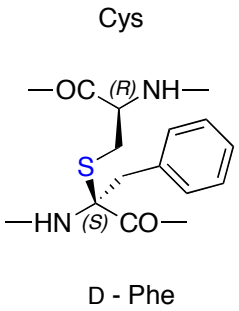

These sulfur to alpha-carbon cross-links are necessary for its antimicrobial activity.[109] Such unique, posttranslationally formed thioether bridges are unprecedented in ribosomally synthesized peptides and proteins, suggesting that subtilosin A is atypical and could be regarded as a new class of bacteriocins.[108] There is only one known example of sulfur to alpha-carbon thioether linkages in nonribosomally synthesized peptides, namely cyclothiazomycin (Figure 39), a natural product with renin inhibitor activity that was isolated from *Streptomyces* species NR0516.[110]

Figure 39. Structure of cyclothiazomycin. Sulfur to alpha-carbon bond is highlighted in red color

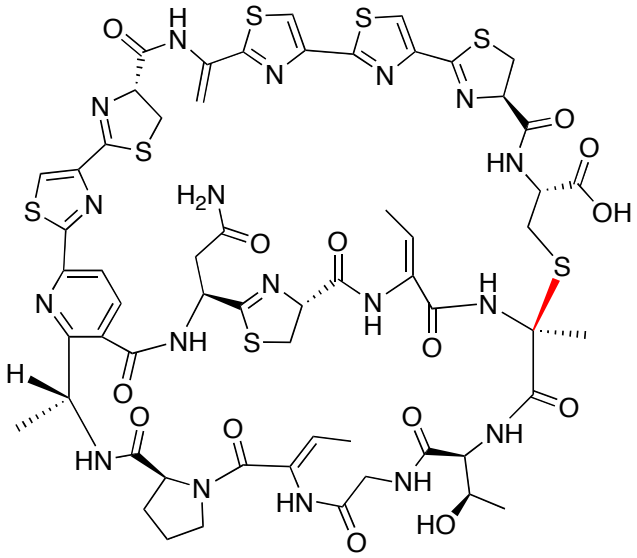

Although sulfur to alpha-carbon linkages are observed in diketopiperazines such as gliotoxin, arantoins and sporidesmins, these linkages constitute parts of di- and trisulfide bonds, indicating that the sulfur atoms are likely derived from residues other than cysteine.[109]

Subtilosin A shows bactericidal activity against Gram-positive bacteria such as *Listeria monocytogenes, Bacillus megatrium*, *Bacillus amyloliquefaciens*, and *Streptococcus faecium*.[95]

4.1.1 Mechanism of action

The mode of action of subtilosin A seems to involve receptor-binding mediated membrane disruption.[111] Subtilosin A with an aliphatic index (relative volume of a protein that is occupied by aliphatic side chains) of 89.43[112] is highly hydrophobic and can interact with the hydrophobic core of phospholipid membranes.[111] Studies with model phospholipid bilayers suggested that subtilosin A adopts an orientation in which the hydrophobic edge of the molecule is inserted into the lipid bilayers. This binding induces a conformational change in the lipid head groups and disorders the hydrophobic region of the bilayers, resulting in membrane permeation and leakage of cell contents.[111]

4.1.2 Structural elucidation studies of subtilosin A

The initial studies[95] on the characterization of subtilosin A were only partially successful and provided incomplete amino acid sequence and peptide structure. Mass spectrometry and amino acid analysis indicated a mass of 3399.9 Da consisting of 32 amino acids and 2 unnatural acid residues (Figure 40). The N-terminus was thought to be blocked by some unknown residue. Unusual cross links were revealed between Cys19 and Glx28 via an unknown Xu residue, and between the N and C termini suggesting that subtilosin A is a cyclic peptide with a novel cross-linked structure.

Figure 40. The proposed primary structure of subtilosin A by Babasaki *et al*.[95]

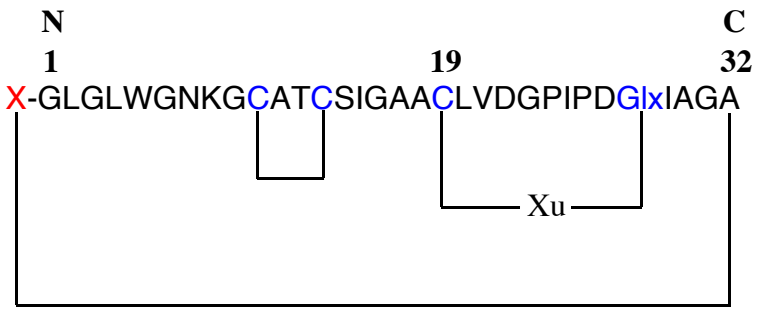

However, their attempts at predicting the correct amino acid sequence and structure were incomplete and required revision. Genetic studies of *Bacillus subtilis* by Zuber and coworkers predicted the correct amino acid sequence of the presubtilosin from the nucleotide sequence.[107] They identified an operon called *alb* (antilisterial bacteriocin) that is responsible for antilisterial activity. The operon *alb* consists of seven genes (*albABCDEFG*) and is preceded by the *sbo* structural gene that encodes a 43 amino acid precursor for subtilosin A that was originally identified and characterized by Babasaki *et al*.[95] Although codons specifying two phenylalanines and a threonine (at positions where postranslational modifications are suggested) are present in the nucleotide sequence, no corresponding residues were detected in the amino acid analysis (partial hydrolysis followed by Edman degradation) suggesting chemical modifications of these residues.[107] Mutations in either the *alb* operon or *sbo* structural gene eliminated antilisterial activity suggesting that the genes of the *sbo-alb* locus are required for the production of antilisterial subtilosin. Subsequent

studies identified that the *sbo-alb* genes are required for subtilosin synthesis as well as immunity (Figure 41).[100]

Figure 41. The *sbo-alb* locus in *Bacillus subtilis*

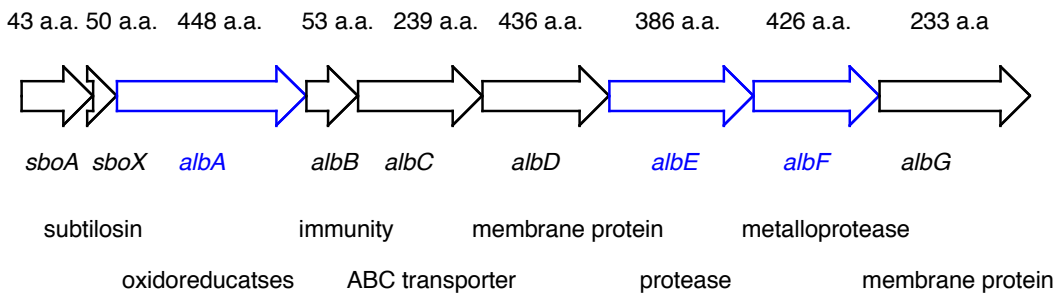

Mutational analyses have shown that two of the genes, *albA* and *albF*, are critical for the production of mature subtilosin.[100] Although the primary functions of the *alb* gene products are not known, sequence homology comparisons with known proteins suggests that some of these gene products (AlbA, AlbE and AlbF) are responsible for the unusual posttranslational modifications of subtilosin A during maturation. Although the products of *albB*, *-C* and *-D* genes are all involved in subtilosin A immunity, the small hydrophobic peptide produced by the *albB* gene appears to be the most critical as a mutation of *albB* gene shows the most severe defect in subtilosin immunity.[100]

Once fully processed to its mature form, subtilosin A, like other bacteriocins from Gram-positive bacteria, is transported to the external environment via membrane associated ATP-binding cassette transporters (ABC-transporters).[113] It was

proposed that AlbC, a member of the ABC family of transport proteins, is likely involved in the export of subtilosin A. The other genes in the operon are thought to have distinct functions as well, but have yet to be elucidated.

Although genetic analysis predicted the correct amino acid sequence for subtilosin A, the proposed cross-links were incomplete and misassigned.[107] Subsequent studies by Stein and coworkers[114] using two-dimensional NMR and MALDI-TOF MS studies revealed inter-residue cross linkages between Cys4 and Phe31, Cys7 and Thr28, and Cys13 and Phe22; However, the exact nature of their connectivity at the molecular level remained uncertain (Figure 42).

Figure 42. The subtilosin A structure proposed by Stein and coworkers[114]

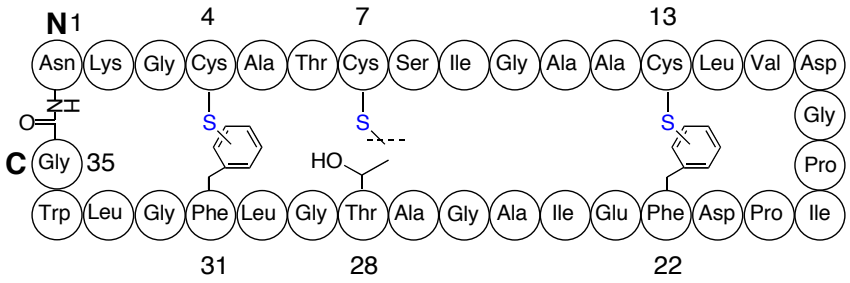

The peptide's mass was found to be 3399.7 Da consistent with that proposed before by Babasaki *et al*.[95] In the NMR solution structure, the proposed posttranslationally modified residues (Phe22, Thr28 and Phe31) were found to be in close proximity to the three-cysteine residues for which thioether modifications were suggested. The cysteine residues were also found to be modified. The mass difference of 6 Da between measured (3400.7 Da) and calculated (3406.7 Da for

subtilosin A with free cysteines) values was attributed to three inter-residue cross linkages with loss of hydrogen from each residue. Also, the calculated monoisotopic mass of subtilosin A (3399.5 ± 0.5 Da) differs from the observed mass (3423.6 ± 0.5 Da) by 24 Da, which is consistent with the loss of one water molecule and six hydrogens. In order to allow for the complete structural assignment of subtilosin A, chemical and spectroscopic methods were undertaken in our group. Dr. Kawulka, a former graduate student from our group, who obtained the primary and tertiary solution structure of subtilosin A using isotopic labeling and multidimensional NMR studies.[108,109] These studies indicated that residues Phe22, Thr28 and Phe31 are modified at their α-carbons. The configurations of all amino acids except for the modified residues are L as determined by GC MS analysis. The stereochemistries of the modified residues are L-Phe22, D-Thr28, and D-Phe31 deduced by extensive NMR analysis.

4.1.3 Physical properties

Subtilosin A is hydrophobic and soluble in methanol, *i*PrOH, glacial acetic acid, 70% formic acid, and dimethyl sulfoxide but insoluble in organic solvents such as dichloromethane, ether and hexane. It is soluble in alkaline solutions but will gradually decompose under basic conditions.[95]

4.1.4 Plausible mechanisms of formation of thioether linkages and N-C cyclization

4.1.4.1 Thioether linkages

Although the exact enzymatic mechanisms of how the cysteine sulfurs are linked to the α-carbons are not known, chemical synthesis of model compounds in our group has provided some insights. In principle, the process could involve nucleophilic attack of the cysteine thiol on an extremely reactive *N*-acyl iminium ion of Phe or Thr residues (Scheme 51).

Scheme 51. Nucleophilic attack of cysteine thiol on a highly reactive *N*-acyl iminium moiety

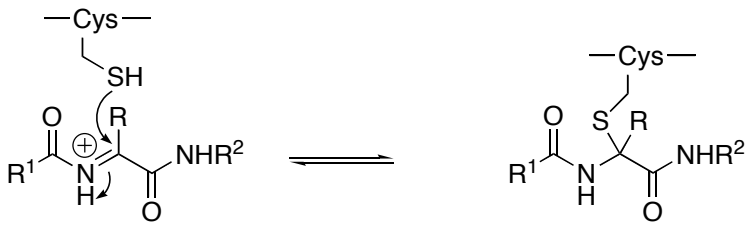

Such highly reactive iminium species could be formed via oxidation reactions that involve enzymatic dehydrogenation or N-hydroxylation followed by dehydration; less likely, the imine species could be formed by α-hydroxylation followed by dehydration as the intermediate hydroxy species could form an α-keto amide (Scheme 52).[109]

Scheme 52. Proposed imine formation mechanisms

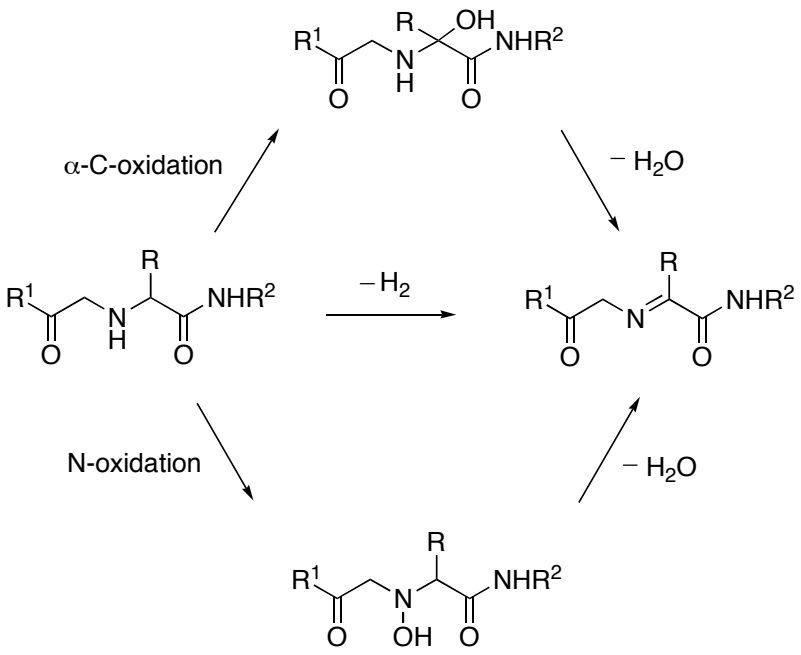

It is currently hypothesized that AlbA is a member of the radical SAM (*S*-adenosylmethionine) super family of enzymes.[107] These radical SAM enzymes contain juxtaposed SAM and [4Fe-4S] clusters that function together during catalysis.[115] One of the biochemical functions of radical SAM enzymes is to perform single electron reductive cleavage to generate a methionine and a strongly oxidizing 5'-deoxyadenosyl radical. This reactive radical intermediate abstracts a hydrogen atom from a substrate to initiate a radical mechanism (Scheme 53).[116]

Scheme 53. Schematic representation of the reaction involving radical SAM

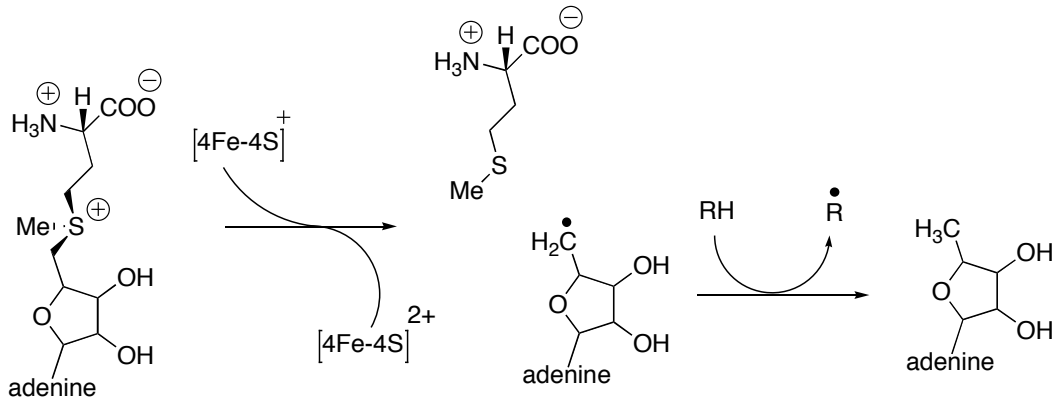

A mechanism similar to the one represented above could be proposed involving radical SAM mediated α-hydrogen abstraction generating a stabilized radical that could combine with a cysteine radical forming a thioether bond (Scheme 54).

Scheme 54. Proposed diradical mechanism

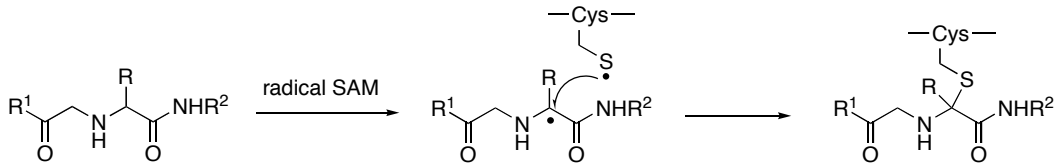

Members of the MoeA/NifB/PqqE family of enzymes containing cysteine clusters that bind Fe-S complexes are thought to be involved in hydration and dehydration reactions of substrate molecules.[117,118] It is also possible that AlbA could be a

member of the MoeA/NifB/PqqE family and might catalyze such oxidation reactions during the maturation of presubtilosin. AlbE and AlbF, based on its N terminal amino acid sequence, are related to known members of the zinc metalloproteases[119-121] and might be involved in critical modifications of presubtilosin.

4.1.4.2 N-C cyclization

Although several circular bacteriocins, cyclotides and cyclic peptides (both ribosomally and nonribosomally synthesized) have been isolated and characterized, the cyclization mechanisms are poorly understood. It has been reported by Peduzzi and coworkers that two enzymes namely, McjB and McjC, catalyze the maturation of microcin J25 (Figure 43), a ribosomally derived small (21 amino acids) circular bacteriocin produced by *Escherichia coli*.[122] Multiple alignment studies using BLAST programs suggested McjC as an ATP/Mg^{2+}-dependent enzyme that could be responsible for the cyclization.

Figure 43. Structure of microcin J25. An amide linkage resulting from side chain macrocyclization is shown in red

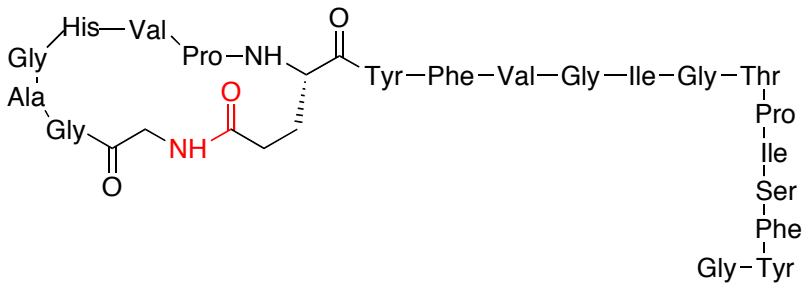

microcin J25

Some cyanobacterial cyclic peptides such as trichamide, ulithiacyclamide, patellamide and microviridins B and C are initially made as linear ribosomal precursors that undergo posttranslational modifications to their mature cyclic forms and as such serve as good models for studying the N to C cyclization. Comparison of the gene clusters of cyanobactins revealed extensive similarities suggesting similar biosynthetic pathways operating among them (Figure 44).[123]

Figure 44. Cyanobactin assembly lines in cyanobacteria. Arrows represent *pat* and *tru* clusters that are involved in the biosynthesis of cyanobactins[123]

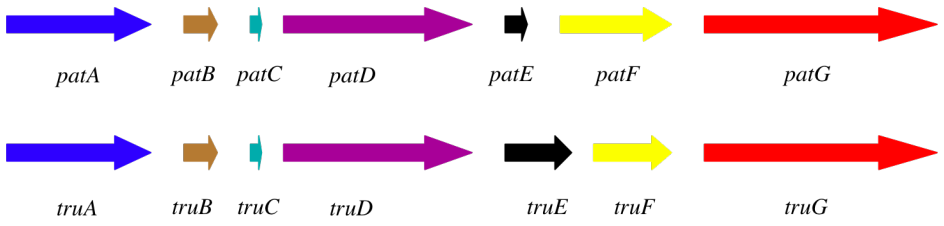

In a recent study, Schmidt and coworkers[124] reported two proteases PatA and PatG (Figure 44) in the *pat* gene cluster are found to be necessary for the cyclization of N and C termini. Computational and sequence alignment studies suggested that PatA and PatG contained a subtilisin-like classical Asp-His-Ser catalytic triad that could be involved in the formation of an activated ester. In their biochemical experiments, they used purified PatA, PatG and two synthetic peptide substrates corresponding to the precursor (PatEdm) and C-terminal fragment (including the recognition sequence (green)), respectively. When incubated, PatA cleaved the precursor PatEdm at two N-terminal sites (Figure 45) and the cleavage products

were identified by mass spectrometry. An active site Ser-Ala mutant of PatA devoid of activity further demonstrated that the activity resided in PatA.

Figure 45. Cleavage of precursor peptide by PatA

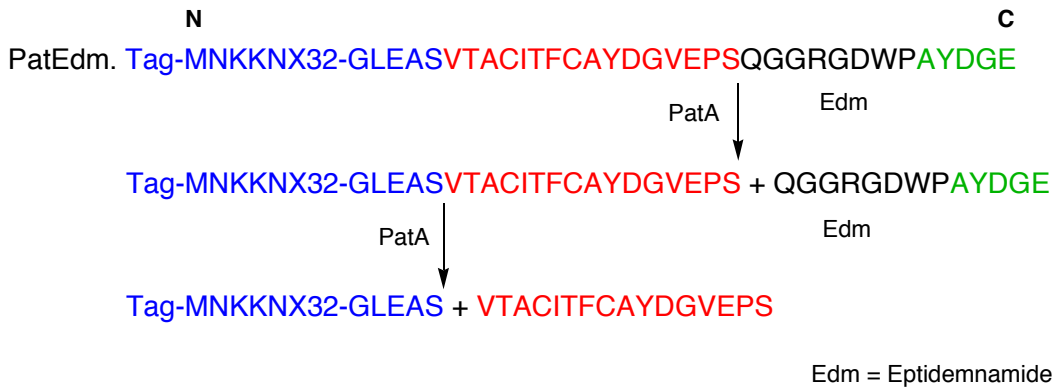

When PatEdm was incubated with PatG, no cleavage products were observed suggesting PatG could only cleave and cyclize the products resulting from PatA catalysis. Additional evidence for this proposal was obtained, when several PatG variants (wild type, a PatG variant and related TruG) cleaved an artificial peptide corresponding to the C-terminal fragment containing recognition sequence (Figure 46). High resolution mass spectrometry showed the formation of both eptidemnamide and the recognition peptide supporting PatG as the N-C cyclization catalyst.

Figure 46. PagG mediated cleavage showing the formation of eptidemnamide and recognition peptide. An amide bond formed by PatG is shown in red

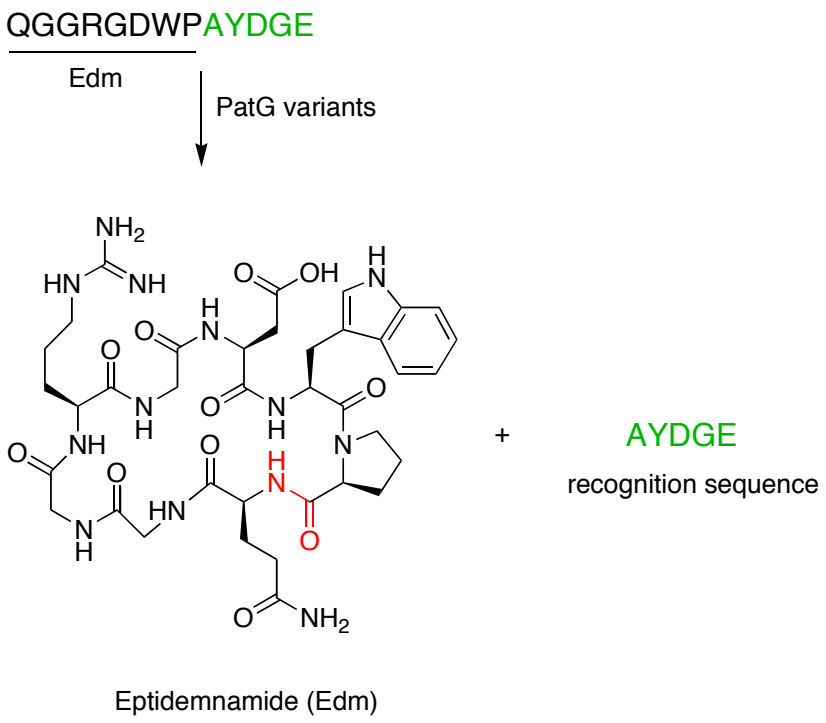

Initially, it was thought that PatG might only be acting as a protease and the peptide could cyclize on its own. Incubation of PatG with C-terminal fragment QGGRGDWP without recognition sequence led to no reaction.[124] All these lines of evidence support a single step no energy (*e.g.* ATP) requiring transamidation mechanism shown in Figure 47. As PatG contains a serine residue at the active site, the reaction could proceed via an activated ester. This activated ester could then undergo nucleophilic attack by the N-terminus of the substrate giving the cyclic peptide and free enzyme.

Figure 47. Proposed transamidation mechanism

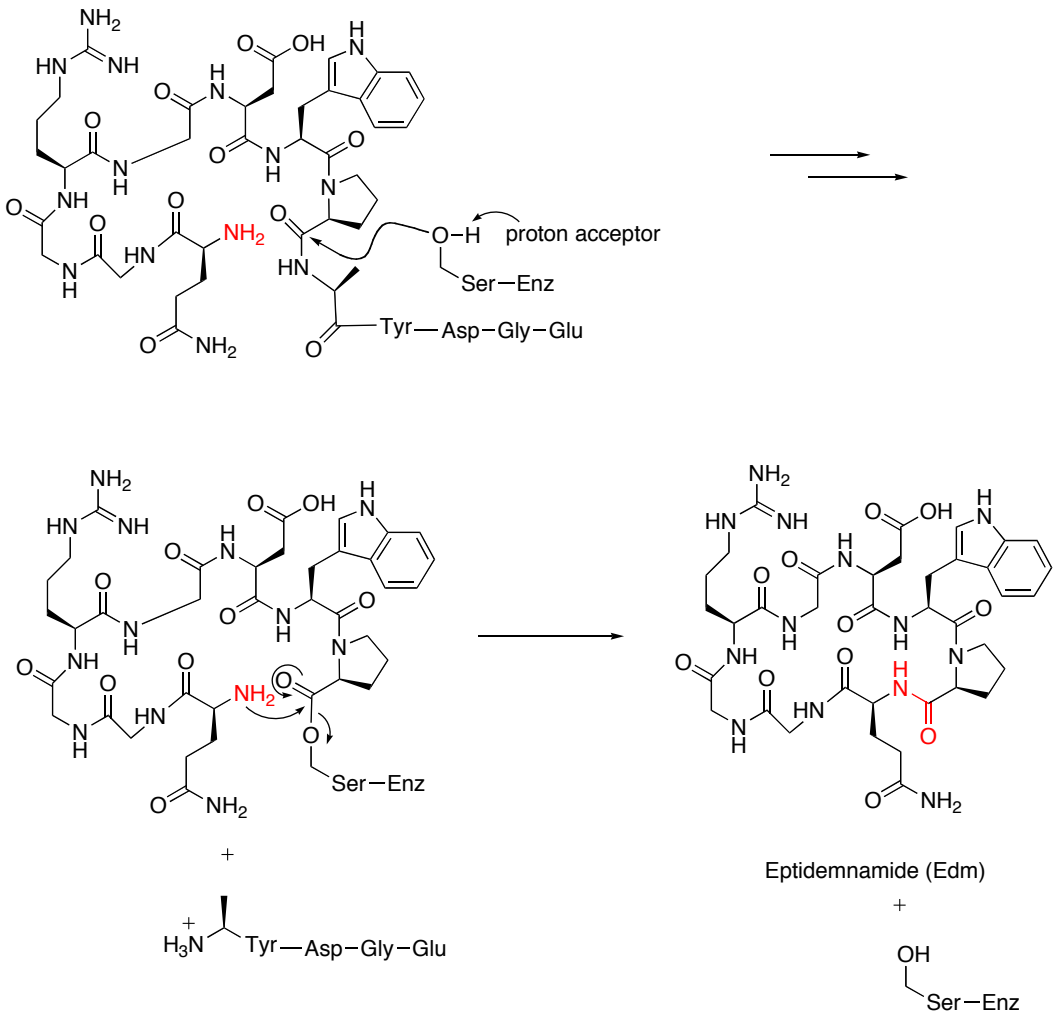

However there are examples in the literature that suggest some cyclizations could proceed via an ATP activated acyl phosphate intermediate. The tricyclic depsipeptides (having an ester and peptide bonds) such as microviridins[125,126] are biosynthesized from their precursors using enzymes related to ATP-grasp enzymes. As the name suggests, the ATP-grasp super family enzymes catalyze ATP mediated condensation of a carboxyl terminus with an amino or thiol

functional groups. The mechanisms proceed via an acyl phosphate intermediates.[127] Some known examples are; D-alanine-D-alanine ligase, glutathione synthetase and biotin carboxylase. A general biosynthetic mechanism is presented (Scheme 55).

Scheme 55. Biosynthetic mechanisms mediated by ATP-grasp enzymes. **5A**. Acyl phosphate pathway; **5B**: Acyl adenylate pathway

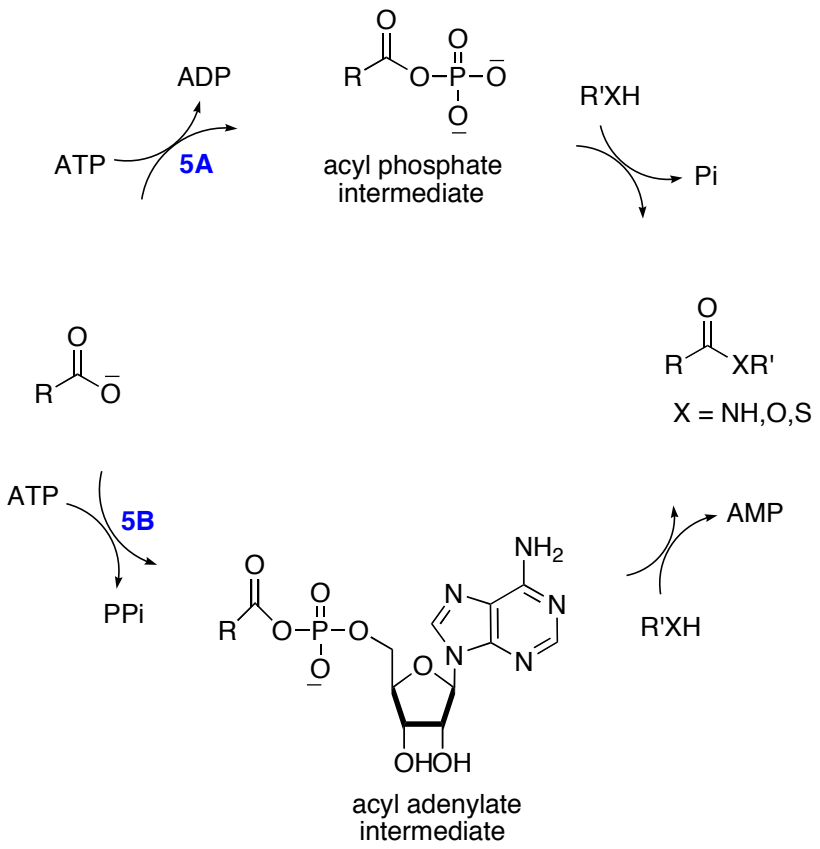

The biosynthetic machinery of microviridin B (Figure 48) revealed two genes namely, *mdnB* and *mdnC*, that encoded ATP-grasp related ligases. Mutational studies and heterologous expression of microviridin B established that MdnB and

MdnC were essential for cyclization, suggesting mechanisms similar to the ones described above may be operating.

Figure 48. Structure of microviridin B. Ester and amide bonds are shown in red

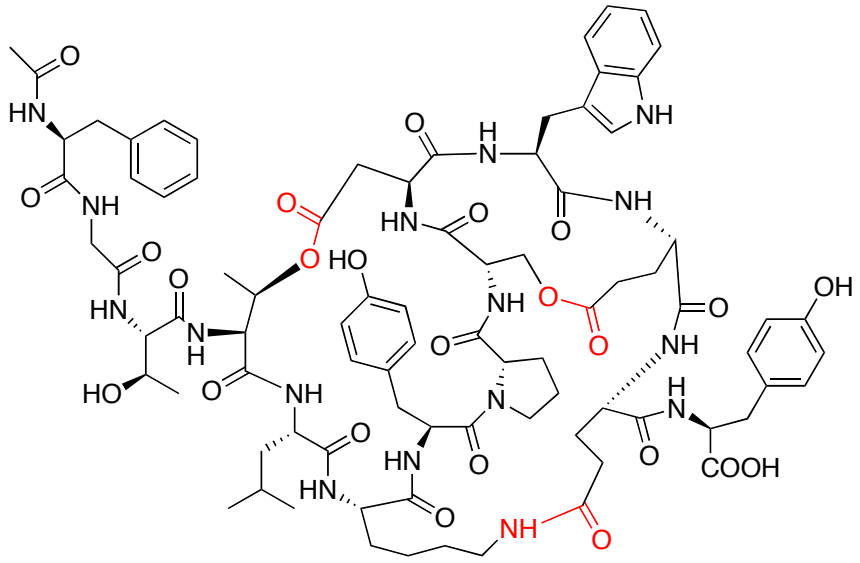

For subtilosin A, which has no C-terminal extension, it is not clear of how the cyclization happens. It is possible that the ones discussed above or some new mechanisms could be operating. Another possibility is that since the structural gene of subtilosin A terminates at the C-terminal glycine, the carboxyl group of the glycine could be activated in some way—for example as an ester, thioester or a phosphate anhydride - so that cyclization occurs. A mechanism in which an activated aminoacyl glycine linked to tRNA, operating in the N to C terminal

cyclization of subtilosin A could be proposed (Scheme 56).

Scheme 56. A possible mechanism of N-C cyclization

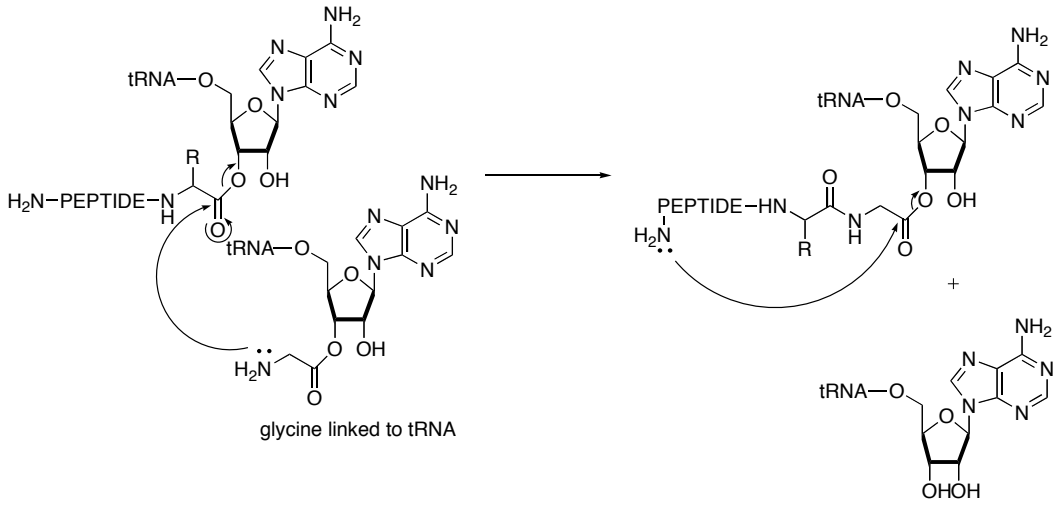

4.1.5 Objectives: Biosynthetic studies

The objective of this project is to elucidate the roles of the *albA*, *albE* and *albF* genes, all of which are likely to be responsible for the unusual and fascinating posttranslational modifications of subtilosin A. The aim would be to find out which if any, of these gene products is involved in generating the sulfur to α-carbon linkages, the removal of the leader peptide and head to tail cyclization. Towards this end, the syntheses of the subtilosin A precursor and the mature linear peptide, by classical solid phase peptide synthesis and a cyclic mature peptide using an on-resin head-to-tail cyclization strategy, were undertaken (Figure 49).

Figure 49. Amino acid sequences of the mature, cyclic and precursor peptides

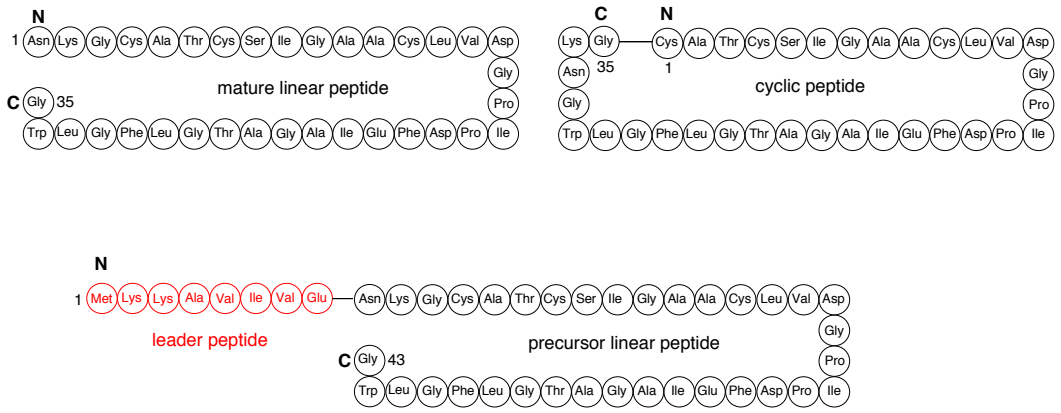

The peptide substrates would then fed to the AlbA, AlbE and AlbF enzymes. Dr. Marco J. van Belkum, a post-doctoral research associate from our group, has been working on the expression and purification of these enzymes. After interaction of the peptide substrates with AlbA, AlbE and AlbF enzymes and analysis of the products, the role of each enzyme could be elucidated.

4.2 RESULTS AND DISCUSSION

The solid phase peptide synthesis was done both manually and using a peptide synthesizer. To minimize aggregation and formation of secondary structures, particularly in the synthesis of long and cyclic peptides, a pseudoproline derivative (e.g. Fmoc-Ala-Thr(ΨMe,Me Pro)-OH) was used wherever possible (Figure 50).

Figure 50. Structure of Fmoc-Ala-Thr(ΨMe,Me Pro)-OH

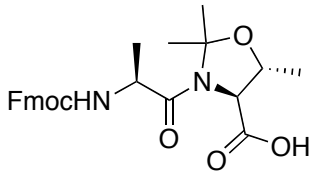

Pseudoproline[128,129] is a dipeptide in which a Ser or Thr residue is reversibly protected as a proline-like TFA labile oxazolidine ring structure. The abbreviation ψPro indicates its relationship to proline. Its incorporation introduces a kink conformation into the peptide backbone, thereby hindering the formation of secondary structures responsible for peptide aggregation. It has the additional advantage of extending the peptide chain by two residues in one step. Pseudoprolines are particularly useful in the synthesis of cyclic peptides.[130-132] By adopting a cis-amide bond conformation, the two ends of the peptide chain are brought closer together, promoting cyclization. During deprotection and resin cleavage, the native peptide is regenerated.

One of the most commonly encountered sequence-dependent side-reactions in solid phase peptide synthesis is the formation of aspartimide.[133-136] This undesirable reaction is particularly serious when bases such as piperdine or diaza(1,3)bicyclo[5.4.0]undecane (DBU) are used for the removal of the Fmoc group.[137,138] Lauer *et al*[139] demonstrated that Asp-Gly sequence is particularly

prone to this side reaction. The aspartimide is susceptible to ring-opening reactions on either of the imide carbonyl carbons by nucleophiles leading to the formation of several by-products. Nucleophilic attack by water yields two deprotected regioisomers with the β-aspartyl peptide being the predominant by-product. Attack by piperidine base yields a mixture of regio isomers with the β-piperidyl amide as the main by-product. Aspartimide formation is also accompanied by base-promoted epimerization (Scheme 57).[140]

Scheme 57. Mechanism of aspartimide and related by-product formation

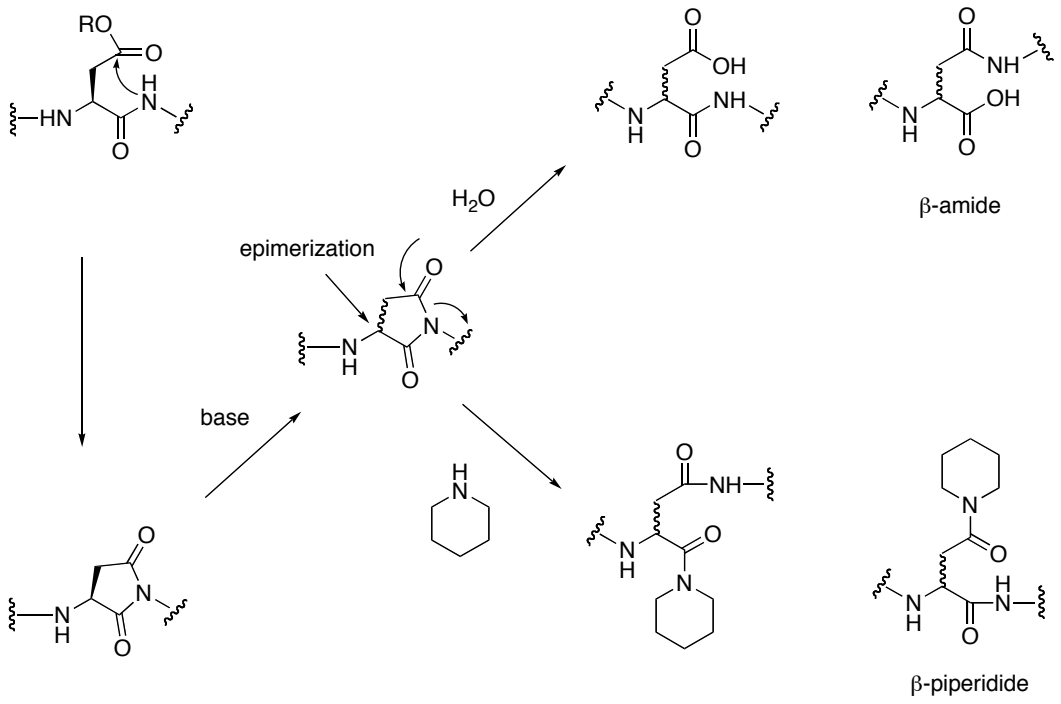

Although, several approaches have been developed to overcome this problem, the use of a preformed dipeptide Fmoc-Asp(O^{t}Bu)-(Dmb)Gly-OH, introduced by Novabiochem® provides complete protection (Figure 51).

Figure 51. Structure of Fmoc-Asp(O^{t}Bu)-(Dmb)Gly-OH

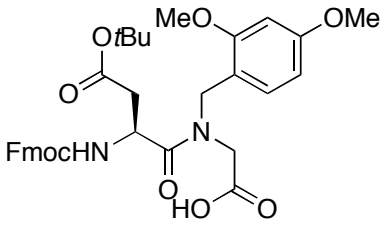

4.2.1 Synthesis of mature peptide

The mature peptide consisting of 35 amino acids was synthesized manually using a Wang resin preloaded with Fmoc-Gly-OH as the C-terminal amino acid. The Fmoc group is removed with 20% piperidine followed by coupling amino acids with PyBOP in the order: Fmoc-Trp(Boc)-OH, Fmoc-Leu-OH, Fmoc-Gly-OH, Fmoc-Phe-OH, Fmoc-Leu-OH and Fmoc-Gly-OH to afford the heptapeptide. A small sample of the resin is cleaved using (95:2.5:2.5) TFA / TIPS / H_2O and analyzed (Scheme 58).

Scheme 58. Synthesis of the heptapeptide

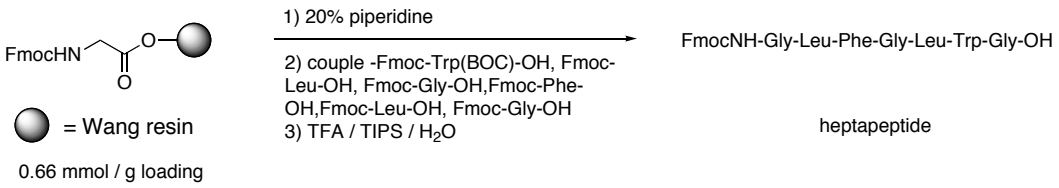

Analysis by MALDI-TOF mass spectrometry indicates a peak at 995 Da ($[M+Na]^+$) that is two units higher than the expected mass (993 Da) for a N-Fmoc protected heptapeptide. Similar results are also observed when the peptide is extended by three or four amino acid residues. An MS/MS analysis of a decapeptide reveals modifications on the tryptophan (Trp) residue showing that it is reduced (Figure 52). In the MS/MS fragmentation nomenclature, b and y ions are formed as a result of amide bond cleavage at the N and C-termini of the backbone peptide respectively.

Figure 52. MS/MS fragmentation nomenclature and analysis of decapeptide indicating modifications on tryptophan residue

Figure 52A. MS/MS fragmentation nomenclature

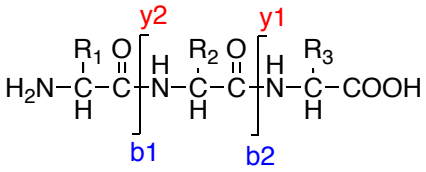

Figure 52B. Structure and mass of decapeptide

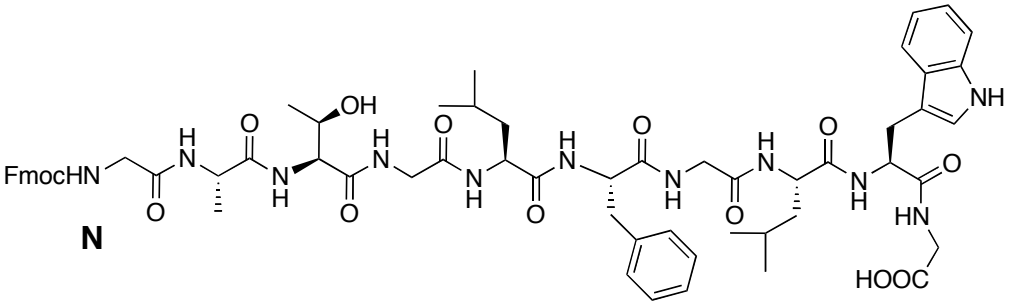

Exact mass : 1199.6

Figure 52C. Structure and mass of decapeptide showing reduced tryptophan (brown)

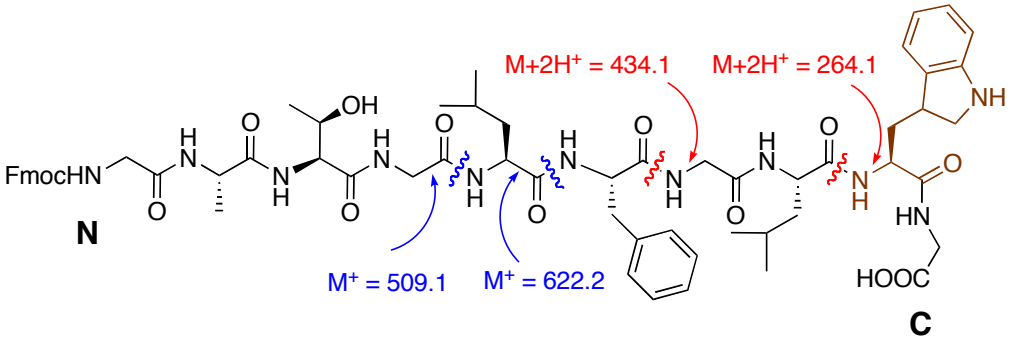

red = y ions
blue = b ions

Exact mass : 1201.6

Observed mass ([M+H]$^+$) : 1202.4

This unwanted reduction of the Trp residue can occur during the resin cleavage step in which triisopropylsilane (TIPS) could serve as a hydride source. A mechanism could be proposed in which protonation at position-3 of the relatively reactive pyrrole ring followed by hydride delivery could generate the reduced product (Scheme 59).

Scheme 59. A plausible mechanism for the tryptophan reduction

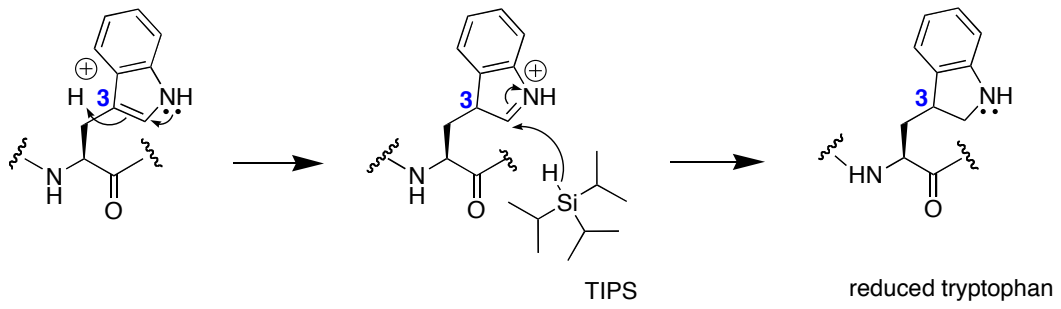

In order to avoid the reduction of the tryptophan residue, a cleavage cocktail in which TIPS is replaced by anisole. The resulting product is reanalyzed as before. The observed mass of 993.4 ($[M+Na]^+$) is consistent with the calculated mass 993.5 Da of the heptapeptide. No reduction of the tryptophan residue is observed. The peptide is extended manually by introducing other amino acids to obtain the desired product consisting of 35 amino acids. Cleavage of the resin using (95:2.5:2.5) TFA / anisole / H_2O followed by MALDI-TOF MS analysis indicates a peak at 3424.3 ($[M+H]^+$) consistent with the calculated mass (3423.6) of the mature linear peptide (Scheme 60).

Scheme 60. Synthesis of the subtilosin A mature linear peptide

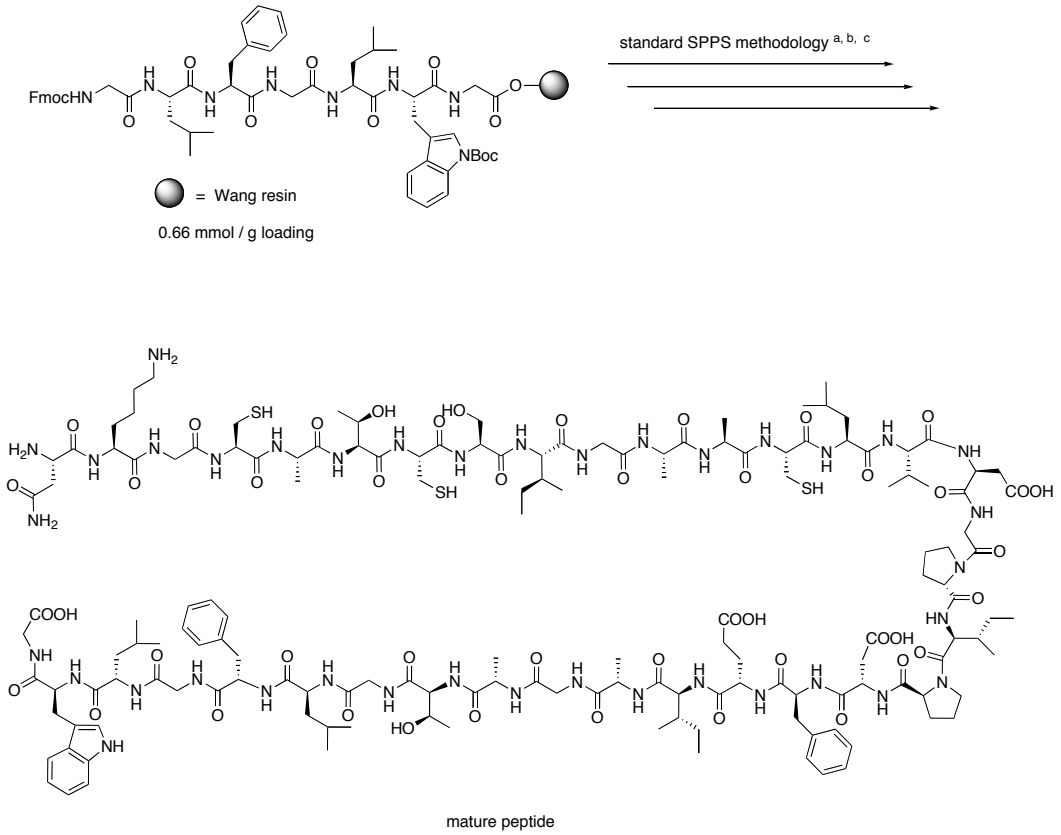

[a] Conditions used for synthesis of **Y** from **X**: (i) 20% piperidine in DMF, (ii) PyBOP, NMM, DMF, (iii) Fmoc-Ala-Thr(ΨMe,Me Pro)-OH; [b] Repeat (i) and (ii) for amino acids: Fmoc-Gly-OH, Fmoc-Ala-OH, Fmoc-Ile-OH, Fmoc-Glu(O^{t}Bu)-OH, Fmoc-Phe-OH, Fmoc-Asp(O^{t}Bu)-OH, Fmoc-Pro-OH, Fmoc-Ile-OH, Fmoc-Pro-OH, Fmoc-Asp(O^{t}Bu)-(Dmb)Gly-OH, Fmoc-val-OH, Fmoc-Leu-OH, Fmoc-Cys(Trt)-OH, Fmoc-Ala-OH, Fmoc-Ala-OH, Fmoc-Gly-OH, Fmoc-Ile-OH, Fmoc-Ser(^{t}Bu)-OH, Fmoc-Cys(Trt)-OH, Fmoc-Ala-Thr(ΨMe,Me Pro)-OH, Fmoc-Cys(Trt)-OH, Fmoc-Gly-OH, Fmoc-Lys(Boc)-OH and Fmoc-Asn(Trt)-OH [c] (i) 20% piperidine in DMF (ii) (95:2.5:2.5) TFA / anisole / H_2O

The sequence of the subtilosin A mature linear peptide was further confirmed by MS / MS analysis (Figure 53).

Figure 53. MS / MS analysis of subtilosin A mature linear peptide

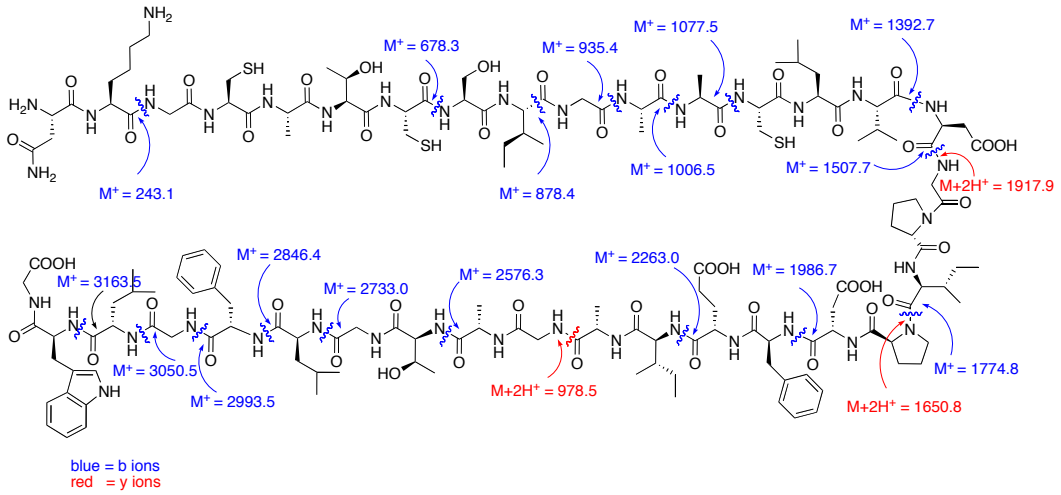

4.2.2 Synthesis of the subtilosin A precursor linear peptide

The mature peptide is extended further by coupling eight more amino acids to obtain the precursor linear peptide (Scheme 61), the mass of which is confirmed by MALDI-TOF mass spectrometry.

Scheme 61. Extension of the mature peptide to the precursor peptide

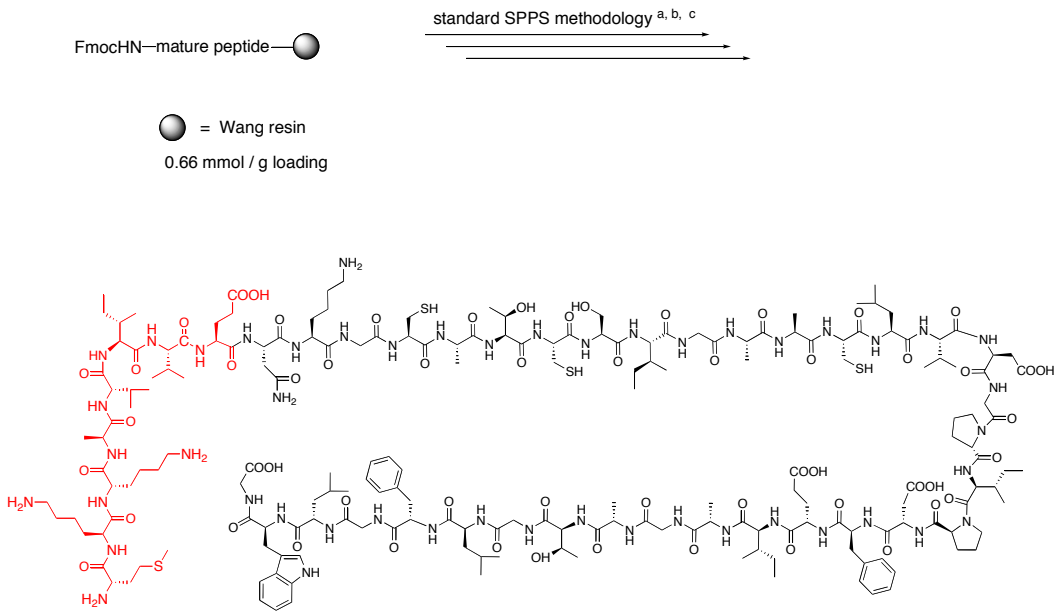

[a] Conditions used for synthesis of precursor peptide: (i) 20% piperidine in DMF, (ii) PyBOP, NMM, DMF, (iii) Fmoc-Glu(O^{t}Bu)-OH [b] Repeat (i) and (ii) for amino acids: Fmoc-Val-OH, Fmoc-Ile-OH, Fmoc-Val-OH, Fmoc-Ala-OH, Fmoc-Lys(Boc)-OH Fmoc-Lys(Boc)-OH Fmoc-Met-OH, [c] (i) 20% piperidine in DMF (ii) (95:2.5:2.5) TFA / anisole / H_2O

The sequence of the subtilosin A precursor linear peptide was further confirmed by MS / MS analysis (Figure 54).

Figure 54. MS / MS analysis of subtilosin A precursor linear peptide

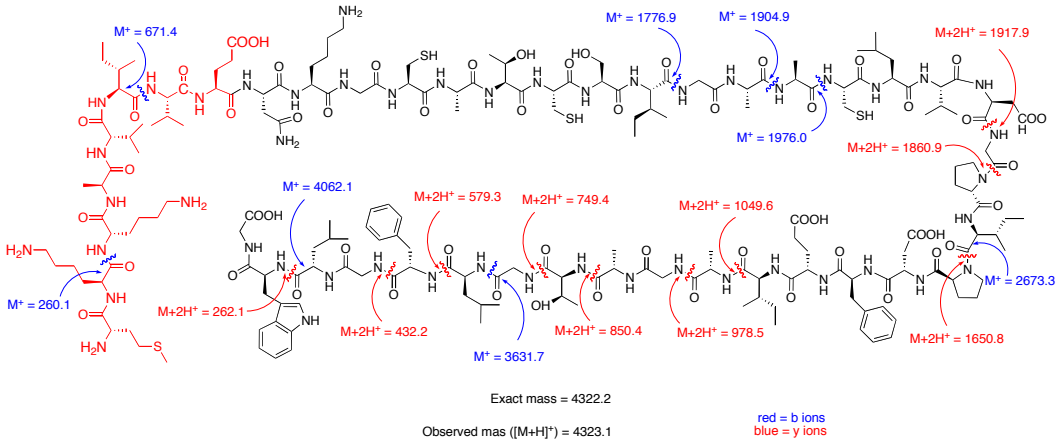

4.2.3 Synthesis of cyclic peptide

Cyclic peptides have gained prominence in medicinal chemistry compared to their linear counterparts. This is due to their enhanced metabolic stability resulting from reduced conformational flexibility, increased potency, receptor selectivity and bioavailability. [141-143] Given the growing and continued interest in cyclic peptides, several methods have been developed for their synthesis.[144,145] Classical methods include preparation of partially protected linear peptides by solution or solid phase chemistry followed by their cyclization in solution under high dilution conditions to avoid or minimize the formation of cyclodimers and oligomers. The

main drawback of using solution phase chemistry to perform the cyclization is the requirement of an additional purification step with the concomitant loss of some product. Head-to-tail cyclization[146,147] presents an attractive alternative for the synthesis of cyclic peptides. In this approach, an amino acid is anchored to a solid support via its side chain. Following solid-phase chain assembly of the linear sequence, lactamization is effected between the carboxyl and amino termini while the peptide is still anchored to the resin. Performing such cyclizations using a low loading resin favors intramolecular reactions over intermolecular reactions, a strategy that is referred to as a "pseudo dilution" effect.[148,149] This solid-phase cyclization method is applicable to peptides where the C-terminal residue has a reactive side chain, such as the side chains of aspartic and glutamic acids,[150] lysine,[151] tyrosine,[152] serine and threonine.[153] For the synthesis of the cyclic peptide, a glutamic acid α-allyl ester, in which the side chain carboxylic acid is anchored to a Wang resin, is used as the C-terminal amino acid. The required amino acids are introduced using an automated peptide synthesizer. Deprotection of a small sample of resin with (94:2.5:2.5:1) TFA /ethane dithiol (EDT) / H_2O / TIPS followed by MALDI-TOF MS analysis indicates the formation of the desired precursor product (Scheme 62).

Scheme 62. Synthesis of a precursor for the cyclic peptide

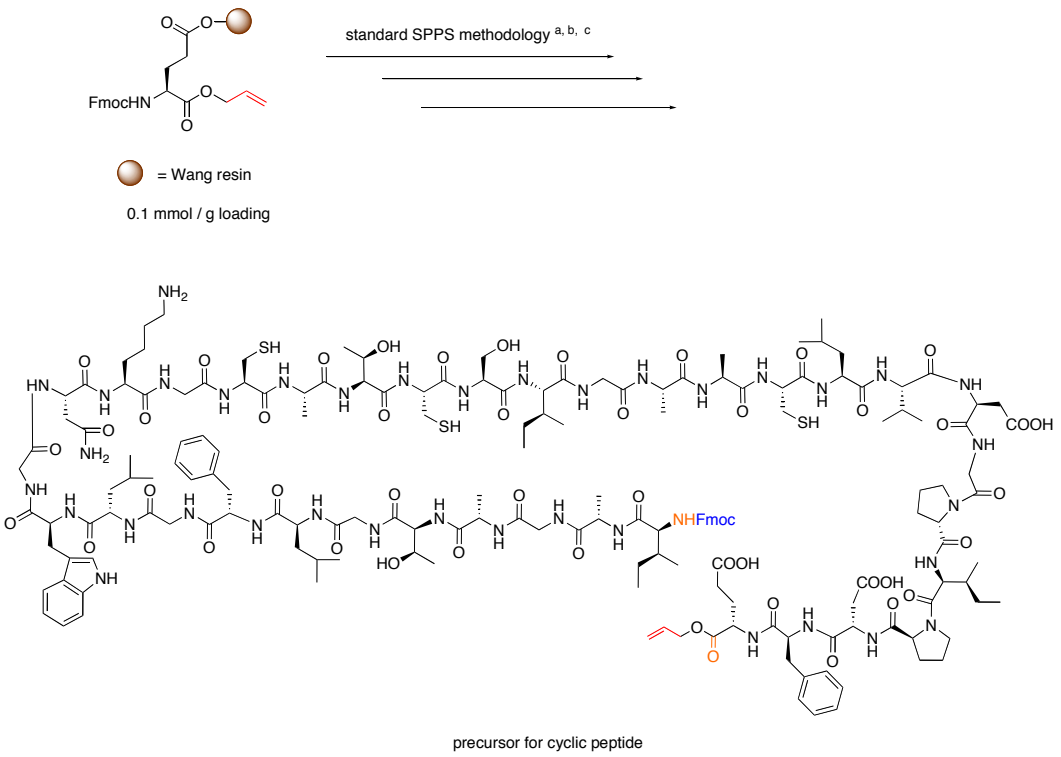

[a] Conditions used in the peptide synthesizer: (i) 22% piperidine in NMP, (ii) HBTU, HOBt, DIPEA, NMP, (iii) Fmoc-Phe-OH [b] Repeat (i) and (ii) for amino acids: Fmoc-Asp(O^{t}Bu)-OH, Fmoc-Pro-OH, Fmoc-Ile-OH, Fmoc-Pro-OH, Fmoc-Asp(O^{t}Bu)-(Dmb)Gly-OH, Fmoc-val-OH, Fmoc-Leu-OH, Fmoc-Cys(Trt)-OH, Fmoc-Ala-OH, Fmoc-Ala-OH, Fmoc-Gly-OH, Fmoc-Ile-OH, Fmoc-Ser(^{t}Bu)-OH, Fmoc-Cys(Trt)-OH, Fmoc-Ala-Thr(ΨMe,Me Pro)-OH, Fmoc-Cys(Trt)-OH, Fmoc-Gly-OH, Fmoc-Lys(Boc)-OH, Fmoc-Asn(Trt)-OH, Fmoc-Gly-OH, Fmoc-Trp(Boc)-OH, Fmoc-Leu-OH, Fmoc-Gly-OH, Fmoc-Phe-OH, Fmoc-Leu-OH, Fmoc-Gly-OH, Fmoc-Ala-Thr(ΨMe,Me Pro)-OH, Fmoc-Gly-OH, Fmoc-Ala-OH, and Fmoc-Ile-OH [c] (94:2.5:2.5:1) TFA / EDT / H_2O / TIPS

The remaining steps are done manually to complete the synthesis. The allyl group is removed in the presence of $Pd(PPh_3)_4$ with $PhSiH_3$ as the scavenger followed by Fmoc deprotection with 20% piperidine, providing a peptide that is ready for

cyclization. On-resin head-to-tail cyclization is effected using PyBOP as the coupling reagent. A small sample of resin is cleaved and analyzed using MALDI-TOF mass spectrometry. A peak at 3406.4 Da ($[M+H]^+$) revealed the formation of the desired cyclic peptide (Scheme 63).

Scheme 63. Synthesis of the cyclic peptide by an on-resin head-to-tail cyclization strategy

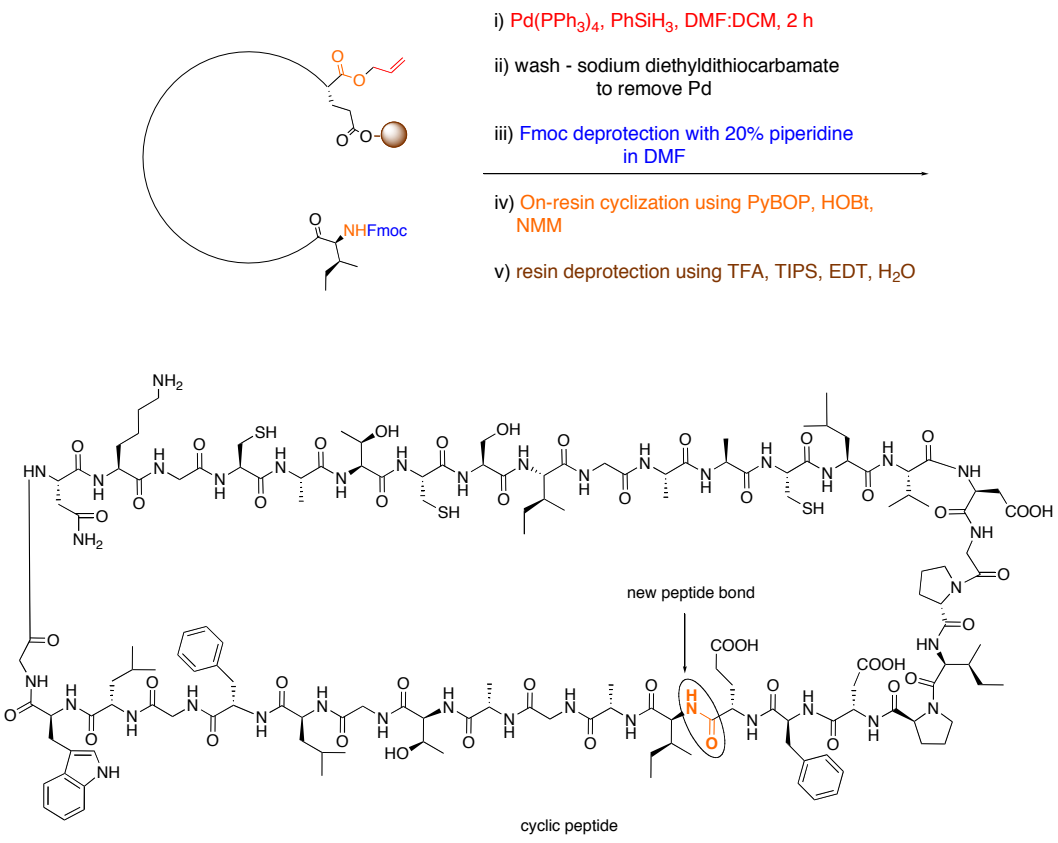

4.2.4 Conclusions and future direction

The precursor and mature peptides have been manually synthesized using solid phase peptide synthesis. The cyclic peptide has been synthesized using a

relatively simple on-resin head-to-tail cyclization strategy. After feeding the peptide substrates to the purified AlbA, AlbC, and AlbF enzymes either separately or in combination followed by analysis of the products using mass spectrometry and biological testing, the role of each enzyme in the biosynthesis of subtilosin A may be elucidated. An understanding of the enzymatic mechanisms of these unusual modifications of subtilosin A could open new doors for making analogues and studying their structure activity relationships. This could possibly provide new methodologies for making new peptides.

CHAPTER 5: EXPERIMENTAL PROCEDURES

5.1 GENERAL PROCEDURES

5.1.1 Reagents, solvents and solutions

All reagents and solvents used were of American Chemical Society (ACS) grade (>99.0% purity) and were purchased from the Aldrich Chemical Company Inc. (Madison, WI), Sigma Chemical Company (St. Louis, MO), Fisher Scientific Ltd. (Ottawa, ON) or Alfa Aesar (Ward Hill, MA). All amino acids, their protected derivatives and resins for SPPS were purchased from the Calbiochem-Novabiochem Corporation (San Diego, CA), Bachem California Inc. (Torrance, CA) or Chem-Impex International Inc. (Wood Dale, IL). These reagents and solvents were used as such unless otherwise specified. Reactions involving air or moisture sensitive reactants were done under an atmosphere of argon. Tetrahydrofuran and diethyl ether were freshly distilled over sodium and benzophenone under an atmosphere of dry argon before use. Dichloromethane, dichloroethane, methanol and triethylamine were distilled over calcium hydride. Ethyl acetate was distilled over potassium carbonate. HPLC grade methanol, dimethylformamide and acetonitrile were used without purification. The solvent removal *in vacuo* refers to the evaporation under reduced pressure below 40 °C using a Buchi rotary evaporator followed by drying (<0.1 mm Hg) to a constant sample mass. Unless otherwise specified, solutions of $NaHCO_3$, HCl, $FeCl_3$, citric acid, lithium hydroxide and sodium thiosulfate refer to aqueous solutions. Brine

refers to a saturated aqueous solution of NaCl. In reactions 'rt' refers to room temperature and 'eq' refers to equivalents.

5.1.2 Purification techniques

Commercially available ACS grade solvents were used for performing column chromatography without further purification. Flash chromatography was performed using Merck type 60, 230-400 mesh silica gel. All reactions and fractions from column chromatography were monitored by thin layer chromatography (TLC) using glass plates with a UV fluorescent indicator (normal SiO_2, Merck 60 F_{254}). TLC spots were visualized using one or more of the following methods: UV absorption by fluorescence quenching; iodine staining; by dipping the TLC plates in a solutions of Ninhydrin:acetic acid:n-butanol (0.6 g:6 mL:200 mL); $Ce(SO_4)\bullet 4H_2O/(NH_4)MoO_{24}\bullet 4H_2O/H_2SO_4/H_2O$ (5 g:12.5 g:28 mL:472 mL) spray.

High performance liquid chromatography (HPLC) was performed using a Varian Prostar chromatograph equipped with a model 325 variable wavelengths UV detector and a Rheodyne 7725i injector fitted with a 20 to 2000 μL sample loop. The columns used were Waters μBondapak C-18 column (WAT015814, 10 μm, 125 Å, 25 x 100 mm), Vydac Protein C_4 (214TP) steel walled column (reverse phase, C_4 column, 10 μm, 300 Å, 22 x 250 mm), Waters Nova-Pak cartridges (reverse phase, 8NVC18, 4 μm C_{18} column, 60 Å, 4 mm, 8 x 100 mm) and Waters μBondapak cartridges (reverse phase μBondapak, WAT037684, C_{18} column, 125

Å, 10 mm, 25 x 100 mm). All HPLC solvents were filtered with a Millipore filtration system under vacuum prior to use.

5.1.3 Instrumentation for compound characterization

Nuclear Magnetic Resonance (NMR) spectra were recorded on a Varian Inova 600, 500, 400 and 300 MHz spectrometers. Chemical shifts for proton and carbon NMR were reported in parts per million (ppm) downfield relative to tetramethylsilane (TMS). For ^{1}H NMR spectra, δ values were referenced to $CDCl_3$ (7.26 ppm), CD_3OD (3.30 ppm), CD_2Cl_2 (5.32 ppm) or DMSO-d_6 (3.53 ppm), and for ^{13}C (75, 100, MHz) spectra, δ values were referenced to $CDCl_3$ (77.0 ppm), CD_3OD (49.0 ppm), CD_2Cl_2 (53.8 ppm) or DMSO-d_6 (39.7 ppm) as the solvents. Selective homonuclear decoupling, shift correlation spectroscopy (gCOSY), heteronuclear multiple quantum coherence (gHMQC) and attached proton test (APT) were used for signal assignments. ^{1}H NMR data were reported in the following order: multiplicity (s, singlet; d, doublet; t, triplet; q, quartet; pent, pentet and m, multiplet), number of protons, coupling constant (*J*) in Hertz (Hz) and assignment. When appropriate, the multiplicity is preceded by br, indicating that the signal was broad. The IR, ^{1}H NMR, and mass spectra of literature compounds are consistent with the assigned structures.

Infrared spectra (IR) were recorded on either a Nicolet Magna-IR 750 with Nic-Plan microscope FT-IR spectrometer or a 20SX FT-IR spectrometer. Cast refers

to the evaporation of a solution on a NaCl plate. Microscope refers to measuring the infrared absorption of minute samples with the aid of photoelectric cells.

Melting points are uncorrected and were determined on a Büchi oil immersion apparatus using open capillary tubes. Optical rotations were measured on a Perkin Elmer 241 polarimeter with a microcell (10 cm, 1 mL) at ambient temperature and are reported in units of 10^{-1} deg cm^2 g^{-1}. All reported optical rotations were referenced against air and were measured at the sodium D line (λ = 589.3 nm) and values reported are valid within ± 1 ˚C.

Mass spectra were recorded using a Kratos AEIMS-50 high resolution mass spectrometer (HRMS) or Micromass ZabSpec Hybrid Sector-TOF positive mode electrospray ionization (ES), 0.5% solution of formic acid in MeCN:H_2O/1:1) instruments or on an Applied Biosystems Voyager Elite MALDI TOF system using either 4-hydroxy-α-cyanocinnamic acid (HCCA) or 3,5-dimethoxy-4-hydroxycinnamic acid (sinapinic acid) as matrices. Microanalyses were performed using a Perkin Elmer 240 or Carlo Erba 1108 elemental analyzers.

5.1.4 Manual Fmoc solid phase peptide synthesis (SPPS)

In the manual solid phase peptide synthesis Fmoc-amino acid (2.0 eq to resin loading) and HOBt (2.0 eq to resin loading) were dissolved in DMF (10 mL) and to the solution was added NMM (3.0 eq to the resin) followed by PyBOP (1.9 eq).

The reaction mixture was then pre-activated for about 3 min and transferred to a pre-swelled (20 min) resin and reacted for 2 h. The completion of coupling reactions were verified by negative Kaiser test. A 20% Ac_2O solution in DMF for 10 min was used for acylating unreacted amino groups (end capping). Subsequent removal of the Fmoc group was achieved using 20% piperidine in DMF and monitored by either Kaiser test or the absorption of dibenzofulvene-piperidine adduct at λ = 301 nm on a UV-Vis spectrophotometer.

5.1.5 Automated Fmoc SPPS

An Applied Bioystems (ABI 433A) peptide synthesizer was used for the automated Fmoc SPPS using the method 'UV *Fastmoc*™ 0.10 mmol'. In the method used, 10 eq of amino acids were used with respect to the resin loading. The coupling reactions were performed in a solution of Fmoc-amino acid (in NMP) with HBTU/HOBt/DIPEA (in DMF) and pre-activating for 2.1 min. The activated reaction mixture was then transferred to the pre-swelled resin and allowed to react for 9.3 min. End capping was performed using a solution of Ac_2O/HOBt/DIPEA in NMP. Deprotection of Fmoc group was achieved with 22% piperidine in NMP and monitored for completion of deprotection based on the absorption of dibenzofulvene-piperidine adduct at λ = 301 nm on a UV-Vis spectrophotometer. The standard cycle time that the synthesizer takes for introducing one amino acid is about 40 min.

5.2 EXPERIMENTAL PROCEDURES AND DATA FOR COMPOUNDS

[5-(4-Chloro-phenyl)furan-2-yl]methanol (32)

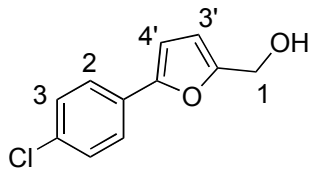

To a solution of furural derivative **31** (2.0 g, 9.66 mmol) in THF was added 1 M solution of $LiAlH_4$ in THF (440 mg, 11.6 mmol) at -5 ˚C, and the reaction mixture was stirred at this temperature for 1 h. The reaction was brought to rt and quenched with 0.5 mL of H_2O followed by 0.5 mL of 15% aq. NaOH. After solvent removal under vacuum, the resulting residue was dissolved with EtOAc (2 x 25 mL) followed by concentrating *in vacuo* to afford **32** in quantitative yield as a solid. IR (microscope) 3583, 2957, 2855, 1896, 1590, 1480, 1236, 1121, 993. cm^{-1}; ^1H NMR ($CDCl_3$, 600 MHz) δ 7.62 (d, 2H, J = 4.8 Hz, H_2), 7.37 (d, 2H, J = 4.8 Hz, H_3), 6.63 (d, 1H, J = 3.0 Hz, $H_{4'}$), 6.38 (d, 1H, J = 3.6 Hz, $H_{3'}$), 4.63 (d, 2H, J = 6.0 Hz, CH_2), 1.83 (t, 1H, J = 6.0 Hz, O<u>H</u>). ^{13}C NMR (100 MHz, $CDCl_3$) δ 154.6, 152.9, 133.1, 129.1, 129.0, 125.1, 110.1, 104.3, 57.6. HRMS (EI) calcd for $C_{11}H_9ClO_2$ (M^+), 208.02911; found, 208.02963.

3-Chloro-5-((5-(4-chlorophenyl)furan-2-yl)methoxy)pyridine (33)

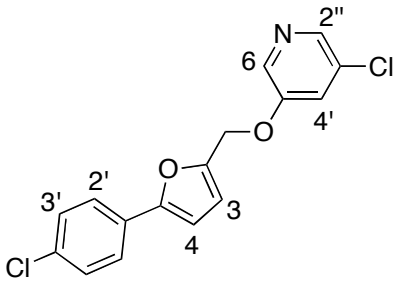

To a solution of PPh_3 (151 mg, 0.56 mmol) in THF (15 mL) was added DEAD (0.09 mL, 0.56 mmol) dropwise at 10 °C. After 30 min of stirring, **32** (100 mg, 0.48 mmol) and 3-chloro-5-pyridinol (75 mg, 0.56 mmol) were added and the cooling bath was removed. The mixture was allowed to stir at rt overnight and concentrated *in vacuo*. The residue was diluted with CH_2Cl_2 (25 mL). The solution was washed with H_2O, saturated $NaHCO_3$ solution and brine. The organic layer was dried over $MgSO_4$. The solvent was removed under vacuum and the crude product was purified by flash column chromatography (SiO_2, 1:3/EtOAc:hexanes) to yield **33** (44 mg, 29%) as an oil. IR (microscope): 3125, 3067, 2932, 1724, 1674, 1575, 1481, 1421, 1310, 1264 cm^{-1}; ^1H NMR (CD_2Cl_2, 600 MHz) δ 8.28 (d, 1H, J = 2.4 Hz, H_6), 8.21 (d, 1H, J = 1.8 Hz, $H_{2''}$), 7.62 (m, 2H, $H_{2'}$), 7.38 (m, 3H, $H_{3'}$ and $H_{4'}$), 6.68 (d, 1H, J = 3.0 Hz, H_4), 6.58 (d, 1H, J = 3.0 Hz, H_3), 5.10 (s, 2H, $OC\underline{H}_2$); ^{13}C NMR (CD_2Cl_2, 100 MHz) δ 154.9, 154.0,

149.2, 141.5, 136.8, 133.6, 132.0, 129.1, 125.4, 121.9, 121.9, 113.3, 106.6, 63.2; HRMS (ES) calcd for $C_{16}H_{12}Cl_2NO_2$ ($[M+H]^+$), 320.0240; found, 320.0234.

3-Bromo-5-((5-(4-chlorophenyl)furan-2yl)methoxy)pyridine (34)

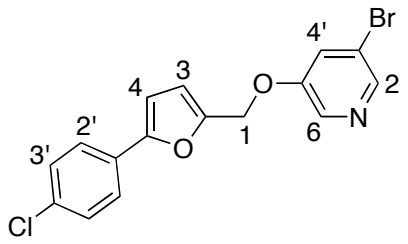

To a solution of PPh_3 (302 mg, 1.15 mmol) in THF (20 mL) was added DEAD (0.18 mL, 1.15 mmol) dropwise at 10 ˚C. After 30 min of stirring, **32** (200 mg, 0.96 mmol) and 3-bromo-5-pyridinol (201 mg, 1.15 mmol) were added and the cooling bath was removed. The mixture was allowed to stir at rt overnight and concentrated *in vacuo*. The residue was diluted with CH_2Cl_2 (15 mL). The solution was washed with H_2O, saturated $NaHCO_3$ solution and brine. The organic layer was dried over $MgSO_4$. The solvent was removed under vacuum and the crude product was purified by flash column chromatography (SiO_2, 1:3/EtOAc:hexanes) to yield **34** (45 mg, 13%) as an oil. IR (microscope): 3064, 2931, 1674, 1573, 1481, 1445 cm^{-1}; ^1H NMR (CD_2Cl_2, 600 MHz) δ 8.32 (d, 1H, J = 2.4 Hz, H_6), 8.30 (d, 1H, J = 1.8 Hz, H_2), 7.62 (d, 2H, J = 9.0 Hz, $H_{2'}$), 7.54 (dd, 1H, J = 2.4, 1.8 Hz, $H_{4'}$), 7.38 (d, 2H, J = 9.0 Hz, $H_{3'}$), 6.67 (d, 1H, J = 3.6 Hz, H_4), 6.58 (d, 1H, J = 3.6 Hz, H_3), 5.10 (s, 2H, OCH_2); ^{13}C NMR (CD_2Cl_2, 100 MHz) δ 129.4, 129.1, 125.4, 124.7, 120.4, 113.3, 106.6, 155.0, 154.0, 149.1,

143.6 137.0, 133.6, 63.2; HRMS (ES) calcd for $C_{16}H_{12}BrClNO_2$ ($[M+H]^+$), 363.9734; found, 363.9728.

5-[5-(4-Chloro-phenyl)-furan-2-ylmethoxy]-2-methyl-pyridine (35)

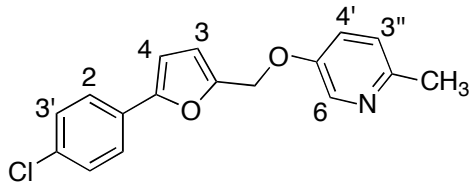

To a solution of PPh_3 (188 mg, 0.71 mmol) in THF (25 mL) was added DEAD (0.11 mL, 0.72 mmol) dropwise at 10 ˚C. After 30 min of stirring, the reaction mixture was brought to rt followed by addition of 5-hydroxy-2-methyl pyridine (78 mg, 0.72 mmol) and **32** (100 mg, 0.48 mmol). The resulting solution was stirred overnight at rt and then the solvent was removed under vacuum. The residue was dissolved in CH_2Cl_2 and the resulting solution was washed with water, saturated $NaHCO_3$ solution, brine, dried over $MgSO_4$ and then concentrated *in vacuo*. The crude was purified by flash column chromatography (SiO_2, 1:3/EtOAc:hexanes) to afford **35** (35 mg, 24%) as a solid. IR (microscope) 2924, 1597, 1494, 1287, 1122, 961 cm^{-1}; ^1H NMR (CD_2Cl_2, 600 MHz) δ 8.26 (s, 1H, H_6), 7.62 (d, 1H, J = 4.8 Hz, H_2), 7.37 (d, 1H, J = 4.8 Hz, $H_{3'}$), 7.26 (dd, 1H, J = 9.0, 3.0 Hz, $H_{4'}$), 7.11 (d, 1H, J = 8.4 Hz, $H_{3''}$), 6.66 (d, 1H, J = 3.6 Hz, H_4), 6.54 (d, 1H, J = 3.6 Hz, H_3), 5.07 (s, 2H, CH_2), 2.47 (s, 3H, CH_3). ^{13}C NMR (100 MHz, CD_2Cl_2) δ 153.7, 152.8, 151.2, 149.9, 136.8, 133.4, 129.1, 125.3, 123.6, 123.2,

112.8, 106.5, 63.1, 41.3, 23.1. HRMS (ES) calcd for $C_{17}H_{15}ClNO_2$ ($[M+H]^+$), 300.0785; found, 300.0789.

2-(4-Chlorophenyl)-5-((3-(trifluoromethyl)phenoxy)methyl)furan (36)

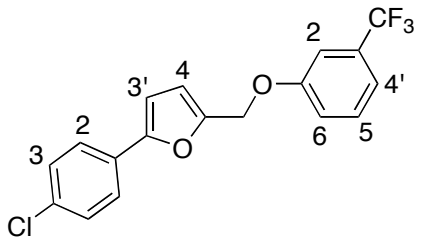

To a solution of PPh_3 (227 mg, 0.87 mmol) in THF (20 mL) was added DEAD (0.14 mL, 0.87 mmol) dropwise at 0 ˚C. After 30 min of stirring, the reaction mixture was brought to rt followed by addition of α,α,α-trifluoro-*meta*-cresol (0.10 mL, 0.87 mmol) and **32** (150 mg, 0.72 mmol). The resulting solution was stirred overnight at rt and then the solvent was removed under vacuum. The residue was dissolved in CH_2Cl_2 and the resulting solution was washed with water, saturated $NaHCO_3$ solution, brine, dried over $MgSO_4$ and then concentrated *in vacuo*. The crude was purified by flash column chromatography (SiO_2, 1:3/EtOAc:hexanes) to afford **36** (21 mg, 9%) as a gum. IR (microscope): 3128, 2930, 1719, 1608, 1492, 1447, 1233, 1202, 1179, 1106, 1118, 1030 cm^{-1}; ^1H NMR (CD_2Cl_2, 600 MHz) δ 7.62 (d, 2H, J = 9.0 Hz, H_2), 7.44 (dd, 1H, $J_1 = J_2 =$ 8.1, Hz, H_5), 7.37 (d, 2H, J = 9.0 Hz, H_3), 7.28 (d, 1H, J = 2.4 Hz, $H_{4'}$), 7.27-7.25 (m, 1H, H_2), 7.20 (dd, 1H, J = 8.4, 2.4 Hz, H_6), 6.67 (d, 2H, J = 3.6 Hz, $H_{3'}$), 6.56 (d, 2H, J = 3.6 Hz, H_4), 5.10 (s, 1H, OCH_2); ^{13}C NMR (CD_2Cl_2, 100 MHz) δ

158.7, 153.7, 149.8, 133.5, 130.3, 129.2, 129.1, 125.3, 122.9, 118.0, 118.0, 112.7, 111.9, 111.9, 106.5, 62.8; HRMS (EI) calcd for $C_{18}H_{12}ClF_3O_2$ (M^+), 352.0477; found, 352.0475.

3-Bromo-5-[5-(4-nitro-phenyl)-furan-2-ylmethoxy]-pyridine (37)

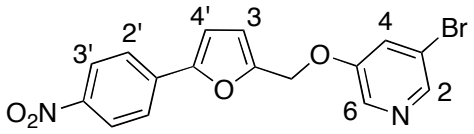

To a solution of PPh_3 (155 mg, 0.59 mmol) in THF (25 mL) was added DEAD (0.09 mL, 0.59 mmol) dropwise at 10 ˚C. After 30 min of stirring, 5-(4-nitrophenyl)furan-2-yl)methanol (100 mg, 0.48 mmol) and 3-bromo-5-pyridinol (119 mg, 0.59 mmol) were added and the cooling bath was removed. The mixture was allowed to stir at rt overnight and concentrated *in vacuo*. The residue was dissolved in CH_2Cl_2 (20 mL) and the resulting solution was washed with H_2O, saturated $NaHCO_3$ solution, brine and then dried over $MgSO_4$. The solvent was removed under vacuum and the crude product was purified by flash column chromatography (SiO_2, 1:3/EtOAc:hexanes) to yield **37** (90 mg, 49%) as a pale yellow solid. IR (microscope) 3073, 2932, 1601, 1558, 1332, 1163, 1026 cm^{-1}; ^1H NMR ($CDCl_3$, 600 MHz) δ 8.35 (d, 2H, J = 1.8 Hz, H_6 and H_2, overlapped), 8.27 (d, 2H, J = 9.0 Hz, $H_{3'}$), 7.81 (d, 2H, J = 9.0 Hz, $H_{2'}$), 7.53 (t, 1H, J = 2.4 Hz, H_4), 6.87 (d, 1H, J = 3.6 Hz, $H_{4'}$), 6.63 (d, 1H, J = 3.6 Hz, H_3), 5.13 (s, 2H, CH_2). ^{13}C NMR (100 MHz, $CDCl_3$) δ 154.5, 152.5, 150.4, 146.7, 143.6, 136.5, 135.6, 124.6,

124.2, 124.1, 113.3, 109.5, 62.7. HRMS (ES) calcd for $C_{16}H_{12}BrN_2O_4$ ($[M+H]^+$), 374.9975; found, 374.9978.

2-[5-(4-Chloro-phenyl)-furan-2-ylmethylsulfanyl]-pyridine (38)

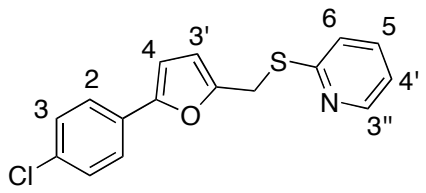

To a solution of PPh_3 (164 mg, 0.63 mmol) in THF (25 mL) was added DEAD (0.1 mL, 0.63 mmol) dropwise at 10 °C. After 30 min of stirring, **32** (100 mg, 0.48 mmol) and 2-mercaptopyridine (69 mg, 0.63 mmol) were added and the cooling bath was removed. The mixture was allowed to stir at rt overnight and concentrated *in vacuo*. The residue was dissolved in CH_2Cl_2 (20 mL) and the resulting solution was washed with H_2O, saturated $NaHCO_3$ solution, brine and then dried over $MgSO_4$. The solvent was removed under vacuum and the crude product was purified by flash column chromatography (SiO_2, 1:3/EtOAc:hexanes) to yield **38** (65 mg, 45%) as a solid. IR (microscope) 3044, 2926,1578, 1481, 1414, 1123, 985. cm^{-1}; ^1H NMR ($CDCl_3$, 400 MHz) δ 8.47 (ddd, 1H, J = 4.9, 1.9, 0.9 Hz, $H_{3''}$), 7.54 (d, 2H, J = 8.8 Hz, H_2), 7.52 (ddd, 1H, J = 8.2, 6.6, 1.8 Hz, H_5), 7.33 (d, 2H, J = 8.8 Hz, H_3), 7.21 (dt, 1H, J = 8.1, 1.1 Hz, H_6), 7.03 (ddd, 1H, J = 7.3, 4.9, 1.9, 1.1 Hz, $H_{4'}$), 6.56 (d, 1H, J = 3.6 Hz, $H_{3'}$), 6.33 (d, 1H, J = 3.2 Hz, H_4). 4.52 (s, 2H, CH_2). ^{13}C NMR (100 MHz, $CDCl_3$) δ 157.7, 152.1, 151.5, 149.3,

135.9, 132.6, 129.2, 128.7, 124.7, 122.3, 119.7, 109.9, 106.4, 26.8. HRMS (EI) calcd for $C_{16}H_{12}ClNOS$ (M^+), 301.0328; found, 301.0382.

3-(Thiophen-2-ylmethoxy)-pyridine (39)

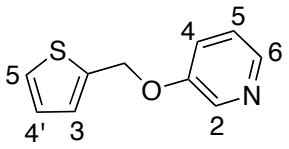

To a solution of PPh_3 (2.75 g, 10.5 mmol) in THF (25 mL) was added DEAD (1.67 mL, 10.5 mmol) dropwise at 10 ˚C, After 30 min of stirring, 2-(hydroxymethyl)thiophene (1.0 g, 8.77 mmol) and 3-hydroxypyridine (1.0 g, 10.5 mmol) were added and the cooling bath was removed. The mixture was allowed to stir at rt overnight and concentrated *in vacuo*. The residue was diluted with CH_2Cl_2 and the resulting solution was washed with H_2O, saturated $NaHCO_3$ solution, brine and then dried over $MgSO_4$. The solvent was removed under vacuum and the crude product was purified by column chromatography (SiO_2, 1:3/EtOAc:hexanes) to yield **39** (800 mg, 48%) as a solid. IR (microscope) 2495, 1773, 1574, 1425, 1257 cm^{-1}; ^1H NMR ($CDCl_3$, 300 MHz) δ 8.38 (d, 1H, J = 2.7 Hz, H_2), 8.24 (dd, 1H, J = 4.2, 1.5 Hz, H_6), 7.36-7.31 (m, 1H, H_4), 7.29-7.17 (m, 2H, H_5), 7.14-7.19 (m, 1H, $H_{4'}$), 7.14-6.97 (m, 1H, H_3), 4.50 (s, 2H, CH_2). ^{13}C NMR (100 MHz, $CDCl_3$) δ 154.4, 142.69, 138.4, 138.3, 127.2, 126.9, 126.6, 123.8, 121.8, 65.3. HRMS (ES) calcd for $C_{10}H_{10}NOS$ ($[M+H]^+$), 192.0477; found, 192.0476.

2-Methyl-5-(thiophen-2-ylmethoxy)pyridine (40)

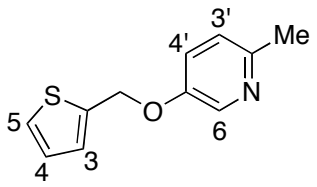

To a solution of PPh_3 (1.72 g, 6.57 mmol) in THF (15 mL) was added DEAD (1.04 mL, 6.57 mmol) dropwise at 10 ˚C. After 30 min of stirring, 5-hydroxy-2-methylpyridine (0.72 g, 6.57 mmol) and 2-(hydroxymethyl)thiophene (0.42 mL, 4.4 mmol) were added and the cooling bath was removed. The mixture was allowed to stir at rt overnight and concentrated *in vacuo*. The residue was diluted with CH_2Cl_2 (50 mL) and the solution was washed with H_2O, saturated $NaHCO_3$ solution and brine. The organic layer was dried over $MgSO_4$. The solvent was removed under vacuum and the crude product was purified by column chromatography (SiO_2, 1:3/EtOAc:hexanes) to yield **40** (270 mg, 30%) as an oil. IR (microscope): 3072, 3021, 2923, 1572, 1495, 1484, 1386, 1264 cm^{-1}; ^1H NMR ($CDCl_3$, 600 MHz) δ 8.26 (d, 1H, J = 3.0 Hz, H_6), 7.33 (dd, 1H, J = 5.4, 1.2 Hz, $H_{3'}$), 7.19 (dd, 1H, J = 8.4, 3.0 Hz, $H_{4'}$), 7.10 (dd, 1H, J = 3.6, 1.2 Hz, H_5), 7.06 (d, 1H, J = 8.4 Hz, H_4), 7.00 (dd, 1H, J = 5.4, 3.6 Hz, H_3), 5.23 (s, 2H, $OC\underline{H}_2$), 2.49 (s, 3H, $ArC\underline{H}_3$); ^{13}C NMR ($CDCl_3$, MHz) δ 152.4, 151.1, 138.6, 137.2, 127.2, 126.9, 126.5, 123.3, 122.9, 65.5, 23.4; HRMS (ES) calcd for $C_{11}H_{12}NOS$ ($[M+H]^+$), 206.0634; found, 206.0635.

3-Bromo-5-((5-(3-nitrophenyl)furan-2-yl)methoxy)pyridine (41)

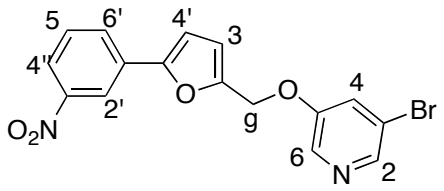

To a solution of PPh_3 (57.4 mg, 0.22 mmol) in THF (15 mL) was added DEAD (0.04 mL, 0.22 mmol) dropwise at 10 ˚C. After 30 min of stirring, 5-[(3-nitrophenyl)furan-2-yl)]methanol (**44**) (40 mg, 0.18 mmol) and 3-bromo-5-pyridinol (38 mg, 0.22 mmol) were added and the cooling bath was removed. The mixture was allowed to stir at rt overnight and concentrated *in vacuo*. The residue was dissolved in CH_2Cl_2 and the resulting solution was washed with H_2O, saturated $NaHCO_3$ solution, brine and then dried over $MgSO_4$. The solvent was removed under vacuum and the crude product was purified by flash column chromatography (SiO_2, 1:3/EtOAc:hexanes) to yield **41** (24 mg, 36%) as a yellow solid. IR (CH_2Cl_2 cast): 3083, 2929, 2866, 1677, 1574, 1555, 1524, 1474, 1349, 862 cm^{-1}; ^1H NMR ($CDCl_3$, 300 MHz) δ 8.50 (t, 1H, J = 2.1 Hz, $H_{2'}$), 8.33 (d, 1H, J = 2.7 Hz, H_6), 8.31 (d, 1H, J = 1.8 Hz, H_2), 8.11 (ddd, 1H, J = 2.4, 0.9, 8.4 Hz, $H_{4'}$), 7.99 (ddd, 1H, J = 1.2, 1.8, 7.8 Hz, $H_{6'}$), 7.59 (t, 1H, J = 7.8 Hz, H_5), 7.54 (dd, 1H, J = 1.8, 2.4 Hz, H_4), 6.85 (d, 1H, J = 3.3 Hz, $H_{4'}$), 6.63 (d, 1H, J = 3.6 Hz, H_3), 5.13 (s, 2H, OC$\underline{H}_2$); ^{13}C NMR ($CDCl_3$, 100 MHz) δ 154.9, 152.6, 150.1,

149.0, 143.7, 137.0, 132.0, 130.1, 129.6, 124.7, 122.3, 120.4, 118.7, 113.3, 108.3, 63.1; HRMS (ES) calcd for $C_{16}H_{12}BrN_2O_4$ ([M+H]$^+$), 374.9975; found, 374.9975.

[5-(3-Nitrophenyl)furan-2-yl)]methanol (44)

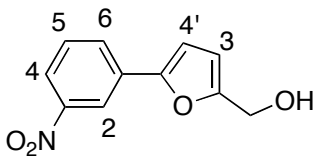

To a solution of 5-(3-nitrophenyl)furan-2-carboxylic acid (**42)** (300 mg, 1.28 mmol) in THF (20 mL) was added dry Et_3N (0.21 mL, 1.54 mmol) followed by ethyl chloroformate (0.15 mL, 1.54 mmol) at 0 ˚C. The reaction mixture was stirred for 2 h at 0 °C and then the precipitate, $Et_3N{\cdot}HCl$, was removed by gravity filtration. To the filtrate was added 1 M solution of $LiAlH_4$ in THF (1.54 mL, 1.54 mmol) at 0 ˚C over a period of 15 min. The reaction mixture was stirred at 0 °C for another 3 h, and then quenched with 5% NaOH (5 mL). The solvent was removed *in vacuo* and the residue was diluted with H_2O (20 mL). The resulting mixture was stirred for another 30 min and then EtOAc (30 mL) was added. The solution was filtered through celite, and then the two layers were separated. The aqueous layer was extracted with EtOAc (2 x 20 mL). The combined organic layer was dried over anhydrous $MgSO_4$ and the solvent was removed to yield the product **44** (157 mg, 56% over two steps). IR (CH_2Cl_2 cast): 3358, 3125, 3087, 2924, 2864, 1620, 1577, 1547, 1523, 1349 cm^{-1}; ^{1}H NMR ($CDCl_3$, 300 MHz) δ 8.50 (t, 1H, J = 2.1 Hz, H_2), 8.10 (ddd, 1H, J = 2.1, 2.4, 8.1 Hz, H_4), 7.96 (ddd,

1H, J = 8.0, 1.4, 1.4 Hz, H_6), 7.55 (t, 1H, J = 8.1 Hz, H_5), 6.77 (d, 1H, J = 3.3 Hz, $H_{4'}$), 6.44 (d, 1H, J = 3.6 Hz, H_3), 4.71 (s, 2H, C<u>H</u>$_2$OH); ^{13}C NMR ($CDCl_3$, 100 MHz) δ 155.2, 151.7, 149.0, 132.4, 129.9, 129.4, 122.0, 118.7, 110.5, 108.2, 57.8; HRMS (ES) calcd for $C_{11}H_9NNaO_4$ ([M+Na]$^+$), 242.04238; found, 242.04264.

3-Bromo-5-(4-methoxy-benzylsulfanyl)-pyridine (45)

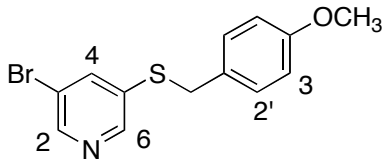

This known compound was prepared according to literature procedure.[55] To a suspension of NaH (60%, 203 mg, 5.06 mmol) in DMF (30 mL) was added 4-methoxybenzylthiol **(47)** (781 mg, 5.06 mmol) followed by 3,5-dibromopyridine (**46)** (1.0 g, 4.22 mmol) at rt. Upon stirring, the reaction mixture became a clear pale yellow colored solution. After the reaction was completed (3 h) as was shown by TLC, DMF was removed *in vacuo*. The residue was dissolved in CH_2Cl_2 (25 mL) and washed with water (25 mL) and brine (25 mL). The organic layer was dried over Na_2SO_4 and concentrated *in vacuo*. The crude product was purified by flash chromatography (SiO_2, 1:2/ EtOAc:hexanes) to yield **45** (900 mg, 69%) as a solid. IR (microscope) 2834, 1653, 1538, 1512, 1439, 1250, 832 cm^{-1}; ^{1}H NMR ($CDCl_3$, 600 MHz) δ 8.45 (d, 1H, J = 2.4 Hz, H_2), 8.39 (d, 1H, J = 1.8 Hz, H_6), 7.68 (t, 1H, J = 2.4 Hz, H_4), 7.18 (d, 1H, J = 8.4 Hz, $H_{2'}$), 6.83 (d, 1H, J = 8.4 Hz, H_3), 4.07 (s, 2H,CH_2), 3.78 (s, 3H, OCH_3). ^{13}C NMR (100 MHz,

$CDCl_3$) δ 159.4, 148.6, 148.4, 139.7, 135.4, 130.2, 128.1, 120.7, 114.4, 55.5, 38.5. HRMS (ES) calcd for $C_{13}H_{13}BrNOS$ ($[M+H]^+$), 309.9895; found, 309.9894.

5-Bromo-*N*-((5-(4-nitrophenyl)furan-2-yl)methyl)pyridin-3-amine (54)

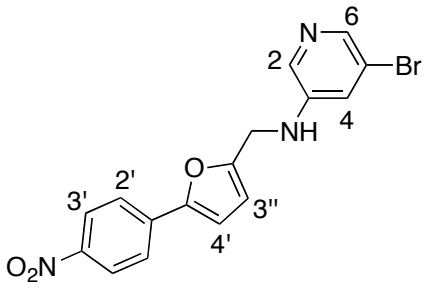

To a solution of PPh_3 (154 mg, 0.56 mmol) in THF (20 mL) was added DEAD (0.09 mL, 0.59 mmol) dropwise at 10 ˚C. After 30 min of stirring, **52** (108 mg, 0.49 mmol) and 3-amino-5-bromopyridine **(53)** (102 mg, 0.59 mmol) were added and the cooling bath was removed. The mixture was allowed to stir at rt overnight. After concentrating *in vacuo* the residue was diluted with CH_2Cl_2 (20 mL) and the solution was washed with H_2O, saturated $NaHCO_3$ solution and brine. The organic layer was then dried over $MgSO_4$. The solvent was removed under vacuum and the crude product was purified by column chromatography (SiO_2, 1:3/EtOAc:hexanes) to yield **54** (90 mg, 49%) as a yellow solid. IR (microscope): 3260, 3108, 3079, 2922, 1602, 1585, 1542, 1513, 1350, 1334, 1294, 1202 cm^{-1}; ^1H NMR (CD_2Cl_2, 500 MHz) δ 8.23 (d, 2H, J = 9.0 Hz, $H_{3'}$), 8.03 (d, 1H, J = 2.5 Hz, H_2), 8.01 (d, 1H, J = 2.0 Hz, H_6), 7.78 (d, 1H, J = 9.5 Hz, $H_{2'}$), 7.18 (dd, 1H, J = 2.5, 2.0 Hz, H_4), 6.87 (d, 1H, J = 3.5 Hz, $H_{4'}$), 6.44 (d, 1H,

J = 3.5 Hz, $H_{3'}$), 4.44 (bs, 3H, CH_2 and $CH_2N\underline{H}$); ^{13}C NMR ($CDCl_3$, 100 MHz) δ 153.2, 151.6, 146.5, 144.3, 139.5, 136.0, 134.2, 124.3, 123.8, 121.3, 121.1, 110.5, 109.8, 40.8; HRMS (ES) calcd for $C_{16}H_{13}N_3O_3Br$ ($[M+H]^+$), 374.0135; found, 374.0135.

(5-Bromo-pyridin-3-yl)-[5-(4-chloro-phenyl)-furan-2-ylmethyl]-amine (55)

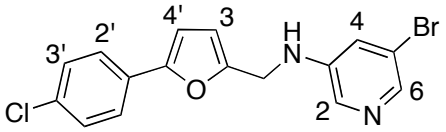

A solution of 3-amino-5-bromopyridine **(53)** (92 mg, 0.53 mmol) and (5-(4-chlorophenyl)furan-2-carbaldehyde (100 mg, 0.49 mmol) in MeOH (20 mL) was cooled to 0 ˚C. Acetic acid (0.060 mL, 0.97 mmol) was added followed by sodium cyanoborohydride (46 mg, 0.73 mmol) and the mixture stirred overnight at rt. The solvent was removed under vacuum and the residue was dissolved in EtOAc (25 mL) and the resulting solution was washed with water, saturated $NaHCO_3$ solution, brine, dried over $MgSO_4$ and then concentrated *in vacuo*. The crude material was purified by flash column chromatography (SiO_2, 1:2/EtOAc:hexanes) to yield **55** (115 mg, 65%) as a white solid. IR (microscope) 3125, 2954, 2932, 1732, 1481, 1249, 963, 830 cm^{-1}; ^1H NMR (CD_2Cl_2, 400 MHz) δ 8.02 (d, 1H, J = 2.4 Hz, H_2), 7.99 (d, 1H, J = 2.0 Hz, H_6), 7.59-7.57 (m, 2H, $H_{2'}$), 7.37 (m, 2H, $H_{3'}$), 7.18 (t, 1H, J = 2.4 Hz, H_4), 6.62 (d, 1H, J = 3.6 Hz, $H_{4'}$),

6.36 (d, 1H, J = 3.6 Hz, H_3), 4.38 (bs, 3H, H_4 and $CH_2N\underline{H}$). ^{13}C NMR (100 MHz, CD_2Cl_2) δ 152.8, 151.7, 144.7, 139.7, 134.9, 133.1, 129.3, 129.0, 125.0, 121.0, 110.0, 106.4, 40.9, (one peak not seen). HRMS (ES) calcd for $C_{16}H_{13}ClBrN_2O$ ($[M+H]^+$), 362.9894; found, 362.9895.

(5-Bromo-pyridin-3-yl)-furan-2-ylmethyl-amine (56)

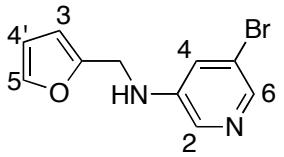

To a solution of furfural (100 mg, 1.04 mmol) in MeOH (20 mL) was added 3-amino-5-bromo pyridine **(53)** (198 mg, 1.14 mmol) and sodium cyanoborohydride (98 mg, 1.56 mmol) and AcOH (0.12 mL, 2.08 mmol) at 0 ˚C. The reaction mixture was stirred overnight at rt and the solvent was removed under vacuum. The residue was dissolved in EtOAc (25 mL) and the resulting solution was washed with water, saturated $NaHCO_3$ solution, brine, dried over $MgSO_4$ and then concentrated *in vacuo*. The crude was purified by flash column chromatography (SiO_2, 1:2/EtOAc:hexanes) to yield **56** (92 mg, 35%) as a white solid. IR (microscope) 3211, 3123, 1586, 1444, 1412, 1325, 1214, 1089, 1001, 919. cm^{-1}; ^1H NMR (CD_2Cl_2, 600 MHz) δ 7.98 (dd, 2H, J = 5.4, 2.4 Hz, $H_{6,2}$), 7.40 (dd, 1H, J = 1.8, 0.6 Hz, H_4), 7.12 (dd, 1H, J = 2.4, 3.0 Hz, H_5), 6.36 (dd, 1H, J = 1.8, 3.0 Hz, $H_{4'}$), 6.28 (dd, 1H, J = 3.0, 0.6 Hz, H_3), 4.32 (s, 2H, CH_2). ^{13}C NMR (100 MHz, CD_2Cl_2) δ 151.6, 142.5, 139.4, 134.5, 121.1, 110.6, 107.7, 40.8. (2 carbon

peaks not observed), HRMS (ES) calcd for $C_{10}H_{10}BrN_2O$ ([M+H]$^+$), 252.9971; found, 252.9969.

Benzofuran-2-ylmethyl-(5-bromo-pyridin-3-yl)-amine (57)

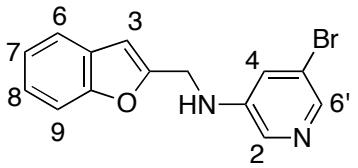

To a solution of benzofuran-2-carboxaldehyde (200 mg, 1.37 mmol) in $ClCH_2CH_2Cl$ (30 mL) at 0 °C was added 3-amino-5-bromo pyridine **(53)** (236 mg, 1.37 mmol) and sodium triacetoxyborohydride (406 mg, 1.92 mmol) followed by AcOH (0.24 mL, 4.10 mmol). After stirring the reaction mixture at rt for overnight (8 h), the solvent was removed under vacuum and the residue was dissolved in EtOAc (20 mL), washed with water, saturated $NaHCO_3$ solution, brine, dried over $MgSO_4$ and then concentrated *in vacuo*. The crude was purified by flash column chromatography (SiO_2, 1:2/EtOAc:hexanes) to yield **57** (225 mg, 54%) as a solid. IR (microscope) 3255, 3054, 2924, 1582, 1473, 1453, 1320, 1254, 942. cm^{-1}; ^{1}H NMR (CD_2Cl_2, 400 MHz) δ 8.04 (d, 1H, J = 2.4 Hz, H_2), 8.01 (d, 1H, J = 2.0 Hz, $H_{6'}$), 7.56-7.53 (m, 1H, H_9), 7.47-7.45 (m, 1H, H_6), 7.30-7.21 (m, 2H, H_8 & H_7), 7.16 (dd, 1H, J = 2.2, 2.2 Hz, H_4), 6.67 (s, 1H, H_3), 4.50 (br, 3H, H_1 & NH). ^{13}C NMR (100 MHz, CD_2Cl_2) δ 155.2, 154.2, 144.6, 139.9, 134.8, 128.3, 124.4, 123.1, 121.1, 121.0, 111.1, 104.4, 41.3, (one peak not observed). HRMS (ES) calcd for $C_{14}H_{12}BrN_2O$ ([M+H]$^+$), 303.0127; found, 303.0129.

Benzo[*b*]thiophen-2-ylmethyl-(5-bromo-pyridin-3-yl)-amine (58)

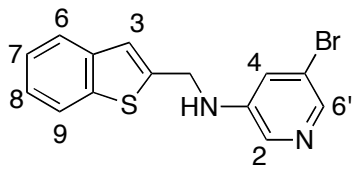

To a solution of benzo[*b*]thiophen-2-carboxaldehyde (765 mg, 4.72 mmol) in $ClCH_2CH_2Cl$ (50 mL) at 0 ˚C was added 3-amino-5-bromo pyridine **(53)** (816 mg, 4.72 mmol) and sodium triacetoxy borohydride (1.4 g, 6.60 mmol) followed by AcOH (0.85 mL, 14.2 mmol). After stirring the reaction mixture at rt for overnight, the solvent was removed under vacuum and the residue was dissolved in EtOAc (25 mL) and the resulting solution was washed with water, saturated $NaHCO_3$ solution, brine, dried over $MgSO_4$ and then concentrated *in vacuo*. The crude was purified by flash column chromatography (SiO_2, 1:2/EtOAc:hexanes) to yield **58** (585 mg, 39%) as a solid. IR (microscope) 3245, 3122, 3078, 3047, 1581, 1446, 1336, 1229, 1129, 866 cm^{-1}; ^1H NMR (CD_2Cl_2, 400 MHz) δ 8.03 (d, 1H, J = 2.8 Hz, H_2), 8.01 (d, 1H, J = 2.0 Hz, $H_{6'}$), 7.81 (dd, 1H, J = 7.8, 1.0 Hz, H_9), 7.74 (dd, 1H, J = 7.0, 1.4 Hz, H_6), 7.38-7.30 (m, 2H, H_8 & H_7), 7.27 (s, 1H, H_3), 7.13 (dd, 1H, J = 2.2, 2.2 Hz, H_4), 4.63 (d, 2H, J = 5.2 Hz, CH_2) 4.56 (d, 1H, J = 4.8 Hz, NH). ^{13}C NMR (100 MHz, $CDCl_3$) δ 144.7, 142.9, 140.0, 139.9, 139.7, 134.8, 124.6, 124.4, 123.5, 122.5, 121.9, 121.09, 121.06, 43.6. HRMS (ES) calcd for $C_{14}H_{12}BrN_2S$ ($[M+H]^+$), 318.9899; found, 318.9898.

***N*-((1*H*-indol-3-yl)methyl)-5-bromopyridin-3-amine (59)**

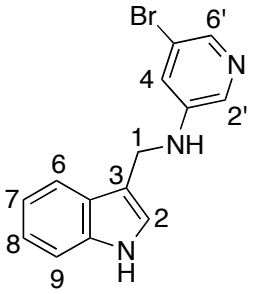

The title compound was obtained from 1*H*-indole-3-carboxaldehyde (214 mg, 1.47 mmol) following the same procedure described for the preparation of **58**. The product **59** was obtained as a solid (102 mg, 23%).IR (microscope) 3402, 3142, 2973, 2869, 1719, 1622, 1585, 1494, 1356, 1129, 934 cm^{-1}; ^{1}H NMR (CD_2Cl_2, 400 MHz) δ 8.37 (br s, 1H, NH), 8.0 (d, 1H, J = 2.4 Hz, $H_{2'}$), 7.97 (d, 1H, J = 2.0 Hz, $H_{6'}$), 7.64 (dd, 1H, J = 0.8 & 8.0 Hz, H_3), 7.43 (dd, 1H, J = 1.0 & 8.2 Hz, H_9), 7.25-7.21 (m, 2H, H_2 & H_2), 7.16-7.12 (m, 2H, H_8 & H_7), 4.49 (d, 2H, J = 4.8 Hz, CH_2), 4.21 (br, 1H, NH). ^{13}C NMR (100 MHz, DMSO-d_6) δ 145.6, 138.9, 136.7, 134.6, 126.7, 123.3, 122.6, 121.1, 120.4, 119.9, 118.8, 112.6, 111.5, 39.6. HRMS (ES) calcd for $C_{14}H_{13}BrN_3$ ($[M+H]^+$), 302.0287; found, 302.0290.

(5-Bromo-pyridin-3-yl)-(1-methyl-1*H*-indol-3-ylmethyl)-amine (60)

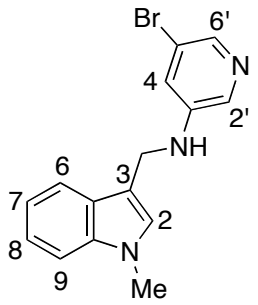

The title compound was obtained from 1-methyl-1*H*-indole-3-carboxaldehyde (250 mg, 1.57 mmol) following the same procedure described for the preparation of **58**. The product **60** was obtained as a solid (130 mg, 26%). IR (microscope) 3270, 3073, 2935, 2887, 1757, 1615, 1583, 1465, 1323, 1100, 923. cm^{-1}; ^{1}H NMR (DMSO-d_6, 400 MHz) δ 7.99 (d, 1H, *J* = 2.4 Hz, $H_{2'}$), 7.75 (d, 1H, *J* = 2.0 Hz, $H_{6'}$), 7.62 (d, 1H, *J* = 8.0 Hz, H_8), 7.38 (d, 1H, *J* = 8.4 Hz, H_7), 7.32 (s, 1H, H_2), 7.17-7.12 (m, 2H, H_4 & H_6), 7.02 (ddd, 1H, *J* = 0.8, 7.4 7.4 Hz, H_9), 6.55 (t, *J* = 5.4 Hz, NH), 4.37 (d, 2H, *J* = 5.2 Hz, CH_2), 3.72 (s, 3H, N-CH_3).^{13}C NMR (100 MHz, DMSO-d_6) δ 146.9, 137.5, 135.8, 134.7, 128.9, 127.5, 122.0, 121.0, 119.8, 119.6, 119.3, 111.3, 110.4, 38.6, 33.0. HRMS (ES) calcd for $C_{15}H_{15}BrN_3$ ($[M+H]^+$), 316.0443; found, 316.0440.

***N*-((5-(4-Aminophenyl)furan-2-yl)methyl)-5-bromopyridin-3-amine (61)**

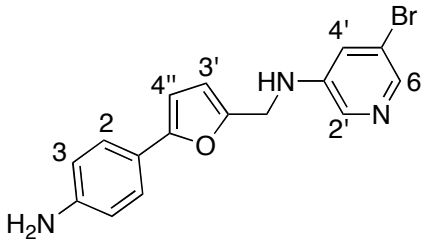

The title compound was prepared by a modified literature procedure.[154] A mixture of **54** (50 mg, 0.13 mmol), hydrazine monohydrate (74 μL, 1.52 mmol), 10% iron powder (5.0 mg) and activated carbon in EtOH (5.0 mL) was heated to reflux for overnight. The reaction mixture was filtered and the filtrate was concentrated under vacuum. The residue was dissolved in EtOAc (8.0 mL) and the resulting solution was washed with water (2 x 3.0 mL) followed by brine. The organic layer was dried over Na_2SO_4 and concentrated *in vacuo* to yield **61** (28 mg, 61%) as a liquid. IR (microscope): 3340, 3223, 3040, 2966, 1620, 1582, 1500, 1289, 1179, 1020 cm^{-1}; ^1H NMR (CD_2Cl_2, 300 MHz) δ 7.99 (d, 1H, J = 2.4 Hz, $H_{2'}$), 7.97 (d, 1H, J = 1.8 Hz, H_6), 7.42 (d, 2H, J = 8.4 Hz, H_2), 7.17 (dd, 1H, $J_1 = J_2$ = 2.3 Hz, $H_{4'}$), 6.67 (d, 2H, J = 8.7 Hz, H_3), 6.37 (d, 1H, J = 3.3 Hz, $H_{3'}$), 6.30 (d, 1H, J = 3.3 Hz, $H_{4''}$), 4.33 (s, 2H, $C\underline{H}_2$), 3.93 (br, 3H, NH and NH_2); ^{13}C NMR (CD_2Cl_2, 100 MHz, - 60 °C) δ 153.7, 149.0, 146.0, 144.4, 137.9, 134.1, 124.4, 120.6, 120.3, 119.9, 114.5, 109.6, 102.4, 40.0; HRMS (ES) calcd for $C_{16}H_{15}N_3OBr$ ($[M+H]^+$), 344.0393; found, 344.0396.

***N*-(4-(5-((5-bromopyridin-3-ylamino)methyl)furan-2-yl)phenyl)methanesulfonamide (62)**

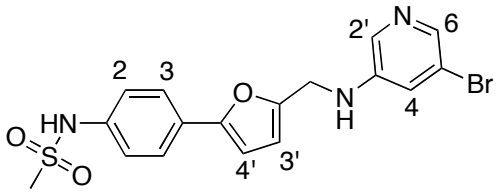

To a solution of **61** (63 mg, 0.18 mmol) in THF was added NEt_3 (19 μL, 0.01 mmol) and methanesulfonyl chloride (14 μL, 0.18 mmol) at 0 ˚C. The reaction mixture was stirred at 0 ˚C for 1 h during which $Et_3N{\cdot}HCl$ was precipitated. After filtration, the organic layer was washed with water, brine and concentrated *in vacuo*. The crude was purified by preparative thin layer chromatography (SiO_2, 1:3/EtOAc:hexanes) to afford **62** (9 mg, 8%) as a gum. IR (CH_2Cl_2 cast): 3387, 3256, 3051, 2928, 2852, 1664, 1583, 1500, 1449, 1325 cm^{-1}; ^1H NMR (CD_2Cl_2, 600 MHz) δ 8.02 (d, 1H, J = 3 Hz, $H_{2'}$), 7.99 (d, 1H, J = 1.8 Hz, H_6), 7.63 (d, 2H, J = 4.2 Hz, H_3), 7.23 (d, 2H, J = 4.2 Hz, H_2), 7.19 (dd, 1H, J = 1.8, 2.4 Hz, H_4), 6.59 (d, 1H, J = 3.6 Hz, $H_{4'}$), 6.51 (br, 1H, SO_2NH), 6.36 (d, 1H, J = 3.6 Hz, $H_{3'}$), 4.39 (bs, 3H, CH_2 and $CH_2N\underline{H}$), 3.01(s, 3H, SO_2CH_3); ^{13}C NMR ($CDCl_3$, 100 MHz) δ 153.3, 151.7, 145.0, 139.6, 136.4, 134.8, 128.2, 125.2, 121.4, 121.2, 110.2, 106.1, 41.0, 39.8 (one peak not seen); HRMS (ES) calcd for $C_{17}H_{17}BrN_3O_3S$ ($[M+H]^+$), 422.0168; found, 422.0161.

Ethyl-(5-bromo-pyridin-3-yl)-[5-(4-nitro-phenyl)-furan-2-ylmethyl]-amine (63)

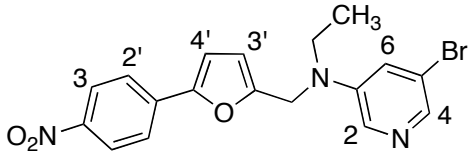

To a solution of **54** (40 mg, 0.11 mmol) and acetaldehyde (7.5 μL, 0.13 mmol) in $ClCH_2CH_2Cl$ (10 mL) was added acetic acid (0.02 mL, 0.33 mmol) followed by sodium triacetoxyborohydride (28 mg, 0.13 mmol) at 0 ˚C. The solution was stirred overnight at rt. The solvent was removed under vacuum and the residue was dissolved in EtOAc (15 mL), and the resulting solution was washed with water, saturated $NaHCO_3$ solution, brine, dried over $MgSO_4$ and then concentrated *in vacuo*. The crude product was purified by flash column chromatography (SiO_2, 1:1/EtOAc:hexanes) to yield **63** (12 mg, 22%) as a yellow gum. IR (microscope) 3072, 2974, 1603, 1574, 1512, 1349, 1331 cm^{-1}; ^1H NMR ($CDCl_3$, 600 MHz) δ 8.23 (d, 2H, J = 7.2 Hz, H_3), 8.15 (d, 1H, J = 2.4 Hz, H_2), 8.02 (br, 1H, H_4), 7.72 (d, 2H, J = 7.2 Hz, $H_{2'}$), 7.26 (bs, 1H, H_6), 6.80 (d, 1H, J = 3.6 Hz, $H_{4'}$), 6.35 (d, 1H, J = 3.6 Hz, $H_{3'}$), 4.53 (s, 2H, $NC\underline{H}_2$), 3.53 (q, 2H, J = 7.2 Hz, $C\underline{H}_2CH_3$), 1.27 (t, 3H, J = 7.2 Hz, CH_3). ^{13}C NMR (100 MHz, $CDCl_3$) δ 153.1, 151.8, 146.7, 145.0, 138.0, 136.2, 132.7, 124.6, 124.0, 121.7, 121.3, 110.9, 109.8, 47.3, 45.6, 12.3. HRMS (ES) calcd for $C_{18}H_{17}BrN_3O_3$ ($[M+H]^+$), 402.0447; found, 402.0451.

_N_-(5-bromopyridin-3-yl)-_N_-((5-(4-nitrophenyl)furan-2-yl)methyl)-cyclopropanecarboxamide (64)

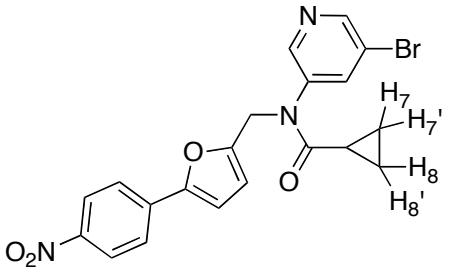

To a stirred solution of **54** (40 mg, 0.11 mmol) in CH_2Cl_2 (5 mL) was added NaOH solution (2M, 5 mL) followed by cyclopropanecarbonyl chloride (27.8 mg, 0.27 mmol) in portions at 10 ˚C. The reaction mixture was stirred for 1 h and the two layers separated. The organic layer was washed with water, brine and then dried with $MgSO_4$. The crude material was concentrated under vaccum. It was purified by flash column chromatography (SiO_2, 1:2/ EtOAc:hexanes) to afford **64** as a yellow solid (12 mg, 26%).IR (microscope): 3096, 3054, 2927, 1645, 1602, 1520, 1442, 1334, 1269, 1211 cm^{-1}; ^1H NMR ($CDCl_3$, 400 MHz) δ 8.68 (d, 1H, J = 2.0 Hz, H_2), 8.49 (d, 1H, J = 2.4 Hz, H_4), 8.24 (d, 2H, J = 9.2 Hz, $H_{4''}$), 7.83 (dd, 1H, $J_1 = J_2$ = 2.2 Hz, H_6), 7.69 (d, 2H, J = 9.2 Hz, H_3), 6.79 (d, 1H, J = 3.2 Hz, $H_{4'}$), 6.40 (d, 1H, J = 3.2 Hz, $H_{3'}$), 4.97 (s, 2H, NC$\underline{H}_2$), 1.26 (br, 1H, $CH_2C\underline{H}CH_2$), 1.14-1.10 (m, 2H, H_7 and H_8), 0.77-0.75 (m, 2H, $H_{7'}$ and $H_{8'}$); ^{13}C NMR ($CDCl_3$, 125 MHz) δ 173.1, 152.0, 151.5, 150.1, 147.8, 146.5, 139.8, 138.4,

135.9, 124.4, 123.8, 120.4, 112.1, 109.8, 46.0, 13.1, 9.4; HRMS (ES) calcd for $C_{20}H_{16}N_3O_4BrNa$ ([M+Na]$^+$), 464.0216; found, 464.0221.

(*S*)-5-(4-Chlorophenyl)-*N*-(6-(dimethylamino)-1-(1,4-dioxo-3,4-dihydrophthalazin-2(1*H*)-yl)-2,6-dioxohexan-3-yl)furan-2-carboxamide (65)

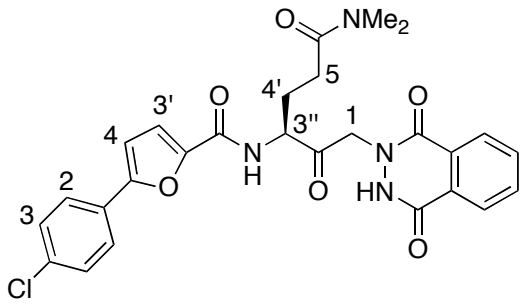

Compound **66** was made by Dr. Zhang[32] in our group and was used for the synthesis of **65**. Compound **66** (25 mg, 0.05 mmol) was treated with TFA/CH_2Cl_2 (3 mL, 1:1 ratio) at 0 ˚C for 1.5 h. The reaction mixture was concentrated under vacuum, and the residue was triturated with Et_2O to obtain the trifluoroacetate salt. In a separate vial a solution of 5-(4-chlorophenyl)furan-2-carboxylic acid (14 mg, 0.06 mmol), HBTU (24 mg, 0.06 mmol) and DIPEA (25.0 μL, 0.14 mmol) in DMF (2.0 mL) was pre-activated for 3 min. The activated solution was then treated with the trifluoroacetate salt in DMF (1.0 mL) for 6 h. The reaction mixture was concentrated under vacuum and the residue was washed with Et_2O (3 x 2.0 mL) and then purified by preparative thin layer chromatography (SiO_2, 1:19/MeOH:CH_2Cl_2) to yield **65** (12.4 mg, 40%) as a solid. $[\alpha]^{25}_D = 3.33°$ (*c* 0.06, MeOH); IR (microscope) 3199, 3051, 2925, 2856, 1675, 1601, 1589, 1477 cm^{-1};

^{1}H NMR (CD_3OD, 600 MHz) δ 8.30-8.28 (m, 1H, Ar<u>H</u>), 8.14-8.12 (m, 1H, Ar<u>H</u>), 7.95-7.91 (m, 2H, Ar<u>H</u>), 7.88 (d, 2H, J = 9.0 Hz, H_2), 7.43 (d, 2H, J = 9.0 Hz, H_3), 7.22 (d, 1H, J = 3.6 Hz, H_4), 6.95 (d, 1H, J = 3.6 Hz, $H_{3'}$), 5.31 (d, 1H, J = 17.4 Hz, H_1), 5.22 (d, 1H, J = 16.8 Hz, H_1), 4.83-4.82 (m, 1H, $H_{3''}$), 3.03 (s, 3H, CH_3), 2.94 (s, 3H, CH_3), 2.66-2.56 (m, 2H, H_5), 2.44-2.39 (m, 1H, $H_{4'}$), 2.20-2.13 (m, 1H, $H_{4'}$); ^{13}C NMR (CD_3OD, 100 MHz) δ 204.5, 174.7, 161.7, 160.7, 156.6, 151.4, 147.5, 135.6, 134.9, 133.5, 130,1, 129,8, 129.6, 127.4, 127.2, 125.9, 125.0, 118.1, 108.8, 70.1, 57.4, 37.6, 35.9, 30.4, 26.3; HRMS (ES) calcd for $C_{27}H_{25}N_4O_6ClNa$ ([M+Na]$^+$), 559.1355; found, 559.1351.

***N*-{5-[5-(4-Nitro-phenyl)-furan-2-ylmethylene]-4-oxo-2-thioxo-thiazolidin-3-yl}-acetamide (67)**

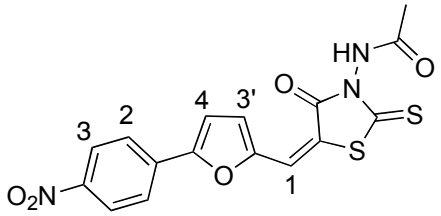

A suspension of 5-(4-nitrophenyl)furan-2-carboxaldehyde (250 mg, 1.15 mmol), *N*-(4-oxo-2-thioxothiazolidin-3-yl)acetamide (220 mg, 1.15 mmol) and NaOAc (378 mg, 4.6 mmol) in AcOH (5.0 mL) was heated to 95 ˚C with stirring for 12 h. Cooling the reaction mixture followed by addition of ice-cold water afforded a bright orange colored solid. After filtration, the solid was washed with absolute EtOH. It was dried *in vauo* to afford **67** as an orange solid (405 mg, 90%). IR (microscope) 3239, 3038, 1729, 1678, 1551, 1347, 1271, 1139 cm^{-1}; ^{1}H NMR

(DMSO-d_6, 600 MHz) δ 8.39 (d, 2H, J = 9.0 Hz, H_3), 8.07 (d, 1H, J = 9.0 Hz, H_2), 7.80 (s, 1H, H_1), 7.61 (d, 1H, J = 3.6 Hz, H_4), 7.45 (d, 1H, J = 3.6 Hz, $H_{3'}$), 2.06 (s, 3H, CH_3). ^{13}C NMR (100 MHz, DMSO-d_6) δ 191.7, 168.4, 163.7, 156.5, 151.5, 147.6, 134.8, 125.9, 125.4, 124.2, 120.0, 117.9, 114.5, 20.9. HRMS (ES) calcd for $C_{16}H_{11}SN_3O_5Na$ ([M+Na]$^+$), 412.0032; found, 412.0034.

5-((5-Bromopyridin-3-yloxy)methyl)-2-(4-chlorophenyl)oxazole (69)

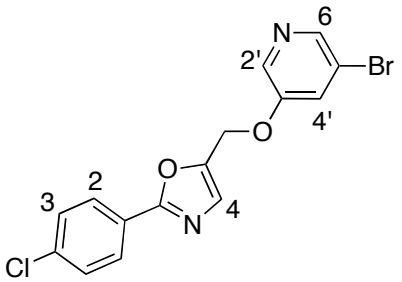

To a solution of PPh_3 (121 mg, 0.46 mmol) in THF (20 mL) was added DEAD (0.07 mL, 0.46 mmol) dropwise at 10 °C. After 30 min of stirring, **74** (81 mg, 0.38 mmol) and 3-bromo-5-pyridinol (80 mg, 0.46 mmol) were added and the cooling bath was removed. The mixture was allowed to stir at rt overnight and concentrated *in vacuo*. The residue was diluted with CH_2Cl_2 (20 mL). The solution was washed with H_2O, saturated $NaHCO_3$ solution, brine and then dried over $MgSO_4$. The solvent was removed under vacuum and the crude product was purified by flash chromatography (SiO_2, 1:3/EtOAc:hexanes) to yield **69** (80 mg, 58%) as a solid. IR (microscope): 3049, 2984, 2934, 1728, 1609, 1577, 1562, 1483, 1456, 1388, 1262, 1221 cm^{-1}; ^{1}H NMR (CD_2Cl_2, 400 MHz) δ 8.33-8.32 (m,

2H, $H_{2'}$ and H_6), 7.99 (d, 2H, J = 9.0 Hz, H_2), 7.52 (dd, 1H, J = 2.0, 2.8 Hz, $H_{4'}$), 7.46 (d, 2H, J = 8.5 Hz, H_3), 7.28 (s, 1H, H_4), 5.17 (s, 2H,OC$\underline{H}_2$); ^{13}C NMR (CD_2Cl_2, 100 MHz) δ 161.3, 153.6, 145.4, 142.8, 136.1, 136.0, 128.9, 128.8, 127.2, 124.9, 123.0, 120.0, 59.5; HRMS (ES) calcd for $C_{15}H_{11}N_2O_2ClBr$ ([M+H]$^+$), 364.9687; found, 364.9684.

5-Bromo-*N*-((2-(4-chlorophenyl)oxazol-5-yl)methyl)pyridin-3-amine (70)

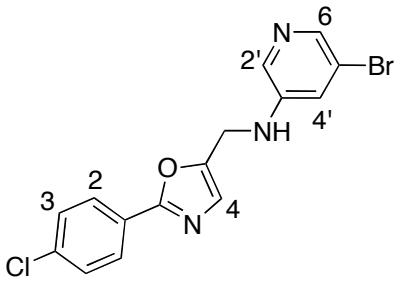

A solution of the aldehyde **75** (40 mg, 0.19 mmol) and 3-amino-5-bromo pyridine **(53)** (40 mg, 0.23 mmol) in $ClCH_2CH_2Cl$ was prepared and cooled to 0 ˚C. Acetic acid (35 μL, 0.58 mmoL) was added followed by sodium triacetoxyborohydride (57 mg, 0.27 mmol) and the mixture was stirred for 12 h at rt. The solvent was removed under vacuum, and the residue was diluted with EtOAc (25 mL). The resulting solution was washed with water, saturated $NaHCO_3$ solution, brine, dried over $MgSO_4$ and then concentrated *in vacuo*. The crude product was purified by column chromatography (SiO_2, 1:2/5% Et_3N in EtOAc:hexanes) to yield **70** (25 mg, 36%) as a solid. IR (microscope): 3208, 3112, 3045, 2968, 2923, 1689,

1584, 1484, 1446, 1327 cm^{-1}; ^1H NMR (CD_2Cl_2, 600 MHz) δ 8.03-8.02 (m, 2H, $H_{2'}$ and H_6), 7.94 (d, 2H, J = 9.0 Hz, H_2), 7.44 (d, 2H, J = 8.4 Hz, H_3), 7.17 (t, 1H, J = 1.8 Hz, $H_{4'}$), 7.08 (s, 1H, H_4), 4.46 (d, 2H, J = 6.0 Hz, NHC$\underline{H}_2$), 4.38 (t, 1H, J = 6.0 Hz, N$\underline{H}$); ^{13}C NMR (CD_2Cl_2, 100 MHz) δ 161.0, 149.1, 144.4, 140.2, 136.6, 134.9, 129.3, 127.7, 126.4, 126.2, 121.2, 121.0, 38.8; HRMS (ES) calcd for $C_{15}H_{12}N_3OClBr$ ($[M+H]^+$), 363.9847; found, 363.9846.

Ethyl 3-diazo-2-oxopropanoate (72)

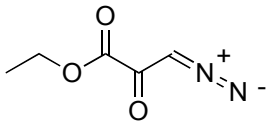

The title compound was prepared by a literature procedure of Müller and Chappellet.[57] To a solution of ethyl chlorooxoacetate **(71)** (1.6 mL, 14 mmol) in THF (20 mL) was added 2 M $TMSCHN_2$ solution in hexane (21 mL, 42 mmol) dropwise at rt over a period of 20 min. After 3 h of stirring at rt, the solvent was removed in vacuo, and the crude product was purified by flash column chromatography (SiO_2, 1:3/EtOAc:hexanes) to yield **72** as a pale yellow solid (1.43 g, 72%). IR (microscope) 3081, 2995, 2163, 2109, 1736, 1626, 1379, 1272, 1115 cm^{-1}; ^1H NMR ($CDCl_3$, 600 MHz) δ 6.16 (s, 1H, CH=N), 4.35 (q, 2H, J = 7.2 Hz, OCH_2), 1.38 (t, 3H, J = 7.2 Hz, CH_3). ^{13}C NMR (100 MHz, $CDCl_3$) δ 177.1, 160.6, 63.2, 57.1, 14.2. HRMS (ES) calcd for $C_5H_7N_2O_3$ ($[M+H]^+$), 143.0451; found, 143.0450.

2-(4-Chlorophenyl)oxazole-5-carboxylic acid ethyl ester (73)

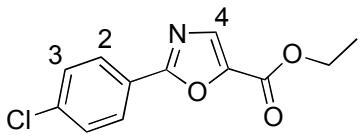

To a stirred suspension of bis-copper acetylacetonate (14 mg) in benzene (12 mL) and 4-chlorobenzonitrile (4.81 g, 34.98 mmol) at reflux temperature was added ethyl diazopyruvate **(72)** (2.3 g, 16.19 mmol) in benzene (20 mL) during a period of 3 h. The reaction mixture was heated for about 3 h until TLC indicated completion of the reaction. The solvent was removed *in vacuo*, and the residue was diluted with saturated $NaHCO_3$ solution (50 mL). The solution was then extracted with EtOAc (3 x 40 mL). The combined organic layers were washed with brine (25 mL), dried over $MgSO_4$ and then concentrated in vacuo. The crude product was purified by column chromatography (SiO_2, 1:4/EtOAc:hexanes) to yield **73** as a solid (600 mg , 15%). IR (microscope) 3089, 2983, 1734, 1605, 1475, 1304, 1151 cm^{-1}; ^1H NMR (CD_2Cl_2, 600 MHz) δ 8.07 (d, 2H, J = 9.0 Hz, H_2), 7.81 (S, 1H, H_4) 7.50 (d, 2H, J = 9.0 Hz, H_3), 4.40 (q, 2H, J = 7.2 Hz, CH_2), 1.40 (t, 3H, J = 7.2 Hz, CH_3). ^{13}C NMR (CD_2Cl_2, 600 MHz) δ 163.2, 157.8, 142.8, 137.8, 135.3, 129.4, 128.6, 125.3, 61.7, 14.2. HRMS (ES) calcd for $C_{12}H_{11}ClNO_3$ ($[M+H]^+$), 252.0422; found, 252.0422.

[2-(4-Chloro-phenyl)-oxazol-5-yl]-methanol (74)

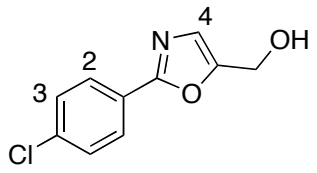

To a solution of **73** (550 mg, 2.19 mmol) in CH_2Cl_2 at -50 °C was added 1 M solution of DIBALH in CH_2Cl_2 (6.6 mL, 6.57 mmol) under argon and the mixture was stirred at this temperature for 1 h. The reaction mixture was brought to rt and quenched with 0.5 mL of saturated NH_4Cl solution, and the solvent was removed under vacuum. The residue was dissolved in EtOAc (20 mL) and the resulting solution was washed with brine, dried over $MgSO_4$ and then concentrated *in vacuo*. The crude was purified by flash column chromatography (SiO_2, 1:2/EtOAc:hexanes) to yield **74** (454 mg, 51%) as a solid. IR (microscope) 3214, 2900, 1695, 1609, 1483, 1410, 1110, 992. cm^{-1}; ^1H NMR ($CDCl_3$, 600 MHz) δ 7.98 (d, 2H, J = 9.0 Hz, H_2), 7.45 (d, 2H, J = 9.0 Hz, H_3), 7.0 (s, 1H, H_4), 4.71 (d, 2H, J = 6.0 Hz, CH_2), 2.0 (t, 1H, J = 6.0 Hz, O<u>H</u>). ^{13}C NMR (100 MHz, $CDCl_3$) δ 161.1, 151.6, 136.5, 129.2, 127.7, 126.3, 126.2, 55.3. . HRMS (ES) calcd for $C_{10}H_9ClNO_2$ ($[M+H]^+$), 210.0316; found, 210.0315.

2-(4-Chloro-phenyl)-oxazole-5-carbaldehyde (75)

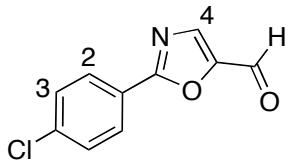

To a solution of **74** in CH_2Cl_2 (15 mL) was added DMP (184 mg, 0.43 mmol) at rt. After stirring for 45 min, a 1:1 mixture of saturated $NaHCO_3$ solution and 1M $Na_2S_2O_3$ was added and stirring continued (10 min) until the reaction mass separates into two clear layers. The layers were separated, the aqueous layer was extracted with CH_2Cl_2 (3x5 mL) and the combined organic layer was washed with saturated $NaHCO_3$ solution, brine and then dried over $MgSO_4$. The solvent was removed under vacuum to afford **75** as a solid (50 mg, 72%). IR (microscope) 3081, 2890, 1689, 1665, 1478, 981 cm^{-1}; ^1H NMR ($CDCl_3$, 400 MHz) δ 9.81 (s, 1H, CHO), 8.12 (d, 2H, J = 8.0 Hz, H_3), 7.95 (s, 1H, H_4), 7.26 (d, 2H, J = 1.2 Hz, H_2). ^{13}C NMR (100 MHz, $CDCl_3$) δ 176.4, 164.5, 150.0, 139.1, 138.6, 129.6, 129.0, 124.8. HRMS (ES) calcd for $C_{10}H_7ClNO_2$ ($[M+H]^+$), 208.0159; found, 208.0161.

(*S*)-2-((2*S*,3*S*)-2-((*S*)-2-Acetamido-3-methylbutanamido)-3-(benzyloxy)butanamido)-4-methylpentanoic acid (76)

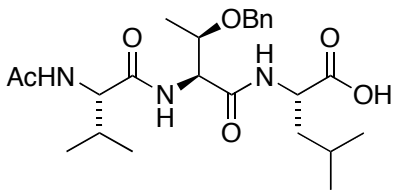

This known compound was prepared according to procedure developed in our group.[34] The tripeptide **90** (0.6 g, 1.07 mmol) was dissolved in TFA/CH_2Cl_2 (20 mL, 1:1 ratio) at 0 °C and stirred for 2 h. Then the reaction mixture was concentrated under vacuum. The residue was triturated with Et_2O (10 mL) to provide the corresponding trifluoroacetate salt as a pale yellow sticky solid. To this trifluoroacetate salt was added CH_2Cl_2 (10 mL) and Et_3N (10 mL) and Ac_2O (10 mL) and stirred overnight. The solvent was removed under vacuum and the residue was diluted with H_2O (10 mL) and extracted with EtOAc (3 x 15 mL). The combined organic layers were washed with brine, dried over $MgSO_4$, filtered, and concentrated *in vacuo* to afford the *N*-acetyl tripeptide **91** that was used in the next reaction without purification. To a solution of *N*-acetyl tripeptide **91** in THF/H_2O (30 mL, 1:1 ratio) at 0 ºC was added LiOH (70 mg, 1.61 mmol) and the reaction was stirred for 2 h until completion as was shown by TLC for the absence of starting material. The reaction mixture was quenched using AcOH and the solvent was removed under vacuum. The solution was treated with H_2O (10 mL) and acidified to pH 3.0 with citric acid followed by extraction with EtOAc (2 x 15 mL). The combined organic layer was washed with brine, dried over $MgSO_4$, filtered, and concentrated *in vacuo* and the crude product was purified by flash chromatography (SiO_2, 1:19/MeOH: CH_2Cl_2) to yield **76** (501 mg, 97%) as a white solid. $[\alpha]^{25}_{D}$ = -25.33° (*c* 0.180, MeOH); IR (microscope) 3293, 3089, 2962, 164, 1550, 1470 cm^{-1}; ^1H NMR (CD_3OD, 600 MHz) δ 7.33-7.23 (m, 5H, Ph<u>H</u>), 4.83 (br, 1H, N<u>H</u>), 4.58 (d, 1H, *J* = 10.8 Hz, OC<u>H</u>$_2$Ph), 4.51 (d, 1H, *J* = 4.2 Hz, NHC<u>H</u>CO(Thr)), 4.48 (d, 1H, *J* = 11.4 Hz, OC<u>H</u>$_2$Ph), 4.45 (br, 1H,

NHC<u>H</u>CO(Leu)), 4.21 (d, 1H, J = 7.2 Hz, NHC<u>H</u>CO(Val)), 4.12-4.07 (m, 1H, CH_3C<u>H</u>OBn(Thr)), 2.12-2.07 (m, 1H, CHC<u>H</u>$(CH_3)_2$(Val)), 1.95 (s, 1H, COC<u>H</u>$_3$), 1.67-1.59 (m, 3H, 2xCHC<u>H</u>$_2$CH(Leu) and 1xCH_2C<u>H</u>$(CH_3)_2$(Leu)), 1.22 (d, 3H, J = 6.0 Hz, CHC<u>H</u>$_3$(Thr)), 0.96 (d, 3H, J = 6.6 Hz, CH(C<u>H</u>$_3$)(Val)), 0.95 (d, 3H, J = 7.2 Hz, CH(C<u>H</u>$_3$)(Val)), 0.89 (d, 3H, J = 6.6 Hz, CH(C<u>H</u>$_3$)(Leu)), 0.87 (d, 3H, J = 6.0 Hz, CH(C<u>H</u>$_3$)(Leu)) ; ^{13}C NMR (CD_3OD, 100 MHz) δ 176.0, 174.1, 173.5, 172.0, 139.6, 129.3, 129.1, 128.8, 128.6, 75.1, 71.3, 59.5, 57.4, 40.8, 30.3, 24.7, 22.2, 21.2, 20.7, 18.5, 17.4, 15.6; HRMS (ES) calcd for $C_{24}H_{37}N_3O_6Na$ ([M+Na]$^+$), 486.2575; found, 486.2573.

(*S*)-4-((*S*)-2-((2*S*,3*R*)-2-((*S*)-2-Acetamido-3-methylbutanamido)-3-(benzyloxy)butanamido)-4-methylpentanamido)-6-fluoro-*N*,*N*-dimethyl-5-oxohexanamide (77)

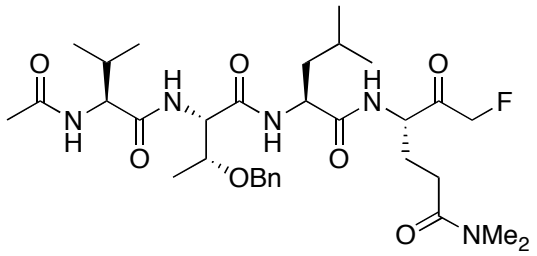

To a solution of fluoroalcohol **94** (15 mg, 0.02 mmol) in DMF (2.0 mL) was added DMP (20 mg, 0.07 mmol) at rt. The mixture was stirred for 1.5 h and the solvent was evaporated under vaccum. The mass was triturated with Et_2O to obtain the crude product (12 mg). The crude (6.0 mg) was purified by HPLC using a Waters μBondapak C-18 column (WAT015814, 10 μm, 125 Å, 25 x 100

mm). The column was operated at a flow rate of 10 mL/min with dual wavelength detection at 220 nm and 254 nm. The method used for the purification started at 30% CH_3CN for 4 min, ramped up to 90% CH_3CN over 36 min and then ramped down to 30% CH_3CN in 2 min followed by flushing with 20% CH_3CN for 5 min. The desired product **77** was isolated at a retention time of t_R = 17.7 min. The solution was frozen and lyophilized to give **77** as a solid (2 mg, 33%). IR (microscope): 3281, 3087, 2961, 2934, 1638, 1585, 1551, 1454; ^{1}H NMR (CD_3CN:D_2O (6:4), 600 MHz) δ 7.33-7.25 (m, 5H, Ar$\underline{H}$), 5.16-4.96 (m, 2H, COC$\underline{H}_2$F), 4.52 (d, 1H, *J* = 11.4 Hz, OC$\underline{H}_2$Ph), 4.43 (d, 1H, *J* = 11.4 Hz, OC$\underline{H}_2$Ph), 4.37 (d, 1H, *J* = 4.2 Hz, αH (Thr)), 4.35-4.33 (m, 1H, αH), 4.23-4.20 (m, 2H, αH), 3.95-3.93 (m, 1H, βH (Thr)), 2.89 (s, 3H, NCH_3), 2.80 (s, 3H, NCH_3), 2.32-2.25 (m, 2H, C$\underline{H}_2$CON$(CH_3)_2$), 2.05-1.99 (m, 2H, C$\underline{H}_2$CH$_2$CON$(CH_3)_2$), 1.78-1.74 (m, 1H, CHC$\underline{H}(CH_3)_2$(Val)), 1.54-1.46 (m, 3H, 2xCHC$\underline{H}_2$CH(Leu) and 1xCH$_2$C$\underline{H}(CH_3)_2$(Leu)), 1.91 (s, 3H, $COCH_3$), 1.11 (d, 3H, *J* = 6.0 Hz, CHC$\underline{H}_3$(Thr)), 0.84 (d, 3H, *J* = 6.0 Hz, CHC$\underline{H}_3$(Val)), 0.83 (d, 3H, *J* = 6.6 Hz, CHC$\underline{H}_3$(Val)), 0.81 (d, 3H, *J* = 6.0 Hz, CHC$\underline{H}_3$(Leu)), 0.78 (d, 3H, *J* = 6.6 Hz, CHC$\underline{H}_3$(Leu)); HRMS (ES) calcd for $C_{32}H_{51}N_5O_7F$ ([M+H]$^+$), 636.3767; found, 636.3765.

(*S*)-*tert*-Butyl 6-(dimethylamino)-1-fluoro-2,6-dioxohexan-3-ylcarbamate (78)

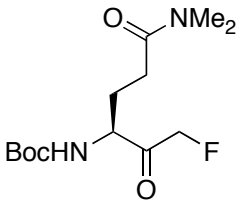

This known compound was synthesized by a modified patented procedure of Palmer.[73] To a solution of *N*-*t*Boc-L-glutamic acid-γ-dimethylamide **81** (1.1 g, 4.0 mmol) in THF (20 mL) was added carbonyl diimidazole (CDI, 0.74 g, 4.0 mmol) at rt. The reaction mixture was stirred for 1 h. Magnesium salt **85** (0.94 g, 2 mmol) was added in the form of a fine powder and the reaction mixture was stirred for another 6 h. The reaction mixture was then washed with 1N HCl (2.0 mL). The aqueous layer was extracted with toluene (2 x 10 mL). The combined organic layer was washed with brine (5 mL), dried with $MgSO_4$ and concentrated under vacuum to about 10 mL at or below 20 ˚C. The toluene solution was hydrogenated over night at 1 atm H_2 with Pd catalyst (0.2 g, 10% w/w). After filtration, the solution was washed with 1N HCl (2 x 25 mL), saturated $NaHCO_3$ solution, brine and then dried over $MgSO_4$. The solvent was removed under vacuum at or below 20 ˚C to give the product **78** (115 mg, 20%) as an oil that was used for next reaction without further purification. IR (CH_2Cl_2 cast): 3300, 2976, 2932, 1740, 1708, 1633, 1509, 1393 cm^{-1}; ^1H NMR ($CDCl_3$, 600 MHz) δ 5.68 (br, 1H, -CO-NH-), 5.12 (dd, 1H, $J_1 = J_2 = 16.8$ Hz $COCH_2F$), 5.01(dd, 1H, $J_1 = J_2 =$

16.2 Hz, $COCH_2F$), 4.46 (br, 1H, αH), 2.97 (s, 3H, -N-CH_3), 2.91 (s, 3H, -N-CH_3), 2.48-2.43 (m, 1H, Hγ), 2.39-2.34 (m, 1H, Hγ), 2.18-2.13 (m, 1H, Hβ), 1.97-1.93 (m, 1H, Hβ), 1.41 (s, 9H, $(CH_3)_3C$); HRMS (ESI) calcd for $C_{13}H_{23}N_2O_4FNa$ ($[M+Na]^+$), 313.1534 found, 313. 15319.

2-*tert*-Butoxycarbonylamino-4-dimethylcarbamoyl-butyric acid benzyl ester (80)

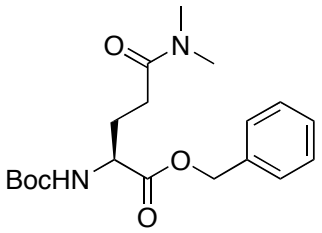

The title compound was prepared by a literature procedure of Ramtohul *et al*.[72] To a solution of Boc-Glu(OBn)-OH **(79)** (5.6 g, 16.6 mmol) in CH_2Cl_2 (70 mL) was added Et_3N (2.3 mL, 18.4 mmol) followed by EtOCOCl (1.7 mL, 17.68 mmol) at 0 °C. After stirring for 30 min at 0 °C, $NHMe_2$•HCl (1.5 g, 18.94 mmol) and Et_3N (2.9 mL, 20.6 mmol) were added to the reaction mixture. The resulting mixture was stirred overnight at rt. The solvent was removed, and the residue was diluted with H_2O (50 mL). The resulting mixture was extracted with EtOAc (3 x 50 mL). The combined organic layer was washed with 1 N HCl (20 mL), brine (20 mL) and dried over $MgSO_4$. The solvent was removed under vacuum, and the crude product was crystallized using CH_2Cl_2/hexanes to afford **80** as a white crystalline solid (4.90 g, 91%); mp 89-91 °C; IR (microscope) 3302, 2976, 2934, 1744, 1711, 1638, 1392, 1212 cm^{-1}; ^1H NMR (CD_2Cl_2, 400 MHz) δ 7.36 (m, 5H, Ph),

5.61 (d, 1H, J = 6.0 Hz, NH), 5.18 (d, 1H, J = 12.6 Hz, OCH_2), 5.12 (d, 1H, J = 12.0 Hz, OCH_2), 4.27-4.24 (m, 1H, αH), 2.88 (s, 6H, NCH_3), 2.34 (m, 2H, $COCH_2$), 2.13 (m, 1H, $COCH_2C\underline{H}_2$), 1.99 (m, 1H, $COCH_2C\underline{H}_2$), 1.41 (s, 9H, Boc). HRMS (ES) calcd for $C_{19}H_{28}N_2O_5Na$ ($[M+Na]^+$), 387.1890; found, 387.1890.

2-*tert*-Butoxycarbonylamino-4-dimethylcarbamoyl-butyric acid (81)

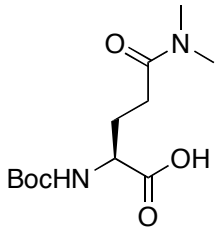

The title compound was prepared by a literature procedure of Ramtohul *et al*.[72] To a stirred solution of **80** (5.0 g, 13.72 mmol) in MeOH (50 mL) was added Pd/C (0.5 g, 10% w/w) at rt. The resulting suspension was stirred under a hydrogen atmosphere for 6 h. Filtration through celite, followed by removal of solvent afforded the crude product, which was recrystallized from CH_2Cl_2/hexanes to afford the product **81** as a white crystalline solid (3.25g, 86%); mp 138-139 °C; IR (microscope) 3327, 2978, 1786, 1711, 1630, 1510, 1166 cm^{-1}; ^1H NMR ($CDCl_3$, 400 MHz) δ 5.68 (bs, 1H, NH), 4.21 (d, 1H, J = 5.6 Hz, NHCH), 3.03 (s, 3H, NCH_3), 2.96 (s, 3H, NCH_3), 2.75-2.69 (m, 1H, $COCH_2$), 2.48-2.41 (m, 1H, $COCH_2$), 2.25-2.20 (m, 1H, $COCH_2C\underline{H}_2$), 2.02-1.93 (m, 1H, $COCH_2C\underline{H}_2$), 1.42 (s, 9H, Boc). HRMS (ES) calcd for $C_{12}H_{21}N_2O_5$ ($[M-H]^-$), 273.1445; found, 273.1445.

Dibenzyl 2-fluoromalonate (83)

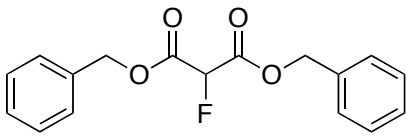

This known compound was synthesized according to the patented procedure of Palmer.[73] A solution of dimethyl fluoromalonate **(82)** (10.2 g, 67.9 mmol), benzyl alcohol (34 mL, 330 mmol) and *para*-toluenesulphonic acid (760 mg, 4 mmol) in toluene in a 3-neck 100-mL round bottom flask that was connected to a Dean-Stark apparatus was heated (80 °C oil bath) *in vacuo* (30 mm of Hg) until all of the toluene had distilled. The reaction mixture was then heated for an additional 5 h. After this the reaction mixture was allowed to cool to 75 °C followed by adding isopropanol (15 mL) and hexane (30 mL). The product crystallized and was placed in the freezer over night. The solid was filtered, washed with hexane and vacuum dried to give dibenzyl fluoromalonate **83** (18.0 g, 88%) as a white crystalline solid; mp 63-64 °C; IR (CH_2Cl_2 cast): 3090, 2991, 2909, 1781, 1763, 1744, 1605, 1497, 1471 cm^{-1}; ^1H NMR (CD_2Cl_2, 600 MHz) δ 7.35 (m, 6H, Ar-H), 7.31 (m, 4H, Ar-H), 5.39 (d, 1H, J_{H-F} = 48 Hz, CH-F), 5.24 (d, 4H, $^5J_{H-F}$ = 3.6 Hz Ar-CH_2-); ^{13}C NMR (CD_2Cl_2, 100 MHz) δ 163.8 (d, $^2J_{C-F}$ = 24.5 Hz), 134.7, 128.9, 128.8, 128.5, 85.5 (d, $^1J_{C-F}$ = 194 Hz), 68.4; HRMS (ESI) calcd for $C_{17}H_{15}FNaO_4$ ($[M+Na]^+$), 325.08466 found, 325.084.

3-(Benzyloxy)-2-fluoro-3-oxopropanoic acid (84)

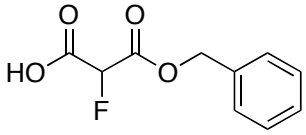

This known compound was synthesized according to the patented procedure of Palmer.[73] A suspension of dibenzyl fluoromalonate **83** (3.0 g, 9.92 mmol) in isopropanol (16 mL) was heated to 45 ˚C, at which the solid was dissolved and a clear solution obtained. To this solution, 1 M aqueous solution of NaOH (10 mL) was added dropwise at this temperature over a period of 45 min. After an additional 10 min, the solution was concentrated to about 7.0 mL and then water (4.0 mL) was added. The pH of the solution was adjusted to 9 with saturated $NaHCO_3$ solution. The mixture was washed with CH_2Cl_2 (2 x 4 mL) to remove benzyl alcohol. The pH of the aqueous layer was adjusted to 2.2 using 5 M HCl. The mixture was then extracted with diisopropyl ether (8.0 mL). The pH of the aqueous layer was readjusted to 1.9 with 5 M HCl followed by further extraction with diisopropyl ether (3 x 8.0 mL). The combined extract was washed with brine (5.0 mL), dried over MgSO4, filtered, and concentrated *in vacuo* below 25 ˚C. The oily residue was triturated with hexane (20 mL) for about 5 h during which the solid product crystallized out. The solid was filtered and dried under vacuum to give the monoester **84** (800 mg, 38%). IR (CH_2Cl_2 cast): 3486-2526 (br), 1760, 1736, 1605, 1586, 1496, 1435 cm^{-1}; ^1H NMR (CD_2Cl_2, 600 MHz) δ 7.37 (m, 5H, Ar-H), 5.39 (d, 1H, $^2J_{H\text{-}F}$ = 48 Hz, CH-F), 5.32 (d, 2H, J = 12.0 Hz, OCH_2), 5.30

(d, 2H, J = 12.0 Hz, OCH_2); ^{13}C NMR ($CDCl_3$, 100 MHz) δ 167.2 (d, $^2J_{C\text{-}F}$ = 24.5 Hz), 163.6 (d, $^2J_{C\text{-}F}$ = 24.5 Hz), 134.7, 129.1, 129.0, 128.7, 85.9 (d, $^1J_{C\text{-}F}$ = 194 Hz), 68.8; HRMS (ES) calcd for $C_{10}H_9FNaO_4$ ($[M+Na]^+$), 235.0377 found, 235.0377.

Benzyl fluoromalonate, magnesium salt (85)

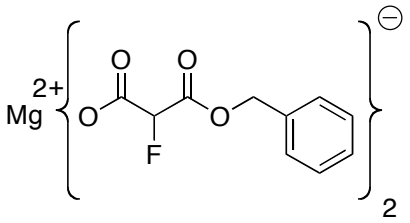

This known compound was synthesized according to the patented procedure of Palmer.[73] To a solution of **84** (1.12 g, 5.28 mol) in THF was added magnesium ethoxide (310 mg, 2.64 mmol) at rt. The solution was stirred for 2 h and filtered. The filtrate was added to hexane (50 mL) with vigorous stirring and the resulting white precipitate was filtered immediately. The precipitate was washed with hexane and dried under vacuum to give **85** (0.90 g, 76%) as a white solid. IR (microscope): 3416, 3066, 3035, 2968, 1732, 1652, 1456, 1428, 1307, 1216 cm^{-1}; ^1H NMR (D_2O, 400 MHz) δ 7.40-7.36 (m, 10H, ArH), 5.36 (d, 2H, $^2J_{H\text{-}F}$ = 49.2 Hz αH), 5.26 (s, 4H, OCH_2); ^{19}F NMR (D_2O, 376 MHz) δ -188.63 (d, $^2J_{H\text{-}F}$ = 49.7 Hz); HRMS (ES) calcd for $C_{30}H_{24}F_3MgO_{12}$ ($[M+C_{10}H_8O_4F]^-$, neutral magnesium salt + anion as a cluster), 657.1075; found, 657.1081

(*S*)-*tert*-Butyl 6-(dimethylamino)-1-fluoro-2-hydroxy-6-oxohexan-3-ylcarbamate (92)

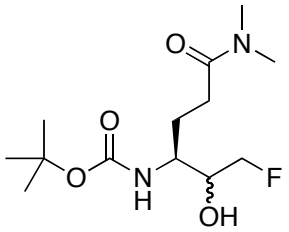

This known compound was synthesized according to the literature procedure of Morris *et al*.[44] To a solution of ketone **78** (150 mg, 0.52 mmol) in EtOH (1 mL) was added a solution of $NaBH_4$ (8.1 mg, 0.21 mmol) in EtOH (1 mL) at 0 °C. The mixture was stirred at 20 °C for 1 h and concentrated *in vacuo*. The reaction mass was dissolved in H_2O (1.5 mL) and acidified to pH 1.5 with 1N H_2SO_4. The mixture was immediately extracted with EtOAc (3 x 3 mL), The combined organic layers were washed with brine (3 mL), dried over MgSO4, filtered, and concentrated *in vacuo* to afford the product **92** (102 mg, 68%) as a white solid. IR (CH_2Cl_2 cast): 3332, 2983, 2943, 2871, 1746, 1677, 1626, 1527, 1448 cm^{-1}; ^1H NMR ($CDCl_3$, 600 MHz) δ 5.23 (br, 1H, NH), 4.53-4.36 (m, 2H, CHC<u>H</u>$_2$F), 3.78-3.74 (m, 1H, C<u>H</u>OH), 3.66-3.62 (m, 1H, αH), 2.97 (s, 3H, NCH_3), 2.91 (s, 3H, NCH_3), 2.45-2.32 (m, 2H, Hγ), 1.97-1.85 (m, 2H, Hβ), 1.41 (s, 9H, $(CH_3)_3C$); HRMS (ESI) calcd for $C_{13}H_{25}N_2O_4FNa$ ($[M+Na]^+$), 315.1690 found, 315.1688.

CrPV peptide substrate (95)

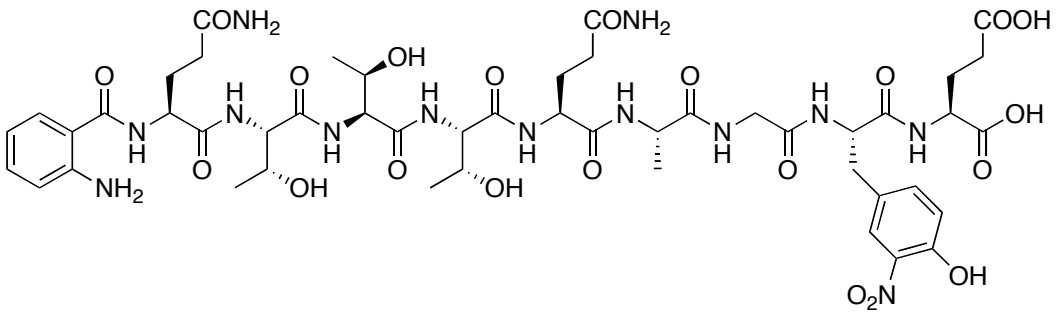

To the resin bound precursor peptide **96** (130 mg, 0.1 mmol) in DMF (4 mL) was added a preactivated solution of 2-(Fmoc-amino)benzoic acid (72 mg, 0.20 mmol), PyBOP (99 mg, 0.19 mmol) and NMM (44 μL, 0.40 mmol) in DMF (8 mL). The coupling was allowed for 2 h under argon bubbling. The completion of coupling reaction was ascertained by negative Kaiser test. Finally the peptide was cleaved from the resin using (95:2.5:2.5) TFA / TIPS / H_2O at rt for 2 h. Concentration of the filtrate *in vacuo,* followed by precipitation with Et_2O provided crude product as a solid. The crude product was purified by reverse phase HPLC using a Waters μBondapak C-18 column (WAT015814, 10 μm, 125 Å, 25 x 100 mm). The column was operated at a flow rate of 10 mL/min with dual wavelength detection at 220 nm and 280 nm. The method used for the purification started at 20% CH_3CN for 2 min and then ramped to 90% CH_3CN over 38 min. The desired product **95** was isolated at a retention time of t_R = 15.7 min. The solution containing the product was frozen and lyophilized to give CrPV peptide substrate **95** as a yellow solid (20 mg, 17%). MALDI-TOF MS Calcd for $C_{48}H_{66}N_{13}O_{21}$ ($[M-H]^-$) 1160.4, found, 1160.5.

Precursor for CrPV (96)

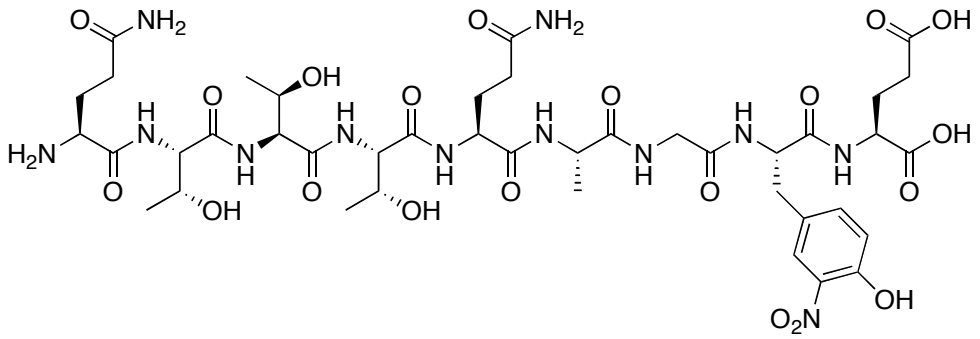

The synthesis of precursor peptide **96** was done on a 0.1 mmol scale (130 mg resin) using an automated peptide synthesizer. For the synthesis, a Wang resin pre-loaded with Fmoc-Glu(O^{t}Bu)-OH with a substitution capacity of 0.77 mmol/g was used. The amino acids were introduced in the order: Fmoc-Tyr(NO_2)-OH, Fmoc-Gly-OH, Fmoc-Ala-OH, Fmoc-Gln(Trt)-OH, Fmoc-Thr(*t*Bu)-OH, Fmoc-Thr(*t*Bu)-OH, Fmoc-Thr(*t*Bu)-OH, Fmoc-Gln(Trt)-OH. The Fmoc group is then removed manually with 20% piperidine followed by treatment of small amount of resin bound peptide with (95:2.5:2.5) TFA / TIPS / H_2O cleaves the product **96** from the solid support. MALDI-TOF MS analysis: Calcd for $C_{41}H_{62}N_{12}O_{20}Na$ ($[M+Na]^+$) 1065.4, found, 1065.5.

IAPV Fluorescent Peptide (98)

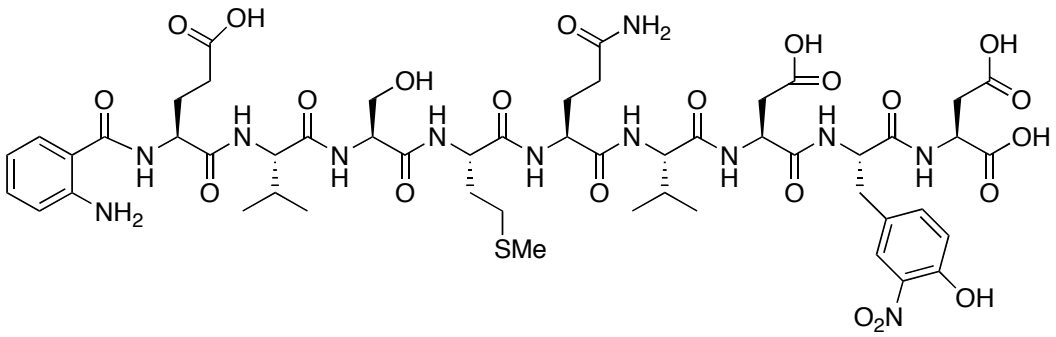

The resin bound precursor peptide **106** (65 mg, 0.05 mmol) for IAPV was pre-swelled in DMF for 30 min. In a seprate vial, an aminobenzoyl dipeptide **105** (84 mg, 0.2 mmol) and PyBOP (99 mg, 0.19 mmol) were dissolved in DMF (10 mL) and to it, NMM (44 μL, 0.4 mmol) was added and allowed to pre-activate for 5 min. The activated amino acid solution was then transferred to resin and reacted for 2 h. The completion of coupling was ascertained by negative Kaiser test. Finally the peptide was cleaved from the resin using (95:2.5:2.5) TFA / TIPS / H_2O at rt for 2 h. Concentration of the filtrate *in vacuo,* followed by precipitation with Et_2O provided crude as an off white solid. The crude product was purified by reverse phase HPLC using a Waters μBondapak C-18 column (WAT015814, 10 μm, 125 Å, 25 x 100 mm). The column was operated at a flow rate of 10 mL/min with dual wavelength detection at 220 nm and 280 nm. The method used for the purification started at 20% CH_3CN for 2 min and then ramped up to 90% CH_3CN over 38 min. The desired product **98** was isolated at a retention time of t_R = 16.8

min. The solution containing the product was frozen and lyophilized to give IAPV peptide substrate **98** (5 mg, 8%) as a solid. MALDI-TOF MS Calcd for $C_{52}H_{72}N_{12}O_{22}SNa$ ($[M+Na]^+$), 1271.5; found, 1271.7.

(*S*)-5-*tert*-Butoxy-2-(2-(*tert*-butoxycarbonylamino)benzamido)-5-oxopentanoic acid (105)

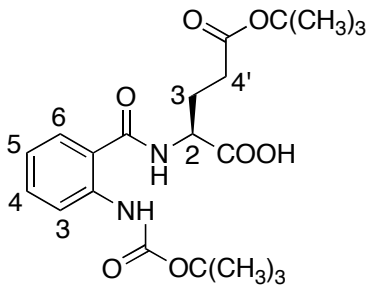

2-Chlorotrityl chloride resin with a loading of 1.1 mmol/g was used for the synthesis. The resin (426 mg, 0.5 mmol substitution capacity) was pre-swelled in CH_2Cl_2 (15 mL) for 20 min. A solution of Fmoc-Glu(O*t*Bu)-OH (426 mg, 1.0 mmol) and DIPEA (0.35 mL, 2.0 mmol) in CH_2Cl_2 (20 mL) was added and allowed to react for 2.5 h. The resin was then washed with CH_2Cl_2 (2 x 20 mL). The Fmoc group was removed using 20% piperidine (3 x 5 mL) in DMF and monitored for completeness by the absorption of dibenzofulvene-piperidine adduct at λ = 301 nm on a UV-Vis spectrophotometer. In a separate vial a solution of 2-(Boc-amino)benzoic acid (237 mg, 1.0 mmol), PyBOP (494 mg, 0.9 mmol) and NMM (0.22 mL, 2.0 mmol) in DMF (10 mL) was pre-activated for 5 min. The activated amino acid solution was then transferred to resin and reacted for 2 h. The completion of coupling was ascertained by negative Kaiser test.

Finally the peptide is cleaved from the resin using mild cleavage cocktail (6:2:2) DCM / TFE / AcOH to obtain the desired protected peptide **105** (207 mg, 98%) as white solid. IR (microscope) 3220, 2980, 2933, 1728, 1647, 1524, 1446, 1249, 1158 cm^{-1}; ^{1}H NMR (CD_2Cl_2, 600 MHz) δ 10.23 (br, 1H, COOH), 8.36 (d, 1H, J = 7.8 Hz, H_6), 7.59-7.55 (m, 2H, PhN<u>H</u>), 7.47-7.44 (m, 1H, H_4), 7.03-7.0 (m, 1H, H_5), 4.65-4.61 (m, 1H, H_2), 2.61-2.56 (m, 1H, $H_{4'}$), 2.46-2.41 (m, 1H, $H_{4'}$), 2.28-2.22 (m, 1H, H_6), 2.16-2.10 (m, 1H, H_6), 1.50 (s, 9H, $CH_2COOC(CH_3)_3$), 1.43 (s, 9H, $NHCOOC(CH_3)_3$). ^{13}C NMR (100 MHz, CD_2Cl_2) δ 174.2, 173.9, 169.5, 152.9, 141.0, 133.1, 127.3, 121.5, 119.6, 118.3, 81.8, 80.4, 31.9, 28.2, 27.9, 26.3. HRMS (ES) calcd for $C_{21}H_{31}N_2O_7$ ($[M+H]^+$), 423.2124; found, 423.2125.

Precurosor for IAPV Fluorescent Peptide (106)

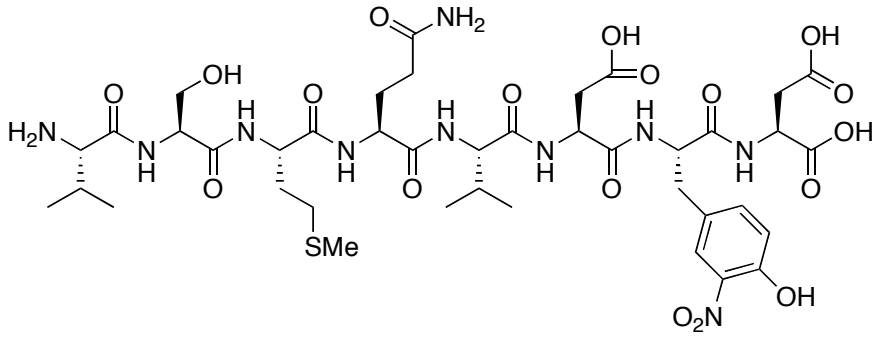

The octamer peptide precursor **106** was prepared using an automated peptide synthesizer. The preloaded resin H-Asp(O*t*Bu)-2-ClTrt with a substitution capacity of 0.77 mmol/g was used for the synthesis. The resin (130 mg, 0.1 mmol substitution capacity) was pre-swelled in NMP for 20 min. The amino acids were

introduced in the order: Fmoc-Tyr(NO_2)-OH, Fmoc-Asp(O*t*Bu)-OH, Fmoc-Val-OH, Fmoc-Gln(Trt)-OH, Fmoc-Met-OH, Fmoc-Ser(*t*Bu)-OH, Fmoc-Val-OH. The formation of the desired precursor peptide **106** was verified by cleaving a small sample of the resin (~15 mg) using (95:2.5:2.5) TFA / TIPS / H_2O and subjected to MALDI-TOF MS analysis: Calcd for $C_{40}H_{60}N_{10}O_{18}SNa$ ($[M+Na]^+$), 1023.4; found, 1023.6.

2-Benzhydrylidene-4-methyl-2*H*-oxazol-5-one (109)

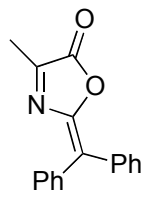

This compound was prepared using a modified literature procedure established in our group.[92] To a suspension of D/L alanine **(107)** (4.0 g, 44.94 mmol) in EtOAc (100 mL) containing propylene oxide (3.5 mL, 50.0 mmol), was added a solution of 2-chloro-2,2-diphenylacetyl chloride (13.2 g, 50.0 mmol) in EtOAc (100 mL). A clear solution was obtained after heating at reflux under argon for 20 h. The solvent was removed under vacuum and the reaction mass was cooled to 0 ˚C and treated with TFAA (15.0 mL). After adding ice cold water (100 mL) and stirring, a large amount of bright orange colored precipitate was formed. The solid was recrystallized from acetonitrile-isopropyl alcohol to afford the product **109** as bright yellow crystals (9.4 g, 80% over two steps); mp 154-156 ˚C; IR

(microscope) 3053, 3034, 1771, 1537, 1441, 1245, 974 cm^{-1}; ^{1}H NMR ($CDCl_3$, 400 MHz) δ 7.45-7.38 (m, 10H, Ph), 2.38 (s, 3H, CH_3). ^{13}C NMR (100 MHz, $CDCl_3$) δ 164.3, 158.2, 151.8, 137.1, 137.0, 132.3, 131.5, 129.5, 129.1, 128.5, 128.2, 125.5, 14.0. HRMS (ES) calcd for $C_{17}H_{14}NO_2$ ($[M+H]^+$), 264.1019; found, 264.1017.

2-(Diphenylacetylamino)propionic acid methyl ester (110)

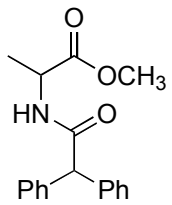

To a solution of alanine diphenyl pseudoxazolone **109** (40 mg, 0.15 mmol) in MeOH (25 mL) at rt was added AcOH (0.02 mL, 0.3 mmol) and sodium cyanoborohydride (14 mg, 0.23 mmol). The mixture was stirred under argon for 12 h. It was quenched by addition dilute HCl (5%). After solvent removal and purification by flash column chromatography (SiO_2, 1:1/EtOAc:hexanes) the title compound **110** was obtained as a solid (12 mg, 27%) IR (microscope) 3243, 3062, 2951, 1734, 1663, 1558, 1455, 1289 cm^{-1}; ^{1}H NMR ($CDCl_3$, 300 MHz) δ 7.39-7.23 (m, 10H, Ar), 6.19 (d, 1H, J = 6.6 Hz, N<u>H</u>), 4.95 (s, 1H, C<u>H</u>-Ph), 4.64 (pent, 1H, J = 7.2 Hz, C<u>H</u>-NH), 3.72 (s, 3H, OC<u>H</u>$_3$), 1.39 (d, 3H, J = 7.2 Hz, NHCHC<u>H</u>$_3$). ^{13}C NMR (100 MHz, $CDCl_3$) δ 173.3, 171.4, 139.2, 128.9, 128.8,

127.3, 59.0, 52.4, 48.3, 18.3. HRMS (EI) calcd for $C_{18}H_{19}NO_3$ (M^+), 297.1365; found, 297.1359.

Methyl 2,2-Diphenyl acetate (111)

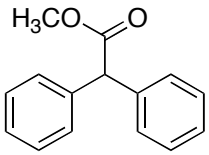

The title compound was isolated as a byproduct. A solution of **109** (100 mg, 0.38 mmol) in MeOH (10 mL) was purged with argon for 30 min. To this solution was added [Rh(I)COD(*R*,*R*)-Et-DuPHOS]$^+$OTf$^-$ (1.1 mg, 0.00152 mmol) followed by hydrogenation at 100 psi for 24 h at 50 °C. The solvent was removed and the resulting mass was purified by flash column chromatography (SiO_2, CH_2Cl_2) to afford **111** (17 mg, 20%) as a wax. IR (microscope): 3087, 3062, 3028, 2950, 1739, 1659, 1599, 1496 cm^{-1}; ^1H NMR ($CDCl_3$, 300 MHz) δ 7.34-7.25 (m, 10H, ArH), 5.05 (s, 1H, αH), 3.75 (s, 3H, OCH_3); HRMS (EI) calcd for $C_{15}H_{14}O_2$ (M^+), 226.0993; found, 226.0996.

4-hydroxy-5-methyl-3,3-diphenylpyrrolidin-2-one (112)

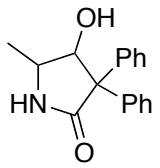

The title compound was isolated as an undesired product when **109** was treated with lithium triethyl borohydride (super hydride). IR (cast) 3256, 3060, 2970, 1698, 1496, 1446 cm^{-1}; ^1H NMR ($CDCl_3$, 300 MHz) δ 7.65-7.62 (m, 2H, ArH), 7.40-7.29 (m, 6H, ArH), 7.17-7.14 (m, 2H, ArH), 5.87 (br, 1H, NH), 4.58 (d, 1H, J = 7.8 Hz, C<u>H</u>OH), 3.31-3.26 (m, 1H, αH), 1.39 (d, 3H, J = 6.3 Hz, CH_3) LRMS (ES) calcd for $C_{17}H_{17}NO_2Na([M+Na]^+)$, 290.1; found, 290.1.

2-Dichloromethylene-4-methyl-2*H*-oxazol-5-one (113)

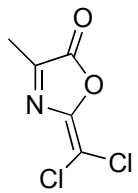

This known compound was prepared according to the literature procedure.[93] To a suspension of **118** (2.5 g, 10.77 mmol) in CH_2Cl_2 (100 mL) was added pyridine (3.92 mL, 48.5 mmol) at -15 ˚C followed by phosphorous-oxychloride dropwise over a period of 15 min. After stirring for 40 min at -15 ˚C, the reaction mixture

was brought to rt and washed with dil HCl (5%, 30 mL), saturated $NaHCO_3$ solution (30 mL), brine, dried over $MgSO_4$ and then concentrated *in vacuo*. The crude was purified by flash column chromatography (SiO_2, 1:9/ MeOH: CH_2Cl_2) to afford **113** (919 mg, 48%) as a solid. IR (microscope) 3102, 2940, 2919, 2586, 2101, 1789, 1650, 1419, 1243 cm^{-1}; ^1H NMR ($CDCl_3$, 400 MHz) δ 2.4 (s, 3H, CH_3). ^{13}C NMR (100 MHz, $CDCl_3$) δ 162.1, 160.6, 151.9, 110.7, 14.2. HRMS (EI) calcd for $C_5H_3Cl_2NO_2$ (M^+), 178.9540; found, 178.9544.

Phenyl trichloroacetate (117)

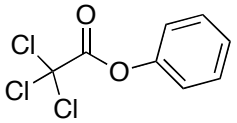

This known compound was prepared according to literature procedure[155] by heating a solution of phenol (10 g, 0.11 mol) in trichloroacetyl chloride (12 mL, 0.11 mol) to reflux for 2 h. The solution was concentrated under vacuum to about 4 mL, and the crude product was purified by flash column chromatography (SiO_2, 1:3/EtOAc:hexanes) to yield **117** (22 g, 90%) as a liquid. IR (microscope) 3064, 1788, 1221, 1182, 1158 cm^{-1}; ^1H NMR ($CDCl_3$, 300 MHz) δ 7.49-7.43 (m, 2H, Ar<u>H</u>), 7.37-7.31 (m, 1H, Ar<u>H</u>), 7.27-7.24 (m, 2H, Ar<u>H</u>); ^{13}C NMR (100 MHz, $CDCl_3$) δ 160.7, 150.8, 130.1, 127.4, 120,7, 89.9; HRMS (EI) calcd for $C_8H_5Cl_3O_2$ (M^+), 237.9355; found, 237.9356.

2-(2,2,2-Trichloroacetamido)propanoic acid (118)

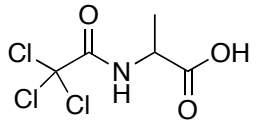

This known compound was prepared according to the literature procedure.[93] To a solution of alanine **(107)** (8.9 g, 100 mmol) in carbonate-bicarbonate buffer solution (2M, 200 mL, pH 9. 2) at rt was added a solution (100 mL) of phenyl trichloroacetate **(117)** (15.0 g, 6.6 mmol) in THF dropwise over a period of an hour. The reaction mixture was concentrated to about 200 mL under vacuum and washed with CH_2Cl_2 (2 x 50 mL) to remove any of the unreacted phenyl trichloroacetate. The aqueous layer was diluted with EtOAc (150 mL) and acidified to pH 3 with 6M HCl. Separation of organic layer followed by concentration of organic layer *in vacuo* afforded the product **118** (3.0 g, 21%) as an off-white solid. IR (microscope): 3312, 3002, 2945, 1716, 1685, 1518, 1458, 1379, 1239 cm^{-1}; ^1H NMR (DMSO-d_6, 600 MHz) δ 9.14 (d, 1H, J = 7.2 Hz, NH), 4.26 (q, 1H, J = 7.2 Hz, αH), 1.37 (d, 3H, J = 7.2 Hz, CH_3); ^{13}C NMR (DMSO-d_6, 100 MHz) δ 172.4, 161.1, 92.5, 49.6, 16.2; HRMS (ES) calcd for $C_5H_6NO_3Cl_3Na$ ($[M+Na]^+$), 255.9306; found, 255.9308.

1,1-Dimethyl-1-phenylbromomethanetricarboxylate (121)

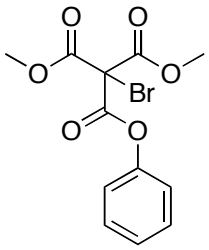

To a solution of **125** (850 mg, 3.34 mmol) in CCl_4 (10.0 mL) was added bromine (0.2 mL, 4.05 mmol) followed by irradiation with a tungsten lamp (250 W). The reaction was run for 2 h. The reaction mixture was washed with 5% Na_2CO_3 solution (2.0 mL) followed by purification using flash column chromatography (SiO_2, 1:9/ diethyl ether:pentane) afforded **121** (1.1 g, 90%) as an oil. IR (microscope): 3017, 2958, 1748, 1591, 1492 cm^{-1}; ^1H NMR (CD_2Cl_2, 600 MHz) δ 7.45-7.42 (m, 2H, ArH), 7.33-7.30 (m, 1H, ArH), 7.16-7.14 (m, 2H, ArH), 3.93 (s, 6H, OCH_3); ^{13}C NMR (CD_2Cl_2, 100 MHz) δ 163.8, 162.4, 150.6, 129.9, 127.0, 122.9, 58.6, 55.0; HRMS (ES) calcd for $C_{16}H_{12}BrClNO_2$ ($[M+H]^+$), 363.97345; found, 363.97281.

Dimethyl-2,3-dicarbomethoxy)butendioate (123)

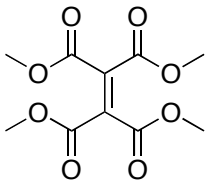

This known compound[156] was prepared by a modified procedure. To a suspension of NaH (60% 9.48 mg, 0.24 mmol) in THF was added dimethyl bromomalonate **(119)** (31 μL, 0.24 mmol) at 0 ˚C, and the reaction mixture was stirred for 30 min, during which product separated as a solid. The product **123** was then separated by filtration (37 mg, 60%). IR (microscope) 2962, 1741, 1731, 1442, 1287, 1248, 1040 cm^{-1}; ^{1}H NMR (CD_2Cl_2, 600 MHz) δ 3.83 (s, 12H, CH_3). ^{13}C NMR (125 MHz, $CDCl_3$) δ 162.6, 135.4, 53.4. HRMS (EI) calcd for $C_{10}H_{12}O_8$ (M^+), 260.0532; found, 260.0531.

2-Methoxycarbonyl-malonic acid methyl ester phenyl ester (125)

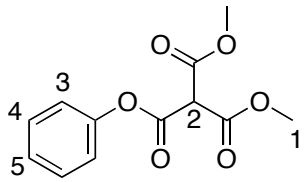

To a suspension of NaH (754 mg, 31.4 mmol) in THF was addded dimethyl malonate **(124)** (2.5 g, 18.9 mmol) at 0 ˚C followed by stirring for 10 min. The resulting solution was treated with phenyl chloroformate (2.36 mL, 18.8 mmol) and stirred for 1 h. The reaction mixture was quenched with dil HCl followed by removal of the solvent under vacuum. The residue was diluted with H_2O and extracted with diethyl ether (2 x 30 mL). The combined organic layer was washed with brine (20 m L) and dried over $MgSO_4$. The solvent was removed under vacuum, and the crude product was purified by column chromatography

(SiO_2, 3:7/ diethyl ether:pentanes) to yield **125** (630 mg, 30%) as an oil. IR (microscope) 3011, 2958, 1746, 1592, 1457, 1315, 1191, 1027 cm^{-1}; ^1H NMR ($CDCl_3$, 300 MHz) δ 7.44-7.37 (m, 2H, H_4), 7.29-7.24 (m, 1H, H_5), 7.18-7.14 (m, 2H, H_3), 4.69 (s, 1H, H_2), 3.87 (s, 6H, H_1). ^{13}C NMR (100 MHz, $CDCl_3$) δ 164.0, 162.4, 150.3, 129.6, 126.5, 121.1, 58.6, 53.5. HRMS (ES) calcd for $C_{12}H_{12}O_6$ (M^+), 252.0636; found, 252.0634.

1,1-Diethyl-2,2-dimethylethene-1,1,2,2-tetracarboxylate (128)

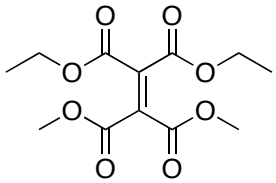

This known compound[94] was prepared by a modified procedure. To a suspension of NaH (60% 0.33 g, 8.37 mmol) in THF was added dimethyl fluoromalonate **(127)** (0.63 g, 4.18 mmol) followed by *t*BuOH (30 mg) at 0 ˚C. Diethyl bromomalonate **(126)** (0.71 mL, 4.18 mmol) was added dropwise over a period of 2 h using a syringe pump. The reaction mixture was then concentrated under vacuum. The residue was diluted with CH_2Cl_2 (30 mL). The resulting solution was washed with water, saturated $NaHCO_3$ solution, brine, dried over $MgSO_4$ and then concentrated *in vacuo*. The crude was purified by flash column chromatography (SiO_2, 2:8/ diethyl ether:pentanes) to yield **128** (220 mg, 18%) as a solid. IR (microscope) 2985, 1744, 1466, 1392, 1306, 1149 cm^{-1}; ^1H NMR

($CDCl_3$, 300 MHz) δ 4.36 (q, 4H, J = 7.2 Hz, OCH_2), 3.86 (s, 6H, OCH_3), 1.35 (t, 6H, J = 7.2 Hz, CH_3). ^{13}C NMR (125 MHz, $CDCl_3$) δ 162.7, 162.2, 136.1, 134.6, 62.6, 53.3, 13.8. HRMS (ES) calcd for $C_{14}H_{16}NaO_8$ ($[M+Na]^+$), 311.0737; found, 311.0737.

2-*tert*-Butoxycarbonylamino-benzoic acid (132)

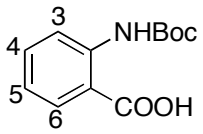

This known compound was prepared according to the literature procedure.[157] Anthranilic acid (1.37 g, 10.0 mmol) and $(Boc)_2O$ (3.12 g, 14.3 mmol) were dissolved in a mixture of 0.5 N NaOH (20.0 mL), dioxane (10.0 mL) and acetonitrile (2.0 mL) and stirred overnight at rt. After the volatile solvent was removed in vacuum, ice and 10% citric acid were added, and the resulting solution was extracted with EtOAc (2 x 60 mL). The combined organic layers were washed with brine, dried over MgSO4, filtered, and concentrated *in vacuo*. The crude was recrystallized from EtOAc–hexane to give **132** (1.35 g, 57%) as a crystalline solid. mp 154-156 ˚C; IR (microscope) 3072, 2980, 1734, 1672, 1254, 1157 cm^{-1}; ^1H NMR ($CDCl_3$, 600 MHz) δ 9.99 (br, 1H, COOH), 8.46 (dd, 1H, J = 9.0, 1.2 Hz, H_6), 8.10 (dd, 1H, J = 7.8, 1.8 Hz, H_3), 7.59-7.56 (m, 1H, H_4), 7.07-7.04 (m, 1H, H_5), 5.32 (s, 1H, NH), 1.53 (s, 9H, $C(CH_3)_3$). ^{13}C NMR (100 MHz,

$CDCl_3$) δ 172.0, 151.0, 142.2, 133.0, 131.1, 121.0, 191.7, 111.7, 80.5, 29.0. HRMS (ES) calcd for $C_{12}H_{15}NNaO_4$ ([M+Na]$^+$), 260.0893; found, 260.0897.

Subtilosin A mature linear peptide

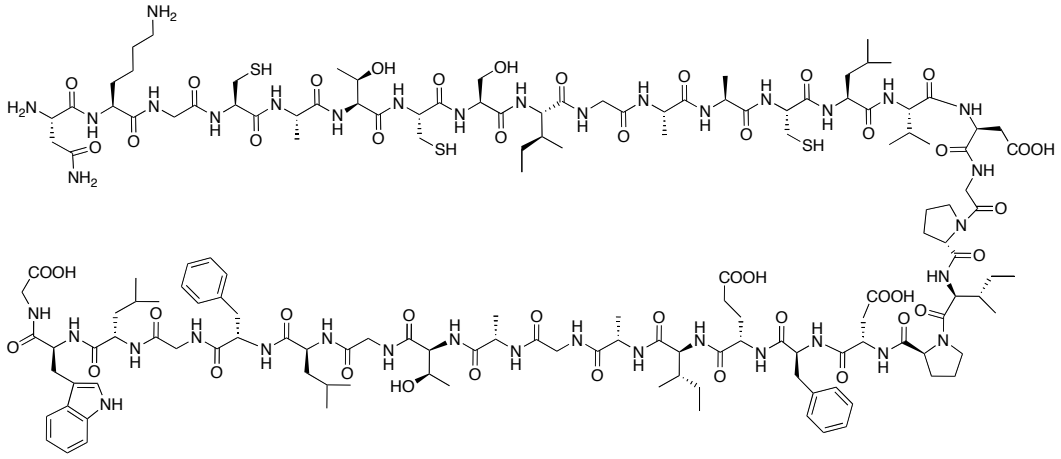

Fmoc-SPPS was carried out manually using a Wang resin (164 mg, 0.1 mmol) preloaded with Fmoc-Gly-OH as the C-terminal amino acid. PyBOP was used as coupling reagent and NMM as base. For the deprotection of Fmoc a 20% piperidine in DMF (3 x 10 mL) was used. The amino acids were introduced in the order: Fmoc-Trp(Boc)-OH, Fmoc-Leu-OH, Fmoc-Gly-OH, Fmoc-Phe-OH, Fmoc-Leu-OH, Fmoc-Gly-OH, Fmoc-Ala-Thr(ΨMe,Me Pro)-OH, Fmoc-Gly-OH, Fmoc-Ala-OH, Fmoc-Ile-OH, Fmoc-Glu(O^{t}Bu)-OH, Fmoc-Phe-OH, Fmoc-Asp(O^{t}Bu)-OH, Fmoc-Pro-OH, Fmoc-Ile-OH, Fmoc-Pro-OH, Fmoc-Asp(O^{t}Bu)-(Dmb)Gly-OH, Fmoc-val-OH, Fmoc-Leu-OH, Fmoc-Cys(Trt)-OH, Fmoc-Ala-OH, Fmoc-Ala-OH, Fmoc-Gly-OH, Fmoc-Ile-OH, Fmoc-Ser(^{t}Bu)-OH, Fmoc-Cys(Trt)-OH, Fmoc-Ala-Thr(ΨMe,Me Pro)-OH, Fmoc-Cys(Trt)-OH, Fmoc-Gly-

OH, Fmoc-Lys(Boc)-OH and Fmoc-Asn(Trt)-OH. Cleavage of a small sample of the resin with (95:2.5:2.5) TFA / anisole / H_2O at rt for 2 h liberated the peptide from the solid support. Concentration of the filtrate *in vacuo,* followed by precipitation with Et_2O gave subtilosin A mature linear peptide as a solid; MALDI-TOF MS Calcd for $C_{152}H_{235}N_{38}O_{46}S_3$ ($[M+H]^+$), 3424.6; found 3424.3.

Subtilosin A precursor linear peptide

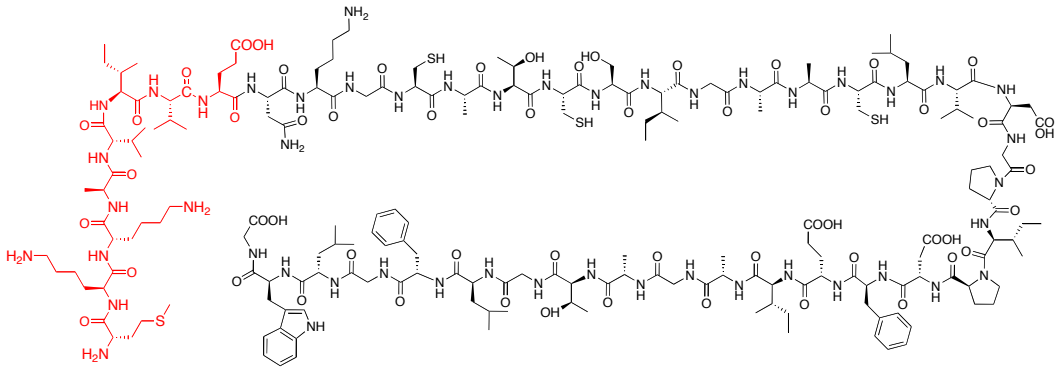

The above mature linear peptide was extended further by coupling the leader sequence amino acids in the order: Fmoc-Glu(O^{t}Bu)-OH, Fmoc-Val-OH, Fmoc-Ile-OH, Fmoc-Val-OH, Fmoc-Ala-OH, Fmoc-Lys(Boc)-OH Fmoc-Lys(Boc)-OH and Fmoc-Met-OH. A small sample of the resin was cleaved with (95:2.5:2.5) TFA / anisole / H_2O at rt for 2 h to liberate the peptide from the solid support. Concentration of the filtrate *in vacuo,* followed by precipitation with Et_2O afforded subtilosin A precursor linear peptide as an off-white solid; MALDI-TOF MS Calcd for $C_{193}H_{309}N_{48}O_{56}S_4$ ($[M+H]^+$), 4323.2; found 4323.1.

Subtilosin A mature cyclic peptide

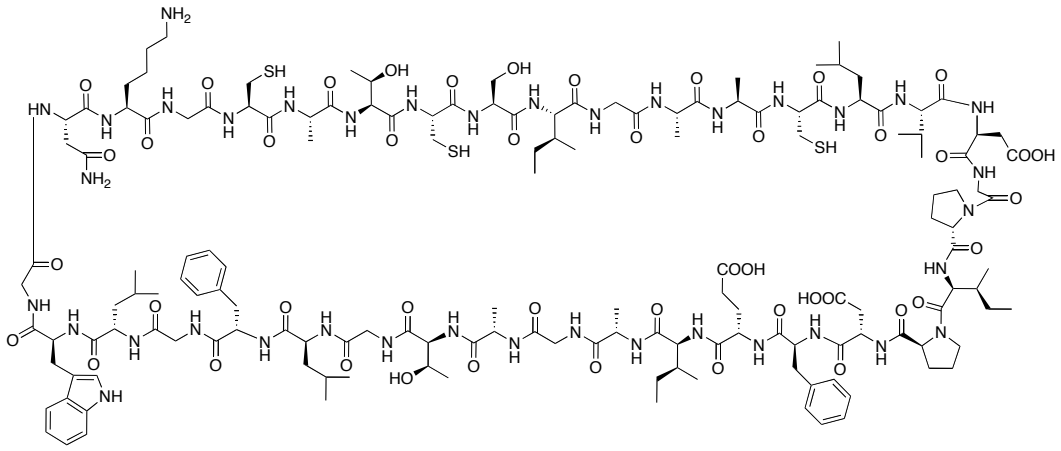

The cyclic peptide was synthesized using a glutamic acid α-allyl ester in which the side chain was anchored to a Wang resin (200 mg, 0.06 mmol). The amino acids were introduced using the peptide synthesizer in the order: Fmoc-Phe-OH, Fmoc-Asp(O^{t}Bu)-OH, Fmoc-Pro-OH, Fmoc-Ile-OH, Fmoc-Pro-OH, Fmoc-Asp(O^{t}Bu)-(Dmb)Gly-OH, Fmoc-val-OH, Fmoc-Leu-OH, Fmoc-Cys(Trt)-OH, Fmoc-Ala-OH, Fmoc-Ala-OH, Fmoc-Gly-OH, Fmoc-Ile-OH, Fmoc-Ser(^{t}Bu)-OH, Fmoc-Cys(Trt)-OH, Fmoc-Ala-Thr(ΨMe,Me Pro)-OH, Fmoc-Cys(Trt)-OH, Fmoc-Gly-OH, Fmoc-Lys(Boc)-OH, Fmoc-Asn(Trt)-OH, Fmoc-Gly-OH, Fmoc-Trp(Boc)-OH, Fmoc-Leu-OH, Fmoc-Gly-OH, Fmoc-Phe-OH, Fmoc-Leu-OH, Fmoc-Gly-OH, Fmoc-Ala-Thr(ΨMe,Me Pro)-OH, Fmoc-Gly-OH, Fmoc-Ala-OH, and Fmoc-Ile-OH to provide a linear fragment on resin. The allyl group was removed by treating the resin bound linear precursor with a solution of $Pd(PPh_3)_4$ (148 mg, 0.128 mmol) and $PhSiH_3$ (78 μL, 0.6 mmol) in 1:1 DMF:CH_2Cl_2 (10

mL) solution for 2 h. The resin bound peptide was washed with CH_2Cl_2 (2 x 5 mL), 0.5% sodium diethyldithiocarbamate in DMF (4 x 5 mL) and then with DMF (2 x 5 mL). Removal of the Fmoc group was achieved with 20% piperidine in DMF (3 x 5 mL) as was ascertained by negative Kaiser test. Analysis of a small sample of resin indicted the formation of the linear peptide. The linear peptide (50 mg, 0.015 mmol) was cyclized by adding a solution of PyBOP (39 mg, 0.08 mmol), HOBt (10 mg, 0.08 mmol) and NMM (16.5 μL, 0.15 mmol) in DMF (10 mL) to the Fmoc deprotected linear fragment and reacting for 4 h. A small sample of the resin was cleaved with (94:2.5:2.5:1) TFA / EDT / H_2O / TIPS at rt for 2 h to liberate the peptide from the solid support. Concentration of the filtrate *in vacuo,* followed by precipitation with Et_2O afforded subtilosin A mature cyclic peptide as an off-white solid; MALDI-TOF MS Calcd for $C_{152}H_{233}N_{38}O_{45}S_3$ ($[M+H]^+$), 3406.6; found 3406.5.

H_2N-Abz-Ser-OH

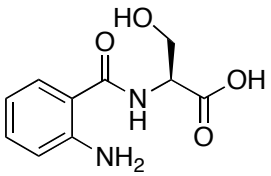

2-Chlorotrityl chloride resin with a loading of 0.65 mmol/g was used for the synthesis. The resin (600 mg, 0.39 mmol substitution capacity) was pre-swelled in CH_2Cl_2 (15 mL) for 20 min. A solution of Fmoc-Ser(O*t*Bu)-OH (300 mg, 0.78

mmol) and DIPEA (0.27 mL, 1.56 mmol) in CH_2Cl_2 (20 mL) was added and allowed to react for 2.5 h. The resin was then washed with CH_2Cl_2 (2 x 20 mL). The Fmoc group was removed using 20% piperidine (3 x 5 mL) in DMF and monitored for completeness by the absorption of dibenzofulvene-piperidine adduct at λ = 301 nm on a UV-Vis spectrophotometer. In a separate vial a solution of 2-(Boc-amino)benzoic acid (185 mg, 0.78 mmol), PyBOP (385 mg, 0.74 mmol) and NMM (0.17 mL, 1.56 mmol) in DMF (10 mL) was pre-activated for 5 min. The activated amino acid solution was then transferred to resin and reacted for 2 h. The completion of coupling was ascertained by negative Kaiser test. Finally the peptide was cleaved from the resin using cleavage cocktail DCM / TFA / TIPS (4.75:4.75:0.5) to obtain the desired peptide H_2N-Abz-Ser-OH (25 mg, 30%) as a solid. ^{1}H NMR (CD_3OD, 300 MHz) δ 7.83 (dd, 1H, J = 7.8, 1.2 Hz, ArH), 7.54-7.48 (m, 1H, ArH), 7.25 (dd, 1H, J = 7.5, 1.2 Hz, ArH), 7.22-7.19 (m, 1H, ArH), 4.75-4.72 (m, 1H, αH), 4.05-3.99 (m, 1H, C$\underline{H}_2$OH); HRMS (ES) calcd for $C_{10}H_{13}N_2O_4$ ([M+H]$^+$), 225.0869; found, 225.0868.

5.3 Enzymatic activity assay

A quenched fluorescence resonance energy transfer (FRET) assay was used to measure the SARS 3CL^{pro} activity using the peptide substrate (Abz-SVTLQSG-Tyr(NO_2)R, 93% purity).[31] The enzyme inhibitions were measured at 22 °C in a reaction mixture of a 50 mM Bis-Tris buffer adjusted to pH 7.0, 2 mM DTT, 10 μM fluorescent substrate, 0.2 μM non-His-tagged protease and inhibitor solution

(1000 μM, 100 μM, 50 μM etc.) without preincubation. Fluorescence was recorded using a Shimadzu RF5301 spectrofluorimeter (λ_{ex} 340 nm, λ_{em} 420 nm) for 3 min and the linear parts of the progression curves were used for the calculation of percentage inhibition. Stock solutions of inhibitors were prepared at 100 mM in DMSO from which dilutions are made. A 7.0 μL of inhibitor solution in DMSO was diluted to a final volume of 700 μL with Bis-Tris buffer for recording fluorescence. The activity of SARS $3CL^{pro}$ is expressed as a percentage of respective control samples. In order to determine the IC_{50} values, at least five different concentrations of the inhibitor were used. The IC_{50} values were determined from % inhibition and log of inhibitor concentration using Microsoft® Excel 2004 for MAC®.

6: REFERENCES

1. Drosten, C.; Gunther, S.; Preiser, W.; van der Werf, S.; Brodt, H. R.; Becker, S.; Rabenau, H.; Panning, M.; Kolesnikova, L.; Fouchier, R. A. M.; Berger, A.; Burguiere, A. M.; Cinatl, J.; Eickmann, M.; Escriou, N.; Grywna, K.; Kramme, S.; Manuguerra, J. C.; Muller, S.; Rickerts, V.; Sturmer, M.; Vieth, S.; Klenk, H. D.; Osterhaus, A.; Schmitz, H.; Doerr, H. W. Identification of a novel coronavirus in patients with severe acute respiratory syndrome. *New. Engl. J. Med.* **2003**, *348*, 1967-1976.
2. Ksiazek, T. G.; Erdman, D.; Goldsmith, C. S.; Zaki, S. R.; Peret, T.; Emery, S.; Tong, S. X.; Urbani, C.; Comer, J. A.; Lim, W.; Rollin, P. E.; Dowell, S. F.; Ling, A. E.; Humphrey, C. D.; Shieh, W. J.; Guarner, J.; Paddock, C. D.; Rota, P.; Fields, B.; DeRisi, J.; Yang, J. Y.; Cox, N.; Hughes, J. M.; LeDuc, J. W.; Bellini, W. J.; Anderson, L. J. A novel coronavirus associated with severe acute respiratory syndrome. *New. Engl. J. Med.* **2003**, *348*, 1953-1966.
3. Fouchier, R. A. M.; Kuiken, T.; Schutten, M.; van Amerongen, G.; van Doornum, J.; van den Hoogen, B. G.; Peiris, M.; Lim, W.; Stohr, K.; Osterhaus, A. Aetiology - Koch's postulates fulfilled for SARS virus. *Nature* **2003**, *423*, 240-240.
4. Guan, Y.; Zheng, B. J.; He, Y. Q.; Liu, X. L.; Zhuang, Z. X.; Cheung, C. L.; Luo, S. W.; Li, P. H.; Zhang, L. J.; Guan, Y. J.; Butt, K. M.; Wong, K. L.; Chan, K. W.; Lim, W.; Shortridge, K. F.; Yuen, K. Y.; Peiris, J. S. M.;

Poon, L. L. M. Isolation and characterization of viruses related to the SARS coronavirus from animals in Southern China. *Science* **2003**, *302*, 276-278.

5. He, J. F.; Peng, G. W.; Min, J.; Yu, D. W.; Liang, W. J.; Zhang, S. Y.; Xu, R. H.; Zheng, H. Y.; Wu, X. W.; Xu, J.; Wang, Z. H.; Fang, L.; Zhang, X.; Li, H.; Yan, X. G.; Lu, J. H.; Hu, Z. H.; Huang, J. C.; Wan, Z. Y.; Hou, J. L.; Lin, J. Y.; Song, H. D.; Wang, S. Y.; Zhou, X. J.; Zhang, G. W.; Gu, B. W.; Zheng, H. J.; Zhang, X. L.; He, M.; Zheng, K.; Wang, B. F.; Fu, G.; Wang, X. N.; Chen, S. J.; Chen, Z.; Hao, P.; Tang, H.; Ren, S. X.; Zhong, Y.; Guo, Z. M.; Liu, Q.; Miao, Y. G.; Kong, X. Y.; He, W. Z.; Li, Y. X.; Wu, C. I.; Zhao, G. P.; Chiu, R. W. K.; Chim, S. S. C.; Tong, Y. K.; Chan, P. K. S.; Tam, J. S.; Lo, Y. M. D. Molecular evolution of the SARS coronavirus during the course of the SARS epidemic in China. *Science* **2004**, *303*, 1666-1669.

6. Marra, M. A.; Jones, S. J. M.; Astell, C. R.; Holt, R. A.; Brooks-Wilson, A.; Butterfield, Y. S. N.; Khattra, J.; Asano, J. K.; Barber, S. A.; Chan, S. Y.; Cloutier, A.; Coughlin, S. M.; Freeman, D.; Girn, N.; Griffith, O. L.; Leach, S. R.; Mayo, M.; McDonald, H.; Montgomery, S. B.; Pandoh, P. K.; Petrescu, A. S.; Robertson, A. G.; Schein, J. E.; Siddiqui, A.; Smailus, D. E.; Stott, J. E.; Yang, G. S.; Plummer, F.; Andonov, A.; Artsob, H.; Bastien, N.; Bernard, K.; Booth, T. F.; Bowness, D.; Czub, M.; Drebot, M.; Fernando, L.; Flick, R.; Garbutt, M.; Gray, M.; Grolla, A.; Jones, S.; Feldmann, H.; Meyers, A.; Kabani, A.; Li, Y.; Normand, S.; Stroher, U.;

Tipples, G. A.; Tyler, S.; Vogrig, R.; Ward, D.; Watson, B.; Brunham, R. C.; Krajden, M.; Petric, M.; Skowronski, D. M.; Upton, C.; Roper, R. L. The genome sequence of the SARS-associated coronavirus. *Science* **2003**, *300*, 1399-1404.

7. Rota, P. A.; Oberste, M. S.; Monroe, S. S.; Nix, W. A.; Campagnoli, R.; Icenogle, J. P.; Penaranda, S.; Bankamp, B.; Maher, K.; Chen, M. H.; Tong, S. X.; Tamin, A.; Lowe, L.; Frace, M.; DeRisi, J. L.; Chen, Q.; Wang, D.; Erdman, D. D.; Peret, T. C. T.; Burns, C.; Ksiazek, T. G.; Rollin, P. E.; Sanchez, A.; Liffick, S.; Holloway, B.; Limor, J.; McCaustland, K.; Olsen-Rasmussen, M.; Fouchier, R.; Gunther, S.; Osterhaus, A.; Drosten, C.; Pallansch, M. A.; Anderson, L. J.; Bellini, W. J. Characterization of a novel coronavirus associated with severe acute respiratory syndrome. *Science* **2003**, *300*, 1394-1399.

8. Ruan, Y. J.; Wei, C. L.; Ee, L. A.; Vega, V. B.; Thoreau, H.; Yun, S. T. S.; Chia, J. M.; Ng, P.; Chiu, K. P.; Lim, L.; Tao, Z.; Peng, C. K.; Ean, L. O. L.; Lee, N. M.; Sin, L. Y.; Ng, L. F. P.; Chee, R. E.; Stanton, L. W.; Long, P. M.; Liu, E. T. Comparative full-length genome sequence analysis of 14 SARS coronavirus isolates and common mutations associated with putative origins of infection. *Lancet* **2003**, *361*, 1779-1785.

9. Stadler, K.; Masignani, V.; Eickmann, M.; Becker, S.; Abrignani, S.; Klenk, H. D.; Rappuoli, R. SARS - Beginning to understand a new virus. *Nat. Rev. Microbiol.* **2003**, *1*, 209-218.

10. Lee, N.; Hui, D.; Wu, A.; Chan, P.; Cameron, P.; Joynt, G. M.; Ahuja, A.; Yung, M. Y.; Leung, C. B.; To, K. F.; Lui, S. F.; Szeto, C. C.; Chung, S.; Sung, J. J. Y. A major outbreak of severe acute respiratory syndrome in Hong Kong. *New. Engl. J. Med.* **2003**, *348*, 1986-1994.

11. Wu, C. Y.; Jan, J. T.; Ma, S. H.; Kuo, C. J.; Juan, H. F.; Cheng, Y. S. E.; Hsu, H. H.; Huang, H. C.; Wu, D.; Brik, A.; Liang, F. S.; Liu, R. S.; Fang, J. M.; Chen, S. T.; Liang, P. H.; Wong, C. H. Small molecules targeting severe acute respiratory syndrome human coronavirus. *Proc. Natl. Acad. Sci. U. S. A.* **2004**, *101*, 10012-10017.

12. http://www.hc-sc.gc.ca/hl-vs/iyh-vsv/diseases-maladies/sars-sras-eng.php#hot (accessed on June 14, 2009)

13. Cinatl, J.; Morgenstern, B.; Bauer, G.; Chandra, P.; Rabenau, H.; Doerr, H. W. Treatment of SARS with human interferons. *Lancet* **2003**, *362*, 293-294.

14. Thiel, V.; Ivanov, K. A.; Putics, A.; Hertzig, T.; Schelle, B.; Bayer, S.; Weissbrich, B.; Snijder, E. J.; Rabenau, H.; Doerr, H. W.; Gorbalenya, A. E.; Ziebuhr, J. Mechanisms and enzymes involved in SARS coronavirus genome expression. *J. Gen. Virol.* **2003**, *84*, 2305-2315.

15. Thiel, V.; Herold, J.; Schelle, B.; Siddell, S. G. Viral replicase gene products suffice for coronavirus discontinuous transcription. *J. Virol.* **2001**, *75*, 6676-6681.

16. Schechter, I.; Berger, A. On Size of Active Site in Proteases .I. Papain. *Biochem. Biophys. Res. Commun.* **1967**, *27*, 157-162.

17. Hegyi, A.; Ziebuhr, J. Conservation of substrate specificities among coronavirus main proteases. *J. Gen. Virol.* **2002**, *83*, 595-599.

18. Anand, K.; Ziebuhr, J.; Wadhwani, P.; Mesters, J. R.; Hilgenfeld, R. Coronavirus main proteinase (3CL(pro)) structure: Basis for design of anti-SARS drugs. *Science* **2003**, *300*, 1763-1767.

19. Yang, H. T.; Yang, M. J.; Ding, Y.; Liu, Y. W.; Lou, Z. Y.; Zhou, Z.; Sun, L.; Mo, L. J.; Ye, S.; Pang, H.; Gao, G. F.; Anand, K.; Bartlam, M.; Hilgenfeld, R.; Rao, Z. H. The crystal structures of severe acute respiratory syndrome virus main protease and its complex with an inhibitor. *Proc. Natl. Acad. Sci. U. S. A.* **2003**, *100*, 13190-13195.

20. Tan, J. Z.; Verschueren, K. H. G.; Anand, K.; Shen, J. H.; Yang, M. J.; Xu, Y. C.; Rao, Z. H.; Bigalke, J.; Heisen, B.; Mesters, J. R.; Chen, K. X.; Shen, X.; Jiang, H. L.; Hilgenfeld, R. pH-dependent conformational flexibility of the SARS-CoV main proteinase (M-pro) dimer: Molecular dynamics simulations and multiple X-ray structure analyses. *J. Mol. Biol.* **2005**, *354*, 25-40.

21. Fan, K. Q.; Wei, P.; Feng, Q.; Chen, S. D.; Huang, C. K.; Ma, L.; Lai, B.; Pei, J. F.; Liu, Y.; Chen, J. G.; Lai, L. H. Biosynthesis, purification, and substrate specificity of severe acute respiratory syndrome coronavirus 3C-like proteinase. *J. Biol. Chem.* **2004**, *279*, 1637-1642.

22. Hsu, W. C.; Chang, H. C.; Chou, C. Y.; Tsai, P. J.; Lin, P. I.; Chang, G. G. Critical assessment of important regions in the subunit association and

catalytic action of the severe acute respiratory syndrome coronavirus main protease. *J. Biol. Chem.* **2005**, *280*, 22741-22748.

23. Li, W. D.; Shi, Z. L.; Yu, M.; Ren, W. Z.; Smith, C.; Epstein, J. H.; Wang, H. Z.; Crameri, G.; Hu, Z. H.; Zhang, H. J.; Zhang, J. H.; McEachern, J.; Field, H.; Daszak, P.; Eaton, B. T.; Zhang, S. Y.; Wang, L. F. Bats are natural reservoirs of SARS-like coronaviruses. *Science* **2005**, *310*, 676-679.

24. Lau, S. K. P.; Woo, P. C. Y.; Li, K. S. M.; Huang, Y.; Tsoi, H. W.; Wong, B. H. L.; Wong, S. S. Y.; Leung, S. Y.; Chan, K. H.; Yuen, K. Y. Severe acute respiratory syndrome coronavirus-like virus in Chinese horseshoe bats. *Proc. Natl. Acad. Sci. U. S. A.* **2005**, *102*, 14040-14045.

25. <http://www.who.int/csr/don/2003_09_24/en/>(2003) (accessed on May 10, 2009)

26. Tong, T. R. Therapies for coronaviruses. Part I of II - viral entry inhibitors. *Expert Opin. Ther. Patents* **2009**, *19*, 357-367.

27. Tong, T. R. Therapies for coronaviruses. Part 2: inhibitors of intracellular life cycle. *Expert Opin. Ther. Patents* **2009**, *19*, 415-431.

28. Turk, B. Targeting proteases: successes, failures and future prospects. *Nat. Rev. Drug Discov.* **2006**, *5*, 785-799.

29. Harrold, M. W. Y., N. S. In *Comprehensive Pharmacy Review*; Shargel, L. M., A. H.; Souney, P. E.; Swanson, L. N., Ed.; Lippincot Williams & Williams: Baltimore, 2004, p 224-253.

30. Ghosh, A. K.; Xi, K.; Ratia, K.; Santarsiero, B. D.; Fu, W. T.; Harcourt, B. H.; Rota, P. A.; Baker, S. C.; Johnson, M. E.; Mesecar, A. D. Design and synthesis of peptidomimetic severe acute respiratory syndrome chymotrypsin-like protease inhibitors. *J. Med. Chem.* **2005**, *48*, 6767-6771.

31. Blanchard, J. E.; Elowe, N. H.; Huitema, C.; Fortin, P. D.; Cechetto, J. D.; Eltis, L. D.; Brown, E. D. High-throughput screening identifies inhibitors of the SARS coronavirus main proteinase. *Chem. Biol.* **2004**, *11*, 1445-1453.

32. Zhang, J. M.; Pettersson, H. I.; Huitema, C.; Niu, C. Y.; Yin, J.; James, M. N. G.; Eltis, L. D.; Vederas, J. C. Design, synthesis, and evaluation of inhibitors for severe acute respiratory syndrome 3C-like protease based on phthalhydrazide ketones or heteroaromatic esters. *J. Med. Chem.* **2007**, *50*, 1850-1864.

33. Wu, C. Y.; King, K. Y.; Kuo, C. J.; Fang, J. M.; Wu, Y. T.; Ho, M. Y.; Liao, C. L.; Shie, J. J.; Liang, P. H.; Wong, C. H. Stable benzotriazole esters as mechanism-based inactivators of the severe acute respiratory syndrome 3CL protease. *Chem. Biol.* **2006**, *13*, 261-268.

34. Jain, R. P.; Pettersson, H. I.; Zhang, J. M.; Aull, K. D.; Fortin, P. D.; Huitema, C.; Eltis, L. D.; Parrish, J. C.; James, M. N. G.; Wishart, D. S.; Vederas, J. C. Synthesis and evaluation of keto-glutamine analogues as potent inhibitors of severe acute respiratory syndrome 3CL(pro). *J. Med. Chem.* **2004**, *47*, 6113-6116.

35. Zhou, L.; Liu, Y.; Zhang, W. L.; Wei, P.; Huang, C. K.; Pei, J. F.; Yuan, Y. X.; Lai, L. H. Isatin compounds as noncovalent SARS coronavirus 3C-like protease inhibitors. *J. Med. Chem.* **2006**, *49*, 3440-3443.

36. Vicik, R.; Busemann, M.; Baumann, K.; Schirmeister, T. Inhibitors of cysteine proteases. *Curr. Top. Med. Chem.* **2006**, *6*, 331-353.

37. Ziebuhr, J.; Snijder, E. J.; Gorbalenya, A. E. Virus-encoded proteinases and proteolytic processing in the Nidovirales. *J. Gen. Virol.* **2000**, *81*, 853-879.

38. Krausslich, H. G.; Wimmer, E. Viral Proteinases. *Annu. Rev. Biochem.* **1988**, *57*, 701-754.

39. Li, X.; Ryan, M. D.; Lamb, J. W. Potato leaf roll virus protein P1 contains a serine proteinase domain. *J. Gen. Virol.* **2000**, *81*, 1857-1864.

40. Niu, C.; Yin, J.; Zhang, J.; Vederas, J. C.; James, M. N. G. Molecular docking identifies the binding of 3-chloropyridine moieties specifically to the S1 pocket of SARS-CoV M-pro. *Bioorg. Med. Chem.* **2008**, *16*, 293-302.

41. Gelb, M. H.; Svaren, J. P.; Abeles, R. H. Fluoro Ketone Inhibitors of Hydrolytic Enzymes. *Biochemistry* **1985**, *24*, 1813-1817.

42. Sani, M.; Sinisi, R.; Viani, F. Peptidyl fluoro-ketones as proteolytic enzyme inhibitors. *Curr. Top. Med. Chem.* **2006**, *6*, 1545-1566.

43. Angliker, H.; Wikstrom, P.; Rauber, P.; Stone, S.; Shaw, E. Synthesis and Properties of Peptidyl Derivatives of Arginylfluoromethanes. *Biochem. J.* **1988**, *256*, 481-486.

44. Morris, T. S.; Frormann, S.; Shechosky, S.; Lowe, C.; Lall, M. S.; GaussMuller, V.; Purcell, R. H.; Emerson, S. U.; Vederas, J. C.; Malcolm, B. A. In vitro and ex vivo inhibition of hepatitis A virus 3C proteinase by a peptidyl monofluoromethyl ketone. *Bioorg. Med. Chem.* **1997**, *5*, 797-807.

45. Launay, S.; Hermine, O.; Fontenay, M.; Kroemer, G.; Solary, E.; Garrido, C. Vital functions for lethal caspases. *Oncogene* **2005**, *24*, 5137-5148.

46. Zhang, H. Z.; Zhang, H.; Kemnitzer, W.; Tseng, B.; Cinatl, J.; Michaelis, M.; Doerr, H. W.; Cai, S. X. Design and synthesis of dipeptidyl glutaminyl fluoromethyl ketones as potent severe acute respiratory syndrome coronovirus (SARS-CoV) inhibitors. *J. Med. Chem.* **2006**, *49*, 1198-1201.

47. Silverman, R. B. *The Organic Chemistry of Enzyme-Catalyzd Reactions*; Academic Press, 2000.

48. Barrila, J.; Bacha, U.; Freire, E. Long-range cooperative interactions modulate dimerization in SARS 3CL(pro). *Biochemistry* **2006**, *45*, 14908-14916.

49. Malcolm, B. A. The Picornaviral 3c Proteinases - Cysteine Nucleophiles in Serine Proteinase Folds. *Protein Sci.* **1995**, *4*, 1439-1445.

50. Gorbalenya, A. E.; Snijder, E. J. Viral cysteine proteinases. *Perspect. Drug Discov. Design* **1996**, *6*, 64-86.

51. Jain, R. P.; Vederas, J. C. Structural variations in keto-glutamines for improved inhibition against hepatitis A virus 3C proteinase. *Bioorg. Med. Chem. Lett.* **2004**, *14*, 3655-3658.

52. Jianmin Zhang. Design, Synthesis and Evaluation of Severe Acute Respiratory Syndrome Coronavirus 3C-Like protease Inhibitors. *Ph. D. Thesis*, *University of Alberta, Edmonton, Alberta.* **2007**.

53. Chen, L. R.; Wang, Y. C.; Lin, Y. W.; Chou, S. Y.; Chen, S. F.; Liu, L. T.; Wu, Y. T.; Chih-Jung, K. B.; Chen, T. S. S.; Juang, S. H. Synthesis and evaluation of isatin derivatives as effective SARS coronavirus 3CL protease inhibitors. *Bioorg. Med. Chem. Lett.* **2005**, *15*, 3058-3062.

54. Zhang, J. M.; Huitema, C.; Niu, C. Y.; Yin, J.; James, M. N. G.; Eltis, L. D.; Vederas, J. C. Aryl methylene ketones and fluorinated methylene ketones as reversible inhibitors for severe acute respiratory syndrome (SARS) 3C-like proteinase. *Bioorg. Med. Chem.* **2008**, *36*, 229-240.

55. Thomas, S. A.; Li, T. M.; Woods, K. W.; Song, X. H.; Packard, G.; Fischer, J. P.; Diebold, R. B.; Liu, X. S.; Shi, Y.; Klinghofer, V.; Johnson, E. F.; Bouska, J. J.; Olson, A.; Guan, R.; Magnone, S. R.; Marsh, K.; Luo, Y.; Rosenberg, S. H.; Giranda, V. L.; Li, Q. Identification of a novel 3,5-disubstituted pyridine as a potent, selective, and orally active inhibitor of Akt1 kinase. *Bioorg. Med. Chem. Lett.* **2006**, *16*, 3740-3744.

56. Frecer, V.; Kabelac, M.; De Nardi, P.; Pricl, S.; Miertus, S. Structure-based design of inhibitors of NS3 serine protease of hepatitis C virus. *J. Mol. Graph.* **2004**, *22*, 209-220.

57. Muller, P.; Chappellet, S. Asymmetric 1,3-dipolar cycloadditions of 2-diazocyclohexane-1,3-diones and alkyl diazopyruvates. *Helv. Chim. Acta* **2005**, *88*, 1010-1021.

58. Copeland, R. A. *Enzymes: A Practical Introduction to Structure, Mechansim and Data Analysis*; 2nd ed.; Wiley, New York, 2000.

59. Ratia, K.; Pegan, S.; Takayama, J.; Sleeman, K.; Coughlin, M.; Baliji, S.; Chaudhuri, R.; Fu, W. T.; Prabhakar, B. S.; Johnson, M. E.; Baker, S. C.; Ghosh, A. K.; Mesecar, A. D. A noncovalent class of papain-like protease/deubiquitinase inhibitors blocks SARS virus replication. *Proc. Natl. Acad. Sci. U. S. A.* **2008**, *105*, 16119-16124.

60. Leung-Toung, R.; Zhao, Y. Q.; Li, W. R.; Tam, T. F.; Karimian, K.; Spino, M. Thiol proteases: Inhibitors and potential therapeutic targets. *Curr. Med. Chem.* **2006**, *13*, 547-581.

61. Jewell, D. A.; Swietnicki, W.; Dunn, B. M.; Malcolm, B. A. Hepatitis-A Virus 3C Proteinase Substrate-Specificity. *Biochemistry* **1992**, *31*, 7862-7869.

62. Lall, M. S.; Jain, R. P.; Vederas, J. C. Inhibitors of 3C cysteine proteinases from picornaviridae. *Curr. Top. Med. Chem.* **2004**, *4*, 1239-1253.

63. http://aginfo.psu.edu/news/2007/1/HoneyBees.htm (accessed on June 02, 2009)

64. Cox-Foster, D. L.; Conlan, S.; Holmes, E. C.; Palacios, G.; Evans, J. D.; Moran, N. A.; Quan, P. L.; Briese, T.; Hornig, M.; Geiser, D. M.; Martinson, V.; vanEngelsdorp, D.; Kalkstein, A. L.; Drysdale, A.; Hui, J.;

Zhai, J. H.; Cui, L. W.; Hutchison, S. K.; Simons, J. F.; Egholm, M.; Pettis, J. S.; Lipkin, W. I. A metagenomic survey of microbes in honey bee colony collapse disorder. *Science* **2007**, *318*, 283-287.

65. Stokstad, E. The case of the empty hives. *Science* **2007**, *316*, 970-972.

66. Barrionuevo, A. In *New York Times* April 24, 2007, p 1.

67. Stokstad, E. Genomics - Puzzling decline of US bees linked to virus from Australia. *Science* **2007**, *317*, 1304-1305.

68. Maori, E.; Lavi, S.; Mozes-Koch, R.; Gantman, Y.; Peretz, Y.; Edelbaum, O.; Tanne, E.; Sela, I. Isolation and characterization of Israeli acute paralysis virus, a dicistrovirus affecting honeybees in Israel: evidence for diversity due to intra- and inter-species recombination. *J. Gen. Virol.* **2007**, *88*, 3428-3438.

69. Mayo, M. A. A summary of taxonomic changes recently approved by ICTV. *Arch. Virol.* **2002**, *147*, 1655-1656.

70. Carly Huitema. Screening, characterization and inhibition of viral cysteine proteinases. *Ph. D. Thesis*, *Univerity of British Columbia, Vancouver.* **2009**.

71. Tate, J.; Liljas, L.; Scotti, P.; Christian, P.; Lin, T. W.; Johnson, J. E. The crystal structure of cricket paralysis virus: the first view of a new virus family. *Nat. Struct. Biol.* **1999**, *6*, 765-774.

72. Ramtohul, Y. K.; James, M. N. G.; Vederas, J. C. Synthesis and evaluation of keto-glutamine analogues as inhibitors of hepatitis A virus 3C proteinase. *J. Org. Chem.* **2002**, *67*, 3169-3178.

73. Palmer, J. T. S. R., CA In *free patents online*; 5210272, U. S. P., Ed. United States of America. http://www.freepatentsonline.com/5210272.html (accessed on Sep 11, 2008)

74. Kaiser, E.; Colescot.Rl; Bossinge.Cd; Cook, P. I. Color Test for Detection of Free Terminal Amino Groups in Solid-Phase Synthesis of Peptides. *Anal. Biochem.* **1970**, *34*, 595-598.

75. Fu, S. C. J.; Birnbaum, S. M. The Hydrolytic Action of Acylase-I on N-Acylamino Acids. *J. Am. Chem. Soc.* **1953**, *75*, 918-920.

76. Michi, K.; Tsuda, H. Enzymatic Resolution of Racemic Amino Acids .6. Hydrolysis of Various N-Acyl Dl-Amino Acids by Mold Acylases. *J. Biochem.* **1958**, *45*, 745-749.

77. Duthaler, R. O. Recent Developments in the Stereoselective Synthesis of Alpha-Amino-Acids. *Tetrahedron* **1994**, *50*, 1539-1650.

78. Hegedus, L. S. Synthesis of Amino-Acids and Peptides Using Chromium Carbene Complex Photochemistry. *Accounts Chem. Res.* **1995**, *28*, 299-305.

79. Schollkopf, U.; Groth, U.; Westphalen, K. O.; Deng, C. Asymmetric Syntheses Via Heterocyclic Intermediates .8. Enantioselective Synthesis of (*R*)-Alpha-Methyl-Alpha-Amino Acids Using L-Valine as Chiral Auxiliary Reagent. *Synthesis* **1981**, 969-971.

80. Schollkopf, U.; Groth, U.; Deng, C. Asymmetric Syntheses Via Heterocyclic Intermediates .6. Enantioselective Synthesis of (*R*)-Amino

Acids Using L-Valine as Chiral Agent. *Angew. Chem.Int. Ed. Engl.* **1981**, *20*, 798-799.

81. Seebach, D.; Boes, M.; Naef, R.; Schweizer, W. B. Alkylation of Amino-Acids without Loss of the Optical-Activity - Preparation of Alpha-Substituted Proline Derivatives - a Case of Self-Reproduction of Chirality. *J. Am. Chem. Soc.* **1983**, *105*, 5390-5398.

82. Williams, R. M.; Sinclair, P. J.; Zhai, D.; Chen, D. Practical Asymmetric Syntheses of Alpha-Amino-Acids through Carbon Carbon Bond Constructions on Electrophilic Glycine Templates. *J. Am. Chem. Soc.* **1988**, *110*, 1547-1557.

83. Evans, D. A.; Britton, T. C.; Ellman, J. A.; Dorow, R. L. The Asymmetric-Synthesis of Alpha-Amino-Acids - Electrophilic Azidation of Chiral Imide Enolates, a Practical Approach to the Synthesis of (*R*)-Alpha-Azido and (*S*)-Alpha-Azido Carboxylic-Acids. *J. Am. Chem. Soc.* **1990**, *112*, 4011-4030.

84. Mansawat, W.; Bhanthumnavin, W.; Vilaivan, T. N-Salicyl-beta-aminoalcohols as a new class of ligand for catalytic asymmetric Strecker reactions. *Tetrahedron Lett.* **2003**, *44*, 3805-3808.

85. Noyori, R. Chemical Multiplication of Chirality - Science and Applications. *Chem. Soc. Rev.* **1989**, *18*, 187-208.

86. Ramtohul, Y. K.; Martin, N. I.; Silkin, L.; James, M. N. G.; Vederas, J. C. Pseudoxazolones, a new class of inhibitors for cysteine proteinases:

inhibition of hepatitis A virus and human rhinovirus 3C proteinases. *Chem. Commun.* **2001**, 2740-2741.

87. Uematsu, N.; Fujii, A.; Hashiguchi, S.; Ikariya, T.; Noyori, R. Asymmetric transfer hydrogenation of imines. *J. Am. Chem. Soc.* **1996**, *118*, 4916-4917.

88. Noyori, R.; Hashiguchi, S. Asymmetric transfer hydrogenation catalyzed by chiral ruthenium complexes. *Accounts Chem. Res.* **1997**, *30*, 97-102.

89. Imamoto, T.; Iwadate, N.; Yoshida, K. Enantioselective hydrogenation of acyclic aromatic N-aryl imines catalyzed by an iridium complex of (S,S)-1,2-bis(tert-butylmethylphosphino)ethane. *Org. Lett.* **2006**, *8*, 2289-2292.

90. Riant, O.; Mostefai, N.; Courmarcel, J. Recent advances in the asymmetric hydrosilylation of ketones, imines and electrophilic double bonds. *Synthesis* **2004**, 2943-2958.

91. Kirton, E. H. M.; Tughan, G.; Morris, R. E.; Field, R. A. Rationalising the effect of reducing agent on the oxazaborolidine-mediated asymmetric reduction of N-substituted imines. *Tetrahedron Lett.* **2004**, *45*, 853-855.

92. Nathaniel I. Martin. Pseudoxazolones as Hepatitis A Virus 3C Proteinase Inhibitors and Bacterially Derived Antimicrobial Peptides. *Ph. D. Thesis*, *University of Alberta, Edmonton, Alberta.* **2004**

93. Steglich, W.; Tanner, H.; Hurnaus, R. 2-Dichlormethylen-Pseudooxazolone-(5). *Chem. Ber.* **1967**, *100*, 1824-1832.

94. Oka, K.; Dobashi, A.; Hara, S. Effects of Strong Pi-Electron Accepting Substituents on Structure Preference for Thiocarbonyl Ylide or Thiirane. *Tetrahedron Lett.* **1980**, *21*, 3579-3582.

95. Babasaki, K.; Takao, T.; Shimonishi, Y.; Kurahashi, K. Subtilosin-a, a New Antibiotic Peptide Produced by Bacillus-Subtilis-168 - Isolation, Structural-Analysis, and Biogenesis. *J. Biochem.* **1985**, *98*, 585-603.

96. Jack, R. W.; Tagg, J. R.; Ray, B. Bacteriocins of Gram-Positive Bacteria. *Microbiol. Rev.* **1995**, *59*, 171-200.

97. Kolter, R.; Moreno, F. Genetics of Ribosomally Synthesized Peptide Antibiotics. *Annu. Rev. Microbiol.* **1992**, *46*, 141-163.

98. Maqueda, M.; Sanchez-Hidalgo, M.; Fernandez, M.; Montalban-Lopez, M.; Valdivia, E.; Martinez-Bueno, M. Genetic features of circular bacteriocins produced by Gram-positive bacteria. *FEMS Microbiol. Rev.* **2008**, *32*, 2-22.

99. Gratia, J. P. Andre Gratia: A forerunner in microbial and viral genetics. *Genetics* **2000**, *156*, 471-476.

100. Zheng, G. L.; Hehn, R.; Zuber, P. Mutational analysis of the sbo-alb locus of Bacillus subtilis : Identification of genes required for subtilosin production and immunity. *J. Bacteriol.* **2000**, *182*, 3266-3273.

101. Klaenhammer, T. R. Genetics of Bacteriocins Produced by Lactic-Acid Bacteria. *FEMS Microbiol. Rev.* **1993**, *12*, 39-86.

102. Nes, I. F.; Hole, H. Class II antimicrobial peptides from lactic acid bacteria. *Biopolymers* **2000**, *55*, 50-61.

103. van Belkum, M. J.; Stiles, M. E. Nonlantibiotic antibacterial peptides from lactic acid bacteria. *Nat. Prod. Rep.* **2000**, *17*, 323-335.

104. Cotter, P. D.; Hill, C.; Ross, R. P. Bacteriocins: Developing innate immunity for food. *Nat. Rev. Microbiol.* **2005**, *3*, 777-788.

105. Maqueda, M.; Galvez, A.; Bueno, M. M.; Sanchez-Barrena, M. J.; Gonzalez, C.; Albert, A.; Rico, M.; Valdivia, E. Peptide AS-48: Prototype of a new class of cyclic bacteriocins. *Curr. Protein Pept. Sci.* **2004**, *5*, 399-416.

106. Kawai, Y.; Kemperman, R.; Kok, J.; Saito, T. The circular Bacteriocins gassericin A and circularin A. *Curr. Protein Pept. Sci.* **2004**, *5*, 393-398.

107. Zheng, G. L.; Yan, L. Z.; Vederas, J. C.; Zuber, P. Genes of the sbo-alb locus of Bacillus subtilis are required for production of the antilisterial bacteriocin subtilosin. *J. Bacteriol.* **1999**, *181*, 7346-7355.

108. Kawulka, K.; Sprules, T.; McKay, R. T.; Mercier, P.; Diaper, C. M.; Zuber, P.; Vederas, J. C. Structure of subtilosin A, an antimicrobial peptide from Bacillus subtilis with unusual posttranslational modifications linking cysteine sulfurs to alpha-carbons of phenylalanine and threonine. *J. Am. Chem. Soc.* **2003**, *125*, 4726-4727.

109. Kawulka, K. E.; Sprules, T.; Diaper, C. M.; Whittal, R. M.; McKay, R. T.; Mercier, P.; Zuber, P.; Vederas, J. C. Structure of subtilosin A, a cyclic antimicrobial peptide from Bacillus subtilis with unusual sulfur to alpha-carbon cross-links: Formation and reduction of alpha-thio-alpha-amino acid derivatives. *Biochemistry* **2004**, *43*, 3385-3395.

110. Aoki, M.; Ohtsuka, T.; Yamada, M.; Ohba, Y.; Yoshizaki, H.; Yasuno, H.; Sano, T.; Watanabe, J.; Yokose, K.; Seto, H. Cyclothiazomycin, a Novel Polythiazole-Containing Peptide with Renin Inhibitory Activity - Taxonomy, Fermentation, Isolation and Physicochemical Characterization. *J. Antibiot.* **1991**, *44*, 582-588.

111. Thennarasu, S.; Lee, D. K.; Poon, A.; Kawulka, K. E.; Vederas, J. C.; Ramamoorthy, A. Membrane permeabilization, orientation, and antimicrobial mechanism of subtilosin A. *Chem. Phys. Lipids* **2005**, *137*, 38-51.

112. Ikai, A. Thermostability and Aliphatic Index of Globular-Proteins. *J. Biochem.* **1980**, *88*, 1895-1898.

113. Havarstein, L. S.; Diep, D. B.; Nes, I. F. A Family of Bacteriocin Abc Transporters Carry out Proteolytic Processing of Their Substrates Concomitant with Export. *Mol. Microbiol.* **1995**, *16*, 229-240.

114. Marx, R.; Stein, T.; Entian, K. D.; Glaser, S. J. Structure of the Bacillus subtilis peptide antibiotic subtilosin a determined by H-1-NMR and matrix assisted laser desorption/ionization time-of-flight mass spectrometry. *J. Protein Chem.* **2001**, *20*, 501-506.

115. Layer, G.; Heinz, D. W.; Jahn, D.; Schubert, W. D. Structure and function of radical SAM enzymes. *Curr. Opin. Chem. Biol.* **2004**, *8*, 468-476.

116. Frey, P. A.; Hegeman, A. D.; Ruzicka, F. J. The radical SAM superfamily. *Crit. Rev. Biochem. Mol. Biol.* **2008**, *43*, 63-88.

117. Solomon, P. S.; Shaw, A. L.; Lane, I.; Hanson, G. R.; Palmer, T.; McEwan, A. G. Characterization of a molybdenum cofactor biosynthetic gene cluster in Rhodobacter capsulatus which is specific for the biogenesis of dimethylsulfoxide reductase. *Microbiology-(UK)* **1999**, *145*, 1421-1429.

118. Wuebbens, M. M.; Rajagopalan, K. V. Investigation of the Early Steps of Molybdopterin Biosynthesis in Escherichia-Coli through the Use of In Vivo Labeling Studies. *J. Biol. Chem.* **1995**, *270*, 1082-1087.

119. Iwata, S.; Lee, J. W.; Okada, K.; Lee, J. K.; Iwata, M.; Rasmussen, B.; Link, T. A.; Ramaswamy, S.; Jap, B. K. Complete structure of the 11-subunit bovine mitochondrial cytochrome bc(1) complex. *Science* **1998**, *281*, 64-71.

120. Oclary, D.; Wahleithner, J. A.; Wolstenholme, D. R. Sequence and Arrangement of the Genes for Cytochrome-B, Urf1, Urf4l, Urf4, Urf5, Urf6 and 5 Transfer-RNAs in Drosophila Mitochondrial-DNA. *Nucleic Acids Res.* **1984**, *12*, 3747-3762.

121. Braun, H. P.; Schmitz, U. K. Are the Core Proteins of the Mitochondrial Bc(1) Complex Evolutionary Relics of a Processing Protease. *Trends Biochem.Sci.* **1995**, *20*, 171-175.

122. Duquesne, S.; Destoumieux-Garzon, D.; Zirah, S.; Goulard, C.; Peduzzi, J.; Rebuffat, S. Two enzymes catalyze the maturation of a lasso peptide in *Escherichia coli*. *Chem. Biol.* **2007**, *14*, 793-803.

123. Donia, M. S.; Ravel, J.; Schmidt, E. W. A global assembly line for cyanobactins. *Nat. Chem. Biol.* **2008**, *4*, 341-343.

124. Lee, J.; McIntosh, J.; Hathaway, B. J.; Schmidt, E. W. Using Marine Natural Products to Discover a Protease that Catalyzes Peptide Macrocyclization of Diverse Substrates. *J. Am. Chem. Soc.* **2009**, *131*, 2122-4

125. Ziemert, N.; Ishida, K.; Liaimer, A.; Hertweck, C.; Dittmann, E. Ribosomal synthesis of tricyclic depsipeptides in bloom-forming cyanobacteria. *Angew. Chem. Int. Ed. Engl.* **2008**, *47*, 7756-7759.

126. Moore, B. S. Extending the Biosynthetic Repertoire in Ribosomal Peptide Assembly. *Angew. Chem. Int. Ed. Engl.* **2008**, *47*, 9386-9388.

127. Murzin, A. G. Structural classification of proteins: New superfamilies. *Curr. Opin. Struct. Biol.* **1996**, *6*, 386-394.

128. Haack, T.; Mutter, M. Serine Derived Oxazolidines as Secondary Structure Disrupting, Solubilizing Building-Blocks in Peptide-Synthesis. *Tetrahedron Lett.* **1992**, *33*, 1589-1592.

129. Mutter, M.; Nefzi, A.; Sato, T.; Sun, X.; Wahl, F.; Wohr, T. Pseudo-Prolines (Psi-Pro) for Accessing Inaccessible Peptides. *Peptide Res.* **1995**, *8*, 145-153.

130. Skropeta, D.; Jolliffe, K. A.; Turner, P. Pseudoprolines as removable turn inducers: Tools for the cyclization of small peptides. *J. Org. Chem.* **2004**, *69*, 8804-8809.

131. Schmiedeberg, N.; Kessler, H. Reversible backbone protection enables combinatorial solid-phase ring-closing metathesis reaction (RCM) in peptides. *Org. Lett.* **2002**, *4*, 59-62.

132. Ehrlich, A.; Heyne, H. U.; Winter, R.; Beyermann, M.; Haber, H.; Carpino, L. A.; Bienert, M. Cyclization of all-L-pentapeptides by means of 1-hydroxy-7-azabenzotriazole-derived uronium and phosphonium reagents. *J. Org. Chem.* **1996**, *61*, 8831-8838.

133. Yang, Y.; Sweeney, W. V.; Schneider, K.; Thornqvist, S.; Chait, B. T.; Tam, J. P. Aspartimide Formation in Base-Driven 9-Fluorenylmethoxycarbonyl Chemistry. *Tetrahedron Lett.* **1994**, *35*, 9689-9692.

134. Nicolas, E.; Pedroso, E.; Giralt, E. Formation of Aspartimide Peptides in Asp-Gly Sequences. *Tetrahedron Lett.* **1989**, *30*, 497-500.

135. Dolling, R.; Beyermann, M.; Haenel, J.; Kernchen, F.; Krause, E.; Franke, P.; Brudel, M.; Bienert, M. Piperidine-Mediated Side Product Formation for Asp(O*t*Bu)-Containing Peptides. *J. Chem. Soc.-Chem. Commun.* **1994**, 853-854.

136. Packman, L. C. *N*-2 Hydroxy-4-Methoxybenzyl (Hmb) Backbone Protection Strategy Prevents Double Aspartimide Formation in a Difficult Peptide Sequence. *Tetrahedron Lett.* **1995**, *36*, 7523-7526.

137. Tam, J. P.; Heath, W. F.; Merrifield, R. B. SN2 Deprotection of Synthetic Peptides with a Low Concentration of HF in Dimethyl Sulfide - Evidence

and Application in Peptide-Synthesis. *J. Am. Chem. Soc.* **1983**, *105*, 6442-6455.

138. Fujii, N.; Otaka, A.; Ikemura, O.; Hatano, M.; Okamachi, A.; Funakoshi, S.; Sakurai, M.; Shioiri, T.; Yajima, H. Studies on Peptides .152. Hard Acid Deprotecting Procedure for Peptide-Synthesis. *Chem. Pharm. Bull.* **1987**, *35*, 3447-3452.

139. Lauer, J. L.; Fields, C. G.; Fields, G. B. Sequence dependence of aspartimide formation during 9-fluorenylmethoxycarbonyl solid-phase peptide synthesis. *Lett. Pept. Sci.* **1995**, *1*, 197-205.

140. Tam, J. P.; Riemen, M. W.; Merrifield, R. B. Mechanisms of Aspartimide Formation the Effects of Protecting Groups Acid Base Temperature and Time. *Peptide Res.* **1988**, *1*, 6-18.

141. Oligino, L.; Lung, F. D. T.; Sastry, L.; Bigelow, J.; Cao, T.; Curran, M.; Burke, T. R.; Wang, S. M.; Krag, D.; Roller, P. P.; King, C. R. Nonphosphorylated peptide ligands for the Grb2 Src homology 2 domain. *J. Biol. Chem.* **1997**, *272*, 29046-29052.

142. Gudmundsson, O. S.; Nimkar, K.; Gangwar, S.; Siahaan, T.; Borchardt, R. T. Phenylpropionic acid-based cyclic prodrugs of opioid peptides that exhibit metabolic stability to peptidases and excellent cellular permeation. *Pharm. Res.* **1999**, *16*, 16-23.

143. Goncalves, M.; Estieu-Gionnet, K.; Lain, G.; Bayle, M.; Betz, N.; Deleris, G. On-resin cyclization of a head-to-tail cyclopeptide using an

allyldimethylsilyl polystyrene resin pre-loaded by metathesis. *Tetrahedron* **2005**, *61*, 7789-7795.

144. Lambert, J. N.; Mitchell, J. P.; Roberts, K. D. The synthesis of cyclic peptides. *J. Chem. Soc.-Perkin Trans. 1* **2001**, 471-484.

145. Jiang, S.; Li, Z.; Ding, K.; Roller, P. P. Recent Progress of Synthetic Studies to Peptide and Peptidomimetic Cyclization. *Curr. Org. Chem.* **2008**, *12*, 1502-1542.

146. Eichler, J.; Lucka, A. W.; Houghten, R. A. Cyclic Peptide Template Combinatorial Libraries - Synthesis and Identification of Chymotrypsin Inhibitors. *Peptide Res.* **1994**, *7*, 300-307.

147. Trzeciak, A.; Bannwarth, W. Synthesis of Head-to-Tail Cyclized Peptides on Solid Support by Fmoc Chemistry. *Tetrahedron Lett.* **1992**, *33*, 4557-4560.

148. Mazur, S.; Jayalekshmy, P. Chemistry of Polymer-Bound Ortho-Benzyne - Frequency of Encounter between Substituents on Cross-Linked Polystyrenes. *J. Am. Chem. Soc.* **1979**, *101*, 677-683.

149. Jayalekshmy, P.; Mazur, S. Pseudodilution, Solid-Phase Immobilization of Benzyne. *J. Am. Chem. Soc.* **1976**, *98*, 6710-6711.

150. Albericio, F.; Vanabel, R.; Barany, G. Solid-Phase Synthesis of Peptides with C-Terminal Asparagine or Glutamine - an Effective, Mild Procedure Based on *N*-Alpha-Fluorenylmethyloxycarbonyl (Fmoc) Protection and Side-Chain Anchoring to a Tris(Alkoxy)Benzylamide (Pal) Handle. *Int. J. Pept. Protein Res.* **1990**, *35*, 284-286.

151. Alsina, J.; Rabanal, F.; Giralt, E.; Albericio, F. Solid-Phase Synthesis of Head-to-Tail Cyclic-Peptides Via Lysine Side-Chain Anchoring. *Tetrahedron Lett.* **1994**, *35*, 9633-9636.

152. Cabrele, C.; Langer, M.; Beck-Sickinger, A. G. Amino acid side chain attachment approach and its application to the synthesis of tyrosine-containing cyclic peptides. *J. Org. Chem.* **1999**, *64*, 4353-4361.

153. Yan, L. Z.; Edwards, P.; Flora, D.; Mayer, J. P. Synthesis of cyclic peptides through hydroxyl side-chain anchoring. *Tetrahedron Lett.* **2004**, *45*, 923-925.

154. Han, B. H.; Shin, D. H.; Cho, S. Y. Organic Sonochemistry - Ultrasonic Acceleration of the Reduction of Aromatic Nitro-Compounds with Hydrazine-Iron in the Presence of Activated Carbon. *Bull. Korean Chem. Soc.* **1985**, *6*, 320-320.

155. Rosen, I.; Stallings, J. P. The Addition-Chlorination of Phenol. *J. Org. Chem.* **1959**, *24*, 1523-1526.

156. Corson, B. B.; Hazzen, R. K.; Thomas, J. S. The mechanism underlying the reaction between aldehydes or ketones and tautomeric substances of the keto-enol Type II The condensation of oxomalonic ester with cyano-acetic and malonic esters. *J. Am. Chem. Soc.* **1928**, *50*, 913-918.

157. Tanaka, F.; Kinoshita, K.; Tanimura, R.; Fujii, I. Relaxing substrate specificity in antibody-catalyzed reactions: Enantioselective hydrolysis of *N*-Cbz-amino acid esters. *J. Am. Chem. Soc.* **1996**, *118*, 2332-2339.

7: APPENDIX A

ISOLATION AND CHARACTERIZATION OF SUBTILOSIN A1 WITH HEMOLYTIC ACTIVITY

7.1 Subtilosin A1

Subtilosin A1[1] (sub A1) is a mutant of subtilosin A in which a threonine residue at position-6 is substituted with an isoleucine (Figure 1).

Figure 1. Amino acid sequence of subtilosin A1. The arrow indicates the position of substitution

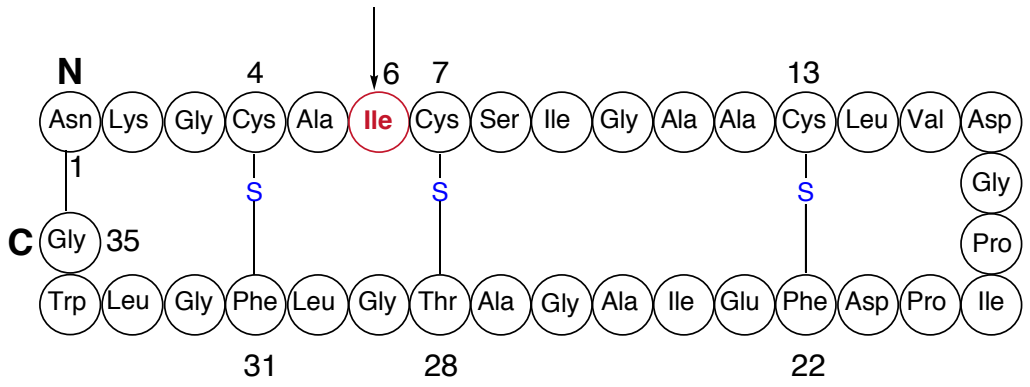

Our collaborators, Dr. Nakano and coworkers at the Oregon Health & Science University, produced the sub A1 mutant via genetic manipulation of a *Bacillus subtilis* strain. They found that sub A1 exhibited hemolytic activity. Interestingly,

the single codon substitution made in the *sboA* gene leads not only to hemolytic activity, but also to significant changes in the antibacterial specificity of the gene product. In addition to its hemolytic activity, sub A1 displays enhanced antibacterial activity against specific bacterial strains. It has been found that a spontaneous subtilosin A resistant mutant (ORB7082) confers resistance to both sub A and sub A1 in the absence of the AlbB immunity peptide. Transformation mapping studies indicated that this *sbr* (subtilosin resistance) mutation conferring resistance is not linked to the *sboA-alb* locus.

7.2 Objective

The overall objective of this collaborative project is to identify the mutation that confers hemolytic and enhanced antimicrobial activities and to examine how a single codon substitution in the *sboA* gene alters its spectrum of activity. Our contribution to this project involves isolation and purification of subtilosin A1 followed by its mass spectral characterization. Antimicrobial studies of subtilosin A (wild type) and subtilosin A1 (mutant) were also done to evaluate their activity against specific bacterial strains.

7.3 Isolation and purification of subtilosin A1

Subtilosin A1 was purified by a modified literature procedure.[2] To isolate subtilosin A1, a fresh colony of ORB6774 was used to inoculate in Difco Luria Broth Base Miller (LB broth). After incubation at 37 °C for 7 h at 200 rpm, 1.5 mL of the culture was transferred to 500 mL NSM (16 g Difco Nutrient broth, 500 mg $MgSO_4 \bullet 7H_2O$, 2 g KCl, 1mM $Ca(NO_3)_2 \bullet 4H_2O$, 0.1mM $MnCl_2 \bullet 4H_2O$, 1μM $FeSO_4 \bullet 7H_2O$ in 500 mL) and incubated at 37 °C for 7 h at 200 rpm. The culture medium was extracted by adding one-quarter volume of *n*-butanol (125 mL) and shaking for 1 h. The mixture was then poured into a separatory funnel and allowed to stand overnight. The two layers were separated and the organic layer was concentrated in vacuo, giving a yellow residue that was subsequently resuspended in methanol (10 mL per liter of cell culture). Purification by reverse phase high performance liquid chromatography (HPLC) yields the desired product subtilosin A1.

7.4 Mass spectrometry studies

To confirm the amino acid substitution, subtilosin A1 was analyzed using matrix assisted laser desorption ionization time of flight (MALDI-TOF) mass spectrometry. The isotopic distribution of the MALDI peak indicated that the average mass of subtilosin A1 is $[M+H]^+$ = 3414.5 Da (Figure 2A). The observed monoisotopic mass of subtilosin A1 $[M+H]^+$ at 3412.5 Da (Figure 2B) is

consistent, within error (0.1 Da) to a theoretical mass (3412.6 Da) resulting from the substitution of Ile for Thr in subtilosin A.

Figure 2. MALDI-TOF mass spectrum of subtilosin A1. **A:** The average mass of pure subtilosin A1; **B:** Expansion of the molecular ion region showing the isotopic distribution pattern for the molecular ion

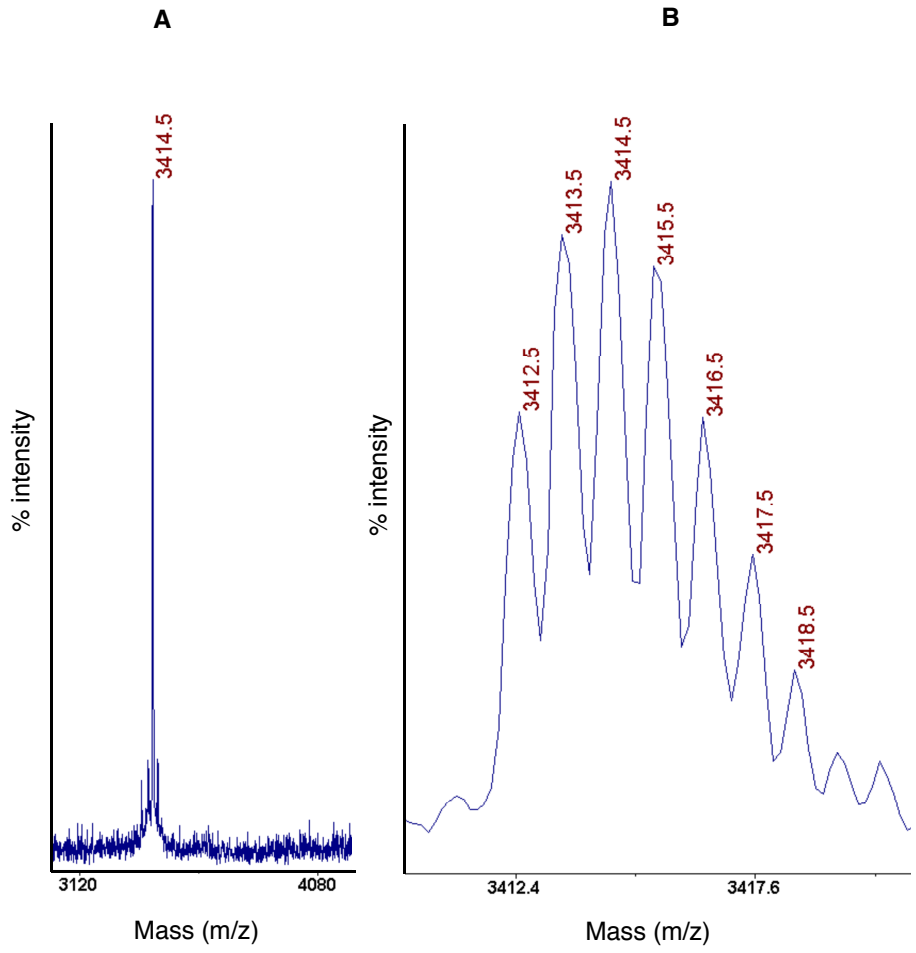

7.5 Antibacterial and hemolytic activity of subtilosin A and subtilosin A1

The antibacterial studies are done by our collaborators Dr. Nakano and coworkers and the results are presented here. Subtilosin A and subtilosin A1 were isolated from JH642 and ORB6774, respectively. Subtilosin A was shown to be more effective against Gram-positive bacteria than Gram-negative bacteria, although a few non-capsulated Gram-negative bacteria were reported to be sensitive to subtilosin A. At the concentrations used (250 μM or less), neither subtilosin A or subtilosin A1 was active against Gram-negative bacteria such as *E. coli*, *P. aeruginosa,* and *E. aerogenes* (data not shown), in contrast to a previous study that reported *E. aerogenes* as being highly sensitive to subtilosin A.[3] All bacteria tested that were sensitive to subtilosin A are more sensitive to subtilosin A1.

In addition to its enhanced antimicrobial activity, subtilosin A1 also shows hemolytic activity, in contrast to subtilosin A (Figure 3). Unlike subtilosin A, which showed no hemolytic activity at concentrations of 250 μM or less, subtilosin A1 exhibited hemolytic activity at 16 μM. These results clearly indicated that the hemolytic activity resulted from the amino acid substitution and this substitution also led to enhanced activity against the bacteria that are sensitive to the wild-type subtilosin A.

Figure 3. Hemolytic activity produced by *B. subtilis* and the variant subtilosin A1. **A.** The JH642 strain (wild) and two mutants that exhibit hemolytic activity were streaked on a rabbit blood agar plate. After incubation for overnight, complete blood lysis zones were observed around the mutant strain colonies, indicating that the mutants produce β-hemolysin. **B.** Hemolytic activity by the variant peptide subtilosin A1.[1]

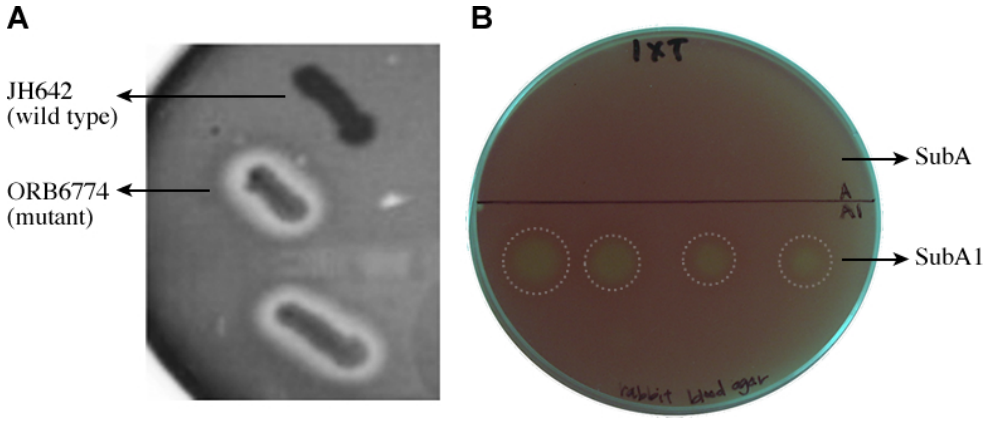

7.6 Conclusions and future direction

Subtilosin A1 was isolated and purified yielding ~3 mg per 1 liter of NSM media. Subsequent analysis by MALDI-TOF MS indicates the successful isolation of desired product. Our collaborators, Dr. Nakano and coworkers, demonstrated that

a single point mutation in the gene encoding subtilosin A confers hemolytic activity that was absent in the wild type form. In addition to its hemolytic activity, subtilosin A1 showed enhanced antibacterial activity against specific bacterial strains compared to the wild type (sub A). The T6I substitution introduces some hydrophobicity into subtilosin A1 which could affect its binding with the target membrane. Alternately, introduction of the bulky Ile side chain could affect the conformation of the peptide, leading to altered activity. These observations suggest possible bioengineering approaches for the production of bacteriocins with altered activities.

7.7 Experimental procedures

7.7.1 Growth and purification of Subtilosin A1

Isolated colonies of *Bacillus subtilis* strain ORB6774 were obtained by overnight incubation at 37 ˚C on DSM agar plates. DSM, which consists of 1.6 g Difco Nutrient broth, 24 mg $MgSO_4$•$7H_2O$, 200 mg KCl, 120 μL of 1N NaOH and 2.6 g agar dissolved in 200 mL milli-Q H_2O, was autoclaved at 121 ˚C for 15 min. Each of the following filter sterilized solutions were added to the cooled media: 0.2 mL each of 1 mM $Ca(NO_3)_2$•$4H_2O$,10 mM $MnCl_2$•$4H_2O$ and 1 mM $FeSO_4$•$7H_2O$.

LB tubes were inoculated with single colonies from DSM agar plates and grown at 37 ˚C for 7 hr at 200 rpm. LB tubes were prepared by dissolving 1.6 g of

Difco™ Luria Broth Base Miller in 100 mL of milli-Q H_2O and autoclaved at 121 ˚C for 15 min.

The grown *B. subtilis* LB culture (1.5 mL) was then added to 500 mL of prewarmed (35-37 ˚C) NSM media and incubated at 37 ˚C for 7 h at 200 rpm. NSM consists of 16 g Difco Nutrient broth, 500 mg $MgSO_4$•$7H_2O$, 2 g KCl, 1mM (118 mg) $Ca(NO_3)_2$•$4H_2O$, O.1mM (9.9 mg) $MnCl_2$•$4H_2O$, 1μM $FeSO_4$•$7H_2O$ (0.139 mg) dissolved in 500 mL milli-Q H_2O and autoclaved at 121 ˚C for 15 min.

The supernatant was extracted by adding one-quarter the volume of *n*-butanol (125 mL) and shaking for 1 hr, then it was poured into a separatory funnel and allowed to stand overnight. The organic layer was concentrated in vacuo and the residue resuspended in methanol (10 mL L^{-1} of cell culture).

7.7.2 HPLC purification

Subtilosin A1 was purified by high performance liquid chromatography (HPLC) using a Waters μBondapak C-18 column (WAT015814, 10 μm, 125 Å, 25 x 100 mm). The column was operated at a flow rate of 10 mL/min with dual wavelength detection at 220 nm and 280 nm. The method used for the purification started at 20% CH_3CN for 5 min and then ramped up to 80% CH_3CN over 28 min. The method was then held constant at 80% CH_3CN for 5 min, before ramping down to 20% CH_3CN in 2 min followed by flushing with 20% CH_3CN for 5 min.

The desired pure product was isolated at a retention time of t_R = 32.9 min. After multiple runs, the fractions containing subtilosin A1 were combined and lyophilized, yielding ~3 mg of subtilosin A1 per 1 liter of NSM media.

7.7.3 Mass spectrometry analysis

Subtilosin A1 was analyzed using matrix assisted laser desorption ionization time of flight (MALDI-TOF) mass spectrometry. Approximately 10 μg/μl subtilosin A1 in a solution of 1:2 acetonitrile (CH_3CN):0.1% trifluoroacetic acid (TFA) was mixed with an equal volume of matrix solution (10 mg/mL sinapinic acid in 50% CH_3CN, 0.1% TFA). 0.4 μl of this mixture was deposited onto a dried layer of matrix (10 mg/mL sinapinic acid in 3:2 acetone:methanol) on a stainless steel target. The sample was then analyzed on an Applied Biosystems Voyager Elite MALDI TOF system equipped with delayed extraction and an ion mirror (reflectron) for improving resolution and mass accuracy. External calibration was performed with a mixture of bovine insulin chain B (oxidized form) and bovine insulin. MALDI-TOF MS: exact mass calculated for $C_{154}H_{230}N_{38}O_{44}S_3$ = 3411.6, found 3412.5 $[M+H]^+$ (Figure 2B).

7.8 References

1. Huang, T.; Geng, H.; Miyyapuram, V. R.; Sit, C. S.; Vederas, J. C.; Nakano, M. M. Isolation of a Variant of Subtilosin A with Hemolytic Activity. *J. Bacteriol.* **2009**, *191*, 5690-5696.
2. Kawulka, K. E.; Sprules, T.; Diaper, C. M.; Whittal, R. M.; McKay, R. T.; Mercier, P.; Zuber, P.; Vederas, J. C. Structure of subtilosin A, a cyclic antimicrobial peptide from Bacillus subtilis with unusual sulfur to alpha-carbon cross-links: Formation and reduction of alpha-thio-alpha-amino acid derivatives. *Biochemistry* **2004**, *43*, 3385-3395.
3. Shelburne, C. E.; An, F. Y.; Dholpe, V.; Ramamoorthy, A.; Lopatin, D. E.; Lantz, M. S. The spectrum of antimicrobial activity of the bacteriocin subtilosin A. *J. Antimicrob. Chemother.* **2007**, *59*, 297-300.

APPENDIX B

SYNTHESIS AND TESTING OF SMALL-MOLECULE INHIBITOR OF *hi*GlmU AGAINST *mtb*GlmU

8.1 Introduction

Amino sugars such as *N*-acetyl glucosamine represent a major constituent of bacterial cell walls. The enzyme *N*-acetylglucosamine-1-phosphate uridyltransferase (GlmU) catalyzes the biosynthesis of uridine-diphospho-*N*-acetylglucosamine (UDP-GlcNAc). In the first step, GlmU transfers an acetyl group from acetyl-CoA to glucosamine-1-phosphate to form *N*-acetylglucosamine-1-phosphate (GlcNAc-1-P). In the second step, an uridyl monophosphate group is transferred from uridine triphosphate (UTP) to GlcNAc-1-P (formed in the first step) to produce UDP-GlcNAc (Scheme 1) and pyrophosphate (PPi).[1-4]

Scheme 1. Biosynthetic pathway for UDP-GlcNAc

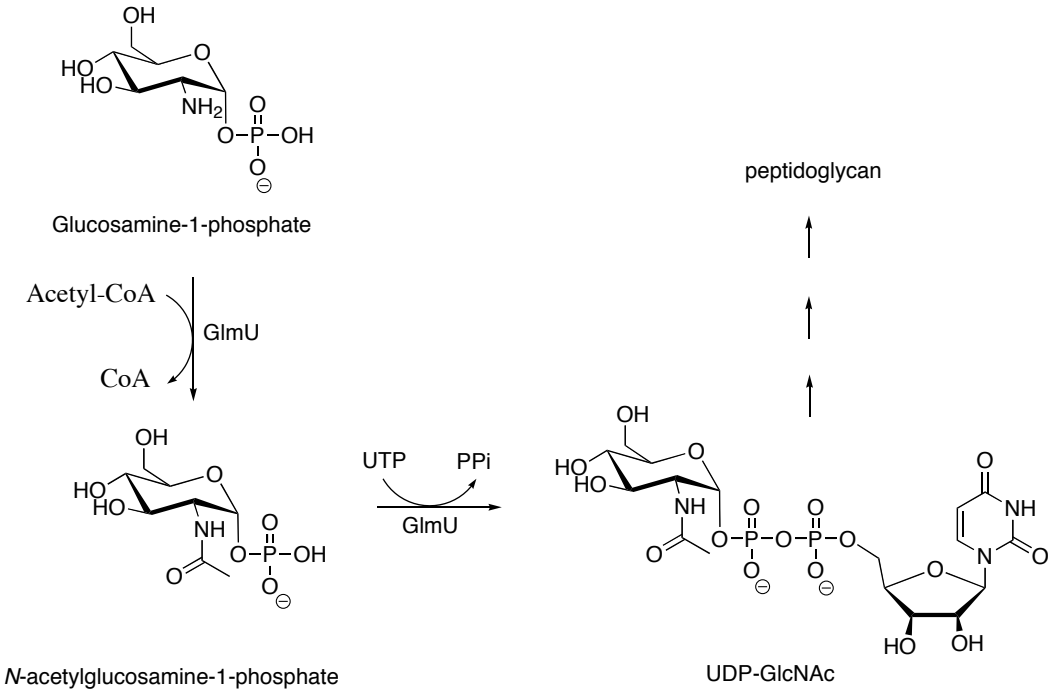

UDP-GlcNAc is an important precursor for the biosynthesis of peptidoglycan and lipopolysaccharide constituents of bacterial cell walls[5]; therefore, GlmU may serve as a potential drug target. For example, inhibition of GlmU in *Mycobacterium tuberculosis* could form the basis of a new treatment against tuberculosis. In developing countries, tuberculosis is by far the most common opportunistic infection. According to the World Health Organization, 8 million cases of tuberculosis (TB) occur each year, resulting in 3 million deaths.[6] Although the currently available anti-tubercular drugs are highly effective, the recent development of drug resistance in certain strains of *M. tuberculosis*

threatens to reduce the effectiveness of current therapies.[7] Since these drugs target a limited number of cellular mechanisms, there is a need for drug candidates that exert their actions through novel mechanisms.[8,9] The gene *glmU* in *Mycobacterium tuberculosis* has been found to be necessary for the growth of the bacterium[10] and is not present in humans. Therefore GlmU has been identified as a potential target for the design of inhibitors against tuberculosis.

The crystal structures of GlmU from *Escherichia coli*, *Streptococcus pneumoniae*, *Haemophilus influenza* and *M. tuberculosis* have been reported.[9,11-14] Mochalkin *et al,*[13] in their recent crystal structure studies of *H. influenza* GlmU (*hi*GlmU) complexes, suggested that GlmU activity follows a sequential substrate-binding order that begins with UTP binding noncovalently to the GlmU enzyme. Upon binding, the uridyltransferase active site remains in the open conformation until *N*-acetylglucosamine-1-phosphate binds and induces a conformational change at the GlcNAc-binding subsite. Following binding of *N*-acetylglucosamine-1-phosphate to the UTP charged uridinyltransfer active site, the unesterified oxygen of GlcNAc-1-P performs a nucleophilic attack on the UTP α-phosphate to complete the enzymatic reaction (Scheme 2).

Scheme 2. Mechanism showing the formation of UDP-GlcNAc

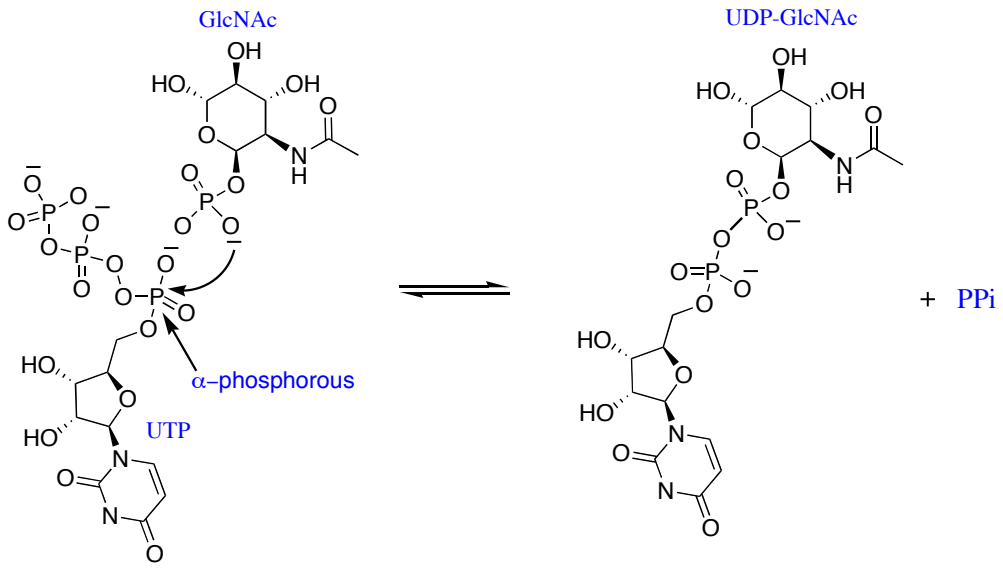

The same group at Pfizer Incorporation reported an X-ray crystal structure of a small-molecule inhibitor (IC_{50} = 18 μM) complexed with GlmU from *Haemophilus influenza* (*hi*GlmU).[14] The studies suggested the inhibitor occupies an allosteric site adjacent to the *N*-acetylglucosamine-1-phosphate substrate binding region and this binding prevents conformational changes required for the transfer of phosphate from UTP to complete the enzymatic reaction. The inhibitor contains a central piperidine ring in which the nitrogen carries a phenethyl ring. The crystal structure indicated a hydrogen bonding interaction between the side chain carboxyl of Glu224 (E224) and the piperidinium nitrogen (Figure 1). An additional hydrogen bonding interaction was seen between the amide oxygen and the terminal nitrogen of Gln231 (Q231).

Figure 1. Schematic representation of *hi*GlmU showing hydrogen-bonding interactions

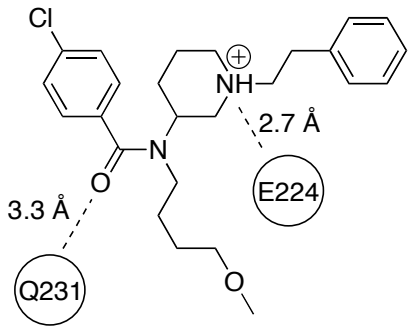

8.2 Objective

As GlmU catalyzes the formation of UDP-GlcNAc, a substrate for the biosynthesis of peptidoglycan and lipopolysaccharides, targeting these biosynthetic pathways might present an attractive approach for the discovery of new antibiotic drugs. One of the interests of our collaborators (Dr. Michael James and coworkers) at the University of Alberta biochemistry department is to find inhibitors that target *Mycobacterium tuberculosis*. The idea was to test the piperidine based inhibitor from *Haemophilus influenza*[14] against GlmU from *Mycobacterium tuberculosis*. Accordingly, we decided to synthesize the compound.

8.3 Results and discussion

The piperidine derivative was synthesized according to a literature procedure.[14] Neither experimental details (except reagents) nor spectroscopic data are provided in the original paper.[14] The commercially available 1-Boc-3-piperidone (**1**) is condensed with 3-methoxy propylamine followed by reduction with sodium triacetoxyborohydride to provide the secondary amine **2**. The crude amine derivative **2** without isolation is treated with 4-chlorobenzoyl chloride to afford the corresponding amide **3**. The Boc protected amide **3** after purification is treated with 4M HCl in dioxane for 30 min to afford the free amine **4** in 60% yield. Reductive amination of **4** with phenylacetaldehyde provides the desired product **5** in 52% yield (Scheme 3).

Scheme 3. Synthesis of piperidine derivative

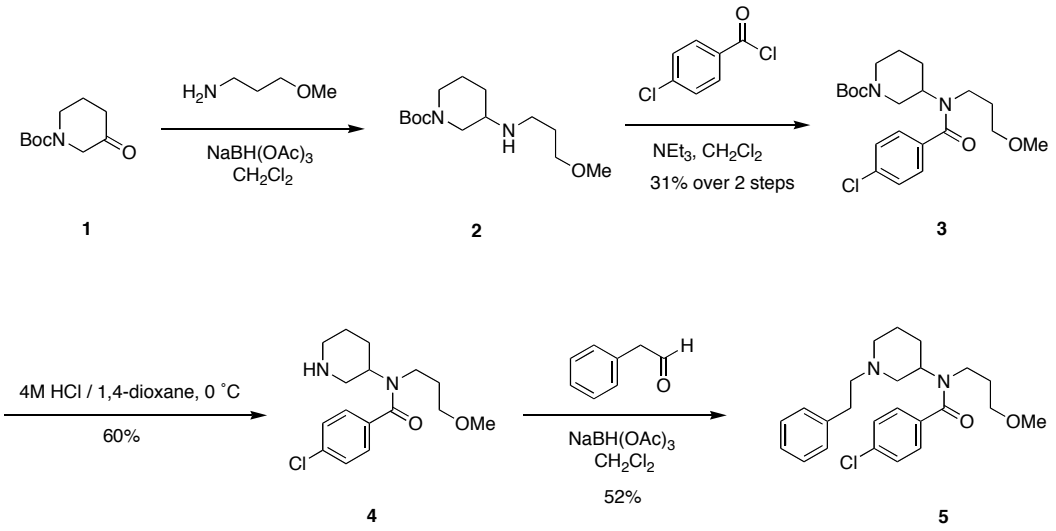

The testing results indicated that the piperidine derivative **5** did not inhibit the enzyme. This could be attributed to differences in the binding sites between the two enzymes. The recently reported crystal structure of GlmU from *Mycobacterium tuberculosis* (*Mtb*)[9] indicated that the *Mtb*GlmU uridyltransferase-domain structure is very similar to that reported for *S. pneumoniae*. It was reported that the piperidine-based inhibitor was inactive against GlmU from *S. pneumoniae*. The GlmU in these organisms contain a Met or a Leu in place of E224 that can disrupt the key bonding interactions with the piperidine protonated nitrogen.

8.4 Summary and future direction

The structural differences at this site among different GlmU enzymes may be the cause of the lack of inhibitory effect of the synthesized compound on *Mtb*GlmU. Further modifications or screening of new libraries may provide new inhibitors.

8.5 Experimental procedures and data for compounds

***tert*-Butyl-3-(4-chloro-*N*-(3-methoxypropyl)benzamido)piperidine-1-carboxylate (3)**

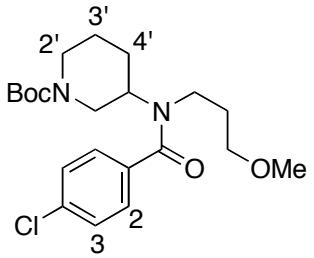

To a solution of 1-Boc-3-piperidone (1.34 g, 6.22 mmol) in $ClCH_2CH_2Cl$ (30.0 mL) at 0 ˚C was added 3-methoxypropylamine (0.64 mL, 6.22 mmol) and sodium triacetoxy borohydride (1.85 g, 8.71 mmol) followed by AcOH (0.93 mL, 15.56 mmol). After stirring the reaction mixture for 6 h, the solvent was removed under vacuum and the residue was dissolved in EtOAc (30.0 mL), washed with water, saturated $NaHCO_3$ solution, brine, dried over $MgSO_4$ and then concentrated *in vacuo* to afford **2** (1.17 g) as a pale pink sticky mass. The crude material was used without purification for the next step. To a solution of **2** (1.17 g, 4.30 mmol) in CH_2Cl_2 (50 mL) at 0 ˚C was added Et_3N (0.84 mL, 6.02 mmol) and a solution of 4-chlorobenzoyl chloride (0.77 mL, 6.03 mmol) in CH_2Cl_2 (5.0 mL) dropwise over a period of 10 min. After stirring for 1 hr at 0 ˚C, the reaction mixture was washed with water, brine and dried over Na_2SO_4, filtered and concentrated *in vacuo*. The crude product was purified by flash chromatography (SiO_2, 8:2/ EtOAc:hexanes) to yield **3** (792 mg, 31% over two steps) as a liquid. IR

(microscope): 2974, 2931, 1692, 1636 1597, 1420, 1265 cm^{-1}; ^1H NMR (CD_2Cl_2, 300 MHz) δ 7.36 (d, 2H, J = 8.7 Hz, H_2), 7.31 (d, 2H, J = 8.7 Hz, H_1), 4.08-4.00 (m, 2H, $C\underline{H}_2OCH_3$), 3.38-3.35 (m, 5H, $C\underline{H}$ and $2xC\underline{H}_2$), 3.27 (s, 3H, $OC\underline{H}_3$), 2.52 (br, 1H, $C\underline{H}_2$), 1.96-1.60 (m, 5H, $C\underline{H}_2$), 1.43 (d, J = 1.8 Hz, $H_{3'}$ or $H_{4'}$), 1.42 (d, J = 1.8 Hz, $H_{3'}$ or $H_{4'}$), 1.39 (s, 9H, $(C\underline{H}_3)_3$); ^{13}C NMR (DMSO-d_6, 125 MHz, 70 °C over night) δ 171.5, 138.5, 129.4, 129.0, 126.6, 70.5, 58.4, 56.8, 50.4, 45.9, 30.3, 29.9, 27.0, no peaks observed for Boc as it fell off; HRMS (ES) calcd for $C_{21}H_{31}N_2O_4ClNa$ ($[M+Na]^+$), 433.1864; found, 433.1857.

4-chloro-*N*-(3-methoxypropyl)-*N*-(1-phenethylpiperidin-3-yl)benzamide (5)

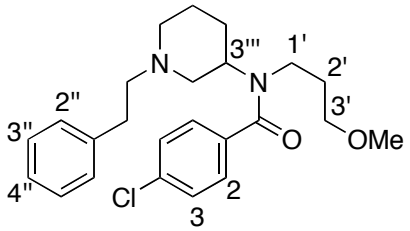

A solution of 4M HCl in dioxane (10.0 mL) was cooled to 0 °C and added to the amide **3** (792 mg, 1.92 mmol). The reaction mixture was stirred at 0 °C for 30 min after which the TLC indicated the completion of the reaction. The reaction mixture was quenched with saturated $NaHCO_3$ solution, washed with water, brine and then concentrated under vacuum to afford the free amine **4** (360 mg, 60%) as an oil. The crude **4** without isolation was carried on to the next step. To a solution of phenylacetaldehyde (0.01 mL, 1.21 mmol) in $ClCH_2CH_2Cl$ (20.0 mL) at 0 °C was added a solution of **4** (250 mg, 0.80 mmol) in $ClCH_2CH_2Cl$ (2.0 mL) and sodium triacetoxy borohydride (256 mg, 1.21 mmol) followed by AcOH (0.01 mL, 1.61 mmol). After stirring the reaction mixture overnight (8 h), the solvent

was removed under vacuum and the residue was dissolved in EtOAc (20.0 mL), washed with water, saturated $NaHCO_3$ solution, brine, dried over $MgSO_4$ and then concentrated *in vacuo*. The crude was purified by flash chromatography (SiO_2, 1:2/EtOAc:hexanes) to yield **5** (172 mg, 52%) as an oil. IR (CH_2Cl_2 cast): 3061, 2953, 1633, 1491, 1452, 1418 cm^{-1}; ^1H NMR (DMSO-d_6, 400 MHz) δ 7.43 (d, 2H, J = 8.8 Hz, H_2), 7.32 (d, 2H, J = 8.8 Hz, H_3), 7.22-7.19 (m, 2H, $H_{3''}$), 7.14-7.12 (m, 3H, $H_{2''}$ and $H_{4''}$), 3.66 (br, 1H, $H_{3'''}$), 3.31-3.27 (m, 4H, $H_{3'}$ and $H_{1'}$), 3.18 (s, 3H, $C\underline{H}_3$), 2.87-2.85 (m, 1H, $C\underline{H}_2$), 2.73-2.65 (m, 3H, $C\underline{H}_2$), 2.55-2.51 (m, 2H, $C\underline{H}_2$), 2.17 (t, 1H, J = 10.6 Hz, $C\underline{H}_2$), 1.9 (t, 1H, J = 10.6 Hz, $C\underline{H}_2$), 1.76-1.70 (m, 3H, $C\underline{H}_2$), 1.64-1.52 (m, 2H, $C\underline{H}_2$), 1.32-1.25 (M, 1H, $C\underline{H}_2$); ^{13}C NMR (DMSO-d_6, 100 MHz) δ 169.1, 135.8, 133. 0, 127.8, 127.7, 127.3, 127.2, 124.9, 74.0, 69.2, 58.5, 57.1, 55.9, 51.9, 32.2, 29.1, 27.8, 23.7; HRMS (ES) calcd for $C_{24}H_{32}N_2O_2Cl$ ($[M+H]^+$), 415.2146; found, 415.2147.

8.6 References

1. Menginlecreulx, D.; Vanheijenoort, J. Identification of the Glmu Gene Encoding N-Acetylglucosamine-1-Phosphate Uridyltransferase in *Escherichia coli*. *J. Bacteriol*. 1993, *175*, 6150-6157.
2. Menginlecreulx, D.; Vanheijenoort, J. Copurification of Glucosamine-1-Phosphate Acetyltransferase and N-Acetylglucosamine-1-Phosphate Uridyltransferase Activities of *Escherichia coli* - Characterization of the Glmu Gene-Product as a Bifunctional Enzyme Catalyzing 2 Subsequent

Steps in the Pathway for Udp-N-Acetylglucosamine Synthesis. *J. Bacteriol*. 1994, *176*, 5788-5795.

3. Gehring, A. M.; Lees, W. J.; Mindiola, D. J.; Walsh, C. T.; Brown, E. D. Acetyltransfer precedes uridylyltransfer in the formation of UDP-N-acetylglucosamine in separable active sites of the bifunctional GlmU protein of *Escherichia coli*. *Biochemistry* 1996, *35*, 579-585.

4. Pompeo, F.; van Heijenoort, J.; Mengin-Lecreulx, D. Probing the role of cysteine residues in glucosamine-1-phosphate acetyltransferase activity of the bifunctional GlmU protein from *Escherichia coli*: Site-directed mutagenesis and characterization of the mutant enzymes. *J. Bacteriol*. 1998, *180*, 4799-4803.

5. Anderson, M. S.; Raetz, C. R. H. Biosynthesis of Lipid-a Precursors in *Escherichia coli* - a Cytoplasmic Acyltransferase That Converts Udp-N-Acetylglucosamine to Udp-3-0-(R-3-Hydroxymyristoyl)-N-Acetylglucosamine. *J. Biol. Chem*. 1987, *262*, 5159-5169.

6. Raviglione, M. C.; Snider, D. E.; Kochi, A. Global Epidemiology of Tuberculosis - Morbidity and Mortality of a Worldwide Epidemic. *JAMA-J. Am. Med. Assoc*. 1995, *273*, 220-226.

7. O'Brien, R. J.; Nunn, P. P. The need for new drugs against tuberculosis - Obstacles, opportunities, and next steps. *Am. J. Respir. Crit. Care Med*. 2001, *163*, 1055-1058.

8. Bates, J. H. Tuberculosis Chemotherapy - the Need for New Antituberculosis Drugs Is Urgent. *Am. J. Respir. Crit. Care Med.* 1995, *151*, 942-943.

9. Zhang, Z.; Bulloch, E. M. M.; Bunker, R. D.; Baker, E. N.; Squire, C. J. Structure and function of GlmU from *Mycobacterium tuberculosis*. *Acta Crystallogr. Sect. D-Biol. Crystallogr.* 2009, *65*, 275-283.

10. Sassetti, C. M.; Boyd, D. H.; Rubin, E. J. Genes required for mycobacterial growth defined by high density mutagenesis. *Mol. Microbiol.* 2003, *48*, 77-84.

11. Brown, K.; Pompeo, F.; Dixon, S.; Mengin-Lecreulx, D.; Cambillau, C.; Bourne, Y. Crystal structure of the bifunctional N-acetylglucosamine 1-phosphate uridyltransferase from *Escherichia coli*: a paradigm for the related pyrophosphorylase superfamily. *Embo J.* 1999, *18*, 4096-4107.

12. Kostrewa, D.; D'Arcy, A.; Takacs, B.; Kamber, N. Crystal structures of Streptococcus pneumoniae N-acetylglucosamine-1-phosphate uridyltransferase, GlmU, in apo form at 2.33 A resolution and in complex with UDP-N-acetylglucosamine and Mg^{2+} at 1.96 A resolution. *J. Mol. Biol.* 2001, *305*, 279-289.

13. Mochalkin, I.; Lightle, S.; Zhu, Y.; Ohren, J. F.; Spessard, C.; Chirgadze, N. Y.; Banotai, C.; Melnick, M.; McDowell, L. Characterization of substrate binding and catalysis in the potential antibacterial target N-acetylglucosamine-1-phosphate uridyltransferase (GlmU). *Protein Sci.* 2007, *16*, 2657-2666.

14. Mochalkin, I.; Lightle, S.; Narasimhan, L.; Bornemeier, D.; Melnick, M.; Vanderroest, S. Structure of a small-molecule inhibitor complexed with GlmU from *Haemophilus influenzae* reveals an allosteric binding site. *Protein Sci*. 2008, *17*, 577-582.